INFORMATION TO USERS

This manuscript has been reproduced from the microfilm master. UMI films the text directly from the original or copy submitted. Thus, some thesis and dissertation copies are in typewriter face, while others may be from any type of computer printer.

The quality of this reproduction is dependent upon the quality of the copy submitted. Broken or indistinct print, colored or poor quality illustrations and photographs, print bleedthrough, substandard margins, and improper alignment can adversely affect reproduction.

In the unlikely event that the author did not send UMI a complete manuscript and there are missing pages, these will be noted. Also, if unauthorized copyright material had to be removed, a note will indicate the deletion.

Oversize materials (e.g., maps, drawings, charts) are reproduced by sectioning the original, beginning at the upper left-hand corner and continuing from left to right in equal sections with small overlaps.

Photographs included in the original manuscript have been reproduced xerographically in this copy. Higher quality 6" x 9" black and white photographic prints are available for any photographs or illustrations appearing in this copy for an additional charge. Contact UMI directly to order.

Bell & Howell Information and Learning
300 North Zeeb Road, Ann Arbor, MI 48106-1346 USA
800-521-0600

UMI®

Reproduced with permission of the copyright owner. Further reproduction prohibited without permission.

Reproduced with permission of the copyright owner. Further reproduction prohibited without permission.

Temple University
Doctoral Dissertation
Submitted to the Graduate Board

Title of Dissertation: (Please type) High Order Finite Difference Method For Incompressible Flow

Author: (Please type) Mr. Cheng Wang

Date of Defense: (Please type) April 11, 2000

Dissertation Examining Committee: (please type)	Read and Approved By: (Signatures)
Professor Jian-Guo Liu Dissertation Advisory Committee Chairperson	
Professor Omar Hijab	
Professor Wei-Shih Yang	
Professor Bo Li	
PROFESSOR Eric Grinberg Examining Committee Chairperson	GRADUATE CHAIR If Member of the Dissertation Examining Committee

Date Submitted to Graduate Board: 4/18/00

Accepted by the Graduate Board of Temple University in partial fulfillment of the requirements for the degree of **Doctor of Philosophy**.

Date 9-18-00

(Dean of the Graduate School)

Reproduced with permission of the copyright owner. Further reproduction prohibited without permission.

Reproduced with permission of the copyright owner. Further reproduction prohibited without permission.

HIGH ORDER FINITE DIFFERENCE METHOD FOR INCOMPRESSIBLE FLOW

A Dissertation

Submitted to

the Temple University Graduate Board

---

in Partial Fulfillment

of the Requirements for the Degree

DOCTOR OF PHILOSOPHY

---

by

Cheng Wang

August 2000

Reproduced with permission of the copyright owner. Further reproduction prohibited without permission.

UMI Number: 9990364

UMI®

UMI Microform 9990364
Copyright 2001 by Bell & Howell Information and Learning Company.
All rights reserved. This microform edition is protected against
unauthorized copying under Title 17, United States Code.

Bell & Howell Information and Learning Company
300 North Zeeb Road
P.O. Box 1346
Ann Arbor, MI 48106-1346

Reproduced with permission of the copyright owner. Further reproduction prohibited without permission.

ABSTRACT

HIGH ORDER FINITE DIFFERENCE METHOD FOR INCOMPRESSIBLE FLOW

by Cheng Wang

Doctor of Philosophy
Temple University, 2000

Advisor: Dr. Jian-Guo Liu

This work is concerned about a set of computational methods for incompressible flow, whose behavior can be governed by Navier-Stokes Equations (NSE). Finite Difference Schemes are concentrated here. The efficiency of these methods lies in the fact that only Poisson solver and heat equation solver are needed at each time stage. No Stokes-type equation needs to be solved and there is no coupling between momentum and kinematic equations. This makes the whole scheme extremely robust. Stability and convergence analysis are also documented. Some numerical examples are presented, along with perfect accuracy check with each scheme. The topics in this thesis include: Gauge formulation and the corresponding implicit gauge method; Second order scheme based on vorticity formulation, along with the choice of vorticity boundary condition; Stability and convergence analysis of Essentially Compact Fourth Order Scheme (EC4); Computation of

Reproduced with permission of the copyright owner. Further reproduction prohibited without permission.

flow on multi-connected domain: A fourth order numerical approximation to Boussinesq flow, which are discussed in each chapter, respectively.

Reproduced with permission of the copyright owner. Further reproduction prohibited without permission.

ACKNOWLEDGEMENTS

I would like to express my deepest thanks to my advisor Professor Jian-Guo Liu, nor only for his subtle guidance, but also for his invaluable assistance and support.

I would also like to thank Professors Wei-Shih Yang, Omar Hijab, from Temple University and Bo Li from University of Maryland for serving as members of my examining committee.

Reproduced with permission of the copyright owner. Further reproduction prohibited without permission.

DEDICATION

I would like to dedicate this work to my mother Shu-Liang Chen and my father Fu-Tang Wang.

Reproduced with permission of the copyright owner. Further reproduction prohibited without permission.

TABLE OF CONTENTS

Reproduced with permission of the copyright owner. Further reproduction prohibited without permission.

Reproduced with permission of the copyright owner. Further reproduction prohibited without permission.

LIST OF TABLES

Reproduced with permission of the copyright owner. Further reproduction prohibited without permission.

Reproduced with permission of the copyright owner. Further reproduction prohibited without permission.

LIST OF FIGURES

Reproduced with permission of the copyright owner. Further reproduction prohibited without permission.

Reproduced with permission of the copyright owner. Further reproduction prohibited without permission.

Reproduced with permission of the copyright owner. Further reproduction prohibited without permission.

CHAPTER 1
INTRODUCTION

The subject of **Computational Fluid Dynamics** has attracted a lot of attentions these years. The starting point of this subject is to design computational methods to approximate Navier-Stokes Equations (NSE), which can describe the motion of incompressible flow very well.

NSE has two widely-used formulations: Velocity-Pressure Formulation and Vorticity-Stream function Formulation. The velocity-pressure formulation with no-flow, no-slip boundary condition can be written as

$$\begin{cases} \boldsymbol{u}_t + (\boldsymbol{u}\cdot\nabla)\boldsymbol{u} + \nabla p = \nu\triangle\boldsymbol{u}\,, & \text{in } \Omega\,, \\ \nabla\cdot\boldsymbol{u} = 0\,, & \text{in } \Omega\,, \\ \boldsymbol{u} = 0\,, & \text{on } \partial\Omega\,. \end{cases} \tag{1.1}$$

where $\boldsymbol{u} = (u, v)$ is the velocity, p is the pressure and ν is the kinematic viscosity.

There are three main difficulties in the numerical simulation of incompressible flow in the primitive formulation:

(D1) The implementation of the incompressibility constraint $\nabla\cdot\boldsymbol{u} = 0$.

(D2) There is no dynamic equation and no boundary condition for the pressure p. Indeed, p is mainly a Lagrange multiplier to assure the incompressibility.

(D3) The implementation of the no penetration and no-slip boundary condition.

To overcome the above difficulties, E and Liu proposed a new formulation, Gauge formulation in [ELG1]. Instead of using primitive variables of NSE, the

Reproduced with permission of the copyright owner. Further reproduction prohibited without permission.

gauge formulation replaces pressure by a gauge variable o and introduces the auxiliary field $\boldsymbol{a} = \boldsymbol{u} - \nabla o$. Then the incompressibility constraint in (1.1) becomes

$$\triangle o = -\nabla \cdot \boldsymbol{a}\,. \tag{1.2}$$

and the momentum equation in (1.1) becomes

$$\boldsymbol{a}_t + (\boldsymbol{u}\cdot\nabla)\boldsymbol{u} + \nabla\Big(\partial_t o - \frac{1}{Re}\triangle o + p\Big) = \frac{1}{Re}\triangle \boldsymbol{a}\,. \tag{1.3}$$

If we impose

$$\partial_t o - \frac{1}{Re}\triangle o = -p\,. \tag{1.4}$$

we obtain the gauge formulation of NSE

$$\begin{cases} \boldsymbol{a}_t + (\boldsymbol{u}\cdot\nabla)\boldsymbol{u} = \dfrac{1}{Re}\triangle \boldsymbol{a}\,, & \text{in } \Omega\,. \\ \triangle \phi = -\nabla\cdot\boldsymbol{a}\,, & \text{in } \Omega\,. \\ \boldsymbol{u} = \boldsymbol{a} + \nabla o\,, & \text{in } \Omega\,. \end{cases} \tag{1.5}$$

One of the main advantages of Gauge formulation is that ϕ is a non-physical variable, so we have the freedom to assign boundary condition for ϕ. Corresponding to the no-flow, no-slip boundary condition $\boldsymbol{u} = 0$ on $\partial\Omega$, we can either prescribe:

$$\frac{\partial o}{\partial \boldsymbol{n}} = 0\,, \qquad \boldsymbol{a}\cdot\boldsymbol{n} = 0\,, \qquad \boldsymbol{a}\cdot\boldsymbol{\tau} = -\frac{\partial o}{\partial \boldsymbol{\tau}}\,, \qquad \text{on } \partial\Omega\,, \tag{1.6}$$

or

$$\phi = 0\,, \qquad \boldsymbol{a}\cdot\boldsymbol{n} = -\frac{\partial \phi}{\partial \boldsymbol{n}}\,, \qquad \boldsymbol{a}\cdot\boldsymbol{\tau} = 0\,. \qquad \text{on } \partial\Omega\,. \tag{1.7}$$

where $\boldsymbol{\tau}$ is the unit tangent vector.

Neumann gauge formulation (1.5) and (1.6) can be written in another form

$$\begin{cases} \boldsymbol{a}_t + (\boldsymbol{u}\cdot\nabla)\boldsymbol{u} = \dfrac{1}{Re}\triangle \boldsymbol{a}\,, & \text{in } \Omega\,. \\ \boldsymbol{a}\cdot\boldsymbol{n} = 0, \quad \boldsymbol{a}\cdot\boldsymbol{\tau} = -\dfrac{\partial o}{\partial \boldsymbol{\tau}}\,, & \text{on } \partial\Omega\,. \end{cases} \tag{1.8a}$$

Reproduced with permission of the copyright owner. Further reproduction prohibited without permission.

$$\begin{cases} \triangle o = -\nabla \cdot \boldsymbol{a}, & \text{in } \Omega, \\ \dfrac{\partial o}{\partial \boldsymbol{n}} = 0, & \text{on } \partial\Omega. \end{cases} \tag{1.8b}$$

(1.8) can be easily solved by finite difference method, which will be discussed in detail in Chapter 2. For simplicity of presentation, we take $Re = 1$. For example, if backward Euler method is used as the time discretization for the momentum equation, we have

$$\frac{\boldsymbol{a}^{n+1} - \boldsymbol{a}^n}{\triangle t} + (\boldsymbol{u}^n \cdot \nabla)\boldsymbol{u}^n = \triangle \boldsymbol{a}^{n+1}, \qquad \text{in } \Omega. \tag{1.9}$$

Still, the boundary conditions for $\boldsymbol{a}$ has to be determined to implement (1.9). To avoid the coupling between the momentum equation and the boundary conditions, we use **explicit** boundary conditions for $\boldsymbol{a}$, which are carried out by vertical extrapolation. For the first order scheme, we can just take

$$\boldsymbol{a}^{n+1} \cdot \boldsymbol{n} = 0, \qquad \boldsymbol{a}^{n+1} \cdot \boldsymbol{\tau} = -\frac{\partial o^n}{\partial \boldsymbol{\tau}}, \qquad \text{on } \partial\Omega. \tag{1.10}$$

Next we update ϕ^{n+1} at time step t^{n+1} by

$$\begin{cases} \triangle o^{n+1} = -\nabla \cdot \boldsymbol{a}^{n+1}, & \text{in } \Omega, \\ \frac{\partial o^{n+1}}{\partial \boldsymbol{n}} = 0, & \text{on } \partial\Omega. \end{cases} \tag{1.11}$$

and the velocity $\boldsymbol{u}^{n+1}$ is determined by the incompressiblity

$$\boldsymbol{u}^{n+1} = \boldsymbol{a}^{n+1} + \nabla o^{n+1}. \tag{1.12}$$

It can be seen that the momentum equation (1.9) is decoupled from the kinematic equation (1.11) due to the fact that the boundary conditions for $\boldsymbol{a}$ in (1.10) are explicit. The resulting scheme is very efficient and the computational cost is reduced to solving a standard heat and Poisson equation.

The main contribution of Chapter 2 is to show that the explicit boundary condition for $\boldsymbol{a}$ in (1.10) is unconditionally stable for Stokes flow. In addition,

Reproduced with permission of the copyright owner. Further reproduction prohibited without permission.

the main convergence theorem for Stokes equations is stated below, which is just Theorem 2.3.1 in Chapter 2:

Theorem 1.1 *Let $(\boldsymbol{u}, \phi)$ be a smooth solution of Stokes equations with smooth initial data $\boldsymbol{u}^0(\boldsymbol{x})$ and let $(\boldsymbol{u}_{\Delta t}, \phi_{\Delta t})$ be the numerical solution of the semi-discrete gauge method with explicit boundary conditions. Then we have*

$$\|\boldsymbol{u} - \boldsymbol{u}_{\Delta t}\|_{L^\infty(0,T;L^2)} \leq C\Delta t\,. \tag{1.13}$$

For the full nonlinear Navier-Stokes equations, the time stepping constraint is reduced to the standard CFL constraint $\frac{\Delta t}{\Delta x} \leq C$. The corresponding convergence theorem is stated below, which is Theorem 2.4.1 in Chapter 2:

Theorem 1.2 *Let $(\boldsymbol{u}, \phi)$ be a smooth solution of the Navier-Stokes equations with smooth initial data $\boldsymbol{u}^0(\boldsymbol{x})$ and let $(\boldsymbol{u}_h, \phi_h)$ be the numerical solution of the gauge method coupled with the MAC spatial discretizations. Assume the CFL constraint $\Delta t \leq Ch$ for some suitable constant C which we will specify in detail later, then we have*

$$\|\boldsymbol{u} - \boldsymbol{u}_h\|_{L^\infty} \leq C(\Delta t + h^2)\,. \tag{1.14}$$

There are some other ways to overcome the three difficulties mentioned for the primitive formulation (1.1). For 2D flow, the first and second difficulties can be eliminated in the vorticity-stream function formulation

$$\begin{cases} \partial_t \omega + \nabla\cdot(\boldsymbol{u}\omega) = \nu\Delta\omega\,. \\ \Delta\psi = \omega\,. \\ u = -\partial_y\psi\,. \qquad v = \partial_x\psi \end{cases} \tag{1.15}$$

where ω denotes the vorticity and the no-flow, no-slip boundary condition can be written in terms of the stream function ψ

$$\psi = C_i, \quad \frac{\partial\psi}{\partial\mathbf{n}} = 0\,, \quad \text{at each } \Gamma_i\,. \tag{1.16}$$

Reproduced with permission of the copyright owner. Further reproduction prohibited without permission.

where C_i is constants at each boundary section Γ_i. In the simply-connected domain, C_0 can be set to be 0. It can be seen that the above formulation has the advantage that it not only eliminates the pressure variable, but also the incompressibility is automatically enforced. Thus it brings a lot of convenience in computation. Yet, the main difficulty in the numerical simulation of (1.15), (1.16) is the boundary condition:

(D3(1)) The implementation of the two boundary conditions for the stream function in (1.16).

(D3(2)) When the vorticity is updated in time (in the momentum equation), there is no definite boundary condition for vorticity.

The methodology to overcome the above difficulties is to solve for the stream function using Dirichlet boundary condition $\psi = 0$ on Γ, and then compute the vorticity at the boundary from the stream function via the kinematic relation and no-slip boundary condition. For example, either **Thom's formula**

$$\omega_{i,0} = \frac{2\psi_{i,1}}{h^2}. \tag{1.17}$$

or **Wilkes-Pearson's formula**

$$\omega_{i,0} = \frac{1}{h^2}(4\psi_{i,1} - \frac{1}{2}\psi_{i,2}). \tag{1.18}$$

can be used as vorticity boundary condition.

In Chapter 3, it will be shown and argued that either Thom's formula or Wilkes' formula, coupled with 2nd order centered difference scheme at the interior points

$$\begin{cases} \partial_t \omega + \widetilde{D}_x(u\omega) + \widetilde{D}_y(v\omega) = \nu \triangle_h \omega, \\ \triangle_h \psi = \omega, \qquad \psi|_\Gamma = 0, \\ u = -\widetilde{D}_y \psi, \qquad v = \widetilde{D}_x \psi, \end{cases} \tag{1.19}$$

give full 2nd order accuracy for the whole scheme. Wilkes' formula gives higher order accuracy for the vorticity on the boundary than Thom's formula by formal

Reproduced with permission of the copyright owner. Further reproduction prohibited without permission.

Taylor expansion. In particular, it will be very useful for non-uniform grids. The main theorem in Chapter 3 can be stated as

Theorem 1.3. *Let $\boldsymbol{u}_e \in L^\infty([0,T];C^{5,\alpha}(\overline{\Omega}))$, v_e, ω_e be the exact solution of the Navier-Stokes equations (1.15), (1.16) and $\boldsymbol{u}_h$, ω_h be the approximate solution of the second order scheme with Pearson-Wilkes formula, then we have*

(1.20)

$$\begin{aligned}&\|\boldsymbol{u}_e - \boldsymbol{u}_h\|_{L^\infty([0,T],L^2)} + \sqrt{\nu}\|\omega_e - \omega_h\|_{L^2([0,T],L^2)}\\ &\le Ch^2\|\boldsymbol{u}_e\|_{L^\infty([0,T],C^{5,\alpha})}\Big(1 + \|\boldsymbol{u}_e\|_{L^\infty([0,T],C^3)}\Big)\exp\left\{\frac{CT}{\nu}(1 + \|\boldsymbol{u}_e\|^2_{L^\infty([0,T],C^1)})\right\},\end{aligned}$$

which is just Theorem 3.4.1. Full 2nd order accuracy is also demonstrated numerically. Our analysis results in almost optimal regularity assumption for the exact solution.

The main contribution of Chapter 3 is to show that Wilkes' formula also has good stability property. In addition, this stability argument can be applied to other long-stencil formulas. It cannot be directly derived from straightforward manipulations since more interior points are involved in the formula. A new methodology is developed to establish this stability analysis. The main idea is to control local terms by global quantities via discrete elliptic regularity for stream function.

In Chapter 4, a fourth order finite difference method based on (1.15), (1.16) is considered. The scheme is essentially compact fourth order scheme (EC4), which was proposed by E and Liu in [ELV2], and can be implemented very efficiently. Motivated by the fourth order approximation to Δ in 2-D

$$\Delta = \frac{\Delta_h + \frac{h^2}{6}D_x^2 D_y^2}{1 + \frac{h^2}{12}\Delta_h} + O(h^4)\,. \tag{1.21}$$

Reproduced with permission of the copyright owner. Further reproduction prohibited without permission.

they discretize NSE in 2-D by

$$\text{(1.22)}\qquad \begin{cases} \partial_t \varpi = (\triangle_h + \dfrac{h^2}{6} D_x^2 D_y^2)\omega - \mathcal{NL}\,. \\ (\triangle_h + \dfrac{h^2}{6} D_x^2 D_y^2)v = \varpi\,. \qquad v\,|_\Gamma = 0\,. \\ (1 + \dfrac{h^2}{12}\triangle_h)\omega = \varpi\,. \end{cases}$$

where the intermediate variable ϖ was introduced as $\varpi = (1 + \frac{h^2}{12}\triangle_h)\omega$, and the approximate nonlinear term $\mathcal{NL}$ is given by

$$\text{(1.23)}\quad \mathcal{NL} = \widetilde{D}_x(1 + \frac{h^2}{6} D_y^2)(u\omega) + \widetilde{D}_y(1 + \frac{h^2}{6} D_x^2)(v\omega) - \frac{h^2}{12}\triangle_h(u\widetilde{D}_x\omega + v\widetilde{D}_y\omega)\,.$$

To compute the third term in (1.23) near the boundary, $u\widetilde{D}_x\omega + v\widetilde{D}_y\omega$ can be set to be 0 on Γ, since the velocity field vanishes on the boundary. In addition, the velocity $\boldsymbol{u} = (-\partial_y\psi, \partial_x\psi)$ can be valued by using the standard long-stencil 4-th order formulas:

$$\text{(1.24)}\qquad u = -\widetilde{D}_y(1 - \frac{h^2}{6} D_y^2)\psi\,, \quad v = \widetilde{D}_x(1 - \frac{h^2}{6} D_x^2)\psi\,.$$

Similar to the second order case discussed in Chapter 3, the vorticity boundary condition is a very important issue. Either **Briley's formula**

$$\text{(1.25)}\qquad \omega_{i,0} = \frac{1}{h^2}(6\psi_{i,1} - \frac{3}{2}\psi_{i,2} + \frac{2}{9}\psi_{i,3})$$

which gives 3rd order accuracy for the vorticity on the boundary, or a new higher order formula

$$\text{(1.26)}\qquad \omega_{i,0} = \frac{1}{h^2}(8\psi_{i,1} - 3\psi_{i,2} + \frac{8}{9}\psi_{i,3} - \frac{1}{8}\psi_{i,4})\,.$$

which will be derived in Chapter 4, and indicates 4th order accuracy for the vorticity on the boundary, can be chosen as the vorticity boundary condition. The use of either boundary condition results in a stable method. The EC4 scheme with Briley's formula was analyzed by E and Liu in [ELV2]. The main result in Chapter 4 can be stated in the following theorem, which is Theorem 4.3.1:

Reproduced with permission of the copyright owner. Further reproduction prohibited without permission.

Theorem 1.4. *Let $\boldsymbol{u}_e \in L^\infty([0,T];C^{7,\alpha}(\overline{\Omega}))$ be the solution of the Navier-Stokes equations and $\boldsymbol{u}_h$ be the approximate solution of EC4, then we have*

$$\begin{aligned}\|\boldsymbol{u}-\boldsymbol{u}_h\|_{L^\infty([0,T];L^2)} \le\ & Ch^4\|\boldsymbol{u}_e\|_{L^\infty([0,T];C^{7,\alpha})} \\ & (1+\|\boldsymbol{u}_e\|_{L^\infty([0,T];C^5)})\exp\left\{\frac{CC^*T}{\nu}\right\}.\end{aligned} \tag{1.27}$$

where $C^* = (1+\|\boldsymbol{u}_e\|_{L^\infty([0,T];C^5)})^2$.

Since the vorticity boundary condition (1.25) or (1.26) are long-stencil formulas, we adopt the similar technique of stability analysis used in the third chapter, which is to control some local terms by the diffusion term via discrete elliptic regularity, thus guarantees the stability of both formulas. To illustrate the idea of both stability and consistency analysis more clearly, we choose to give a detailed analysis of both formulas in a simple 1-D Stokes model in Section 4.2. The consistency analysis for Briley's formula is implemented by Strang type expansion; while that of our new 4-th order vorticity boundary condition is more straightforward, no correction term is needed. Physical no-slip boundary conditions are used throughout.

In Chapter 5, an application of finite difference method based on vorticity and stream-function variables to multi-connected computational domain is considered. As discussed above, using the vorticity and stream-function variables is an effective way to compute 2D incompressible flow due to the fact that the incompressibility constraint for the velocity is automatically satisfied, the pressure variable is eliminated, and high order schemes can be efficiently implemented. However, the difficulty arises in the multi-connected computational domain in determining the constants of the stream function on the boundary of "holes". This is an especially difficult task for the calculation of unsteady flows, since these constants vary with time to reflect the total fluxes of the flow in each sub-channels. An efficient method in finite difference setting is presented to attack this task. For simplicity of presentation, the following domain is chosen:

Reproduced with permission of the copyright owner. Further reproduction prohibited without permission.

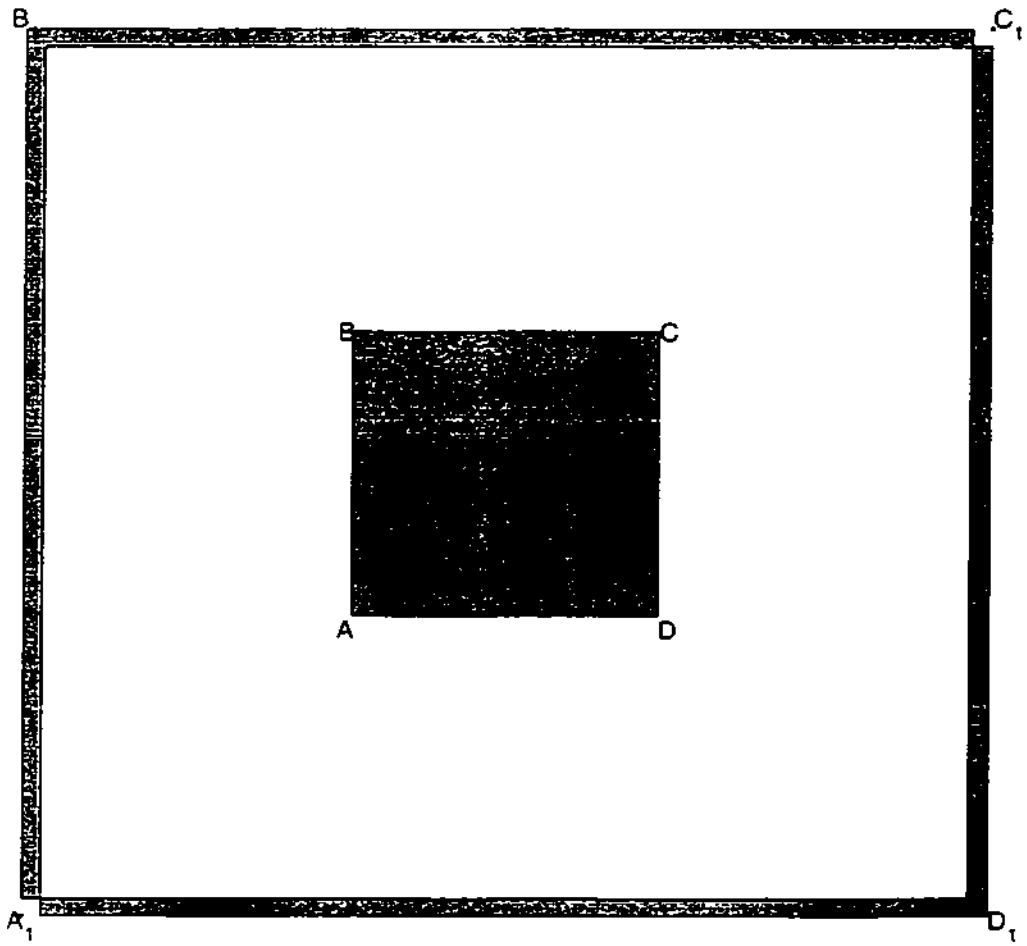

Figure 1.1: An example of multi-connected Domain

The outer boundary $A_1B_1C_1D_1$ is denoted as Γ_0, the inner boundary $ABCD$ is denoted as Γ_1. In more detail, A, B, C, D have grid indices (n,n), (n,m), (m,m), and (m,n), and A_1, B_1, C_1, D_1 have grid indices $(0,0)$, $(0,N)$, (N,N), $(N,0)$, respectively. n and m are given by $n=\frac{1}{3}N$, $m=\frac{2}{3}N$, and the grid size is chosen as $\Delta x=\Delta y=h$.

The starting point of the discussion in Chapter 5 is the following equivalent formulation of the incompressible NSE for the multi-connected domain in terms of vorticity-stream function formulation

(1.28a) $$\partial_t\omega+(\boldsymbol{u}\cdot\nabla)\omega=\nu\Delta\omega\,.$$

Reproduced with permission of the copyright owner. Further reproduction prohibited without permission.

(1.28b) $$\Delta \psi = \omega .$$

(1.28c) $$\psi |_{\Gamma_i} = C_i . \qquad \frac{\partial \psi}{\partial \boldsymbol{n}} = 0 . \qquad \text{at each } \Gamma_i .$$

(1.28d) $$\int_{\Gamma_i} \frac{\partial \omega}{\partial \boldsymbol{n}} = 0 . \qquad \text{for } 0 \le i \le k .$$

(1.28e) $$u = -\partial_y \psi , \qquad v = \partial_x \psi .$$

where the derivation of the boundary condition $\int_{\Gamma_i} \frac{\partial \omega}{\partial \boldsymbol{n}} = 0$ in (1.28d) is based on NSE with the primitive variable formulation. Since the stream function is uniquely determined up to a constant, the constant at the outer boundary Γ_0 can be automatically set as 0, i.e. $C_0 = 0$.

The key part is the computation of Poisson equation (1.28b) and enforcement of boundary conditions (1.28c), (1.28d). The standard centered difference approximation to (1.28b) and the use of Dirichlet boundary condition in (1.28c) leads to

(1.29) $$\begin{cases} \Delta_h \psi = \omega , & \text{in } \Omega , \\ \psi |_{\Gamma_0} = 0 , \quad \psi |_{\Gamma_1} = C_1 . \end{cases}$$

Yet, the constant C_1 is not known yet. In Chapter 5 it will be shown that such constant has to be obtained through the boundary condition in (1.28d).

As mentioned in Chapter 3, the no-slip boundary condition $\frac{\partial \psi}{\partial \boldsymbol{n}} = 0$ can be converted into the boundary condition for the vorticity by local formulas, such as Thom's formula. Especially, on AD, one boundary section of Γ_1, Thom's formula indicates

(1.30) $$\omega_{i,n} = \frac{2\psi_{i,n-1} - 2\psi_{i,n}}{h^2} .$$

The boundary condition $\int_{\Gamma_1} \frac{\partial \omega}{\partial \boldsymbol{n}} = 0$ can be implemented by finite difference approximation. Using the one-sided difference operator $\frac{4\omega_{n-1,j} - \omega_{n-2,j} - 3\omega_{n,j}}{2h}$

Reproduced with permission of the copyright owner. Further reproduction prohibited without permission.

as the second order approximation to $\frac{\partial \omega}{\partial n}$ (at the boundary section AB), and plugging into the boundary condition (1.28d) results in

$$\int_{\Gamma_1}^{(0)} \omega = \frac{4}{3}\int_{\Gamma_1}^{(1)} \omega - \frac{1}{3}\int_{\Gamma_1}^{(2)} \omega . \tag{1.31}$$

The notation $\int_{\Gamma_1}^{(k)} f$ is introduced as

$$\int_{\Gamma_1}^{(k)} f = \int_{AB} f_{n-k,j} + \int_{BC} f_{i,m+k} + \int_{CD} f_{m+k,j} + \int_{DA} f_{i,n-k} , \tag{1.32}$$

where the trapezoid rule is applied to the integration at each boundary sections. The substitution of Thom's formula (1.30) into the left hand side of (1.31), along with the fact that ψ is a constant C_1 on the boundary Γ_1, gives

$$C_1 = \frac{1}{|\Gamma_1|}\Big(\int_{\Gamma_1}^{(1)} \psi - \frac{4}{3}h^2 \int_{\Gamma_1}^{(1)} \omega + \frac{1}{3}h^2 \int_{\Gamma_1}^{(2)} \omega\Big) . \tag{1.33}$$

It is argued in detail in Chapter 5 that the formula (1.33) plays the role of a bridge between the constant C_1 and the boundary condition (1.28d). Then the coupled system (1.29), (1.33) will be used to compute ψ and the constant C_1 by a fixed point iteration.

As can be seen, the right hand side of (1.33) depends on C_1. Thus an operator ϕ can be introduced by (1.33): for any constant C, denote ψ as the solution of the system

$$\begin{cases} \Delta_h \psi = \omega , & \text{in } \Omega . \\ \psi|_{\Gamma_0} = 0 , \quad \psi|_{\Gamma_1} = C . \end{cases} \tag{1.34}$$

and define

$$\phi(C) = \frac{1}{|\Gamma_1|}\Big(\int_{\Gamma_1}^{(1)} \psi - \frac{4}{3}h^2 \int_{\Gamma_1}^{(1)} \omega + \frac{1}{3}h^2 \int_{\Gamma_1}^{(2)} \omega\Big) . \tag{1.35}$$

Obviously, the fixed point of ϕ, i.e. the constant C such that $\phi(C) = C$, along with ψ determined by (1.34), is exactly the solution of the coupled system (1.29), (1.33). The existence and uniqueness of the fixed point can be guaranteed

Reproduced with permission of the copyright owner. Further reproduction prohibited without permission.

by the following Proposition stating that o is in fact a contraction mapping, which is Proposition 5.2.1:

Proposition 1.5 *For any $C_1, C_2 \in R$, we have*

$$|o(C_1) - o(C_2)| \leq C^*|C_1 - C_2|. \qquad \text{where } C^* = 1 - h. \tag{1.36}$$

The above proposition provides a means for solving the system (1.29), (1.33) by iteration procedure: once the k-th iteration for the constant $C_1^{(k)}$ is obtained, solve the stream function $\psi^{(k)}$ using the boundary condition $C_1^{(k)}$, then update the constant $C_1^{(k+1)}$by $(k+1)$-th iteration: $C_1^{(k+1)} = o(C_1^{(k)})$. The proposition indicates that this iteration procedure converges to the real solution of (1.29), (1.33).

In addition, the momentum equation and the velocity field in (1.28a), (1.28e) can be treated by the second order finite difference method in the same way as in Chapter 3, which can be written as (1.19). The whole scheme can be implemented very effectively through the explicit treatment of time discretization, such as fourth order Runge-Kutta time stepping, as discussed in detail in [ELV1]. That makes the whole scheme extremely effective.

Similar procedure and scheme can also be applied to the fourth order method, the EC4 scheme, which was considered in Chapter 4. The scheme (1.22)-(1.24) can be carried out here to deal with multi-connected domain. Briley's formula (1.25) is also valid here. Still, the boundary condition $\int_{\Gamma_1} \frac{\partial \omega}{\partial n} = 0$ is used to obtain the value for C_1. Yet, the implementation is a little different from the second order case. The reason is that the vorticity in the interior points has to be determined by a Poisson-like equation and the boundary condition for ω, which, in turn, depends on the stream function and C_1, by Briley's formula. To avoid the coupling between the two systems, we express $\frac{\partial \omega}{\partial n}$ in terms of a third order derivative of ψ: as can be seen, on the boundary section AD of Γ_1, $\frac{\partial \omega}{\partial n} = -\partial_y^3 \psi$.

Reproduced with permission of the copyright owner. Further reproduction prohibited without permission.

On the other hand, ∂_y^3 can be approximated by

$$\partial_y^3 v_{i,n} \sim \frac{1}{h^3}\left(15v_{i,n-1} - 6v_{i,n-2} + v_{i,n-3} - 10v_{i,n}\right). \tag{1.37}$$

Plugging into the boundary condition $\int_{\Gamma_1} \frac{\partial \omega}{\partial \boldsymbol{n}} = 0$, we arrive at an equality similar to (1.32)

$$\int_{\Gamma_1}^{(0)} v = \frac{3}{2}\int_{\Gamma_1}^{(1)} v - \frac{3}{5}\int_{\Gamma_1}^{(2)} v + \frac{1}{10}\int_{\Gamma_1}^{(3)} v. \tag{1.38}$$

Since v is a constant C_1 on Γ_1, we have

$$C_1 = \frac{3}{2|\Gamma_1|}\int_{\Gamma_1}^{(1)} v - \frac{3}{5|\Gamma_1|}\int_{\Gamma_1}^{(2)} v + \frac{1}{10|\Gamma_1|}\int_{\Gamma_1}^{(3)} v. \tag{1.39}$$

Again, the formula (1.39) plays the role of a bridge between the constant C_1 and the boundary condition $\int_{\Gamma_1} \frac{\partial \omega}{\partial \boldsymbol{n}} = 0$. Of course, the right hand side of (1.39) depends on C_1. Then we need to solve (1.39) along with the following Poisson-like equation

$$\begin{cases} \left(\triangle_h + \frac{h^2}{6}D_x^2 D_y^2\right)v = (1 + \frac{h^2}{12}\triangle_h)\omega, \\ v\,|_{\Gamma_0} = 0, \qquad v\,|_{\Gamma_1} = C_1. \end{cases} \tag{1.40}$$

which is a coupled system.

A similar procedure of iteration can be carried out in the fourth order method. First, we define the operator o: for any constant C, let ψ be the solution satisfying

$$\begin{cases} \left(\triangle_h + \frac{h^2}{6}D_x^2 D_y^2\right)\psi = (1 + \frac{h^2}{12}\triangle_h)\omega, \\ \psi\,|_{\Gamma_0} = 0, \qquad \psi\,|_{\Gamma_1} = C. \end{cases} \tag{1.41}$$

and $o(C)$ is defined by

$$o(C) = \frac{3}{2|\Gamma_1|}\int_{\Gamma_1}^{(1)} \psi - \frac{3}{5|\Gamma_1|}\int_{\Gamma_1}^{(2)} \psi + \frac{1}{10|\Gamma_1|}\int_{\Gamma_1}^{(3)} \psi. \tag{1.42}$$

Reproduced with permission of the copyright owner. Further reproduction prohibited without permission.

The following proposition, which is Proposition 5.3.1, states that o in (1.42) is also a contraction mapping.

Proposition 1.6 *For any two constants C_1, C_2, we have*

$$|o(C_1) - o(C_2)| \leq C^*|C_1 - C_2| . \qquad \text{where } C^* = 1 - O(h) . \tag{1.43}$$

A similar method for solving the system (1.39), (1.40) can be obtained by the iteration procedure: once the k-th iteration for the constant $C_1^{(k)}$ is obtained, solve the stream function $\psi^{(k)}$ using the boundary condition $C_1^{(k)}$ in (1.40), then update the constant $C_1^{(k+1)}$ by $(k+1)$-th iteration: $C_1^{(k+1)} = o(C_1^{(k)})$. The above proposition guarantees that this iteration procedure converges to the real solution of (1.39), (1.40).

Some numerical experiments including an accuracy check of a forced flow, flow past a cooling system, etc., are documented in Chapter 5.

In Chapter 6, a fourth order finite difference method for 2-D unsteady incompressible Oberbeck-Boussinesq equations is considered. Boussinesq equation in vorticity-stream function formulation can be written as

$$\begin{cases} \partial_t \theta + (\boldsymbol{u}\cdot\nabla)\theta = \kappa\triangle\theta , \\ \partial_t \omega + (\boldsymbol{u}\cdot\nabla)\omega = Ri\partial_x\theta + \nu\triangle\omega , \\ \triangle\psi = \omega , \\ u = -\partial_y\psi , \qquad v = \partial_x\psi \end{cases} \tag{1.44}$$

where κ is the heat conductivity and Ri is the Richardson number. In a simply-connected domain, the natural no-flow, no-slip boundary condition can be written as (1.16) with $C = 0$. For the temperature θ, either the Dirichlet boundary condition $\theta\ |_\Gamma = \theta_b$ where θ_b is a given distribution for the temperature on the boundary; or, the Neumann boundary condition $\frac{\partial\theta}{\partial\boldsymbol{n}} = \theta_f$ on Γ, where θ_f is a given heat flux on the boundary, can be imposed.

Reproduced with permission of the copyright owner. Further reproduction prohibited without permission.

The temperature transport equation is treated explicitly by long-stencil fourth order approximations to ∂_x, ∂_y, and $\triangle$

$$(1.45)\quad \partial_t\theta + u\widetilde{D}_x(1-\frac{h^2}{6}D_x^2)\theta + v\widetilde{D}_y(1-\frac{h^2}{6}D_y^2)\theta = \kappa\Big(\triangle_h - \frac{h^2}{12}(D_x^4+D_y^4)\Big)\theta\,.$$

The temperature at "ghost points" is evaluated by one-sided extrapolation near the boundary and some information from the original PDE.

If the Dirichlet boundary condition for the temperature is imposed, $\theta_{i,0}$ can be given accurately on the boundary. Accordingly, (1.45) shall be updated at interior points. Thus only one "ghost point" value $\theta_{i,-1}$ needs to be obtained. Local Taylor expansion near the boundary along with some information from the PDE, gives us

$$(1.46)\quad \theta_{i,-1} = \frac{20}{11}\theta_{i,0} - \frac{6}{11}\theta_{i,1} - \frac{4}{11}\theta_{i,2} + \frac{1}{11}\theta_{i,3} + \frac{12}{11}h^2(\frac{1}{\kappa}\partial_t\theta_b - \partial_x^2\theta_b) + O(h^5)\,.$$

The detailed derivation can be found in Chapter 6.

A similar derivation can be carried out to obtain the "ghost point" values for θ if the Neumann boundary condition for the temperature is imposed. In this case, (1.45) is updated at every computational point. This in turn requires that we determine two "ghost point" values $\theta_{i,-1}$ and $\theta_{i,-2}$ to carry out (1.45). The same strategy of one-sided approximations is applied. The approximated evaluation for $\theta_{i,1}$ and $\theta_{i,2}$ can be written as

$$(1.47)\qquad \theta_{i,-1} = \theta_{i,1} - 2h\theta_f - \frac{h^3}{3}\Big(\frac{1}{\kappa}\theta_{ft} - \frac{1}{\kappa}\omega_{i,0}\widetilde{D}_x(1-\frac{h^2}{6}D_x^2)\theta_{i,0} - \theta_{fxx}\Big)\,.$$

$$(1.48)\qquad \theta_{i,-2} = \theta_{i,2} - 4h\theta_f - \frac{8h^3}{3}\Big(\frac{1}{\kappa}\theta_{ft} - \frac{1}{\kappa}\omega_{i,0}\widetilde{D}_x(1-\frac{h^2}{6}D_x^2)\theta_{i,0} - \theta_{fxx}\Big)\,.$$

The detailed derivation is also given in Chapter 6.

The momentum equation in (1.43) can be treated as the same way as the EC4 scheme discussed in Chapter 4. The only difference is the gravity term

Reproduced with permission of the copyright owner. Further reproduction prohibited without permission.

$Ri\partial_x\theta$. which can be treated by the following approximation

$$
\begin{aligned}
(1+\frac{h^2}{12}\triangle)\partial_x = \quad & \widetilde{D}_x(1+\frac{h^2}{12}D_y^2-\frac{h^2}{12}D_x^2)+O(h^4) \\
= \quad & \widetilde{D}_x+\frac{h^2}{12}\widetilde{D}_xD_y^2-\frac{h^2}{12}\widetilde{D}_xD_x^2+O(h^4)\,.
\end{aligned}
\tag{1.49}
$$

The whole scheme coupled with explicit Runge-Kutta time stepping gives a very efficient fourth order method for Boussinesq equations. Its efficiency can be seen in that only two standard Poisson-like equations are required to be solved at each Runge-Kutta time stage in the computation. An example of the Loren flow is presented. in which the full accuracy can be seen. The numerical simulation of a strong shear flow induced by a temperature jump. is resolved by two perfectly matching resolutions.

Reproduced with permission of the copyright owner. Further reproduction prohibited without permission.

CHAPTER 2

CONVERGENCE AND ANALYSIS OF GAUGE METHOD

2.1 Introduction and Review

We start with the homogeneous, incompressible Navier-Stokes equations (NSE) with no-slip boundary condition:

$$\begin{cases} \boldsymbol{u}_t + (\boldsymbol{u}\cdot\nabla)\boldsymbol{u} + \nabla p = \dfrac{1}{Re}\triangle \boldsymbol{u}\,, & \text{in } \Omega\,, \\ \nabla\cdot\boldsymbol{u} = 0\,, & \text{in } \Omega\,, \\ \boldsymbol{u} = 0\,, & \text{on } \partial\Omega\,. \end{cases} \tag{2.1.1}$$

where $\boldsymbol{u} = (u, v)$ is the velocity, p is the pressure and Re is the Reynolds number.

A new formulation, Gauge formulation was proposed by E and Liu in [ELG1]. Instead of using primitive variables of NSE, the gauge method replaces pressure by a gauge variable ϕ and introduces the auxiliary field $\boldsymbol{a} = \boldsymbol{u} - \nabla\phi$. Then the incompressibility constraint in (2.1.1) becomes

$$\triangle\phi = -\nabla\cdot\boldsymbol{a}\,. \tag{2.1.2}$$

and the momentum equation in (2.1.1) becomes

$$\boldsymbol{a}_t + (\boldsymbol{u}\cdot\nabla)\boldsymbol{u} + \nabla\Big(\partial_t\phi - \frac{1}{Re}\triangle\phi + p\Big) = \frac{1}{Re}\triangle\boldsymbol{a}\,. \tag{2.1.3}$$

If we impose

$$\partial_t\phi - \frac{1}{Re}\triangle\phi = -p\,. \tag{2.1.4}$$

Reproduced with permission of the copyright owner. Further reproduction prohibited without permission.

we obtain the gauge formulation of NSE

$$\begin{cases} \boldsymbol{a}_t + (\boldsymbol{u}\cdot\nabla)\boldsymbol{u} = \dfrac{1}{Re}\triangle\boldsymbol{a}. & \text{in } \Omega. \\ \triangle\phi = -\nabla\cdot\boldsymbol{a}. & \text{in } \Omega. \\ \boldsymbol{u} = \boldsymbol{a} + \nabla o. & \text{in } \Omega. \end{cases} \tag{2.1.5}$$

One of the main advantages of gauge formulation is that o is a non-physical variable, so we have the freedom to assign boundary condition for ϕ. As pointed out in [ELG1], corresponding to the no-slip boundary condition $\boldsymbol{u} = 0$ on $\partial\Omega$, we can either prescribe:

$$\frac{\partial\phi}{\partial\boldsymbol{n}} = 0. \qquad \boldsymbol{a}\cdot\boldsymbol{n} = 0. \qquad \boldsymbol{a}\cdot\boldsymbol{\tau} = -\frac{\partial\phi}{\partial\boldsymbol{\tau}}. \qquad \text{on } \partial\Omega. \tag{2.1.6}$$

or

$$\phi = 0. \qquad \boldsymbol{a}\cdot\boldsymbol{n} = -\frac{\partial o}{\partial\boldsymbol{n}}. \qquad \boldsymbol{a}\cdot\boldsymbol{\tau} = 0. \qquad \text{on } \partial\Omega. \tag{2.1.7}$$

where $\boldsymbol{\tau}$ is the unit tangent vector. The system (2.1.5), (2.1.6) is called Neumann gauge formulation and (2.1.5), (2.1.7) is called Dirichlet gauge formulation. In this chapter, we will concentrate on the Neumann formulation, while we will give a brief description of the analysis with respect to the Dirichlet formulation.

The idea of gauge formulation has a long history. For example, Oseledets first used an impulse variable to reformulate Euler equations as in a Hamiltonian system in [OV]; Buttke first used an impulse variable as a computational method in [BT]; Maddocks and Pego used an impulse variable to formulate an unconstrained Hamiltonian for the Euler equation in [MP]; In [ELG3], E and Liu found that the velocity impulse formulation of Buttke [BT] is marginally ill-posed for the inviscid flow and they presented numerical evidence of this instability. In [RS], Russo and Smereka studied the connection of different impulse/gauge formulations, especially the stretching effects.

Reproduced with permission of the copyright owner. Further reproduction prohibited without permission.

We can write the Neumann gauge formulation (2.1.5) and (2.1.6) in another form

$$\text{(2.1.8a)} \qquad \begin{cases} \boldsymbol{a}_t + (\boldsymbol{u}\cdot\nabla)\boldsymbol{u} = \dfrac{1}{Re}\triangle\boldsymbol{a}\,. & \text{in } \Omega\,. \\ \boldsymbol{a}\cdot\boldsymbol{n} = 0\,, \quad \boldsymbol{a}\cdot\boldsymbol{\tau} = -\dfrac{\partial o}{\partial \boldsymbol{\tau}}\,. & \text{on } \partial\Omega\,. \end{cases}$$

$$\text{(2.1.8b)} \qquad \begin{cases} \triangle o = -\nabla\cdot\boldsymbol{a}\,. & \text{in } \Omega\,. \\ \dfrac{\partial o}{\partial \boldsymbol{n}} = 0\,, & \text{on } \partial\Omega\,. \end{cases}$$

With this new formulation at hand, we can easily solve (2.1.8) by finite difference [ELG1], finite element [ELG2], or other kinds of numerical techniques. We only consider finite difference here. In this chapter, we are mainly concerned with the case wherever the Reynolds number is of O(1), which requires us to treat the diffusion term implicitly. For simplicity in this presentation, we take $Re = 1$. For example, if backward Euler method is used as our time discretization for the momentum equation, we have

$$\text{(2.1.9)} \qquad \frac{\boldsymbol{a}^{n+1} - \boldsymbol{a}^n}{\triangle t} + (\boldsymbol{u}^n\cdot\nabla)\boldsymbol{u}^n = \triangle\boldsymbol{a}^{n+1}\,, \qquad \text{in } \Omega\,.$$

It is evident that the implementation of (2.1.9) requires that the boundary conditions for $\boldsymbol{a}$ be determined. To avoid the coupling between the momentum equation and the boundary conditions, we use **explicit** boundary conditions for $\boldsymbol{a}$, which are carried out by vertical extrapolation. For the first order scheme, we can just take

$$\text{(2.1.10)} \qquad \boldsymbol{a}^{n+1}\cdot\boldsymbol{n} = 0\,, \qquad \boldsymbol{a}^{n+1}\cdot\boldsymbol{\tau} = -\frac{\partial o^n}{\partial \boldsymbol{\tau}}\,. \qquad \text{on } \partial\Omega\,.$$

Next we update o^{n+1} at time step t^{n+1} by

$$\text{(2.1.11)} \qquad \begin{cases} \triangle o^{n+1} = -\nabla\cdot\boldsymbol{a}^{n+1}\,. & \text{in } \Omega\,. \\ \dfrac{\partial o^{n+1}}{\partial \boldsymbol{n}} = 0\,, & \text{on } \partial\Omega\,. \end{cases}$$

Reproduced with permission of the copyright owner. Further reproduction prohibited without permission.

and the velocity $\boldsymbol{u}^{n+1}$ is determined by the incompressiblity

$$\boldsymbol{u}^{n+1} = \boldsymbol{a}^{n+1} + \nabla o^{n+1}. \tag{2.1.12}$$

We shall emphasize that the momentum equation (2.1.9) is decoupled from the kinematic equation (2.1.11) due to the fact that the boundary conditions for $\boldsymbol{a}$ in (2.1.10) are explicit. The resulting scheme is very efficient and the computational cost is reduced to solving a standard heat and Poisson equation. As reported in [ELG1], full accuracy was obtained with this explicit boundary conditions.

2.1.1 Stability of the Explicit Boundary Condition

One of the main concerns in the computations is the stability of the scheme. The main observation of this chapter is that the explicit boundary conditions (2.1.10) are unconditionally stable for Stokes equations, where nonlinear terms are neglected. Using the method mentioned above, we can write our scheme as:

$$\begin{cases} \frac{\boldsymbol{a}^{n+1}-\boldsymbol{a}^{n}}{\Delta t} = \Delta \boldsymbol{a}^{n+1}, & \text{in } \Omega, \\ \boldsymbol{a}^{n+1}\cdot\boldsymbol{n} = 0, \qquad \boldsymbol{a}^{n+1}\cdot\boldsymbol{\tau} = -\frac{\partial o^{n}}{\partial \boldsymbol{\tau}}, & \text{on } \partial\Omega, \end{cases} \tag{2.1.13}$$

then, we obtain ϕ^{n+1} via (2.1.11), finally, the velocity is given by (2.1.12).

For the convenience of our analysis below, we introduce $\hat{\boldsymbol{u}}^{n} = \boldsymbol{a}^{n+1} + \nabla\phi^{n}$, the system (2.1.13), (2.1.11), (2.1.12) can be reformulated as:

$$\begin{cases} \frac{\hat{\boldsymbol{u}}^{n} - \boldsymbol{u}^{n}}{\Delta t} + \Delta\nabla o^{n} = \Delta\hat{\boldsymbol{u}}^{n}, & \text{in } \Omega, \\ \hat{\boldsymbol{u}}^{n} = 0, & \text{on } \partial\Omega, \end{cases} \tag{2.1.14a}$$

$$\begin{cases} \boldsymbol{u}^{n+1} - \hat{\boldsymbol{u}}^{n} + \nabla(\phi^{n} - o^{n+1}) = 0, & \text{in } \Omega, \\ \nabla\cdot\boldsymbol{u}^{n+1} = 0, & \text{in } \Omega, \\ \frac{\partial(\phi^{n} - o^{n+1})}{\partial \boldsymbol{n}} = \boldsymbol{n}\cdot\boldsymbol{u}^{n+1} = 0, & \text{on } \partial\Omega. \end{cases} \tag{2.1.14b}$$

This formulation is similar to the pressure increment formulation of the second order projection method in [BCG], [VKJ]. So we can apply similar techniques used in [ELP1] to analyze the stability of the system (2.1.14).

Reproduced with permission of the copyright owner. Further reproduction prohibited without permission.

The basic technique used here is just standard energy estimate. As can be seen, if we take the inner product of the equation in (2.1.14a) with $2\hat{\boldsymbol{u}}^n$, and use the boundary conditions for $\hat{\boldsymbol{u}}^n$ in (2.1.14a), we have

$$\begin{aligned} &\|\hat{\boldsymbol{u}}^n\|^2 - \|\boldsymbol{u}^n\|^2 + \|\hat{\boldsymbol{u}}^n - \boldsymbol{u}^n\|^2 + 2\triangle t\,\|\nabla\hat{\boldsymbol{u}}^n\|^2 \\ &= -2\triangle t \int_\Omega \hat{\boldsymbol{u}}^n\cdot\nabla\triangle\phi^n\,d\boldsymbol{x} = 2\triangle t\int_\Omega(\nabla\cdot\hat{\boldsymbol{u}}^n)\triangle\phi^n\,d\boldsymbol{x} \equiv I\,. \end{aligned} \tag{2.1.15}$$

Taking the divergence of the first equation in (2.1.14b), we get

$$\nabla\cdot\hat{\boldsymbol{u}}^n = \triangle(\phi^n - \phi^{n+1})\,. \tag{2.1.16}$$

Plugging back in to the last term in the right hand side of (2.1.15), we have

$$\begin{aligned} I &= -2\triangle t\int_\Omega \triangle(\phi^{n+1} - \phi^n)\triangle\phi^n\,d\boldsymbol{x} \\ &= -\triangle t(\|\triangle\phi^{n+1}\|^2 - \|\triangle\phi^n\|^2) + \triangle t\|\triangle(\phi^{n+1} - \phi^n)\|^2 \\ &= -\triangle t(\|\triangle\phi^{n+1}\|^2 - \|\triangle\phi^n\|^2) + \triangle t\|\nabla\cdot\hat{\boldsymbol{u}}^n\|^2\,, \end{aligned} \tag{2.1.17}$$

where in the last step we used (2.1.16) again. We note that $\|\nabla\cdot\hat{\boldsymbol{u}}^n\|$ can be controlled by the diffusion term $\|\nabla\hat{\boldsymbol{u}}^n\|$. The combination of (2.1.15) and (2.1.17) results in

$$\begin{aligned} &\|\hat{\boldsymbol{u}}^n\|^2 - \|\boldsymbol{u}^n\|^2 + \|\hat{\boldsymbol{u}}^n - \boldsymbol{u}^n\|^2 + \triangle t\|\nabla\hat{\boldsymbol{u}}^n\|^2 \\ &\qquad +\triangle t(\|\triangle\phi^{n+1}\|^2 - \|\triangle\phi^n\|^2) \le 0\,. \end{aligned} \tag{2.1.18}$$

Next, we need to do energy estimate of the first equation in (2.1.14b). As can be seen, the incompressibility of $\boldsymbol{u}^{n+1}$ together with the boundary condition $\boldsymbol{u}^{n+1}\cdot\boldsymbol{n} = 0$ on $\partial\Omega$ for the normal component of $\boldsymbol{u}^{n+1}$, can guarantee that u^{n+1} is orthogonal to the gradient of $\phi^n - \phi^{n+1}$, i.e.

$$\int_\Omega \boldsymbol{u}^{n+1}\cdot\nabla(\phi^n - \phi^{n+1})\,d\boldsymbol{x} = 0\,. \tag{2.1.19}$$

If we take the inner product of the first equation in (2.1.14b) with $2\boldsymbol{u}^{n+1}$, we have

$$\|\boldsymbol{u}^{n+1}\|^2 - \|\hat{\boldsymbol{u}}^n\|^2 + \|\boldsymbol{u}^{n+1} - \hat{\boldsymbol{u}}^n\|^2 = 0\,. \tag{2.1.20}$$

Reproduced with permission of the copyright owner. Further reproduction prohibited without permission.

Finally, the combination of (2.1.18) and (2.1.20) results in

$$\|\boldsymbol{u}^{n+1}\|^2 - \|\boldsymbol{u}^n\|^2 + \Delta t\|\nabla\tilde{\boldsymbol{u}}^n\|^2 + \Delta t(\|\Delta\phi^{n+1}\|^2 - \|\Delta\phi^n\|^2) \leq 0\,. \tag{2.1.21}$$

Then the proof is completed, to wit, that the gauge method with explicit boundary conditions (2.1.10) is unconditionally stable for Stokes equations. The analysis in this chapter follows the philosophy used above.

Remark 2.1.1 The above arguments can also be applied in regard to the gauge method using the Dirichlet formulation. The only difference is that the boundary condition for the gauge variable analogous to (2.1.14b) will be $\phi^n - \phi^{n+1} = \boldsymbol{\tau}\cdot\boldsymbol{u}^{n+1} = 0$. Since $\boldsymbol{u}^{n+1}$ is divergence-free, (2.1.19) is still valid, which in turn yields (2.1.20). (2.1.15)-(2.1.18) are the same. Finally, (2.1.21) still holds. In other words, the gauge method with explicit boundary conditions (2.1.10), either in the Neumann or Dirichlet formulation, is unconditionally stable for Stokes equations.

2.1.2 Connection between Projection Method and Gauge Method

The gauge method shares many similarities with the projection method [ELG1]. The analysis of projection method has been thoroughly studied in [S1, S2, ELP1, WB]. We will adopt analyses and techniques similar to those used in [ELP1]. One of the main differences between the gauge method and the projection method is that the gauge method is a direct discretization of partial differential equations (2.1.5), while the projection method is a fractional splitting of the Navier-Stokes equations with some artificial numerical boundary conditions. Consequently, the projection method results in a singular perturbation of the original PDE and numerical boundary layers [OI2, ELP1]. This subtle fact is reflected in our analysis of the numerical method by the fact that the consistency analysis of the gauge method is much easier than that of the projection method,

Reproduced with permission of the copyright owner. Further reproduction prohibited without permission.

with regular expansions of the numerical scheme, and no numerical boundary layers are included. One of the other advantages of the gauge method is that it overcomes some difficulties in the numerical computations of the incompressible flow, such as the approximate projection in the projection methods [ABS] and the pressure boundary conditions [GS]. Extension of the gauge method to the 3D case is also straightforward.

2.2 Time and Space Discretizations

We will use backward Euler method as our first order time discretization, Crank-Nicholson method as our second order time discretization, and MAC grids as our spatial discretization. Since our analysis in the following chapters is close to that of the projection method, we adopt similar notations as in [ELP1].

2.2.1 Time Discretization

Backward Euler

The backward Euler time discretization of (2.1.8) with explicit boundary conditions for $\boldsymbol{a}$ can be written as

$$\text{(2.2.1)} \qquad \begin{cases} \dfrac{\boldsymbol{a}^{n+1}-\boldsymbol{a}^{n}}{\triangle t}+(\boldsymbol{u}^{n}\cdot\nabla)\boldsymbol{u}^{n}=\triangle\boldsymbol{a}^{n+1}. & \text{in } \Omega. \\ \boldsymbol{a}^{n+1}\cdot\boldsymbol{n}=0. \qquad \boldsymbol{a}^{n-1}\cdot\boldsymbol{\tau}=-\dfrac{\partial\phi^{n}}{\partial\boldsymbol{\tau}}. & \text{on } \partial\Omega, \end{cases}$$

and

$$\text{(2.2.2)} \qquad \begin{cases} \triangle\phi^{n+1}=-\nabla\cdot\boldsymbol{a}^{n+1}. & \text{in } \Omega. \\ \dfrac{\partial\phi^{n+1}}{\partial\boldsymbol{n}}=0. & \text{on } \partial\Omega. \end{cases}$$

and the velocity is given by

$$\text{(2.2.3)} \qquad \boldsymbol{u}^{n+1}=\boldsymbol{a}^{n+1}+\nabla\phi^{n+1}.$$

Reproduced with permission of the copyright owner. Further reproduction prohibited without permission.

Crank-Nicholson

We can also discretize (2.1.8) using second order Crank-Nicholson method. with explicit boundary conditions for $\boldsymbol{a}$

$$\text{(2.2.4)} \qquad \begin{cases} \dfrac{\boldsymbol{a}^{n+1}-\boldsymbol{a}^{n}}{\triangle t}+(\boldsymbol{u}^{n+\frac{1}{2}}\cdot\nabla)\boldsymbol{u}^{n+\frac{1}{2}}=\triangle\dfrac{1}{2}(\boldsymbol{a}^{n}+\boldsymbol{a}^{n-1}). & \text{in } \Omega. \\ \boldsymbol{a}^{n+1}\cdot\boldsymbol{n}=0. \qquad \boldsymbol{a}^{n+1}\cdot\boldsymbol{\tau}=-(2\dfrac{\partial o^{n}}{\partial\boldsymbol{\tau}}-\dfrac{\partial o^{n-1}}{\partial\boldsymbol{\tau}}). & \text{on } \partial\Omega. \end{cases}$$

where the term $(\boldsymbol{u}^{n+\frac{1}{2}}\cdot\nabla)\boldsymbol{u}^{n+\frac{1}{2}}$ is defined as $\frac{3}{2}(\boldsymbol{u}^{n}\cdot\nabla)\boldsymbol{u}^{n}-\frac{1}{2}(\boldsymbol{u}^{n-1}\cdot\nabla)\boldsymbol{u}^{n-1}$. On the boundary, $\boldsymbol{a}$ is determined by the second order one-sided extrapolation of ϕ in the previous time steps, which is called the Crank-Nicholson method. ϕ^{n+1} at time t^{n+1} is still determined by $\boldsymbol{a}$ via (2.2.2), and the velocity can be calculated by (2.2.3).

Remark 2.2.1 As can be seen, if the **implicit** boundary conditions for the auxiliary field $\boldsymbol{a}$ in the momentum equation is adopted, for example, if the implicit boundary conditions for $\boldsymbol{a}$ is imposed when we solve $\boldsymbol{a}$ by backward Euler time-discretization

$$\text{(2.2.5)} \qquad \begin{cases} \dfrac{\boldsymbol{a}^{n+1}-\boldsymbol{a}^{n}}{\triangle t}+(\boldsymbol{u}^{n}\cdot\nabla)\boldsymbol{u}^{n}=\triangle\boldsymbol{a}^{n+1}. & \text{in } \Omega. \\ \boldsymbol{a}^{n+1}\cdot\boldsymbol{n}=0, \qquad \boldsymbol{a}^{n+1}\cdot\boldsymbol{\tau}=-\dfrac{\partial\phi^{n+1}}{\partial\boldsymbol{\tau}}. & \text{on } \partial\Omega. \end{cases}$$

coupled with the kinematic equation

$$\text{(2.2.6)} \qquad \begin{cases} \triangle\phi^{n+1}=-\nabla\cdot\boldsymbol{a}^{n+1}. & \text{in } \Omega. \\ \dfrac{\partial\phi^{n+1}}{\partial\boldsymbol{n}}=0. & \text{on } \partial\Omega. \end{cases}$$

$$\text{(2.2.7)} \qquad \boldsymbol{u}^{n+1}=\boldsymbol{a}^{n+1}+\nabla o^{n+1}.$$

then by (2.2.3), the relation among the velocity $\boldsymbol{u}$, the auxiliary field $\boldsymbol{a}$ and the

Reproduced with permission of the copyright owner. Further reproduction prohibited without permission.

gauge variable o. (2.2.5)-(2.2.7) can be rewritten as

$$\text{(2.2.8)}\qquad \begin{cases} \dfrac{\boldsymbol{u}^{n+1}-\boldsymbol{u}^{n}}{\triangle t}+(\boldsymbol{u}^{n}\cdot\nabla)\boldsymbol{u}^{n}+\nabla\tilde{p}^{n+1}=\triangle\boldsymbol{u}^{n+1}. & \text{in } \Omega. \\ \nabla\cdot\boldsymbol{u}^{n+1}=0. & \text{in } \Omega. \\ \boldsymbol{u}^{n+1}=0. & \text{on } \partial\Omega. \end{cases}$$

where

$$\text{(2.2.9)}\qquad \tilde{p}^{n+1}=-\frac{o^{n+1}-o^{n}}{\triangle t}+\triangle o^{n+1}.$$

which becomes the standard backward Euler discretization of the Navier-Stokes equations. The convergence of this scheme is straightforward. However, to implement the implicit boundary conditions in (2.2.5), one has to iterate the system between (2.2.5) and (2.2.6), which is very costly. Extensive computational evidence shows that this iteration is not necessary, and accuracy is still maintained with the explicit boundary conditions for $\boldsymbol{a}$ in (2.2.1). Our analysis will give a theoretical insight into this.

2.2.2 Dirichlet Formulation

If we prescribe the Dirichlet boundary condition (2.1.7) of o, the corresponding first order scheme analogous to (2.2.1)-(2.2.3) becomes

$$\text{(2.2.10)}\qquad \begin{cases} \dfrac{\boldsymbol{a}^{n+1}-\boldsymbol{a}^{n}}{\triangle t}+(\boldsymbol{u}^{n}\cdot\nabla)\boldsymbol{u}^{n}=\triangle\boldsymbol{a}^{n+1}. & \text{in } \Omega. \\ \boldsymbol{a}^{n+1}\cdot\boldsymbol{n}=-\dfrac{\partial\phi^{n}}{\partial\boldsymbol{n}}. \qquad \boldsymbol{a}^{n+1}\cdot\boldsymbol{\tau}=0. & \text{on } \partial\Omega. \end{cases}$$

$$\text{(2.2.11)}\qquad \begin{cases} \triangle\phi^{n+1}=-\nabla\cdot\boldsymbol{a}^{n+1}. & \text{in } \Omega. \\ \phi^{n+1}=0. & \text{on } \partial\Omega. \end{cases}$$

$$\text{(2.2.12)}\qquad \boldsymbol{u}^{n+1}=\boldsymbol{a}^{n+1}+\nabla o^{n+1}.$$

Reproduced with permission of the copyright owner. Further reproduction prohibited without permission.

It is only necessary to solve three Poisson-like equations with Dirichlet boundary conditions. This gives some advantage in the iterative methods for the linear system generated by the finite element method [ELG2]. Similarly, the corresponding second order method using the Crank-Nicholson time discretization becomes

$$\text{(2.2.13)} \qquad \begin{cases} \dfrac{\boldsymbol{a}^{n+1}-\boldsymbol{a}^n}{\triangle t}+(\boldsymbol{u}^{n+\frac{1}{2}}\cdot\nabla)\boldsymbol{u}^{n-\frac{1}{2}}=\triangle\dfrac{1}{2}(\boldsymbol{a}^{n+1}+\boldsymbol{a}^n)\,. & \text{in } \Omega\,. \\ \boldsymbol{a}^{n+1}\cdot\boldsymbol{n}=-2\dfrac{\partial\phi^n}{\partial\boldsymbol{n}}+\dfrac{\partial\phi^{n-1}}{\partial\boldsymbol{n}}\,. \qquad \boldsymbol{a}^{n+1}\cdot\boldsymbol{\tau}=0\,. & \text{on } \partial\Omega\,, \end{cases}$$

along with (2.2.11), which gives us ϕ^{n+1} at the time step t^{n+1}, and (2.2.12), which updates the velocity $\boldsymbol{u}^{n+1}$.

We will show later that this Dirichlet gauge method with explicit boundary conditions is still stable. Yet, since the lack of the normal compatibility on the boundary, there are some problems in the expansions of the numerical scheme. We can only get $\sqrt{\triangle t}$ order error estimate. However, it is hoped that this is only a theoretical difficulty, which will not influence practical computations.

2.2.3 Space Discretization

We will concentrate on the situation when $\Omega=[-1,1]\times[0,2\pi]$ with periodic boundary conditions in the y direction and no-slip boundary conditions in the x direction: $\boldsymbol{u}(x,0,t)=\boldsymbol{u}(x,2\pi,t)$, $\boldsymbol{u}(-1,y,t)=\boldsymbol{u}(1,y,t)=0$. $\partial'\Omega$ is used to denote the part of the boundary at $x=\pm1$. It is assumed that $\triangle x=\triangle y=h$. The analysis of the spatial discretization with standard grids is quite difficult. In this chapter, we only consider the MAC staggered grids for spatial discretization. Here the gauge variable ϕ (also the pressure p) is evaluated at the points (i,j), the gauge variable a (also the u velocity) is evaluated at the points $(i\pm1/2,j)$, and the gauge variable b (also the v velocity) is evaluated at the points $(i,j\pm1/2)$. The discrete divergence of $\boldsymbol{a}$ (also $\boldsymbol{u}$ and $\tilde{\boldsymbol{u}}$) is computed at the points (i,j):

$$(\nabla_h\cdot\boldsymbol{a})_{i,j}=\frac{a_{i+1/2,j}-a_{i-1/2,j}}{h}+\frac{b_{i,j+1/2}-b_{i,j-1/2}}{h}\,.$$

Reproduced with permission of the copyright owner. Further reproduction prohibited without permission.

Other differential operators are defined as: (For brevity, we just write out the definition of these operators on $\boldsymbol{a}$, o, where the same definition can be applied to $\boldsymbol{u}$, $\hat{\boldsymbol{u}}$ and p)

$$(\triangle_h a)_{i-1/2,j} = \frac{a_{i+3/2,j} - 2a_{i+1/2,j} + a_{i-1/2,j}}{h^2} + \frac{a_{i-1/2,j+1} - 2a_{i-1/2,j} + a_{i+1/2,j-1}}{h^2}.$$

$$(\triangle_h b)_{i,j-1/2} = \frac{b_{i+1,j+1/2} - 2b_{i,j+1/2} + b_{i-1,j-1/2}}{h^2} + \frac{b_{i,j+3/2} - 2b_{i,j+1/2} + b_{i,j-1/2}}{h^2}.$$

$$(\phi_x)_{i+1/2,j} = \frac{\phi_{i+1,j} - \phi_{i,j}}{h}. \quad (\phi_y)_{i,j-1/2} = \frac{\phi_{i,j+1} - \phi_{i,j}}{h}.$$

$$\overline{a}_{i,j+1/2} = \frac{1}{4}(a_{i+1/2,j} + a_{i-1/2,j} + a_{i+1/2,j+1} + a_{i-1/2,j+1}).$$

$$\overline{b}_{i+1/2,j} = \frac{1}{4}(b_{i+1,j+1/2} + b_{i+1,j-1/2} + b_{i,j+1/2} + b_{i,j-1/2}).$$

$$\mathcal{N}_h(\boldsymbol{u}, a)_{i+1/2,j} = u_{i+1/2,j}\frac{a_{i+3/2,j} - a_{i-1/2,j}}{2h} + \overline{v}_{i+1/2,j}\frac{a_{i+1/2,j+1} - a_{i+1/2,j-1}}{2h}.$$

$$\mathcal{N}_h(\boldsymbol{u}, b)_{i,j-1/2} = \overline{u}_{i,j+1/2}\frac{b_{i+1,j+1/2} - b_{i-1,j+1/2}}{2h} + v_{i,j-1/2}\frac{b_{i,j+3/2} - b_{i,j-1/2}}{2h}.$$

Clearly the truncation errors of these approximations are of second order. The first momentum equation (for a) is implemented at right arrow points, the second momentum equation is implemented at upper arrow points, and the (discrete) Poisson equation for ϕ is implemented at dot points.

The boundary condition $u = 0$ is imposed at the vertical physical boundary Γ_y, whereas $v = 0$ is imposed by $v_{0,j+1/2} + v_{1,j-1/2} = 0$. Similarly, the boundary condition $v = 0$ is imposed at the horizontal physical boundary Γ_y, where $u = 0$ is imposed by $u_{i+1/2,0} + u_{i-1/2,1} = 0$. Consequently, the boundary condition $a = 0, b = -\partial_y o$ at the left vertical boundary is implemented by

$$a = 0. \qquad b_{1,j+1/2} + b_{0,j+1/2} = -\frac{\phi_{1,j+1} - \phi_{1,j}}{h} - \frac{\phi_{0,j+1} - \phi_{0,j}}{h}. \tag{2.2.14}$$

Similar boundary conditions for $\boldsymbol{a}$ are imposed at the other three boundaries.

One of the main advantage of the MAC grids is that the spatial discretization of (2.2.2) and (2.2.3),

$$\triangle_h \phi^{n+1} = -\nabla_h \cdot \boldsymbol{a}^{n+1}, \qquad \boldsymbol{u}^{n+1} = \boldsymbol{a}^{n+1} + \nabla_h \phi^{n+1},$$

Reproduced with permission of the copyright owner. Further reproduction prohibited without permission.

gives an exact projection

$$\boldsymbol{a}^{n+1} = \boldsymbol{u}^{n+1} - \nabla_h \phi^{n+1}, \quad \nabla_h \cdot \boldsymbol{u}^{n+1} = 0.$$

and the Neumann boundary condition

$$\frac{\partial \phi^{n+1}}{\partial \boldsymbol{n}} = 0. \qquad \text{on } \partial\Omega.$$

gives the boundary condition for the normal component of $\boldsymbol{u}$.

$$\boldsymbol{n} \cdot \boldsymbol{u}^{n+1} = 0. \qquad \text{on } \partial'\Omega.$$

Therefore we can rewrite the full discrete scheme analogous to (2.2.1)-(2.2.3) in the following form which will be used in the convergence and error analysis:

(2.2.15a)
$$\begin{cases} \dfrac{\boldsymbol{a}^{n+1} - \boldsymbol{a}^n}{\Delta t} + \mathcal{N}_h(\boldsymbol{u}^n, \boldsymbol{u}^n) = \Delta_h \boldsymbol{a}^{n+1}. & \text{in } \Omega. \\ \boldsymbol{a}^{n+1} = -\nabla_h \phi^n. & \text{on } \partial'\Omega. \end{cases}$$

(2.2.15b)
$$\begin{cases} \boldsymbol{u}^{n+1} = \boldsymbol{a}^{n+1} + \nabla_h \phi^{n+1}. & \text{in } \Omega. \\ \nabla_h \cdot \boldsymbol{u}^{n+1} = 0. & \text{in } \Omega. \\ \boldsymbol{n} \cdot \boldsymbol{u}^{n+1} = 0. & \text{on } \partial'\Omega. \end{cases}$$

2.3 Spatially Continuous Case for Stokes Equations

We have already shown the unconditional stability of the gauge method with explicit boundary conditions in the introduction. Now our theorem of convergence for Stokes equations is stated.

Theorem 2.3.1 *Let $(\boldsymbol{u}, \phi)$ be a smooth solution of Stokes equations with smooth initial data $\boldsymbol{u}^0(\boldsymbol{x})$ and let $(\boldsymbol{u}_{\Delta t}, \phi_{\Delta t})$ be the numerical solution of the semi-discrete gauge method with explicit boundary conditions* (2.1.10)-(2.1.13). *Then we have*

(2.3.1)
$$\|\boldsymbol{u} - \boldsymbol{u}_{\Delta t}\|_{L^\infty(0,T,L^2)} \leq C\Delta t.$$

Reproduced with permission of the copyright owner. Further reproduction prohibited without permission.

The convergence proof follows the standard strategy of consistency and stability estimates. We have already proven the stability of the scheme in the introduction. In the consistency part, we first make a transformation of the numerical scheme. Instead of directly comparing the numerical solutions with the exact solutions, we compare them with the ones constructed from the exact field, o. The constructed fields satisfy exactly the boundary conditions in the numerical scheme. The advantage of this approach is that no error term appears in the boundary conditions. This simplifies the energy estimates used in the stability part of the proof.

For simplicity, we just do first order expansions in the spatially continuous case. In the fully discrete case, second order expansions are required to establish the a priori estimates needed in the convergence proof.

2.3.1 Truncation Error and Consistency Analysis

We follow the strategy of Strang [STR] in constructing a high order expansion from the exact solutions to satisfy the numerical scheme up to high order. This will enable us to give a sharper *a priori* estimate.

By introducing the new variable $\hat{\boldsymbol{u}}^n = \boldsymbol{a}^{n+1} + \nabla o^n$, we obtained (2.1.14), an equivalent reformulation of the scheme (2.1.13), (2.1.11), (2.1.12).

Let $\boldsymbol{u}_e(\boldsymbol{x}, t)$ and $p_e(\boldsymbol{x}, t)$ be the exact solutions of Stokes Equations, i.e.

$$\begin{cases} \partial_t \boldsymbol{u}_e + \nabla p_e = \triangle \boldsymbol{u}_e\,, & \text{in } \Omega\,. \\ \nabla \cdot \boldsymbol{u}_e = 0\,, & \text{in } \Omega\,. \\ \boldsymbol{u}_e = 0\,, & \text{on } \partial\Omega\,. \end{cases} \tag{2.3.2}$$

and let $o_e(\boldsymbol{x}, t)$ be a solution of the following heat equation with Neumann boundary condition

$$\begin{cases} \partial_t \phi_e = \triangle o_e - p_e\,, & \text{in } \Omega\,. \\ \dfrac{\partial \phi_e}{\partial \boldsymbol{n}} = 0\,, & \text{on } \partial\Omega\,, \end{cases} \tag{2.3.3}$$

Reproduced with permission of the copyright owner. Further reproduction prohibited without permission.

where the initial data $o_e(\boldsymbol{x}, 0)$ is chosen from the following Poisson equation

$$\begin{cases} \triangle \phi_e(\boldsymbol{x}, 0) = p_e(\boldsymbol{x}, 0) + C_1 \,, & \text{in } \Omega \,. \\ \dfrac{\partial o_e(\boldsymbol{x}, 0)}{\partial \boldsymbol{n}} = 0 \,, & \text{on } \partial\Omega \,. \end{cases} \tag{2.3.4}$$

where C_1 is a constant such that $C_1 = -\int_\Omega p_e(\boldsymbol{x}, 0)\, d\boldsymbol{x}$ to maintain the consistency that follows from the Neumann boundary condition. Obviously, if we introduce $\boldsymbol{a}_e = \boldsymbol{u}_e - \nabla o_e$, then $(\boldsymbol{a}_e, \phi_e)$ is an exact solution of Stokes equations in gauge formulation.

Next, we let $\boldsymbol{u}_1$ be a solution of Stokes equations with the prescribed boundary conditions and initial data

$$\begin{cases} \partial_t \boldsymbol{u}_1 + \nabla p_1 = \triangle \boldsymbol{u}_1 \,, & \text{in } \Omega \,. \\ \nabla \cdot \boldsymbol{u}_1 = 0 \,, & \text{in } \Omega \,. \\ \boldsymbol{u}_1 = \partial_t \nabla \phi_e \,. & \text{on } \partial\Omega \,. \\ \boldsymbol{u}_1(\boldsymbol{x}, 0) = 0 \,. \end{cases} \tag{2.3.5}$$

By the construction of $\phi_e(\boldsymbol{x}, 0)$, we have

$$\partial_t o_e(\boldsymbol{x}, 0) = \triangle \phi_e(\boldsymbol{x}, 0) - p_e(\boldsymbol{x}, 0) = C_1 \,. \qquad \text{on } \partial\Omega \,. \tag{2.3.6}$$

which implies that $\partial_t \nabla \phi_e(\boldsymbol{x}, 0) = 0$ on the boundary, so we can choose $\boldsymbol{u}_1(\boldsymbol{x}, 0) = 0$ as in (2.3.5).

Consequently, we let

$$\hat{\boldsymbol{u}}_1 = \boldsymbol{u}_1 + \partial_t \boldsymbol{a}_e \,. \tag{2.3.7}$$

and construct approximate profiles

$$U^{**} = \boldsymbol{u}_e + \triangle t \hat{\boldsymbol{u}}_1 \,, \qquad U^{*} = \boldsymbol{u}_e + \triangle t \boldsymbol{u}_1 \,. \qquad \Phi = o_e \,. \tag{2.3.8}$$

Reproduced with permission of the copyright owner. Further reproduction prohibited without permission.

Lemma 2.3.1 *We have*

$$\text{(2.3.9a)}\qquad \begin{cases} \dfrac{U^{*n}-U^n}{\Delta t}+\Delta\nabla\Phi^n=\Delta U^{*n}+\Delta t\boldsymbol{f}^n\,, & \text{in } \Omega\,,\\ U^{*n}=0\,, & \text{on } \partial\Omega\,. \end{cases}$$

$$\text{(2.3.9b)}\qquad \begin{cases} U^{n+1}-U^{*n}+\nabla(\Phi^n-\Phi^{n-1})=\Delta t^2\boldsymbol{g}^n\,, & \text{in } \Omega\,,\\ \nabla\cdot U^{n+1}=0\,, & \text{in } \Omega\,,\\ \dfrac{\partial(\Phi^n-\Phi^{n+1})}{\partial\boldsymbol{n}}=\boldsymbol{n}\cdot U^{n-1}=0\,, & \text{on } \partial\Omega\,. \end{cases}$$

$$\text{(2.3.9c)}\qquad U^0=\boldsymbol{u}^0\,, \qquad \text{in } \Omega\,.$$

where $\boldsymbol{f}^n$, $\boldsymbol{g}^n$ *are some bounded functions.*

Proof. Substituting (2.3.8) into the equation (2.3.9a) and by direct calculations, we obtain

$$\begin{aligned} &\frac{U^{*n}-U^n}{\Delta t}+\Delta\nabla\Phi^n-\Delta\tilde{U}^n\\ &=\hat{\boldsymbol{u}}_1-\boldsymbol{u}_1+\Delta\nabla o_e-\Delta\boldsymbol{u}_e-\Delta t\Delta\hat{\boldsymbol{u}}_1\\ &=(\partial_t\boldsymbol{a}_e-\Delta\boldsymbol{a}_e)-\Delta t\Delta\hat{\boldsymbol{u}}_1\\ &=-\Delta t\Delta\hat{\boldsymbol{u}}_1=O(\Delta t)\,, \qquad \text{in } \Omega\,. \end{aligned} \tag{2.3.10}$$

In the last step we used the fact that $(\boldsymbol{u}_e, \boldsymbol{a}_e)$ is the exact solution of Stokes equations in gauge formulation, i.e.

$$\text{(2.3.11)}\qquad \partial_t\boldsymbol{a}_e-\Delta\boldsymbol{a}_e=0\,, \qquad \text{in } \Omega\,.$$

By the construction of $\hat{\boldsymbol{u}}_1$ and the boundary condition for $\boldsymbol{u}_1$, we have

$$\text{(2.3.12)}\qquad \hat{\boldsymbol{u}}_1^n=\boldsymbol{u}_1^n+\partial_t\boldsymbol{a}_e^n=\partial_t\boldsymbol{u}_e^n=0\,, \qquad \text{on } \partial\Omega\,,$$

which shows that

$$\text{(2.3.13)}\qquad U^{*n}=0\,, \qquad \text{on } \partial\Omega\,.$$

Reproduced with permission of the copyright owner. Further reproduction prohibited without permission.

For the equation in (2.3.9b), by direct calculations and Taylor expansions of U and Φ w.r.t. time t, we have

$$\begin{aligned} & U^{n+1} - \widehat{U}^n + \nabla(\Phi^n - \Phi^{n+1}) \\ &= \boldsymbol{u}_e^n + \triangle t \partial_t \boldsymbol{u}_e^n + \triangle t \boldsymbol{u}_1^n + O(\triangle t^2) \\ &\quad -\boldsymbol{u}_e^n - \triangle t \widehat{\boldsymbol{u}}_1^n - \triangle t \partial_t \nabla o_e^n + O(\triangle t^2) \\ &= \triangle t \partial_t \boldsymbol{a}_e^n + \triangle t (\boldsymbol{u}_1^n - \widehat{\boldsymbol{u}}_1^n) + O(\triangle t^2) \\ &= O(\triangle t^2), \qquad \text{in } \Omega. \end{aligned} \tag{2.3.14}$$

Since both $\boldsymbol{u}_e$ and $\boldsymbol{u}_1$ are divergence free, we obtain

$$\nabla \cdot U^{n+1} = 0, \qquad \text{in } \Omega. \tag{2.3.15}$$

and by the construction of our U and Φ, we have

$$\frac{\partial \Phi^{n+1}}{\partial \boldsymbol{n}} = \boldsymbol{n} \cdot U^{n+1} = 0, \qquad \text{on } \partial\Omega. \tag{2.3.16}$$

Then we complete the consistency analysis of the first order gauge method with explicit boundary conditions. Lemma 2.3.1 is proven.

2.3.2 Proof of Theorem 2.3.1

We define the error functions

$$\boldsymbol{e}^n = U^n - \boldsymbol{u}^n, \qquad \hat{\boldsymbol{e}}^n = U^{*n} - \hat{\boldsymbol{u}}^n, \qquad q^n = \Phi^n - o^n. \tag{2.3.17}$$

In Section 2.1, by making a transformation, we got (2.1.14), which is an equivalent formulation of (2.1.13), (2.1.11), (2.1.12). Subtracting (2.3.9) from (2.1.14), we get the equations for the error functions:

$$\begin{cases} \dfrac{\hat{\boldsymbol{e}}^n - \boldsymbol{e}^n}{\triangle t} = \triangle \hat{\boldsymbol{e}}^n - \nabla \triangle q^n + \triangle t \boldsymbol{f}^n, & \text{in } \Omega, \\ \hat{\boldsymbol{e}}^n = 0, & \text{on } \partial\Omega. \end{cases} \tag{2.3.18a}$$

$$\begin{cases} \boldsymbol{e}^{n+1} - \hat{\boldsymbol{e}}^n + \nabla (q^n - q^{n+1}) = \triangle t^2 \boldsymbol{g}^n, & \text{in } \Omega, \\ \nabla \cdot \boldsymbol{e}^{n+1} = 0, & \text{in } \Omega, \\ \dfrac{\partial (q^n - q^{n+1})}{\partial \boldsymbol{n}} = \boldsymbol{e}^{n+1} \cdot \boldsymbol{n} = 0, & \text{on } \partial\Omega. \end{cases} \tag{2.3.18b}$$

Reproduced with permission of the copyright owner. Further reproduction prohibited without permission.

(2.3.18c) $$\boldsymbol{e}^0 = 0\,. \qquad \text{in } \Omega\,.$$

It can be seen that the system (2.3.18) is very similar to (2.1.14), except for the local truncation error terms $\Delta t \boldsymbol{f}^n$, $\Delta t^2 \boldsymbol{g}^n$. So most of the energy estimate techniques we used in Section 2.1 can be carried out here similarly. The estimates corresponding to the local error terms can be given by the Cauchy inequality. We will omit some of the details in the following analysis.

Taking the inner product of (2.3.18a) with $2\hat{\boldsymbol{e}}^n$ and by the fact that $\hat{\boldsymbol{e}}^n$ vanishes on the boundary, we have

(2.3.19)
$$\begin{aligned} &\|\hat{\boldsymbol{e}}^n\|^2 - \|\boldsymbol{e}^n\|^2 + \|\hat{\boldsymbol{e}}^n - \boldsymbol{e}^n\|^2 + 2\Delta t\,\|\nabla\hat{\boldsymbol{e}}^n\|^2 \\ &\qquad \le \Delta t^3\,\|\boldsymbol{f}^n\|^2 + \Delta t\,\|\hat{\boldsymbol{e}}^n\|^2 - 2\Delta t\int_\Omega \hat{\boldsymbol{e}}^n\cdot\nabla\Delta q^n\,d\boldsymbol{x}\,. \end{aligned}$$

Taking the inner product of the first equation in (2.3.18b) with $2\boldsymbol{e}^{n+1}$ and using a similar argument as in Section 2.1, i.e., that $\boldsymbol{e}^{n+1}$ is orthogonal to the gradient of $q^n - q^{n+1}$, we arrive at

(2.3.20) $$\|\boldsymbol{e}^{n+1}\|^2 - \|\hat{\boldsymbol{e}}^n\|^2 + \|\boldsymbol{e}^{n+1} - \hat{\boldsymbol{e}}^n\|^2 \le \Delta t\|\boldsymbol{e}^{n+1}\|^2 + \Delta t^3\|\boldsymbol{g}^n\|^2\,.$$

Combining (2.3.19) and (2.3.20), we get

(2.3.21)
$$\begin{aligned} &\|\boldsymbol{e}^{n+1}\|^2 - \|\boldsymbol{e}^n\|^2 + \|\hat{\boldsymbol{e}}^n - \boldsymbol{e}^n\|^2 + \|\boldsymbol{e}^{n+1} - \hat{\boldsymbol{e}}^n\|^2 + 2\Delta t\|\nabla\hat{\boldsymbol{e}}^n\|^2 \\ &\le C\,\Delta t\,(\|\boldsymbol{e}^n\|^2 + \|\boldsymbol{e}^{n+1}\|^2) + \Delta t^3(\|\boldsymbol{f}^n\|^2 + \|\boldsymbol{g}^n\|^2) - 2\Delta t\int_\Omega \hat{\boldsymbol{e}}^n\cdot\nabla\Delta q^n\,d\boldsymbol{x}\,. \end{aligned}$$

Similar to the analysis in (2.1.17), the estimate of the last term in (2.3.21) is

Reproduced with permission of the copyright owner. Further reproduction prohibited without permission.

determined by integration by parts and then using the first equation in (2.3.18b).

$$
\begin{aligned}
I &\equiv -2\triangle t \int_\Omega \hat{\boldsymbol{e}}^n \cdot \nabla \triangle q^n \, d\boldsymbol{x} \\
&= 2\triangle t \int_\Omega (\nabla \cdot \hat{\boldsymbol{e}}^n) \triangle q^n \, d\boldsymbol{x} \\
&= -2\triangle t \int_\Omega \triangle (q^{n+1} - q^n) \triangle q^n \, d\boldsymbol{x} - 2\triangle t^3 \int_\Omega (\nabla \cdot \boldsymbol{g}^n) \triangle q^n \, d\boldsymbol{x} \\
&= -\triangle t (\|\triangle q^{n+1}\|^2 - \|\triangle q^n\|^2) + \triangle t \|\triangle (q^{n+1} - q^n)\|^2 \\
&\quad -2\triangle t^3 \int_\Omega (\nabla \cdot \boldsymbol{g}^n) \triangle q^n \, d\boldsymbol{x} \\
&= -\triangle t (\|\triangle q^{n+1}\|^2 - \|\triangle q^n\|^2) + \triangle t \|\nabla \cdot \hat{\boldsymbol{e}}^n\|^2 + \triangle t^5 \|\boldsymbol{g}^n\|^2 \\
&\quad +2\triangle t^3 \int_\Omega (\nabla \cdot \hat{\boldsymbol{e}}^n)(\nabla \cdot \boldsymbol{g}^n) \, d\boldsymbol{x} - 2\triangle t^3 \int_\Omega (\nabla \cdot \boldsymbol{g}^n) \triangle q^n \, d\boldsymbol{x} .
\end{aligned} \tag{2.3.22}
$$

It is given by (2.3.22) that

$$
\begin{aligned}
I \le & -\triangle t (\|\triangle q^{n+1}\|^2 - \|\triangle q^n\|^2) + \triangle t \|\nabla \hat{\boldsymbol{e}}^n\|^2 + \triangle t^2 \|\triangle q^n\|^2 \\
& +2\triangle t^4 \|\nabla \cdot \boldsymbol{g}^n\|^2 + \triangle t^2 \|\nabla \hat{\boldsymbol{e}}^n\|^2 + \triangle t^5 \|\boldsymbol{g}^n\|^2 .
\end{aligned} \tag{2.3.23}
$$

Going back to (2.3.21), we obtain

$$
\begin{aligned}
& \|e^{n+1}\|^2 - \|\boldsymbol{e}^n\|^2 + \triangle t \|\nabla \hat{\boldsymbol{e}}^n\|^2 + \triangle t (\|\triangle q^{n+1}\|^2 - \|\triangle q^n\|^2) \\
& \le C \triangle t \, (\|\boldsymbol{e}^n\|^2 + \|\boldsymbol{e}^{n+1}\|^2) + \triangle t^2 \|\triangle q^n\|^2 + C \triangle t^3 (\|\boldsymbol{f}^n\|^2 + \|\boldsymbol{g}^n\|^2 + \triangle t \|\boldsymbol{g}^n\|_{H^1}^2) .
\end{aligned} \tag{2.3.24}
$$

Applying the discrete Grownwall lemma to the last inequality, we arrive at the following result

$$
\|\boldsymbol{e}^n\| + \triangle t^{1/2} \, \|\nabla \hat{\boldsymbol{e}}^n\| + \triangle t^{1/2} \, \|\triangle q^n\| \le C \triangle t . \tag{2.3.25}
$$

Thus the proof of Theorem 2.3.1 is finished.

Reproduced with permission of the copyright owner. Further reproduction prohibited without permission.

2.4 Spatially Discrete Case for the Full Navier-Stokes Equations

Theorem 2.4.1 *Let $(\boldsymbol{u}, \phi)$ be a smooth solution of the Navier-Stokes equations (2.1.1) with smooth initial data $\boldsymbol{u}^0(\boldsymbol{x})$ and let $(\boldsymbol{u}_h, \phi_h)$ be the numerical solution of the gauge method (2.2.15) coupled with the MAC spatial discretizations. Assume the CFL constraint $\Delta t \leq Ch$ for some suitable constant C which we will specify in detail later, then we have*

$$\|\boldsymbol{u} - \boldsymbol{u}_h\|_{L^\infty} \leq C(\Delta t + h^2). \tag{2.4.1}$$

Some Notations

For $\boldsymbol{a} = (a, b), \boldsymbol{c} = (c, d), \boldsymbol{u} = (u, v)$, we define the following discrete inner products on the MAC grids:

(2.4.2)

$$\langle \boldsymbol{a}, \boldsymbol{c} \rangle = h^2 \sum_{i=1}^{N-1} \sum_{j=1}^{N} a_{i+1/2,j} c_{i+1/2,j} + h^2 \sum_{i=1}^{N} \sum_{j=1}^{N} b_{i,j-1/2} d_{i,j-1/2},$$

$$\langle \boldsymbol{u}, \nabla_h \phi \rangle = h \sum_{i=1}^{N-1} \sum_{j=1}^{N} u_{i+1/2,j} (\phi_{i+1,j} - \phi_{i,j}) + h \sum_{i=1}^{N} \sum_{j=1}^{N} v_{i,j-1/2} (\phi_{i,j+1} - \phi_{i,j}).$$

$$\langle \nabla_h \cdot \boldsymbol{u}, \phi \rangle = h \sum_{i=1}^{N-1} \sum_{j=1}^{N} (u_{i+1/2,j} - u_{i-1/2,j}) \phi_{i,j} + h \sum_{i=1}^{N} \sum_{j=1}^{N} (v_{i,j+1/2} - v_{i,j-1/2}) \phi_{i,j},$$

and discrete norms

$$\|\boldsymbol{u}\| = (\boldsymbol{u}, \boldsymbol{u})^{1/2}, \qquad \|\boldsymbol{u}\|_\infty = \max_{i,j} |\boldsymbol{u}_{i,j}|. \tag{2.4.3}$$

Next we state some preliminary lemmas excerpted from [ELP3] which are needed in the proof of the theorem.

Reproduced with permission of the copyright owner. Further reproduction prohibited without permission.

Lemma 2.4.1 *We have the following*

(i) *Inverse inequality:*

$$\|f\|_\infty \le \frac{C}{h}\|f\| . \tag{2.4.4}$$

(ii) *Poincare inequality: suppose* $f\,|_{x=\pm 1} = 0$. *then*

$$\|f\| \le C\|\nabla_h f\| . \tag{2.4.5}$$

(iii) *Suppose* $\boldsymbol{n}\cdot\boldsymbol{u}\,|_{x=\pm 1} = 0$, *then we have*

$$\langle \boldsymbol{u}, \nabla_h \phi\rangle = -\langle \nabla_h\cdot\boldsymbol{u}, \phi\rangle . \tag{2.4.6}$$

(iv) *Suppose* $\boldsymbol{u}\,|_{x=\pm 1} = 0$, *then we have*

$$2\langle \boldsymbol{u}, \Delta_h \boldsymbol{u}\rangle \le -\|\nabla_h \boldsymbol{u}\|^2 - \|\nabla_h\cdot\boldsymbol{u}\|^2 . \tag{2.4.7}$$

(v) *Suppose* $\boldsymbol{a}\,|_{x=\pm 1} = 0$ *and* $\boldsymbol{c}\cdot\boldsymbol{n}\,|_{x=\pm 1} = 0$. *then we have*

$$|\langle \boldsymbol{a}, \mathcal{N}_h(\boldsymbol{u}, \boldsymbol{c})\rangle| \le C\|\boldsymbol{c}\|\|\nabla_h \boldsymbol{a}\|\|\boldsymbol{u}\|_{W^{1,\infty}} . \tag{2.4.8}$$

Lemma 2.4.2 *Let* $(\boldsymbol{u}, p)$ *be a solution of the Navier-Stokes equations with smooth initial data* $\boldsymbol{u}^0(\boldsymbol{x})$. *Let* $(\boldsymbol{u}_0, p_0)$ *be a solution of the following system:*

$$\begin{cases} \partial_t \boldsymbol{u}_0 + \nabla_h p_0 + \mathcal{N}_h(\boldsymbol{u}_0, \boldsymbol{u}_0) = \Delta_h \boldsymbol{u}_0 , & \text{in } \Omega . \\ \nabla_h\cdot\boldsymbol{u}_0 = 0 , & \text{in } \Omega . \\ \boldsymbol{u}_0 = 0 , & \text{at } \ x = \pm 1 . \\ \boldsymbol{u}_0(\cdot, 0) = \boldsymbol{u}^0(\cdot) , & \text{in } \Omega . \end{cases} \tag{2.4.9}$$

Then $(\boldsymbol{u}_0, p_0)$ *is smooth in the sense that its discrete derivatives are bounded. Moreover, we have*

$$\|\boldsymbol{u} - \boldsymbol{u}_0\|_{L^\infty} + \|p - p_0\|_{L^\infty} \le Ch^2 . \tag{2.4.10}$$

Reproduced with permission of the copyright owner. Further reproduction prohibited without permission.

Remark 2.4.1 Let ϕ_0 be the solution of the following discrete heat equation:

$$\text{(2.4.11)} \qquad \begin{cases} \partial_t \phi_0 - \Delta_h \phi_0 + p_0 = 0\,, & \text{in } \Omega\,, \\ \dfrac{\partial \phi_0}{\partial \boldsymbol{x}} = 0\,, & \text{at } \ x = \pm 1\,, \\ \phi_0(\cdot, 0) = \phi^0(\cdot)\,, & \text{in } \Omega\,. \end{cases}$$

and a^0 is denoted as

$$\text{(2.4.12)} \qquad \boldsymbol{a}^0 = \boldsymbol{u}^0 - \nabla_h \phi^0\,.$$

Then the solution $(\boldsymbol{u}_0, \phi_0)$ of the decoupled system (2.4.9), (2.4.11) is smooth in the sense that its discrete derivatives are bounded and

$$\text{(2.4.13)} \qquad \|\boldsymbol{u} - \boldsymbol{u}_0\|_{L^\infty} + \|\phi - \phi_0\|_{L^\infty} \le Ch^2\,.$$

where $(\boldsymbol{u}, \phi)$ is the solution of Navier-Stokes equations in the gauge formulation with initial data $\boldsymbol{u}^0$.

Lemma 2.4.3 *Let $(\boldsymbol{u}, p)$ be a solution of the linear system of ODE*

$$\text{(2.4.14)} \qquad \begin{cases} \partial_t \boldsymbol{u} + \nabla_h p + \mathcal{N}_h(\boldsymbol{u}_0, \boldsymbol{u}) + \mathcal{N}_h(\boldsymbol{u}, \boldsymbol{u}_0) = \Delta_h \boldsymbol{u} + \boldsymbol{f}\,, & \text{in } \Omega\,, \\ \nabla_h \cdot \boldsymbol{u} = 0\,, & \text{in } \Omega\,, \\ \boldsymbol{u} = \boldsymbol{g}\,, & \text{at } \ x = \pm 1\,, \\ \boldsymbol{u}(\cdot, 0) = \boldsymbol{u}^0(\cdot)\,, & \text{in } \Omega\,. \end{cases}$$

where $\boldsymbol{f}$, $\boldsymbol{g}$, and $\boldsymbol{u}_0$ are smooth and satisfy some compatibility conditions. Then $(\boldsymbol{u}, p)$ is smooth in the sense that its divided differences of various orders are bounded.

Remark 2.4.2 Once again, let ϕ be the solution of the discrete heat equation

$$\text{(2.4.15)} \qquad \begin{cases} \partial_t \phi - \Delta_h \phi + p = 0\,, & \text{in } \Omega\,, \\ \dfrac{\partial \phi}{\partial \boldsymbol{n}} = 0\,, & \text{on } \partial'\Omega\,. \end{cases}$$

Reproduced with permission of the copyright owner. Further reproduction prohibited without permission.

Then the solution $(\boldsymbol{u}, \phi)$ of the decoupled system (2.4.14), (2.4.15) is also smooth in the sense that its divided differences of various orders are bounded.

2.4.1 Consistency Analysis of Spatial Discretization with MAC grid

As pointed out in Section 2.2, the numerical scheme can be written in the form of (2.2.15) for the convenience of our analysis. Similar to the spatially continuous case, if we introduce $\hat{\boldsymbol{u}}^n = \boldsymbol{a}^{n-1} + \nabla_h o^n$, (2.2.15) is equivalent to:

$$\text{(2.4.16a)} \qquad \begin{cases} \frac{\hat{\boldsymbol{u}}^n - \boldsymbol{u}^n}{\Delta t} + \mathcal{N}_h(\boldsymbol{u}^n, \boldsymbol{u}^n) + \Delta_h \nabla_h o^n = \Delta_h \hat{\boldsymbol{u}}^n, & \text{in } \Omega, \\ \hat{\boldsymbol{u}}^n = 0, \qquad \text{at} \qquad x = \pm 1. \end{cases}$$

$$\text{(2.4.16b)} \qquad \begin{cases} \boldsymbol{u}^{n+1} - \hat{\boldsymbol{u}}^n + \nabla_h (o^n - o^{n+1}) = 0, & \text{in } \Omega, \\ \nabla_h \cdot \boldsymbol{u}^{n+1} = 0, & \text{in } \Omega, \\ \frac{\partial (o^{n+1} - o^n)}{\partial \boldsymbol{n}} = \boldsymbol{n} \cdot \boldsymbol{u}^{n+1} = 0, & \text{at} \quad x = \pm 1. \end{cases}$$

We note that (2.4.16) is almost a discrete version of (2.1.14), except for the appearance of $\mathcal{N}_h(\boldsymbol{u}^n, \boldsymbol{u}^n)$, a nonlinear term.

Let $\boldsymbol{u}_0(\boldsymbol{x}, t)$, $o_0(\boldsymbol{x}, t)$ be solutions of the decoupled system (2.4.10), (2.4.12), which are guaranteed by Lemma 2.4.2 and Remark 2.4.1 to be smooth in the sense that the divided differences of various orders are bounded.

Next, we denote $\boldsymbol{u}_1(\boldsymbol{x}, t)$ as the solution of the following system

$$\text{(2.4.17a)} \qquad \begin{cases} \partial_t \boldsymbol{u}_1 + \nabla_h p_1 + \mathcal{N}_h(\boldsymbol{u}_0, \boldsymbol{u}_1) + \mathcal{N}_h(\boldsymbol{u}_1, \boldsymbol{u}_0) \\ = \Delta_h \boldsymbol{u}_1 + \partial_t \Delta_h \boldsymbol{a}_0 - \frac{1}{2} \partial_t^2 \boldsymbol{a}_0, & \text{in } \Omega, \\ \nabla_h \cdot \boldsymbol{u}_1 = 0, & \text{in } \Omega, \\ \boldsymbol{u}_1 \mid_{x=\pm 1} = \partial_t \nabla_h o_0 \mid_{x=\pm 1}. \end{cases}$$

with suitable initial data for $\boldsymbol{u}_1$, and let $o_1(\boldsymbol{x}, t)$ be the solution of the following discrete heat equation

$$\text{(2.4.17b)} \qquad \begin{cases} \partial_t \phi_1 - \Delta_h \varphi_1 + p_1 = 0, & \text{in } \Omega, \\ \frac{\partial \phi_1}{\partial \boldsymbol{n}} = 0, & \text{on } \partial' \Omega. \end{cases}$$

Reproduced with permission of the copyright owner. Further reproduction prohibited without permission.

with suitable initial data for ϕ_1. We know from Lemma 2.4.3 and Remark 2.4.2 that (2.4.17) has a smooth solution.

Let $\boldsymbol{u}_2(\boldsymbol{x}, t)$ be the solution of the (spatially) discrete Stokes equations with the prescribed boundary condition and some suitable initial data

$$\text{(2.4.18)} \qquad \begin{cases} \partial_t \boldsymbol{u}_2 + \nabla_h p_2 = \triangle_h \boldsymbol{u}_2 . & \text{in } \Omega . \\ \nabla_h \cdot \boldsymbol{u}_2 = 0 . & \text{in } \Omega . \\ \boldsymbol{u}_2 \mid_{x=\pm 1} = (\frac{1}{2}\partial_t^2 \nabla_h \phi_0 - \partial_t \boldsymbol{u}_1 + \partial_t \nabla_h \phi_1) \mid_{x=\pm 1} . \end{cases}$$

Subsequently, we let

$$\text{(2.4.19)} \qquad \hat{\boldsymbol{u}}_1 = \boldsymbol{u}_1 + \partial_t \boldsymbol{a}_0 .$$

and

$$\text{(2.4.20)} \qquad \hat{\boldsymbol{u}}_2 = \boldsymbol{u}_2 + \frac{1}{2}\partial_t^2 \boldsymbol{a}_0 + \partial_t \boldsymbol{u}_1 - \partial_t \nabla_h \phi_1 .$$

Now we construct

$$\text{(2.4.21)} \qquad \begin{cases} U^{*n} = \boldsymbol{u}_0 + \triangle t \hat{\boldsymbol{u}}_1 + \triangle t^2 \hat{\boldsymbol{u}}_2 . \\ U^n = \boldsymbol{u}_0 + \triangle t \boldsymbol{u}_1 + \triangle t^2 \boldsymbol{u}_2 . \\ \Phi^n = \phi_0 + \triangle t \phi_1 . \end{cases}$$

and substitute them into (2.4.16). Similar to the computations and arguments in the spatially continuous case and doing Taylor expansions of $\boldsymbol{u}_h$ and $\nabla_h \phi$ w.r.t. time t, we obtain

$$\text{(2.4.22a)} \qquad \begin{cases} \dfrac{U^{*n} - U^n}{\triangle t} + \mathcal{N}_h(U^n, U^n) + \triangle_h \nabla_h \Phi^n = \triangle_h \tilde{U}^n + \triangle t^2 \boldsymbol{f}^n . & \text{in } \Omega . \\ U^{*n} = 0 . & \text{at } \ x = \pm 1 . \end{cases}$$

$$\text{(2.4.22b)} \qquad \begin{cases} U^{n+1} - U^{*n} + \nabla_h (\Phi^n - \Phi^{n+1}) = \triangle t^3 \boldsymbol{g}^n . & \text{in } \Omega . \\ \nabla_h \cdot U^{n+1} = 0 . & \text{in } \Omega . \\ \dfrac{\partial \Phi^{n+1}}{\partial \boldsymbol{n}} = \boldsymbol{n} \cdot U^{n+1} = 0 . & \text{at } \ x = \pm 1 . \end{cases}$$

Reproduced with permission of the copyright owner. Further reproduction prohibited without permission.

where $\boldsymbol{f}^n$ and $\boldsymbol{g}^n$ are bounded and smooth if $(\boldsymbol{u}_0, \phi_0)$ is sufficiently smooth. It can be seen that the only difference between (2.4.22) and (2.4.16) is the higher order truncations error terms $\Delta t^2 \boldsymbol{f}^n$, $\Delta t^3 \boldsymbol{g}^n$.

It is obvious that

$$\max_{0 \le t^n \le T} \|U^n(\cdot)\|_{W^{1,\infty}} \le C^* . \tag{2.4.23}$$

Under the compatible condition

$$\partial_t \nabla_h \phi_0(\boldsymbol{x}, 0) = 0 , \qquad \text{on } \partial' \Omega . \tag{2.4.24}$$

we can choose

$$\boldsymbol{u}_1(\boldsymbol{x}, 0) = 0 . \tag{2.4.25}$$

Then we have a second order approximate initial data

$$U^0(\boldsymbol{x}) = \boldsymbol{u}_0(\boldsymbol{x}, 0) + \Delta t^2 \boldsymbol{w}^0(\boldsymbol{x}) , \tag{2.4.26}$$

where $\boldsymbol{w}^0$ is a bounded function.

2.4.2 Convergence Proof

Assume a priori that

$$\max_{0 \le t^n \le T} \|\boldsymbol{u}^n\|_{W^{1,\infty}} \le \tilde{C} . \tag{2.4.27}$$

In the following estimate, the constant will sometimes depend on C^* and $\tilde{C}$. We define

$$\boldsymbol{e}^n = U^n - \boldsymbol{u}^n , \qquad \hat{\boldsymbol{e}}^n = U^{*n} - \hat{\boldsymbol{u}}^n , \qquad q^n = \Phi^n - \phi^n . \tag{2.4.28}$$

The following system of error equations is obtained by (2.4.22) and (2.4.16)

(2.4.29a)

$$\begin{cases} \dfrac{\hat{\boldsymbol{e}}^n - \boldsymbol{e}^n}{\Delta t} + \mathcal{N}_h(\boldsymbol{e}^n, U^n) + \mathcal{N}_h(\boldsymbol{u}^n, \boldsymbol{e}^n) + \nabla_h \Delta_h q^n = \Delta_h \hat{\boldsymbol{e}}^n + \Delta t^2 \boldsymbol{f}^n . & \text{in } \Omega , \\ \hat{\boldsymbol{e}}^n = 0 . \qquad \text{at} \quad x = \pm 1 . \end{cases}$$

Reproduced with permission of the copyright owner. Further reproduction prohibited without permission.

$$\text{(2.4.29b)}\qquad \begin{cases} \boldsymbol{e}^{n+1} - \hat{\boldsymbol{e}}^n + \nabla_h(q^n - q^{n-1}) = \triangle t^3 \boldsymbol{g}^n\,, & \text{in } \Omega\,. \\ \nabla_h \cdot \boldsymbol{e}^{n+1} = 0\,, & \text{in } \Omega\,. \\ \dfrac{\partial q^{n+1}}{\partial \boldsymbol{n}} = \boldsymbol{n}\cdot\boldsymbol{e}^{n+1} = 0\,, & \text{at } \ x = \pm 1\,. \end{cases}$$

$$\text{(2.4.29c)}\qquad \boldsymbol{e}^0 = \triangle t^2\, \boldsymbol{w}^0\,, \qquad \text{in } \Omega\,.$$

The system (2.4.29) is similar to the system of the error equations for the spatially continuous Stokes equations, (2.3.18). At the first glance, (2.4.29) is almost a discrete version of (2.3.18). Then most of the techniques used in Section 2.3 can be applied here. Moreover, there are also some differences: the appearance of nonlinear error terms $\mathcal{N}_h(\boldsymbol{e}^n, U^n)$ and $\mathcal{N}_h(\boldsymbol{u}^n, \boldsymbol{e}^n)$, and the local truncation error terms appearing in (2.4.29) are of higher order than those of (2.3.18). We make higher order expansions in the spatially discrete case so that we can establish the $W^{1,\infty}$ estimate for the numerical $\boldsymbol{u}^n$. This estimate is needed for nonlinear error terms so that part (v) of Lemma 2.4.1 can be applied. By making higher order expansions as we did in the consistency analysis part, the only thing we need to do is to apply the *a priori* estimate (2.4.27).

Taking the inner product of the equation in (2.4.29a) with $2\hat{\boldsymbol{e}}^n$, we obtain

$$\begin{aligned} &\|\hat{\boldsymbol{e}}^n\|^2 - \|\boldsymbol{e}^n\|^2 + \|\hat{\boldsymbol{e}}^n - \boldsymbol{e}^n\|^2 - 2\triangle t\, \langle \hat{\boldsymbol{e}}^n, \Delta_h \hat{\boldsymbol{e}}^n \rangle \\ &\le \triangle t^5 \|\boldsymbol{f}^n\|^2 + \triangle t\, \|\hat{\boldsymbol{e}}^n\|^2 - 2\triangle t\, \langle \hat{\boldsymbol{e}}^n, \mathcal{N}_h(\boldsymbol{e}^n, U^n) \rangle \\ &-2\triangle t\, \langle \hat{\boldsymbol{e}}^n, \mathcal{N}_h(\boldsymbol{u}^n, \boldsymbol{e}^n) \rangle - 2\triangle t\, \langle \hat{\boldsymbol{e}}^n, \nabla_h \Delta_h q^n \rangle\,. \end{aligned} \qquad \text{(2.4.30)}$$

By Lemma 2.4.1, parts (iv) and (v), and the a priori estimate (2.4.27), we get

(2.4.31)

$$\begin{aligned} &\|\hat{\boldsymbol{e}}^n\|^2 - \|\boldsymbol{e}^n\|^2 + \|\hat{\boldsymbol{e}}^n - \boldsymbol{e}^n\|^2 + \triangle t\, \|\nabla_h \hat{\boldsymbol{e}}^n\|^2 + \triangle t\, \|\nabla_h \cdot \hat{\boldsymbol{e}}^n\|^2 \\ &\quad \le \triangle t^5 \|\boldsymbol{f}^n\|^2 + C\triangle t(\|\hat{\boldsymbol{e}}^n\|^2 + \|\boldsymbol{e}^n\|^2) + \tfrac{1}{2}\triangle t\, \|\nabla_h \hat{\boldsymbol{e}}^n\|^2 - 2\triangle t\, \langle \hat{\boldsymbol{e}}^n, \nabla_h \Delta_h q^n \rangle\,. \end{aligned}$$

Once again, as can be seen, to use Lemma 2.4.1(v), we must have an a priori estimate (2.4.27). This requires us to do second order expansions in the spatially discrete case.

Reproduced with permission of the copyright owner. Further reproduction prohibited without permission.

By the triangle inequality for the discrete L^2 norm

$$\|\widehat{\boldsymbol{e}}^n\| \le \|\widehat{\boldsymbol{e}}^n - \boldsymbol{e}^n\| + \|\boldsymbol{e}^n\| . \tag{2.4.32}$$

we have

$$\begin{aligned} &\|\widehat{\boldsymbol{e}}^n\|^2 - \|\boldsymbol{e}^n\|^2 + \tfrac{7}{8}\|\widehat{\boldsymbol{e}}^n - \boldsymbol{e}^n\|^2 + \triangle t\,\|\nabla_h \widehat{\boldsymbol{e}}^n\|^2 + \triangle t\,\|\nabla_h \cdot \widehat{\boldsymbol{e}}^n\|^2 \\ &\le \triangle t^5 \|\boldsymbol{f}^n\|^2 + C\triangle t \|\boldsymbol{e}^n\|^2 + \tfrac{1}{2}\triangle t\,\|\nabla_h \widehat{\boldsymbol{e}}^n\|^2 - 2\triangle t\,\langle \widehat{\boldsymbol{e}}^n, \nabla_h \Delta_h q^n\rangle . \end{aligned} \tag{2.4.33}$$

Taking the inner product of the first equation in (2.4.29b) with $2\boldsymbol{e}^{n+1}$ and applying Lemma 2.4.1(iii) yields

$$\|\boldsymbol{e}^{n+1}\|^2 - \|\widehat{\boldsymbol{e}}^n\|^2 + \|\boldsymbol{e}^{n+1} - \widehat{\boldsymbol{e}}^n\|^2 \le \triangle t\,\|\boldsymbol{e}^{n+1}\|^2 + \triangle t^5 \|\boldsymbol{g}^n\|^2 . \tag{2.4.34}$$

Combining (2.4.33) and (2.4.34), we get

(2.4.35)

$$\begin{aligned} &\|\boldsymbol{e}^{n+1}\|^2 - \|\boldsymbol{e}^n\|^2 + \tfrac{7}{8}\|\widehat{\boldsymbol{e}}^n - \boldsymbol{e}^n\|^2 + \|\boldsymbol{e}^{n+1} - \widehat{\boldsymbol{e}}^n\|^2 + \tfrac{1}{2}\triangle t\|\nabla_h \widehat{\boldsymbol{e}}^n\|^2 + \triangle t\|\nabla_h \cdot \widehat{\boldsymbol{e}}^n\|^2 \\ &\quad \le \triangle t^5(\|\boldsymbol{f}^n\|^2 + \|\boldsymbol{g}^n\|^2) + C\,\triangle t(\|\boldsymbol{e}^n\|^2 + \|\boldsymbol{e}^{n+1}\|^2) - 2\triangle t\,\langle \widehat{\boldsymbol{e}}^n, \nabla_h \Delta_h q^n\rangle . \end{aligned}$$

Estimating the last term in (2.4.35) is similar to (2.3.22)

$$\begin{aligned} I &\equiv -2\triangle t\langle \widehat{\boldsymbol{e}}^n, \nabla_h \Delta_h q^n\rangle \\ &= 2\triangle t\langle \nabla_h \cdot \widehat{\boldsymbol{e}}^n, \Delta_h q^n\rangle \\ &= -2\triangle t\langle \Delta_h(q^{n+1} - q^n), \Delta_h q^n\rangle - 2\triangle t^4\langle \nabla_h \cdot \boldsymbol{g}^n, \Delta_h q^n\rangle \\ &= -\triangle t(\|\Delta_h q^{n+1}\|^2 - \|\Delta_h q^n\|^2) + \triangle t\|\Delta_h(q^{n+1} - q^n)\|^2 \\ &\qquad -2\triangle t^4\langle \nabla_h \cdot \boldsymbol{g}^n, \Delta_h q^n\rangle \\ &= -\triangle t(\|\Delta_h q^{n+1}\|^2 - \|\Delta_h q^n\|^2) + \triangle t\|\nabla_h \cdot \widehat{\boldsymbol{e}}^n\|^2 + \triangle t^7\|\boldsymbol{g}^n\|^2 \\ &\qquad +2\triangle t^4\langle \nabla_h \cdot \widehat{\boldsymbol{e}}^n, \nabla_h \cdot \boldsymbol{g}^n\rangle - 2\triangle t^4\langle \nabla_h \cdot \boldsymbol{g}^n, \Delta_h q^n\rangle . \end{aligned} \tag{2.4.36}$$

Then (2.4.36) gives us

$$\begin{aligned} I \le\ &-\triangle t(\|\Delta_h q^{n+1}\|^2 - \|\Delta_h q^n\|^2) + \triangle t\|\nabla_h \cdot \widehat{\boldsymbol{e}}^n\|^2 + \triangle t^2\|\Delta_h q^n\|^2 \\ &+2\triangle t^6\|\nabla_h \cdot \boldsymbol{g}^n\|^2 + \triangle t^2\|\nabla_h \cdot \widehat{\boldsymbol{e}}^n\|^2 + \triangle t^7\|\boldsymbol{g}^n\|^2 . \end{aligned} \tag{2.4.37}$$

Reproduced with permission of the copyright owner. Further reproduction prohibited without permission.

Going back to (2.4.35), we obtain

(2.4.38)

$$\|e^{n+1}\|^2 - \|e^n\|^2 + \tfrac{1}{2}\|\nabla_h \widehat{e}^n\|^2 + \Delta t(\|\Delta_h q^{n+1}\|^2 - \|\Delta_h q^n\|^2)$$
$$\leq C\Delta t(\|e^n\|^2 + \|e^{n+1}\|^2) + \Delta t^2\|\Delta_h q^n\|^2 + C\Delta t^5(\|f^n\|^2 + \|g^n\|^2 + \Delta t\|g^n\|_{H^1}^2).$$

Grownwall Lemma gives

$$\|e^n\| + \Delta t\|\nabla_h \widehat{e}^n\| + \Delta t^{1/2}\|\Delta_h q^n\| + \leq C_1\Delta t^2. \tag{2.4.39}$$

By the inverse inequality (2.4.4) we have

$$\|e^n\|_{L^\infty} + h\|e^n\|_{W^{1,\infty}} + \Delta t^{1/2}\|\Delta_h q^n\|_{L^\infty} \leq C_1\frac{\Delta t^2}{h}. \tag{2.4.40}$$

Under the CFL constraint

$$\Delta t \leq \sqrt{\frac{1}{C_1}}\Delta x, \tag{2.4.41}$$

where C_1 only depends on the exact solution (u_0, o_0) and the a priori constant $\tilde{C}$ for the estimate of $\|u^n\|_{W^{1,\infty}}$ in (2.4.27), we have

$$\|e^{n+1}\|_{L^\infty} \leq \sqrt{C_1}\Delta t, \quad \|e^{n-1}\|_{W^{1,\infty}} \leq 1. \tag{2.4.42}$$

Therefore in (2.4.27) we can choose

$$\tilde{C} = 1 + \max_{n\leq\left[\frac{T}{\Delta t}\right]} \|U^n(\cdot)\|_{W^{1,\infty}}, \tag{2.4.43}$$

such that $\tilde{C}$ depends only on the exact solution (u_0, o_0). This gives

$$\|u_0 - u_h\|_{L^\infty} \leq C\Delta t. \tag{2.4.44}$$

By Lemma 2.4.2, we have

$$\|u - u_h\|_{L^\infty} \leq C(\Delta t + h^2). \tag{2.4.46}$$

This completes the proof of Theorem 2.4.1.

Reproduced with permission of the copyright owner. Further reproduction prohibited without permission.

2.5 Analysis and Error Estimate of the Dirichlet Gauge Formulation

Finally we look at the gauge method with Dirichlet boundary condition for ϕ. For simplicity, we will concentrate on the spatially continuous case for Stokes equations:

$$\text{(2.5.1)} \qquad \begin{cases} \dfrac{\boldsymbol{a}^{n+1}-\boldsymbol{a}^n}{\triangle t} = \triangle \boldsymbol{a}^{n+1}, & \text{in } \Omega, \\ \boldsymbol{a}^{n+1}\cdot\boldsymbol{n} = -\dfrac{\partial \phi^n}{\partial \boldsymbol{n}}, \quad \boldsymbol{a}^{n+1}\cdot\boldsymbol{\tau} = 0, & \text{on } \partial\Omega. \end{cases}$$

and

$$\text{(2.5.2)} \qquad \begin{cases} \triangle \phi^{n+1} = -\nabla\cdot\boldsymbol{a}^{n+1}, & \text{in } \Omega, \\ \phi^{n+1} = 0, & \text{on } \partial\Omega. \end{cases}$$

$$\text{(2.5.3)} \qquad \boldsymbol{u}^{n+1} = \boldsymbol{a}^{n+1} + \nabla\phi^{n+1}.$$

Next we state our theorem for Dirichlet gauge formulation:

Theorem 2.5.1 *Let $(\boldsymbol{u}, \phi)$ be a smooth solution of Stokes equation (2.2.1) with smooth initial data $\boldsymbol{u}^0(\boldsymbol{x})$ and let $(\boldsymbol{u}_{\triangle t}, \phi_{\triangle t})$ be the numerical solution for the semi-discrete gauge method with Dirichlet boundary condition for the gauge variable (2.5.1)-(2.5.3). Then we have*

$$\text{(2.5.4)} \qquad \|\boldsymbol{u} - \boldsymbol{u}_{\triangle t}\|_{L^\infty(0,T;L^2)} \le C\sqrt{\triangle t}.$$

The analysis carried out in Section 2.2 can be applied to this formulation similarly. First we make a transformation. If we introduce $\hat{\boldsymbol{u}}^n = \boldsymbol{a}^{n+1} + \nabla\phi^n$, (2.5.1)-(2.5.3) can also be reformulated as

$$\text{(2.5.5a)} \qquad \begin{cases} \dfrac{\hat{\boldsymbol{u}}^n - \boldsymbol{u}^n}{\triangle t} + \triangle\nabla\phi^n = \triangle\hat{\boldsymbol{u}}^n, & \text{in } \Omega, \\ \hat{\boldsymbol{u}}^n = 0, & \text{on } \partial\Omega. \end{cases}$$

Reproduced with permission of the copyright owner. Further reproduction prohibited without permission.

$$\text{(2.5.5b)}\qquad \begin{cases} \boldsymbol{u}^{n+1} - \hat{\boldsymbol{u}}^n + \nabla(\phi^n - \phi^{n-1}) = 0\,, & \text{in } \Omega\,. \\ \nabla\cdot\boldsymbol{u}^{n+1} = 0\,, & \text{in } \Omega\,. \\ (\phi^n - \phi^{n+1}) = 0\,, & \text{on } \partial\Omega\,. \end{cases}$$

Note that (2.5.5) is the same as (2.1.14) except for the boundary condition for ϕ.

We will repeat the procedure in Section 2.2: let $\boldsymbol{u}_e(\boldsymbol{x},t), p_e(\boldsymbol{x},t)$ be the exact solution of the Stokes Equations

$$\text{(2.5.6a)}\qquad \begin{cases} \partial_t \boldsymbol{u}_e + \nabla p_e = \triangle \boldsymbol{u}_e\,, & \text{in } \Omega\,. \\ \nabla\cdot\boldsymbol{u}_e = 0\,, & \text{in } \Omega\,. \\ \boldsymbol{u}_e = 0\,, & \text{on } \partial\Omega\,. \end{cases}$$

and let $\phi_e(\boldsymbol{x},t)$ be a solution of the following heat equation with Dirichlet boundary condition

$$\text{(2.5.6b)}\qquad \begin{cases} \partial_t \phi_e = \triangle \phi_e - p_e\,, & \text{in } \Omega\,. \\ \phi_e = 0\,, & \text{on } \partial\Omega\,. \end{cases}$$

However, there is some trouble when we try to construct $\boldsymbol{u}_1$ in the expansion of the numerical scheme. As can be seen, (2.3.5) does not necessarily have a solution in the Dirichlet gauge formulation. Since $\partial_t\nabla\phi_e$ is not orthogonal to the normal vector at the boundary, this leads to the incompatibility of the boundary condition for $\boldsymbol{u}_1$. Yet, to continue our analysis, we can still construct an arbitrary field $\boldsymbol{u}_1$ such that

$$\text{(2.5.7)}\qquad \boldsymbol{u}_1 = \partial_t\nabla\phi_e\,, \qquad \text{on } \partial\Omega\,.$$

We still adopt the notation in **2.3**: let $\hat{\boldsymbol{u}}_1 = \boldsymbol{u}_1 + \partial_t \boldsymbol{a}_e$, and construct

$$\text{(2.5.8)}\qquad U^* = \boldsymbol{u}_e + \triangle t\hat{\boldsymbol{u}}_1\,, \qquad U = \boldsymbol{u}_e + \triangle t\boldsymbol{u}_1\,, \qquad \Phi = \phi_e\,.$$

It must be mentioned here that U is not divergence free up to an order $O(\triangle t)$

$$\text{(2.5.9)}\qquad \nabla\cdot U = \triangle t h\,, \qquad \text{where} \qquad h = \nabla\cdot\boldsymbol{u}_1\,.$$

Reproduced with permission of the copyright owner. Further reproduction prohibited without permission.

This fact will reduce a $\sqrt{\Delta t}$ factor in our estimate as we can see later. Using similar arguments as in Lemma 2.3.1, we have the following system analogous to (2.3.9)

$$\text{(2.5.10a)} \qquad \begin{cases} \dfrac{U^{*n} - U^n}{\Delta t} + \Delta \nabla \Phi^n = \Delta U^{*n} + \Delta t \boldsymbol{f}^n, & \text{in } \Omega, \\ U^{*n} = 0, & \text{on } \partial\Omega. \end{cases}$$

$$\text{(2.5.10b)} \qquad \begin{cases} U^{n+1} - U^{*n} + \nabla(\Phi^n - \Phi^{n-1}) = \Delta t^2 \boldsymbol{g}^n, & \text{in } \Omega, \\ \nabla \cdot U^{n+1} = \Delta t \boldsymbol{h}^{n+1}, & \text{in } \Omega, \\ \Phi^n - \Phi^{n+1} = 0, & \text{on } \partial\Omega, \\ U^0 = \boldsymbol{u}^0 + \Delta t \boldsymbol{w}^0, & \text{in } \Omega. \end{cases}$$

where $\boldsymbol{f}^n$, $\boldsymbol{g}^n$, $\boldsymbol{h}^{n+1}$ and $\boldsymbol{w}^0$ are some bounded functions.

Using the same notation as in (2.3.17)

$$\text{(2.5.11)} \qquad \boldsymbol{e}^n = U^n - \boldsymbol{u}^n, \qquad \hat{\boldsymbol{e}}^n = U^{*n} - \hat{\boldsymbol{u}}^n, \qquad q^n = \Phi^n - o^n.$$

and subtracting (2.5.10) from (2.5.5), we get the system of error equations:

$$\text{(2.5.12a)} \qquad \begin{cases} \dfrac{\hat{\boldsymbol{e}}^n - \boldsymbol{e}^n}{\Delta t} = \Delta \hat{\boldsymbol{e}}^n - \nabla \Delta q^n + \Delta t \boldsymbol{f}^n, & \text{in } \Omega, \\ \hat{\boldsymbol{e}}^n = 0, & \text{on } \partial\Omega. \end{cases}$$

$$\text{(2.5.12b)} \qquad \begin{cases} \boldsymbol{e}^{n+1} - \hat{\boldsymbol{e}}^n + \nabla(q^n - q^{n-1}) = \Delta t^2 \boldsymbol{g}^n, & \text{in } \Omega, \\ \nabla \cdot \boldsymbol{e}^{n+1} = \Delta t \boldsymbol{h}^{n+1}, & \text{in } \Omega, \\ q^n - q^{n+1} = 0, & \text{on } \partial\Omega, \\ \boldsymbol{e}^0 = \Delta t \boldsymbol{w}^0, & \text{in } \Omega. \end{cases}$$

We will continue to do energy estimates as in Section 2.2. Applying the same procedure, taking the inner product of the first equation of (2.5.12a) with $2\hat{\boldsymbol{e}}^n$ we get:

$$\text{(2.5.13)} \qquad \begin{aligned} &\|\hat{\boldsymbol{e}}^n\|^2 - \|\boldsymbol{e}^n\|^2 + \|\hat{\boldsymbol{e}}^n - \boldsymbol{e}^n\|^2 + 2\Delta t \|\nabla \hat{\boldsymbol{e}}^n\|^2 \\ &\quad \le \Delta t^3 \|\boldsymbol{f}^n\|^2 + C\,\Delta t \|\boldsymbol{e}^n\|^2 - 2\Delta t \int_\Omega \hat{\boldsymbol{e}}^n \cdot \nabla \Delta q^n \, d\boldsymbol{x}. \end{aligned}$$

Reproduced with permission of the copyright owner. Further reproduction prohibited without permission.

Taking the inner product of the equation of (2.5.12b) with $2\boldsymbol{e}^{n+1}$ yields

$$\begin{aligned}(2.5.14)\qquad &\|\boldsymbol{e}^{n+1}\|^2 - \|\widehat{\boldsymbol{e}}^n\|^2 + \|\boldsymbol{e}^{n+1} - \widehat{\boldsymbol{e}}^n\|^2 \\ &\quad \le \Delta t\|\boldsymbol{e}^{n+1}\|^2 + \Delta t^3\|\boldsymbol{g}^n\|^2 - 2\int_\Omega \boldsymbol{e}^{n+1}\cdot\nabla(q^n - q^{n+1})\,d\boldsymbol{x}\,.\end{aligned}$$

Next, we estimate the last term of the right hand side, which is caused by the fact that U^n is not divergence-free:

$$\begin{aligned}I_1 &\equiv -2\int_\Omega \boldsymbol{e}^{n+1}\cdot\nabla(q^n - q^{n-1})\,d\boldsymbol{x} = 2\int_\Omega(\nabla\cdot\boldsymbol{e}^{n-1})(q^n - q^{n+1})\,d\boldsymbol{x} \\ &= 2\Delta t\int_\Omega \boldsymbol{h}^{n+1}(q^n - q^{n+1})\,d\boldsymbol{x} \qquad (2.5.15)\\ &\le C\Delta t^2\|\boldsymbol{h}^{n+1}\|^2 + C_1\|q^n - q^{n+1}\|^2\,.\end{aligned}$$

Since $q^n - q^{n+1} = 0$ on the boundary, by the Poincare inequality, we have

$$\begin{aligned}\|q^n - q^{n+1}\|^2 &\le C_2\|\nabla(q^n - q^{n-1})\|^2 \\ &\le C_2\|(\boldsymbol{e}^{n+1} - \widehat{\boldsymbol{e}}^n) + \Delta t^2\boldsymbol{g}^n\|^2 \qquad (2.5.16)\\ &\le \tfrac{3}{2}C_2\|\boldsymbol{e}^{n+1} - \widehat{\boldsymbol{e}}^n\|^2 + C\Delta t^4\|\boldsymbol{g}^n\|^2\,.\end{aligned}$$

Since we can always adjust C_1 such that $C_1C_2 \le \frac{1}{3}$, (2.5.14)-(2.5.16) gives

$$\begin{aligned}(2.5.17)\qquad &\|\boldsymbol{e}^{n+1}\|^2 - \|\widehat{\boldsymbol{e}}^n\|^2 + \tfrac{1}{2}\|\boldsymbol{e}^{n+1} - \widehat{\boldsymbol{e}}^n\|^2 \\ &\quad \le \Delta t\|\boldsymbol{e}^{n+1}\|^2 + C\Delta t^2\|\boldsymbol{h}^{n+1}\|^2 + \Delta t^3\|\boldsymbol{g}^n\|^2\,.\end{aligned}$$

The estimates in (2.3.22), (2.3.23) are still valid here. Finally we obtain

$$\begin{aligned}&\|\boldsymbol{e}^{n+1}\|^2 - \|\boldsymbol{e}^n\|^2 + \tfrac{1}{2}\Delta t\|\nabla\widehat{\boldsymbol{e}}^n\|^2 + \Delta t(\|\Delta q^{n+1}\|^2 - \|\Delta q^n\|^2) \\ &\quad \le C\,\Delta t\,(\|\boldsymbol{e}^n\|^2 + \|\boldsymbol{e}^{n+1}\|^2) + \Delta t^2\|\Delta q^n\|^2 \qquad (2.5.18)\\ &\quad\quad + C\Delta t^2\|\boldsymbol{h}^{n+1}\|^2 + C\Delta t^3(\|\boldsymbol{f}^n\|^2 + \|\boldsymbol{g}^n\|^2 + \Delta t\|\boldsymbol{g}^n\|_{H^1}^2)\,.\end{aligned}$$

Applying the discrete Grownwall lemma to the last inequality, we arrive at

$$(2.5.19)\qquad \|\boldsymbol{e}^n\| + \Delta t^{1/2}\,\|\nabla\widehat{\boldsymbol{e}}^n\| + \Delta t^{1/2}\,\|\Delta q^n\| \le C\sqrt{\Delta t}\,.$$

where only the $\sqrt{\Delta t}$ error estimate for the velocity field is available. Theorem 2.5.1 is now proven.

Reproduced with permission of the copyright owner. Further reproduction prohibited without permission.

CHAPTER 3
ANALYSIS OF SECOND ORDER SCHEME

3.1 Preliminary

The 2-D Navier-Stokes equations in vorticity-stream function formulation read:

$$\text{(3.1.1)} \qquad \begin{cases} \partial_t \omega + \nabla \cdot (\boldsymbol{u}\omega) = \nu \triangle \omega \,, \\ \triangle \psi = \omega \,, \\ u = -\partial_y \psi \,, \qquad v = \partial_x \psi \end{cases}$$

with the no-slip boundary condition written in terms of the stream function ψ:

$$\text{(3.1.2)} \qquad \psi = 0, \quad \frac{\partial \psi}{\partial \mathbf{n}} = 0 \,.$$

Here $\boldsymbol{u} = (u, v)$ denotes the velocity field, ω denotes the vorticity.

Many finite difference schemes, e.g., [QL], [ELV1], [ELV2], have been proposed to solve (3.1.1), (3.1.2) numerically. The main difficulty and confusion of straightforward discretizations of (3.1.1) and (3.1.2) includes two points: there are two boundary conditions for stream function in (3.1.2), while on the other hand when we time march vorticity in the dynamic equation, there is no definite boundary condition for vorticity (see [QL]). The methodology we employ to overcome this difficulty is to solve for the stream function using Dirichlet boundary condition $\psi = 0$ on Γ, and then compute the vorticity at the boundary from the stream function via the kinematic relation and no-slip boundary condition.

Reproduced with permission of the copyright owner. Further reproduction prohibited without permission.

The subject of vorticity boundary condition has a long history, going back to Thom's formula in 1933. See [THOM], [OI1], [QL], [ELV1]. Recently, an efficient explicit time stepping was proposed by E and Liu in [ELV1], which is very suitable for unsteady flow at high Reynolds number.

The convergence analysis of this subject has attracted considerable attentions recently. For example, the 2nd order scheme with Thom's formula on the boundary was analyzed by Wetton and Hou in [HW]. It was always very confusing that Thom's formula still achieves full 2nd order accuracy even the formal Taylor expansion of it only indicates 1st order accuracy of the vorticity on the boundary. Their analysis resorts to Strang type high order expansions, which are quite complicated. A technical assumption of one-sided physical, one-sided periodic boundary condition was imposed.

In this chapter, we perform a simple, clean analysis of the second order scheme with Wilkes' formula for the vorticity on the boundary. As we can see, both centered difference, which is used at interior points, and the boundary condition for vorticity give us 2nd order accuracy. This fact is reflected in our paper that our consistency analysis is more straightforward, no Strang type expansion is needed. Yet, people are always doubtful about its stability, since it involves more interior points than Thom's formula. In fact, direct calculations and standard local estimates cannot work it out as we can see later. We overcome this difficulty, which comes from the boundary term, by adopting a new technique: applying Cauchy inequality to bound local terms by some global terms, then applying discrete elliptic regularity to control the global terms by the diffusion term, which therefore guarantees the stability of Wilkes' formula. The combination of the consistency and stability leads to the convergence of the scheme, as we can see in our main theorem. The physical no-slip boundary condition on both sides is imposed in our analysis.

Reproduced with permission of the copyright owner. Further reproduction prohibited without permission.

In Section 3.2 we describe our second order scheme for 2-D NSE with a $[0,1] \times [0,1]$ box for the domain. Then, in Section 3.3, we give the detailed stability analysis of Wilkes' formula in the case of linear Stokes equations. In Section 3.4, we show the convergence of the second order scheme with Wilkes' formula. In Section 3.5, we give the numerical accuracy check for both Thom's formula and Wilkes' formula.

3.2 Description of the Second Order Scheme

We look at Navier-Stokes equations in 2-D when no-slip boundary condition is imposed on both sides. For simplicity of presentation, we take the computation domain as $\Omega = [0,1] \times [0,1]$ with grid size $\triangle x = \triangle y = h$. The no-slip boundary conditions are imposed at $\{y = 0,1\}$ and $\{x = 0,1\}$, denoted by Γ_x and Γ_y, respectively. The associated numerical grids will be denoted by $\{x_i = i/N, y_j = j/N,\ i,j = 0,1,\cdots,N\}$. At these grid points, NSE can be discretized by standard centered difference formulas:

$$\text{(3.2.1)} \qquad \begin{cases} \partial_t \omega + \widetilde{D}_x(u\omega) + \widetilde{D}_y(v\omega) = \nu \triangle_h \omega\,, \\ \triangle_h \psi = \omega\,, \qquad \psi\,|_\Gamma = 0\,. \\ u = -\widetilde{D}_y \psi\,, \qquad v = \widetilde{D}_x \psi\,. \end{cases}$$

where $\widetilde{D}_x$, $\widetilde{D}_y$ are the centered difference operators

$$\text{(3.2.2)} \qquad \widetilde{D}_x u_{i,j} = \frac{u_{i+1,j} - u_{i-1,j}}{2h}\,, \qquad \widetilde{D}_y u_{i,j} = \frac{u_{i,j+1} - u_{i,j-1}}{2h}\,.$$

and $\triangle_h$ is the standard 5-point Laplacian $\triangle_h = D_x^2 + D_y^2$, where

$$\text{(3.2.3)} \qquad D_x^2 u_{i,j} = \frac{u_{i-1,j} - 2u_{i,j} + u_{i+1,j}}{h^2}\,, \quad D_y^2 u_{i,j} = \frac{u_{i,j-1} - 2u_{i,j} + u_{i,j+1}}{h^2}\,.$$

As we pointed out in the introduction, there are two boundary conditions for ψ. The Dirichlet boundary condition $\psi = 0$ on Γ was implemented to solve the

Reproduced with permission of the copyright owner. Further reproduction prohibited without permission.

stream function via the vorticity as in (3.2.1). Yet the normal boundary condition, $\frac{\partial \psi}{\partial n} = 0$, cannot be enforced directly. The way to overcome this difficulty is to convert it into the boundary condition for the vorticity. As we can see, by the fact that $\psi|_\Gamma = 0$, we have the approximation for the vorticity on the boundary (say on Γ_x, $j = 0$)

$$\omega_{i,0} = D_y^2 \psi_{i,0} = \frac{1}{h^2}(\psi_{i,1} + \psi_{i,-1}) = \frac{2\psi_{i,1}}{h^2} - \frac{2}{h}\frac{\psi_{i,1} - \psi_{i,-1}}{2h} \tag{3.2.4}$$

where (-1) refers to the "ghost" grid point outside of the computational domain. If we take $\frac{\psi_{i,1}-\psi_{i,-1}}{2h} = 0$, which implies that $\psi_{-1} = \psi_1$, as a second order normal boundary condition for $(\partial_y \psi)_{i,0} = 0$, we arrive at **Thom's formula**

$$\omega_{i,0} = \frac{2\psi_{i,1}}{h^2}. \tag{3.2.5}$$

We should mention here that by formal Taylor expansion, Thom's formula is only first order accurate for ω on the boundary. More sophisticated consistency analysis can guarantee the scheme is indeed 2nd order accurate, which was first proved in [HW].

The vorticity on the boundary can also be determined by other approximations of ψ_{-1}. For example, if we use a 3rd order one-sided approximation for the normal boundary condition $(\partial_y \psi)_{i,0} = 0$

$$(\partial_y \psi)_{i,0} = \frac{-\psi_{i,-1} + 3\psi_{i,1} - \frac{1}{2}\psi_{i,2}}{3h} = 0, \qquad \psi_{i,-1} = 3\psi_{i,1} - \frac{1}{2}\psi_{i,2}, \tag{3.2.6}$$

and plug back into the difference vorticity formula $\omega_{i,0} = \frac{1}{h^2}(\psi_{i,1} + \psi_{i,-1})$ as in (3.2.4), we have **Wilkes-Pearson's formula**

$$\omega_{i,0} = \frac{1}{h^2}(4\psi_{i,1} - \frac{1}{2}\psi_{i,2}). \tag{3.2.7}$$

See [PT] for more details. This formula gives us 2nd order accuracy for the vorticity on the boundary.

Reproduced with permission of the copyright owner. Further reproduction prohibited without permission.

The scheme (3.2.1), along with the vorticity boundary condition we mentioned above, either (3.2.5) or (3.2.7), can be implemented very efficiently via explicit treatment of the diffusion term and 4th order Runge-Kutta time-stepping.

3.3 Stability of Wilkes' Formula for Stokes Equations

One of the main concerns in the computations of Navier-Stokes equations are numerical stabilities. For simplicity, we only consider Stokes equations in this section, where nonlinear terms are neglected. The second order scheme applied to Stokes equations corresponding to (3.2.1) will turn out to be

$$\text{(3.3.1)} \qquad \begin{cases} \partial_t \omega = \nu \Delta_h \omega , \\ \Delta_h \psi = \omega , \qquad \psi \mid_\Gamma = 0 . \end{cases}$$

and either Thom's formula (3.2.5) or Wilkes' formula (3.2.7) can be chosen to implement (3.3.1).

Now we introduce some notations.

Notation. We will use the discrete L^2-norm and the discrete L^2-inner product

$$\text{(3.3.2)} \qquad \|u\| = \langle u , u \rangle^{1/2} , \qquad \langle u , v \rangle = \sum_{1 \le i,j \le N-1} u_{i,j} \, v_{i,j} \, h^2 .$$

For $u \mid_\Gamma = 0$, we introduce the notation $\|\nabla_h u\|$ by

$$\text{(3.3.3)} \qquad \|\nabla_h u\|^2 = \sum_{j=1}^{N-1} \sum_{i=0}^{N-1} (D_x^+ u_{i,j})^2 h^2 + \sum_{i=1}^{N-1} \sum_{j=0}^{N-1} (D_y^+ u_{i,j})^2 h^2 .$$

where $D_x^+ u$, $D_y^+ u$ are defined as

$$\text{(3.3.4)} \qquad D_x^+ u_{i,j} = \frac{u_{i+1,j} - u_{i,j}}{h} , \quad D_y^+ u_{i,j} = \frac{u_{i,j+1} - u_{i,j}}{h} .$$

First, we look at the stability argument of Thom's formula, which is straightforward. For Stokes equations, the stability analysis can be described as following:

Reproduced with permission of the copyright owner. Further reproduction prohibited without permission.

multiplying the equation in (3.3.1) by $-v$ we have $-\langle v, \partial_t \omega \rangle + \langle v, \Delta_h \omega \rangle = 0$. The first term is exactly

$$-\langle v, \partial_t \omega \rangle = -\langle v, \partial_t \Delta_h v \rangle = \frac{1}{2}\frac{d}{dt}\|\nabla_h v\|^2 . \tag{3.3.5}$$

where in the second step we used the fact that v vanishes on the boundary. The second term can be estimated via summing by parts

$$\langle v, \Delta_h \omega \rangle = \langle \Delta_h v, \omega \rangle + \mathcal{B} = \|\omega\|^2 + \mathcal{B} . \tag{3.3.6}$$

where we used the fact that $\Delta_h v = \omega$, and the boundary term $\mathcal{B}$ is decomposed into four parts: $\mathcal{B} = \mathcal{B}_1 + \mathcal{B}_2 + \mathcal{B}_3 + \mathcal{B}_4$

$$\begin{aligned} \mathcal{B}_1 &= \sum_{i=1}^{N-1} \psi_{i,1}\omega_{i,0} , \mathcal{B}_2 = \sum_{i=1}^{N-1} v_{i,N-1}\omega_{i,N} , \\ \mathcal{B}_3 &= \sum_{j=1}^{N-1} v_{1,j}\omega_{0,j} , \mathcal{B}_4 = \sum_{j=1}^{N-1} v_{N-1,j}\omega_{N,j} . \end{aligned} \tag{3.3.7}$$

As we can see, to ensure the stability of the scheme, an estimate to control the boundary term $\mathcal{B}$ is required. For simplicity of the presentation, we only consider $\mathcal{B}_1$ here. The other three boundary terms can be treated in the same way. We apply Thom's boundary condition (3.2.5) to recover $\mathcal{B}_1$

$$\mathcal{B}_1 = \sum_{i=1}^{N-1} v_{i,1} \cdot \frac{2\psi_{i,1}}{h^2} = \sum_{i=1}^{N-1} \frac{2v_{i,1}^2}{h^2} \geq 0 . \tag{3.3.8}$$

The other three boundary terms can be treated in the same way. Then we have the estimate $\mathcal{B} \geq 0$, whose substitution into (3.3.6), along with (3.3.5) gives us the stability of the second order scheme (3.3.1) with Thom's formula (3.2.5). This observation was first made by Meth in [MKZ]. It was also used in [HW] to prove the convergence of Thom's formula.

As we can see, Wilkes' formula (3.2.7) involves more interior points than Thom's formula (3.2.5). A natural question arises: is Wilkes' formula stable?

Reproduced with permission of the copyright owner. Further reproduction prohibited without permission.

We follow the procedure above. As we can see, (3.3.5), (3.3.6) are still valid. The only difference is the boundary term $\mathcal{B}$, which is still represented as in (3.3.7). Similarly, we only consider $\mathcal{B}_1$ here. Here, Wilkes' boundary condition (3.2.7) is applied to recover $\mathcal{B}_1$

$$\mathcal{B}_1 = \sum_{i=1}^{N-1} \frac{\psi_{i,1}}{h^2}(4v_{i,1} - \frac{1}{2}v_{i,2}) . \tag{3.3.9}$$

However, a direct calculation cannot control $\mathcal{B}_1$, since two interior points v_1 and v_2 of stream function are involved in Wilkes' formula. So the straightforward argument (3.3.8) does not work here. To overcome this difficulty, we can apply the property that v vanishes on the boundary and then rewrite the term $4v_{i,1} - \frac{1}{2}v_{i,2}$ as

$$4v_{i,1} - \frac{1}{2}v_{i,2} = 3v_{i,1} - \frac{1}{2}h^2 D_y^2 v_{i,1} . \tag{3.3.10}$$

The purpose of this transformation is to control local terms by global terms as we can see later. Now $\mathcal{B}_1$ can be estimated via applying Cauchy inequality for $v_{i,1}D_y^2 v_{i,1}$

$$\begin{aligned} \mathcal{B}_1 = & \sum_{i=1}^{N-1} \frac{\psi_{i,1}}{h^2}(3\psi_{i,1} - \frac{1}{2}h^2 D_y^2 v_{i,1}) \\ \geq & \sum_{i=1}^{N-1} (\frac{3\psi_{i,1}^2}{h^2} - \frac{1}{2h^2}\frac{1^2}{2^2}\psi_{i,1}^2 - \frac{1}{2}|D_y^2 v_{i,1}|^2 h^2) \\ \geq & -\sum_{i=1}^{N-1} \frac{1}{2}|D_y^2 \psi_{i,1}|^2 h^2 , \end{aligned} \tag{3.3.11}$$

where we used the fact that $3 - \frac{1}{2}\cdot\frac{1^2}{2^2} \geq 0$ in the last step. Repeating the same argument for $\mathcal{B}_2$, $\mathcal{B}_3$ and $\mathcal{B}_4$, we arrive at

$$\begin{aligned} \mathcal{B} \geq & -\frac{1}{2}\sum_{i=1}^{N-1}(|D_y^2 v_{i,1}|^2 + |D_y^2 v_{i,N-1}|^2)h^2 - \frac{1}{2}\sum_{j=1}^{N-1}(|D_x^2 v_{1,j}|^2 + |D_x^2 v_{N-1,j}|^2)h^2 \\ \geq & -\frac{1}{2}\|D_x^2 v\|^2 - \frac{1}{2}\|D_y^2 v\|^2 . \end{aligned} \tag{3.3.12}$$

Reproduced with permission of the copyright owner. Further reproduction prohibited without permission.

As can be seen, the transformation (3.3.10) and the application of Cauchy inequality helps us to bound the boundary term, which is a local term, by global terms $\|D_x^2 v\|^2$ and $\|D_y^2 v\|^2$. Our next aim is to control the terms $\|D_x^2 v\|^2$ and $\|D_y^2 v\|^2$ by $\|\omega\|^2$ appearing in the diffusion term. The following lemma is resorted.

Lemma 3.3.1 *For any v such that $v|_\Gamma = 0$, we have*

$$\|D_x^2 v\|^2 + \|D_y^2 v\|^2 \le \|(D_x^2 + D_y^2) v\|^2 = \|\omega\|^2 \tag{3.3.13}$$

Proof. Since $v_{i,j}$ is zero on Γ, we can take Sine transforms for $\{v_{i,j}\}$ in both i-direction and j-direction, i.e.,

$$v_{i,j} = \sum_{k,\ell} \widehat{v}_{k,\ell} \sin(k\pi x_i) \sin(\ell\pi y_j) . \tag{3.3.14}$$

Then Parserval equality gives

$$\sum_{i,j} (v_{i,j})^2 = \sum_{k,\ell} \left|\widehat{v}_{k,\ell}\right|^2 . \tag{3.3.15}$$

If we introduce

$$f_k = -\frac{4}{h^2} \sin^2(\frac{k\pi h}{2}) , \qquad g_\ell = -\frac{4}{h^2} \sin^2(\frac{\ell\pi h}{2}) , \tag{3.3.16}$$

we obtain the Fourier expansion of $D_x^2 v$ and $D_y^2 v$

$$\begin{aligned} D_x^2 v_{i,j} &= \sum_{k,l} f_k \widehat{v}_{k,l} \sin(k\pi x_i) \sin(\ell\pi y_j) , \\ D_y^2 v_{i,j} &= \sum_{k,l} g_\ell \widehat{v}_{k,l} \sin(k\pi x_i) \sin(\ell\pi y_j) , \end{aligned} \tag{3.3.17}$$

which implies that

$$\sum_{i,j} |\omega_{i,j}|^2 = \sum_{i,j} |\Delta_h v_{i,j}|^2 = \sum_{k,\ell} |g_\ell + f_k|^2 \, |\widehat{v}_{k,\ell}|^2 . \tag{3.3.18}$$

Since $f_k \le 0$, $g_\ell \le 0$, which indicates that $(f_k + g_\ell)^2 \ge f_k^2 + g_\ell^2$, we arrive at

$$\sum_{i,j} |\omega_{i,j}|^2 \ge \sum_{k,\ell} (f_k^2 + g_\ell^2) |\widehat{v}_{k,\ell}|^2 = \sum_{i,j} (|D_x^2 v_{i,j}|^2 + |D_y^2 v_{i,j}|^2) . \tag{3.3.20}$$

Reproduced with permission of the copyright owner. Further reproduction prohibited without permission.

which shows exactly (3.3.13).

The combination of Lemma 3.3.1 and (3.3.12) gives us that $B \geq -\frac{1}{2}\|\omega\|^2$. Plugging back into (3.3.6), along with (3.3.5), we have the stability estimate of the second order scheme with Wilkes' boundary condition

$$\frac{1}{2}\frac{d}{dt}\|\nabla_h \psi\|^2 + \frac{1}{2}\nu\|\omega\|^2 \leq 0\,. \tag{3.3.20}$$

Remark 3.3.1 The purpose of Lemma 3.3.1 is to control L^2 norms of $D_x^2\psi$ and $D_y^2\psi$ by the discrete Laplacian of ψ, which enables us to control local terms by the global diffusion term. In fact it is a discrete version of the elliptic regularity for (discrete) Poisson equation.

Remark 3.3.2 Let's review our stability analysis for Wilkes' formula. The main difficulty comes from the boundary term. Our trick is to rewrite it via the boundary condition for vorticity, therefore convert it into an expression in terms of ψ near the boundary. Next, we apply Cauchy inequality to bound it by $\|D_x^2\psi\|^2$ and $\|D_y^2\psi\|^2$. Then we can apply an estimate like (3.3.13), control $\|D_x^2\psi\|^2$ and $\|D_y^2\psi\|^2$ by $\|\omega\|^2$, which leads to the bound of the boundary term by the diffusion term.

This methodology is quite general. The original idea of it was proposed in [ELV2] to show the stability of a fourth order method. We will use it in the next chapter to study higher order vorticity boundary conditions in 4-th order scheme.

Reproduced with permission of the copyright owner. Further reproduction prohibited without permission.

3.4 Analysis Of Second Order Scheme for 2-D NSE

We state our main theorem in our paper.

Theorem 3.4.1. *Let $\boldsymbol{u}_e \in L^\infty([0,T]; C^{5,\alpha}(\bar{\Omega}))$. v_e, ω_e be the exact solution of the Navier-Stokes equations (3.1.1), (3.1.2) and $\boldsymbol{u}_h$, ω_h be the approximate solution of the second order scheme (3.2.1) with Pearson-Wilkes formula (3.2.7), we have*

(3.4.1)

$$\|\boldsymbol{u}_e - \boldsymbol{u}_h\|_{L^\infty([0,T],L^2)} + \sqrt{\nu}\|\omega_e - \omega_h\|_{L^2([0,T],L^2)}$$
$$\leq Ch^2\|\boldsymbol{u}_e\|_{L^\infty([0,T],C^{5,\alpha})}\Big(1 + \|\boldsymbol{u}_e\|_{L^\infty([0,T],C^3)}\Big)\exp\left\{\frac{CT}{\nu}(1 + \|\boldsymbol{u}_e\|^2_{L^\infty([0,T],C^1)})\right\}.$$

In the convergence proof, we follow the standard procedure of consistency, stability and error analysis. Difficulty in the consistency analysis arises from the fact that centered difference is used at the interior points, while one-sided formula is used for the vorticity on the boundary. This difficulty is overcome by our construction of an approximate vorticity through finite differences of the exact stream function. All of the truncation errors are then lumped into the momentum equation. Since Wilkes' formula is second order accurate on the boundary, we can avoid Strang type expansion. This results in an easy consistency analysis near the boundary, which shows that the error function for the vorticity on the boundary is of order $O(h^2)$. The stability of Wilkes' formula has already been established in Section 3.3. Our error analysis follows the strategy and arguments in Section 3.3.

Reproduced with permission of the copyright owner. Further reproduction prohibited without permission.

3.4.1 Consistency Analysis

Let $\Psi_{i,j} = \psi_e(x_i, y_j)$ for $-1 \le i, j \le N+1$. (here we extended ψ_e smoothly to $[-\delta, 1+\delta]^2$), and construct U, V, Ω through the finite difference of Ψ to maintain the consistency, especially near the boundary.

$$(3.4.2)\quad U_{i,j} = -\widetilde{D}_y \Psi\,, \qquad V_{i,j} = \widetilde{D}_x \Psi\,, \qquad \Omega_{i,j} = \triangle_h \Psi\,, \qquad \text{for } 0 \le i, j \le N\,.$$

Then direct Taylor expansion for ψ_e up to the boundary gives us that at grid points (x_i, y_j), $0 \le i, j \le N$,

$$\begin{aligned} U &= u_e - \frac{h^2}{6}\partial_y^3 \psi_e + O(h^3)\|\psi_e\|_{C^4}\,. \\ V &= v_e + \frac{h^2}{6}\partial_x^3 \psi_e + O(h^3)\|\psi_e\|_{C^4}\,. \\ \Omega &= \omega_e + \frac{h^2}{12}(\partial_x^4 + \partial_y^4)\psi_e + O(h^4)\|\psi_e\|_{C^6}\,. \end{aligned} \tag{3.4.3}$$

It is obvious that at these grid points, (including boundary points)

$$(3.4.4)\quad |U - u_e| + |V - v_e| + |\Omega - \omega_e| \le Ch^2 \|\psi_e(\cdot, t)\|_{C^4}\,.$$

Now we look at the local truncation errors. We will show that the constructed U, V, Ω constructed in (3.4.2) satisfy the numerical scheme (3.2.1), (3.2.7) up to $O(h^2)$ error. First we look at the diffusion term. (3.4.3) indicates

$$(3.4.5)\quad \triangle_h \Omega = \triangle_h \omega_e + O(h^2)\|\psi_e\|_{C^6}\,.$$

which along with Taylor expansion of ω_e that

$$(3.4.6)\quad \triangle_h \omega_e = \triangle \omega_e + O(h^2)\|\omega_e\|_{C^4} = \triangle \omega_e + O(h^2)\|\psi_e\|_{C^6}\,.$$

leads to the estimate of the diffusion term: at grid points (x_i, y_j), $1 \le i, j \le N-1$.

$$(3.4.7)\quad \triangle_h \Omega = \triangle \omega_e + O(h^2)\|\psi_e(\cdot, t)\|_{C^6}\,.$$

Reproduced with permission of the copyright owner. Further reproduction prohibited without permission.

The nonlinear convection terms can be treated in a similar fashion. (3.4.3) implies that at grid points (x_i, y_j), $0 \le i, j \le N$.

$$(3.4.8) \qquad U\Omega = u_e\omega_e - \frac{h^2}{6}\omega_e\partial_y^3 v_e + \frac{h^2}{12}u_e(\partial_x^4 + \partial_y^4)v_e + O(h^3)\|v_e\|_{C^6}\|v_e\|_{C^4}\,.$$

which leads to the estimate at interior grid points (x_i, y_j), $1 \le i, j \le N-1$.

$$(3.4.9) \qquad \begin{aligned} \widetilde{D}_x(U\Omega) = &\ \widetilde{D}_x(u_e\omega_e) - \frac{h^2}{6}\widetilde{D}_x(\omega_e\partial_y^3 v_e) \\ + &\ \frac{h^2}{12}\widetilde{D}_x\Big(u_e(\partial_x^4 + \partial_y^4)v_e\Big) + O(h^2)\|v_e\|_{C^4}\|v_e\|_{C^6} \\ = &\ \widetilde{D}_x(u_e\omega_e) + O(h^2)\|v_e\|_{C^4}\|v_e\|_{C^6}\,. \end{aligned}$$

Moreover, Taylor expansion for $u_e\omega_e$ gives $\widetilde{D}_x(u_e\omega_e) = \partial_x(u_e\omega_e) + O(h^2)\|u_e\omega_e\|_{C^3}$, thus

$$(3.4.10) \qquad \widetilde{D}_x(u_e\omega_e) = \partial_x(u_e\omega_e) + O(h^2)\|v_e\|_{C^5}\|v_e\|_{C^3}\,.$$

Then we arrive at

$$(3.4.11) \qquad \widetilde{D}_x(U\Omega) = \partial_x(u_e\omega_e) + O(h^2)\|v_e\|_{C^4}\|v_e\|_{C^6}\,.$$

The similar result can be obtained for $\widetilde{D}_y(V\Omega)$

$$(3.4.12) \qquad \widetilde{D}_y(V\Omega) = \partial_y(v_e\omega_e) + O(h^2)\|v_e\|_{C^4}\|v_e\|_{C^6}\,.$$

Next we deal with the time marching term $\partial_t\Omega$. The strategy here is to control the difference between $\partial_t\Omega$ and $\partial_t\omega_e$ by $O(h^2)$ of $\|\partial_t v_e\|_{C^4}$

$$(3.4.13) \qquad \partial_t\Omega - \partial_t\omega_e = \triangle_h\partial_t v_e - \triangle\partial_t\psi_e = (\triangle_h - \triangle)\partial_t v_e = O(h^2)\|\partial_t v_e\|_{C^4}\,.$$

Yet, to get an estimate of $\|\partial_t v_e\|_{C^4}$, we have to apply Schauder estimate to the following Poisson equation

$$(3.4.14) \qquad \begin{cases} \triangle(\partial_t v_e) = \partial_t\omega_e\,, & \text{in } \Omega\,, \\ \partial_t v_e = 0\,. & \text{on } \Gamma\,. \end{cases}$$

Reproduced with permission of the copyright owner. Further reproduction prohibited without permission.

which gives us that for $\alpha > 0$.

$$\|\partial_t v_e\|_{C^{4,\alpha}} \le C\|\partial_t \omega_e\|_{C^{2,\alpha}} \le C(\|v_e\|_{C^{6,\alpha}} + \|v_e\|_{C^{5,\alpha}}\|v_e\|_{C^{3,\alpha}}) . \tag{3.4.15}$$

where in the second step we applied the exact vorticity equation that $\partial_t \omega_e + \boldsymbol{u}_e \cdot \nabla \omega_e = \nu \triangle \omega_e$. The combination of (3.4.13) and (3.4.15) gives us

$$\partial_t \Omega - \partial_t \omega_e = O(h^2)(\|\psi_e\|_{C^{6,\alpha}} + \|v_e\|_{C^{5,\alpha}}\|v_e\|_{C^{3,\alpha}}) . \tag{3.4.16}$$

Combining (3.4.7), (3.4.11), (3.4.12) and (3.4.16), and applying the original PDE of the exact solution that $\partial_t \omega_e + \nabla \cdot (\boldsymbol{u}_e \omega_e) = \nu \triangle \omega_e$, we conclude that

$$\partial_t \Omega + \widetilde{D}_x(U\Omega) + \widetilde{D}_y(V\Omega) = \triangle_h \Omega + O(h^2)\|v_e\|_{C^{6,\alpha}}(1 + \|v_e\|_{C^4}) . \tag{3.4.17}$$

which verifies our claim.

Finally we look at our constructed Ω on the boundary. Our aim is to show that Ω satisfies Wilkes' formula applied to Ψ up to an $O(h^2)$ error. The verification of it is straightforward. We only consider Γ_x, $j = 0$ here. The other three boundaries can be dealt with in the same way. One-sided Taylor expansion for Ψ in the y-th direction near the boundary shows that

$$\begin{aligned} \frac{1}{h^2}(4\Psi_{i,1} - \frac{1}{2}\Psi_{i,2}) &= \partial_y^2 \psi_e(x_i, 0) + O(h^2)\|v_e\|_{C^4} \\ &= \omega_e(x_i, 0) + O(h^2)\|v_e\|_{C^4} . \end{aligned} \tag{3.4.18}$$

On the other hand, (3.4.4) gives us that the difference between $\Omega_{i,0}$ and $\omega_e(x_i, 0)$ on Γ_x is also of order $O(h^2)\|v_e\|_{C^4}$, then we arrive at

$$\Omega_{i,0} = \frac{1}{h^2}(4\Psi_{i,1} - \frac{1}{2}\Psi_{i,2}) + O(h^2)\|v_e\|_{C^4} . \tag{3.4.19}$$

Thus the consistency analysis is completed.

3.4.2 Error Estimate

For $0 \le i, j \le N$, we define

(3.4.20)

$$\tilde{v}_{i,j} = v_{i,j} - \Psi_{i,j} , \quad \tilde{\omega}_{i,j} = \omega_{i,j} - \Omega_{i,j} , \quad \tilde{u}_{i,j} = u_{i,j} - U_{i,j} , \quad \tilde{v}_{i,j} = v_{i,j} - V_{i,j} .$$

Reproduced with permission of the copyright owner. Further reproduction prohibited without permission.

Then the above consistency analysis gives the following system for the error functions

$$\text{(3.4.21)}\qquad \begin{cases} \partial_t\tilde{\omega} + \widetilde{D}_x(\tilde{u}\Omega + u\tilde{\omega}) + \widetilde{D}_y(\tilde{v}\Omega + v\tilde{\omega}) = \nu\triangle_h\tilde{\omega} + \boldsymbol{f}\,. \\ \triangle_h\tilde{\psi} = \tilde{\omega}\,. \qquad \tilde{\psi}\,|_\Gamma = 0\,. \\ \tilde{u} = -\widetilde{D}_y\tilde{\psi}\,, \quad \tilde{v} = \widetilde{D}_x\tilde{\psi}\,, \qquad \tilde{u}\,|_{\Gamma_y} = 0\,. \qquad \tilde{v}\,|_{\Gamma_x} = 0\,. \end{cases}$$

where $|\boldsymbol{f}| \le Ch^2\|\boldsymbol{u}_e\|_{C^{5,\alpha}}(1 + \|\boldsymbol{u}_e\|_{C^3})$. On the boundary, (say at Γ_x, $j = 0$) we have

$$\text{(3.4.22)}\qquad \tilde{\omega}_{i,0} = \frac{1}{h^2}(4\tilde{\psi}_{i,1} - \frac{1}{2}\tilde{\psi}_{i,2}) + h^2\boldsymbol{e}_i\,.$$

where $|\boldsymbol{e}_i| \le C\|\boldsymbol{u}_e\|_{C^3}$. (3.4.22) comes from Wilkes' formula (3.2.7) and our estimate (3.4.19). In other words, the error function of vorticity and the error function of stream function satisfy Wilkes' formula up to an $O(h^2)$ error.

As we can see, the system (3.4.21), (3.4.22) is very similar to the second order scheme (3.2.1) along with the Wilkes' formula (3.2.7) except for the error terms $\boldsymbol{f}$ and $h^2\boldsymbol{e}$. In other words, as we showed in the consistency part, the constructed solutions satisfy the numerical scheme except for some local truncation errors. We have already shown the stability of the scheme in Section 3, so we can apply the same procedure to estimate the error functions. The error terms corresponding to $\boldsymbol{f}$ and $\boldsymbol{e}$ can be estimated by Cauchy inequalities.

Multiplying the vorticity dynamic error equation in (3.4.21) by $-\tilde{\omega}$, we have

$$\text{(3.4.23)}\quad -\langle\tilde{\omega}, \partial_t\tilde{\omega}\rangle + \langle\tilde{\omega}, \triangle_h\tilde{\omega}\rangle = \langle\tilde{\psi}, \widetilde{D}_x(\tilde{u}\Omega + u\tilde{\omega})\rangle + \langle\tilde{\omega}, \widetilde{D}_y(\tilde{v}\Omega + v\tilde{\omega})\rangle - \langle\tilde{\omega}, \boldsymbol{f}\rangle\,.$$

The first term, which is corresponding to time evolution term, can be dealt with in the way as in (3.3.5) since $\tilde{\psi}$ also vanishes on the boundary, i.e.

$$\text{(3.4.24)}\qquad -\langle\tilde{\omega}, \partial_t\tilde{\omega}\rangle = -\langle\tilde{\psi}, \partial_t\triangle_h\tilde{\psi}\rangle = \frac{1}{2}\frac{d}{dt}\|\nabla_h\tilde{\psi}\|^2\,.$$

The term $-\langle\tilde{\omega}, \boldsymbol{f}\rangle$ can be controlled by standard Cauchy inequality. Then the rest of our work will be concentrated on the estimates of the diffusion term and the convection terms. We will resort to Lemma 3.4.1 and Lemma 3.4.2 as below.

Reproduced with permission of the copyright owner. Further reproduction prohibited without permission.

Lemma 3.4.1 *For sufficiently small h, we have*

$$\langle \tilde{\omega}, \Delta_h \tilde{\omega} \rangle \geq \frac{1}{2}\|\tilde{\omega}\|^2 - h^4 . \tag{3.4.25}$$

Proof. Our proof of (3.4.25) follows the procedure of stability analysis in Section 3.3 Summing by parts and using the fact that $\tilde{\omega}\,|_\Gamma = 0$ gives us

$$\langle \tilde{\omega}, \Delta_h \tilde{\omega} \rangle = \langle \tilde{\omega}, (D_x^2 + D_y^2)\tilde{\omega} \rangle = \langle D_x^2 \tilde{\omega}, \tilde{\omega} \rangle + \langle D_y^2 \tilde{\omega}, \tilde{\omega} \rangle + \mathcal{B} = \|\tilde{\omega}\|^2 + \mathcal{B} , \tag{3.4.26}$$

where the boundary term $\mathcal{B}$ can also be decomposed into $\mathcal{B} = \mathcal{B}_1 + \mathcal{B}_2 + \mathcal{B}_3 + \mathcal{B}_4$ as in (3.3.7)

$$\begin{aligned} \mathcal{B}_1 &= \sum_{i=1}^{N-1} \tilde{\psi}_{i,1}\tilde{\omega}_{i,0} , \mathcal{B}_2 = \sum_{i=1}^{N-1} \tilde{\psi}_{i,N-1}\tilde{\omega}_{i,N} , \\ \mathcal{B}_3 &= \sum_{j=1}^{N-1} \tilde{\psi}_{1,j}\tilde{\omega}_{0,j} , \mathcal{B}_4 = \sum_{j=1}^{N-1} \tilde{\psi}_{N-1,j}\tilde{\omega}_{N,j} . \end{aligned} \tag{3.4.27}$$

The estimate of $\mathcal{B}_1$ is also similar to that in Section 3.3. The only difference here is that $\tilde{\omega}_{i,0}$, the error of vorticity on the boundary as in (3.4.22), includes one more error term $h^2 \boldsymbol{e}_i$, whose L^2 product with $\tilde{\psi}$ can be estimated by Cauchy inequality. By (3.4.22), we can express $\mathcal{B}_1$ as

$$\mathcal{B}_1 = \sum_{i=1}^{N-1} \tilde{\psi}_{i,1}\tilde{\omega}_{i,0} = \frac{1}{h^2}\sum_{i=1}^{N-1} \tilde{\psi}_{i,1}(4\tilde{\psi}_{i,1} - \frac{1}{2}\tilde{\psi}_{i,2}) + h^2 \sum_{i=1}^{N-1} \tilde{\psi}_{i,1}\boldsymbol{e}_i \equiv I_1 + I_2 . \tag{3.4.28}$$

As we mentioned just now, I_2 can be controlled by Cauchy inequality directly

$$I_2 = \sum_i h^2 \tilde{\psi}_{i,1}\boldsymbol{e}_i \geq -\frac{1}{2}\sum_{i=1}^{N-1} \frac{\tilde{\psi}_{i,1}^2}{h^2} - \frac{1}{2}\sum_{i=1}^{N-1} h^6 \boldsymbol{e}_i^2 \geq -\frac{1}{2}\sum_{i=1}^{N-1} \frac{\tilde{\psi}_{i,1}^2}{h^2} - Ch^5\|\boldsymbol{u}_e\|_{C^3}^2 , \tag{3.4.29}$$

where in the last step we applied our estimate that $|\boldsymbol{e}_i| \leq C\|\boldsymbol{u}_e\|_{C^3}$and the fact that $h = \frac{1}{N}$. The estimate of I_1 follows our stability analysis in Section 3.3. First, we rewrite the term appearing in the parentheses as the way in (3.3.10):

$$4\tilde{\psi}_{i,1} - \frac{1}{2}\tilde{\psi}_{i,2} = 3\tilde{\psi}_{i,1} - \frac{1}{2}h^2(D_y^2\tilde{\psi})_{i,1} . \tag{3.4.30}$$

Reproduced with permission of the copyright owner. Further reproduction prohibited without permission.

which is still valid since $\tilde{\psi}$ vanishes on the boundary. The purpose of this transformation is still to control local terms by global terms as we can see later. Next, plugging (3.4.30) back into I_1

(3.4.31)
$$I_1 = \frac{1}{h^2}\sum_{i=1}^{N-1}\tilde{\omega}_{i,1}\Big(3\tilde{\omega}_{i,1} - \frac{1}{2}h^2(D_y^2\tilde{\omega})_{i,1}\Big) = \frac{3}{h^2}\sum_{i=1}^{N-1}\tilde{\omega}_{i,1}^2 - \frac{1}{2}\sum_{i=1}^{N-1}\tilde{\omega}_{i,1}(D_y^2\tilde{\omega})_{i,1}\,.$$

and applying Cauchy inequality to the second term $\tilde{\omega}_{i,1}(D_y^2\tilde{\psi})_{i,1}$, we arrive at

(3.4.32)
$$\begin{aligned} I_1 &\geq \frac{3}{h^2}\sum_{i=1}^{N-1}\tilde{\omega}_{i,1}^2 - \frac{1}{8h^2}\sum_{i=1}^{N-1}\tilde{\omega}_{i,1}^2 - \frac{1}{2}\sum_{i=1}^{N-1}\Big|(D_y^2\tilde{\psi})_{i,1}\Big|^2 h^2 \\ &\geq \frac{2}{h^2}\sum_{i=1}^{N-1}\tilde{\omega}_{i,1}^2 - \frac{1}{2}\sum_{i=1}^{N-1}\Big|D_y^2\tilde{\psi}_{i,1}\Big|^2 h^2\,. \end{aligned}$$

Finally, (3.4.29) and (3.4.32) gives that for sufficiently small h,

(3.4.33)
$$\mathcal{B}_1 \geq \frac{1}{h^2}\sum_{i=1}^{N-1}\tilde{\omega}_{i,1}^2 - \frac{1}{2}\sum_{i=1}^{N-1}\Big|D_y^2\tilde{\psi}_{i,1}\Big|^2 h^2 - \frac{1}{4}h^4\,.$$

The treatment of the other three boundary terms is essentially the same. Now we recover $\mathcal{B}$ by global terms $\|D_x^2\tilde{\psi}\|^2$ and $\|D_y^2\tilde{\psi}\|^2$

(3.4.34)
$$\mathcal{B} \geq -\frac{1}{2}\|D_y^2\tilde{\psi}\|^2 - \frac{1}{2}\|D_x^2\tilde{\psi}\|^2 - h^4\,.$$

As we can see, since $\tilde{\psi}|_\Gamma = 0$, Lemma 3.3.1 is still valid for $\tilde{\psi}$ and $\tilde{\omega}$, i.e.

(3.4.35)
$$\|D_x^2\tilde{\psi}\|^2 + \|D_y^2\tilde{\psi}\|^2 \leq \|(D_x^2 + D_y^2)\tilde{\psi}\|^2 = \|\tilde{\omega}\|^2\,.$$

Substituting (3.4.35) into (3.4.34), plugging back into (3.4.26), we obtain (3.4.25) finally. Lemma 3.4.1 is proved.

Lemma 3.4.2 *Assume a-prior that the error function for the velocity field satisfy*

(3.4.36)
$$\|\tilde{\boldsymbol{u}}\|_{L^\infty} \leq 1\,,$$

then we have

(3.4.37)
$$(\tilde{\psi}, \tilde{D}_x(\tilde{u}\Omega + u\tilde{\omega})) \leq \frac{8C_1^2}{\nu}\|\nabla_h\tilde{\psi}\|^2 + \frac{\nu}{6}\|\tilde{\omega}\|^2\,.$$

Reproduced with permission of the copyright owner. Further reproduction prohibited without permission.

and

$$(3.4.38)\qquad (\tilde{v}, \widetilde{D}_y(\tilde{v}\Omega + v\tilde{\omega})) \le \frac{8C_1^2}{\nu}\|\nabla_h \tilde{v}\|^2 + \frac{\nu}{6}\|\tilde{\omega}\|^2 .$$

where $C_1 = 1 + \|\boldsymbol{u}_e\|_{C^1}$.

Proof. We will only prove (3.4.37). The proof of (3.4.38) is essentially the same. By the a-prior bound (3.4.36) and our construction of U and Ω, we have

$$(3.4.39)\qquad \begin{aligned} &\|u\|_{L^\infty} \le \|U\|_{L^\infty} + \|\tilde{u}\|_{L^\infty} \le \|\partial_y \psi_e\|_{C^1} + 1 \le \|\boldsymbol{u}_e\|_{C^0} + 1 \le C_1 \\ &\|\Omega\|_{L^\infty} \le \|\partial_x^2 \psi_e\|_{C^0} + \|\partial_y^2 \psi_e\|_{C^0} \le \|\boldsymbol{u}_e\|_{C^1} \le C_1 . \end{aligned}$$

where $C_1 = \|\boldsymbol{u}_e\|_{C^1} + 1$. Summing by parts and applying (3.4.36), we obtain

(3.4.40)

$$\begin{aligned} \langle \tilde{v}, \widetilde{D}_x(\tilde{u}\Omega + u\tilde{\omega})\rangle &= -\langle \widetilde{D}_x\tilde{\psi}, \tilde{u}\Omega + u\tilde{\omega}\rangle \\ &\le C_1\|\nabla_h\tilde{\psi}\|(\|\tilde{u}\| + \|\tilde{\omega}\|) \le \frac{8C_1^2}{\nu}\|\nabla_h\tilde{v}\|^2 + \frac{\nu}{6}\|\tilde{\omega}\|^2 . \end{aligned}$$

where we used the fact that the norms $\|\widetilde{D}_x\tilde{\psi}\|$, $\|\widetilde{D}_y\tilde{\psi}\|$ are bounded by $\|\nabla_h\tilde{v}\|$.

$$(3.4.41)\qquad \|\tilde{u}\| = \|\widetilde{D}_y\tilde{\psi}\| \le \|\nabla_h\tilde{\psi}\| , \qquad \|\tilde{v}\| = \|\widetilde{D}_x\tilde{\psi}\| \le \|\nabla_h\tilde{v}\| .$$

since $\tilde{v}$ vanishes on the boundary. Lemma 3.4.2 is proved.

Now go back to our convergence analysis. First we assume that (3.4.36) holds. Plugging (3.4.37), (3.4.38), (3.4.25) along with (3.4.24) back into (3.4.23), we obtain

$$(3.4.42)\qquad \frac{1}{2}\frac{d}{dt}\|\nabla_h\tilde{v}\|^2 \le C\|\boldsymbol{f}\|^2 + \frac{16C_1^2}{\nu}\|\nabla_h\tilde{v}\|^2 - \frac{\nu}{6}\|\tilde{\omega}\|^2 + h^4 .$$

where we absorbed the term $C\|\tilde{\psi}\|^2$ generated by Cauchy inequality: $|(\tilde{v}, \boldsymbol{f})| \le C\|\tilde{v}\|^2 + C\|\boldsymbol{f}\|^2$ into the coefficient of $\|\nabla_h\tilde{\psi}\|^2$, which is valid since we can apply Poincare inequality for $\tilde{v}$ that

$$(3.4.43)\qquad \|\tilde{v}\|^2 \le C\|\nabla_h\tilde{\psi}\|^2 ,$$

Reproduced with permission of the copyright owner. Further reproduction prohibited without permission.

by the fact that $\tilde{\omega}$ vanishes on the boundary. Applying Gronwall inequality to (3.4.42), we have

$$
\begin{aligned}
&\|\nabla_h \tilde{\omega}\|^2 + \frac{\nu}{6}\int_0^t \|\tilde{\omega}\|^2\, dt \\
&\le C(\exp\frac{16C_1^2 t}{\nu})\int_0^t (\|\boldsymbol{f}(\cdot,s)\|^2 + h^4)\, ds + CTh^4 \\
&\le Ch^4 \exp\left\{\frac{16C_1^2 t}{\nu}\right\}\left(\|\boldsymbol{u}_e\|^2_{C^{5,\alpha}}(1+\|\boldsymbol{u}_e\|_{C^3})^2 + T\right).
\end{aligned}
\tag{3.4.44}
$$

Thus, we have proved

(3.4.45)

$$
\begin{aligned}
&\|\boldsymbol{u}(\cdot,t) - \boldsymbol{u}(t)\|_{L^2} + \sqrt{\nu}\Big(\int_0^T \|\tilde{\omega}\|^2 dt\Big)^{\frac{1}{2}} \\
&\qquad \le Ch^2\Big(\|\boldsymbol{u}_e\|_{C^{5,\alpha}}(1+\|\boldsymbol{u}_e\|_{C^3})\exp\left\{\frac{CT}{\nu}(1+\|\boldsymbol{u}_e\|_{C^1})^2\right\} + T\Big).
\end{aligned}
$$

which implies (3.4.1). Using the inverse inequality, we have

$$
\|\tilde{\boldsymbol{u}}\|_{L^\infty} \le Ch\,. \tag{3.4.46}
$$

Now we can resort to a standard trick which asserts that (3.4.36) will never be violated if h is small enough. Theorem 3.4.1 is proved.

3.5 Numerical Tests and Accuracy Check

In this section we check the numerical accuracy of our second order scheme, with either Thom's formula or Wilkes' formula. The computational domain is $[0,1]^2$. The exact stream function, velocity and vorticity are chosen to be

$$
\begin{aligned}
\psi_e(\boldsymbol{x},t) &= \tfrac{1}{2\pi^2}\sin^2(\pi x)\sin^2(\pi y)\cos t\,, \\
u_e(\boldsymbol{x},t) &= -\tfrac{1}{2\pi}\sin^2(\pi x)\sin(2\pi y)\cos t\,, \\
v_e(\boldsymbol{x},t) &= \tfrac{1}{2\pi}\sin(2\pi x)\sin^2(\pi y)\cos t\,, \\
\omega_e(\boldsymbol{x},t) &= \Big(\sin^2(\pi x)\sin(2\pi y) + \sin^2(\pi y)\sin(2\pi x)\Big)\cos t\,.
\end{aligned}
\tag{3.5.1}
$$

Reproduced with permission of the copyright owner. Further reproduction prohibited without permission.

The force term will come out if we substitute (3.5.1) into the momentum equation

$$\partial_t \omega_e + \nabla \cdot (\boldsymbol{u}_e \omega_e) = \nu \triangle \omega_e + \boldsymbol{f} \,. \tag{3.5.2}$$

where $\boldsymbol{f}$ is expressed as

(3.5.3)

$$\begin{aligned} \boldsymbol{f} = \; & -\sin t(\sin^2(\pi x)\cos(2\pi y) + \sin^2(\pi y)\cos(2\pi x)) \\ & + \frac{1}{2}\sin(2\pi y)\sin(2\pi x)\cos^2 t[-\sin^2(\pi x)(1 - 4\sin^2(\pi y)) \\ & \qquad + \sin^2(\pi y)(1 - 4\sin^2(\pi x))] \\ & - 4\pi^2 \nu \cos t \left[\cos(2\pi x)\cos(2\pi y) - \sin^2(\pi y)\cos(2\pi x) - \sin^2(\pi x)\cos(2\pi y)\right] . \end{aligned}$$

We apply our second order numerical scheme (3.2.1), along with either Thom's formula (3.2.5) or Wilkes' formula (3.2.7) as the boundary condition for vorticity. The force term $\boldsymbol{f}$ as in (3.5.3) is added when we update the momentum equation in (3.2.1). The viscosity $\nu = 0.001$, and the final time is taken to be $t = 6.0$. Explicit treatment of the diffusion term and the fourth order Runge-Kutta time stepping were used (see E and Liu [ELV1] for detail). The absolute errors between the numerical and exact solutions are listed in Table 3.1, 3.2. As can be seen in Table 3.1, if the second order method with Thom's boundary condition is used, exactly second order accuracy, in both L^1, L^2 and L^∞ norms, is achieved for the stream function. The vorticity achieves almost second order accuracy in L^1, L^2 norms and a little less than second order accuracy in L^∞ norm. It can be seen in Table 3.2 that the second order scheme with Wilkes' formula on the boundary indicates almost the same result as that with Thom's formula: exactly second order accuracy for both stream function and vorticity in L^1, L^2 norms, exactly second order accuracy in L^∞ norm for stream function and a little less than second order accuracy in L^∞ norm for vorticity. In other words, the orders of accuracy of these two formulas for both stream function and vorticity are almost the same.

Reproduced with permission of the copyright owner. Further reproduction prohibited without permission.

Table 3.1: Error and order of accuracy for stream function and vorticity at $t = 6$ when the second order scheme with **Thom's formula** for the vorticity at the boundary are used. CFL=0.5, where CFL $= \frac{\Delta t}{\Delta x}$.

	N	L^1 error	L^1 order	L^2 error	L^2 order	L^∞ error	L^∞ order
ψ	32	3.79e-05		5.73e-05		1.53e-04	
	64	9.45e-06	2.00	1.43e-05	2.00	3.83e-05	2.00
	128	2.36e-06	2.00	3.58e-06	2.00	9.56e-06	2.00
	256	5.90e-07	2.00	8.94e-07	2.00	2.39e-06	2.00
ω	32	7.49e-04		1.01e-03		2.44e-03	
	64	1.96e-04	1.93	2.61e-04	1.95	6.57e-04	1.89
	128	5.07e-05	1.95	6.74e-05	1.95	2.26e-04	1.54
	256	1.29e-05	1.98	1.72e-05	1.97	6.50e-05	1.80

Table 3.2: Errors and order of accuracy for stream function and vorticity at $t = 6$ when the second order scheme with **Wilkes' formula** for the vorticity at the boundary are used. CFL=0.5, where CFL $= \frac{\Delta t}{\Delta x}$.

	N	L^1 error	L^1 order	L^2 error	L^2 order	L^∞ error	L^∞ order
ψ	32	3.71e-05		5.67e-05		1.52e-04	
	64	9.35e-06	1.99	1.42e-05	2.00	3.81e-05	2.00
	128	2.35e-06	1.99	3.57e-06	2.00	9.55e-06	2.00
	256	5.89e-07	2.00	8.94e-07	2.00	2.39e-06	2.00
ω	32	7.78e-04		1.06e-03		2.46e-03	
	64	1.99e-04	1.97	2.66e-04	1.99	7.58e-04	1.70
	128	5.09e-05	1.97	6.76e-05	1.98	2.07e-04	1.87
	256	1.29e-05	1.98	1.72e-05	1.98	6.09e-05	1.77

Reproduced with permission of the copyright owner. Further reproduction prohibited without permission.

CHAPTER 4
CONVERGENCE OF A FOURTH ORDER METHOD

4.1 Preliminary

As the same in Chapter 3, we start with the 2-D NSE in vorticity-stream function formulation:

$$\begin{cases} \partial_t \omega + \nabla \cdot (\boldsymbol{u}\omega) = \nu \triangle \omega , \\ \triangle \psi = \omega , \\ u = -\partial_y \psi , \qquad v = \partial_x \psi \end{cases} \tag{4.1.1}$$

with the no-slip boundary condition written in terms of the stream function ψ:

$$\psi = 0, \quad \frac{\partial \psi}{\partial \mathbf{n}} = 0 . \tag{4.1.2}$$

Here $\boldsymbol{u} = (u, v)$ denotes the velocity field, ω denotes the vorticity.

The subject of fourth order schemes for (4.1.1), (4.1.2) has attracted considerable attention recently. For example, E and Liu proposed Essentially Compact fourth order scheme (EC4) in [ELV2], and proved the fourth order convergence of the method. Their analysis resorts to Strang type high order expansion. A technical assumption of one-sided physical, one-sided periodic boundary condition was also imposed.

The purpose of this paper is to give a thorough analysis of the fourth order scheme proposed by them. The boundary condition for vorticity will also be

Reproduced with permission of the copyright owner. Further reproduction prohibited without permission.

analyzed in detail. Briley's formula, which was derived in [BRL], was used in [ELV2]. We will derive a new formula in this paper, which gives higher order accuracy for the vorticity on the boundary by formal Taylor expansion. First we present the main idea of the convergence analysis and an accuracy check for a 1-D model for the Stokes problem. The advantage of this 1-D model is its simplicity: we can easily see why Briley's formula gives full 4th order accuracy although the formal Taylor expansion of it only indicates 3rd order accuracy on the boundary. This is accomplished by making expansions which are implemented by a third order polynomial. Then we treat the full Navier-Stokes equations in 2-D with a $[0, 1]^2$ box as the domain, with the physical boundary condition (4.1.2) applied on all boundaries. We then present the convergence proof for the analogous 4th order (EC4) scheme with our new 4-th order vorticity boundary condition. The use of this new boundary condition simplifies the consistency analysis. No Strang type expansion is needed.

The procedure of our convergence proof is standard: consistency analysis and error estimate. Consistency analysis is similar to that in the second chapter. Yet there are still some differences since our fourth order scheme involves an intermediate variable for vorticity. We construct the approximate intermediate vorticity variable via finite difference of the exact stream function, and recover the approximate vorticity by solving a linear system, whose eigenvalues are controlled, through the approximate intermediate vorticity variable with suitable boundary conditions. To maintain higher order consistency for vorticity, which will be needed when we compute its finite difference, we add an $O(h^4)$ correction term to the exact vorticity on the boundary when we set our boundary condition for the approximate vorticity. The approximate velocity will be constructed via finite differences of the exact stream function. Then we can show that the constructed profiles satisfy the numerical scheme up to $O(h^4)$ truncation error, including

Reproduced with permission of the copyright owner. Further reproduction prohibited without permission.

the vorticity on the boundary. Next, we perform a stability analysis and error estimate. We adopt the technique used in E and Liu [ELV2] and in the second chapter. The basic strategy is to use energy estimates, with special care taken at the boundary. Standard local estimates do not work for the boundary terms, due to the interior points of stream function involved in the boundary vorticity formula, so we have to apply elliptic regularity at the discrete level, and then control these local terms by global terms.

In Section 4.2 we outline the main idea of the EC4 scheme for a 1-D model for the Stokes problem. Stability of both two boundary conditions will be established there, which is accompanied by numerical accuracy check. The rigorous convergence proof of the method with Briley's formula as vorticity boundary condition will also be presented, by which we hope to explain the ideas in our consistency analysis clearly, including Strang type expansion and the construction of the approximate profiles. In Section 4.3 we look at the EC4 applied to 2-D full Navier-Stokes equations, and present the convergence analysis for the scheme, where the new 4-th order vorticity boundary condition is applied.

4.2 Convergence and Accuracy Check for 1-D Model

To explain the idea of our fourth order scheme more clearly, in this section we consider a simple 1-D model for Stokes equations, where nonlinear terms are neglected. The purpose of the introduction of this model is to catch main features and difficulties both in computation and analysis. The idea developed here can be applied to full 2-D nonlinear case as we can see in Section 4.3. This 1-D model

Reproduced with permission of the copyright owner. Further reproduction prohibited without permission.

reads

$$\begin{cases} \partial_t \omega = \nu(\partial_x^2 - k^2)\omega\,, \\ (\partial_x^2 - k^2)\psi = \omega\,, \\ v = \partial_x \psi = 0\,, \qquad \text{at } x = -1, 1\,. \end{cases} \tag{4.2.1}$$

whose solution is the k-th mode solution of the unsteady Stokes equations in the domain $[-1, 1] \times [0, 2\pi]$

$$\begin{cases} \partial_t \omega = \nu \Delta \omega\,, \\ \Delta \psi = \omega\,. \end{cases} \tag{4.2.2}$$

where the no-slip boundary condition, $\psi = \partial_x \psi = 0$, is imposed at $x = -1, 1$, and periodic boundary conditions are imposed in the y direction. An exact solution of (4.2.1) is

$$\omega_e(x, t) = \cos(\mu x) \exp\left\{-\nu(k^2 + \mu^2)t\right\}\,, \tag{4.2.3}$$

where μ satisfies $\mu \tan \mu + k \tanh k = 0$. See [OI2] and [ELV1] for detail. For simplicity we take $k = 1$.

4.2.1 Description of Fourth Order Schemes

Essentially compact fourth order scheme (EC4) for 2-D Navier-Stokes equations was proposed by E and Liu in [ELV2]. We can use the similar idea to deal with the 1-D model (4.2.1). As we can see, the operator $\partial_x^2 - 1$ can be approximated by compact difference operator

$$\partial_x^2 - 1 = \frac{(1 - \frac{h^2}{12})D_x^2 - 1}{1 + \frac{h^2}{12} D_x^2} + O(h^4)\,. \tag{4.2.4}$$

Applying (4.2.4) to both the diffusion term in vorticity equation and the kinematic relation between stream function and vorticity in (4.2.1), and multiplying both equations by $1 + \frac{h^2}{12} D_x^2$, we obtain the following system

$$\begin{cases} \partial_t \overline{\omega} = \nu\Big((1 - \dfrac{h^2}{12})D_x^2 - 1\Big)\omega\,, \\ \Big((1 - \dfrac{h^2}{12})D_x^2 - 1\Big)v = \overline{\omega}\,, \qquad v = 0\,. \quad \text{on } x = -1, 1\,. \end{cases} \tag{4.2.5}$$

Reproduced with permission of the copyright owner. Further reproduction prohibited without permission.

where the auxiliary term $\overline{\omega}$ was introduced as

$$\overline{\omega} = (1 + \frac{h^2}{12} D_x^2)\omega \,. \tag{4.2.6}$$

As we pointed out in the second chapter where we deal with second order scheme, there are two boundary conditions for ψ. The situation here is similar. The Dirichlet boundary condition $\psi = 0$ on $x = -1, 1$ can be implemented to solve the stream function via (4.2.5). Yet the normal boundary condition $\partial_x \psi = 0$, which cannot be enforced directly, will be converted into the boundary condition for the vorticity. For example, Briley's formula

$$\omega_0 = \frac{1}{h^2}(6\psi_1 - \frac{3}{2}\psi_2 + \frac{2}{9}\psi_3) - \frac{11}{3h}\left(\frac{\partial \psi}{\partial x}\right)_0 \tag{4.2.7}$$

was used in the EC4 scheme (see [BRL], [ELV2]). We should remark here that Briley's formula is only third order accurate for the vorticity on the boundary by formal local Taylor expansion. Later we will show that it still preserves 4th order accuracy. It was first proved in [ELV2]. Next, we derive our new 4th order vorticity boundary condition. First, we use a 4th order approximation of $\omega = (\partial_x^2 - 1)\psi$ on the boundary:

$$\omega_0 = \frac{1}{12h^2}\Big(16(\psi_{-1} + \psi_1) - (\psi_{-2} + \psi_2)\Big) + O(h^4) \,. \tag{4.2.8}$$

where (-1), (-2) refer to the "ghost" grid points outside of the computational domain. Note that we need five points of ψ to obtain fourth order accuracy for ω, which is different from the second order case, where we only need three points of ψ as we discussed in the second chapter. Then we prescribe the values for the "ghost" points of ψ using the no-slip boundary condition $\frac{\partial \psi}{\partial x} = 0$, on $x = -1, 1$ along with a 6-th order one-sided approximations for ψ:

$$\psi_{-1} = 10\psi_1 - 5\psi_2 + \frac{5}{3}\psi_3 - \frac{1}{4}\psi_4 - 5h\left(\frac{\partial \psi}{\partial x}\right)_0 + O(h^6) \,. \tag{4.2.9}$$

Reproduced with permission of the copyright owner. Further reproduction prohibited without permission.

and

$$v_{-2} = 80v_1 - 45v_2 + 16v_3 - \frac{5}{2}v_4 - 30h\left(\frac{\partial v}{\partial x}\right)_0 + O(h^6). \tag{4.2.10}$$

Combining (4.2.8), (4.2.9) and (4.2.10), we obtain

$$v_0 = \frac{1}{h^2}(8v_1 - 3v_2 + \frac{8}{9}v_3 - \frac{1}{8}v_4) - \frac{25}{6h}\left(\frac{\partial v}{\partial x}\right)_0. \tag{4.2.11}$$

We will use this new formula to perform our analysis of 2-D EC4 scheme in Section 4.3. The system (4.2.5), (4.2.6) along with the boundary condition (4.2.7) or (4.2.11) can be implemented very efficiently via an explicit time stepping procedure introduced by E and Liu in [ELV2].

4.2.2 Stability Analysis of the Scheme

One of the main concerns in the higher order schemes are their numerical stabilities. We will have a look at the 4th order scheme with the boundary conditions we mentioned above. First we introduce some notations. **Notation.** We will use the discrete L^2-norm and the discrete L^2-inner product

$$\|u\| = \langle u, u\rangle^{1/2}, \qquad \langle u, v\rangle = \sum_{1\le i\le N-1} u_i v_i h, \tag{4.2.12}$$

For $u_0 = u_N = 0$, we introduce the notation $\|\nabla_h u\|$ by defining

$$\|\nabla_h u\|^2 = \sum_{0\le i\le N-1} (D_x^+ u_i)^2\ h, \qquad \text{where } D_x^+ u_i = \frac{u_{i+1} - u_i}{h}. \tag{4.2.13}$$

Similar notations of L^2 norms and inner products, one sided difference norms in 2-D analogous to (4.2.12), (4.2.13) can also be introduced. Note that in 2-D case, the discrete inner product $\langle u, v\rangle$ will turn out to be $\sum_{1\le i,j\le N-1} u_{i,j} v_{i,j} h^2$; moreover, $\|\nabla_h u\|^2$ includes two parts, for both $D_x^+ u_{i,j}$ and $D_y^+ u_{i,j}$, where the forward difference operators D_x^+, D_y^+ can be defined similarly as in (4.2.13). We will use these 2-D notations in Section 4.3.

Reproduced with permission of the copyright owner. Further reproduction prohibited without permission.

4.2.2.1 Stability of Briley's Formula

We look at the fourth order scheme (4.2.5), (4.2.6) with Briley's formula (4.2.7) first. The first step here is to multiply (4.2.5) by $-(1+\frac{h^2}{12}D_x^2)v$

(4.2.14)

$$-\langle(1+\frac{h^2}{12}D_x^2)v,(1+\frac{h^2}{12}D_x^2)\partial_t\omega\rangle+\Big\langle(1+\frac{h^2}{12}D_x^2)v,\Big((1-\frac{h^2}{12})D_x^2-1\Big)\omega\Big\rangle=0.$$

The first term, which is corresponding to the time marching term, can be estimated by the discrete kinematic relation between v and ω as in (4.2.5)

(4.2.15)

$$\begin{aligned}
&-\langle(1+\frac{h^2}{12}D_x^2)v,(1+\frac{h^2}{12}D_x^2)\partial_t\omega\rangle\\
&=-\Big\langle(1+\frac{h^2}{12}D_x^2)v,\partial_t\Big((1-\frac{h^2}{12})D_x^2-1\Big)\psi\Big\rangle\\
&=-\langle(1+\frac{h^2}{12}D_x^2)v,\partial_t(1-\frac{h^2}{12})D_x^2\psi\rangle-\langle(1+\frac{h^2}{12}D_x^2)v,-\partial_t v\rangle\\
&=\frac{1}{2}(1-\frac{h^2}{12})\frac{d}{dt}\|\nabla_h v\|^2-\frac{h^2}{24}(1-\frac{h^2}{12})\frac{d}{dt}\|D_x^2\psi\|^2+\frac{1}{2}\frac{d}{dt}\|v\|^2-\frac{h^2}{24}\frac{d}{dt}\|\nabla_h v\|^2\\
&=\frac{1}{2}\frac{d}{dt}\Big((1-\frac{h^2}{6})\|\nabla_h v\|^2+\|v\|^2-\frac{h^2}{12}(1-\frac{h^2}{12})\|D_x^2 v\|^2\Big).
\end{aligned}$$

and the second term, which is corresponding to the diffusion term, can be estimated via summing by parts

(4.2.16)

$$\begin{aligned}
&\Big\langle(1+\frac{h^2}{12}D_x^2)v,\Big((1-\frac{h^2}{12})D_x^2-1\Big)\omega\Big\rangle\\
&=\langle\tilde{v},(1-\frac{h^2}{12})D_x^2\tilde{\omega}\rangle+\langle v,-\omega\rangle+\langle\frac{h^2}{12}D_x^2\psi,(1-\frac{h^2}{12})D_x^2\omega\rangle+\langle\frac{h^2}{12}D_x^2 v,-\omega\rangle\\
&=\langle(1-\frac{h^2}{12})D_x^2 v,\omega\rangle+\frac{1}{h}(1-\frac{h^2}{12})(v_1\omega_0+v_{N-1}\omega_N)+\langle-v,\omega\rangle\\
&\quad+\langle(1-\frac{h^2}{12})D_x^2 v,\frac{h^2}{12}D_x^2\omega\rangle+\langle-\psi,\frac{h^2}{12}D_x^2\omega\rangle+\frac{1}{h}\cdot\frac{h^2}{12}(v_1\omega_0+v_{N-1}\omega_N)\\
&=\Big\langle\Big((1-\frac{h^2}{12})D_x^2-1\Big)v,(1+\frac{h^2}{12}D_x^2)\omega\Big\rangle+\frac{1}{h}(v_1\omega_0+v_{N-1}\omega_N)\\
&=\|(1+\frac{h^2}{12}D_x^2)\omega\|^2+\frac{1}{h}(v_1\omega_0+v_{N-1}\omega_N).
\end{aligned}$$

As we can see in (4.2.16), we have to control the boundary term to ensure the stability. Here we decompose the boundary term into two parts $\mathcal{B}=\mathcal{B}_1+\mathcal{B}_2$.

Reproduced with permission of the copyright owner. Further reproduction prohibited without permission.

where $\mathcal{B}_1 = \frac{1}{h}\omega_1\omega_0$ and $\mathcal{B}_2 = \frac{1}{h}\omega_{N-1}\omega_N$. For simplicity of presentation, we only consider $\mathcal{B}_1$ here. $\mathcal{B}_2$ can be treated in the same way.

We can apply Briley's formula (4.2.7) to update $\mathcal{B}_1$

$$\mathcal{B}_1 = \frac{\omega_1}{h^3}(6\omega_1 - \frac{3}{2}\psi_2 + \frac{2}{9}\omega_3)\,. \tag{4.2.17}$$

However, a straightforward calculation cannot guarantee a bound of $\mathcal{B}_1$. The difficulty comes from the fact that three interior points of stream function are involved in Briley's formula. Here we apply the similar technique used in [ELV2] and our previous paper when we dealt with second order scheme with Wilkes' formula in the second chapter: as can be seen, the term $(6\omega_1 - \frac{3}{2}\psi_2 + \frac{2}{9}\omega_3)$ can be rewritten as

$$6\omega_1 - \frac{3}{2}\psi_2 + \frac{2}{9}\psi_3 = \frac{11}{3}\psi_1 - \frac{19}{18}h^2D_x^2\psi_1 + \frac{2}{9}h^2D_x^2\psi_2\,, \tag{4.2.18}$$

which is valid since $\omega_0 = \omega_N = 0$. The purpose of this transformation is to control the local terms in (4.2.17) by global quantities as we can see later. Now (4.2.18), along with Cauchy inequalities applied to $\omega_1 D_x^2\psi_1$ and $\omega_2 D_x^2\psi_2$, gives us the estimate of $\mathcal{B}_1$

$$\begin{aligned}
\mathcal{B}_1 &= \frac{\omega_1}{h^3}(\frac{11}{3}\omega_1 - \frac{19}{18}h^2D_x^2\psi_1 + \frac{2}{9}h^2D_x^2\psi_2) \\
&\geq \frac{11\omega_1^2}{3h^3} - \frac{1}{2h^3}\frac{19^2}{18^2}\psi_1^2 - \frac{1}{2}|D_x^2\psi_1|^2h - \frac{1}{2h^3}\frac{2^2}{9^2}\psi_1^2 - \frac{1}{2}|D_x^2\psi_2|^2h \qquad (4.2.19)\\
&\geq \frac{2\omega_1^2}{h^3} - \frac{1}{2}|D_x^2\psi_1|^2h - \frac{1}{2}|D_x^2\psi_2|^2h\,.
\end{aligned}$$

where in the last step we used the fact that $\frac{11}{3} - \frac{1}{2}(\frac{19^2}{18^2} + \frac{2^2}{9^2}) \geq 2$. The term $\mathcal{B}_2$ can be estimated in a similar fashion. Now we arrive at

$$\mathcal{B} \geq -\frac{1}{2}\sum_{i=1,2N-1,N-2} h|D_x^2\psi_i|^2 \geq -\frac{1}{2}\|D_x^2\psi\|^2\,. \tag{4.2.20}$$

As mentioned earlier, the transformation (4.2.18) and the application of Cauchy inequalities give us a bound of the boundary term, which is a local term,

Reproduced with permission of the copyright owner. Further reproduction prohibited without permission.

by a global term $\|D_x^2 v\|^2$. Next, we need to control $\|D_x^2 v\|^2$ by $\|\varpi\|^2$ appearing in the diffusion term, which can be resorted to the following lemma.

Lemma 4.2.1 *For $v_0 = v_N = 0$, we have*

$$\|(1-\frac{h^2}{12})D_x^2 v\| \le \|\Big((1-\frac{h^2}{12})D_x^2 - 1\Big)v\| = \|(1+\frac{h^2}{12}D_x^2)\omega\| = \|\varpi\| . \tag{4.2.21}$$

Proof. The boundary condition $w_0 = v_N = 0$ indicates that we can Sine transform v.

$$w_i = \sum_k \widehat{w}_k \sin(k\pi x_i) . \tag{4.2.22}$$

The Parserval equality gives that

$$\sum_i (w_i)^2 = \sum_k (\widehat{w}_k)^2 . \tag{4.2.23}$$

We let $f_k = -\frac{4}{h^2}\sin^2(\frac{k\pi h}{2})$, then we have $D_x^2 w_i = \sum_k f_k \widehat{v}_k \sin(k\pi x_i)$, which in turn shows the Parserval equality for $(1-\frac{h^2}{12})D_x^2 v$ and $\Big((1-\frac{h^2}{12})D_x^2 - 1\Big)v$

$$\begin{aligned} &\|(1-\frac{h^2}{12})D_x^2 w\|^2 = h\sum_k (1-\frac{h^2}{12})^2 f_k^2 \widehat{v}_k^2 . \\ &\|\Big((1-\frac{h^2}{12})D_x^2 - 1\Big)w\|^2 = h\sum_k \Big((1-\frac{h^2}{12})f_k - 1\Big)^2 \widehat{v}_k^2 . \end{aligned} \tag{4.2.24}$$

On the other hand, $f_k \le 0$ implies that $(1-\frac{h^2}{12})^2 f_k^2 \le \Big((1-\frac{h^2}{12})f_k - 1\Big)^2$. Then we obtain (4.2.21). Lemma 4.2.1 is proved.

Plugging (4.2.21) back into (4.2.20), we obtain

$$\mathcal{B} \ge -\frac{1}{2(1-\frac{h^2}{12})}\|(1+\frac{h^2}{12}D_x^2)\omega\|^2 \ge -\frac{2}{3}\|\varpi\|^2 . \tag{4.2.25}$$

Substituting (4.2.25) into (4.2.16), along with (4.2.15), and denoting "energy" E as

$$E = (1-\frac{h^2}{6})\|\nabla_h w\|^2 + \|w\|^2 - \frac{h^2}{12}(1-\frac{h^2}{12})\|D_x^2 v\|^2 . \tag{4.2.26}$$

Reproduced with permission of the copyright owner. Further reproduction prohibited without permission.

we finally arrive at

$$\frac{1}{2}\frac{dE}{dt} + \frac{1}{2}\nu\|\varpi\|^2 \le 0\,. \tag{4.2.27}$$

This completes the stability analysis of the fourth order scheme (4.2.5) with Briley's formula (4.2.7).

4.2.2.2 Stability of the New Fourth Order Formula

The stability of the fourth order scheme (4.2.5) with our new 4-th order vorticity boundary condition (4.2.11) can also be ensured by similar arguments. (4.2.15), (4.2.16) are still valid here. The only difference here is the estimate of the boundary term $\mathcal{B} = \mathcal{B}_1 + \mathcal{B}_2$, where $\mathcal{B}_1$ can be expressed as

$$\mathcal{B}_1 = \frac{1}{h}\psi_1\omega_0 = \frac{\psi_1}{h^3}(8\psi_1 - 3\psi_2 + \frac{8}{9}\psi_3 - \frac{1}{8}\psi_4)\,. \tag{4.2.28}$$

by our new 4-th order formula (4.2.11). Note that one more interior point of ψ is involved in our vorticity boundary formula. The estimate of $\mathcal{B}_1$ in (4.2.28) also follows our procedure above. First, we rewrite the term $(8\psi_1 - 3\psi_2 + \frac{8}{9}\psi_3 - \frac{1}{8}\psi_4)$ as

$$8\psi_1 - 3\psi_2 + \frac{8}{9}\psi_3 + \frac{1}{8}\psi_4 = \frac{25}{6}\psi_1 - \frac{115}{72}h^2D_x^2\psi_1 + \frac{23}{36}h^2D_x^2\psi_2 - \frac{1}{8}h^2D_x^2\psi_3\,. \tag{4.2.29}$$

and then repeat the procedure and argument as in (4.2.19), which gives that

$$\begin{aligned}
\mathcal{B}_1 &= \frac{\psi_1}{h^3}(\frac{25}{6}\psi_1 - \frac{115}{72}h^2D_x^2\psi_1 + \frac{23}{36}h^2D_x^2\psi_2 - \frac{1}{8}h^2D_x^2\psi_3) \\
&\ge \frac{25\psi_1^2}{6h^3} - \frac{1}{2h^3}\frac{115^2}{72^2}\psi_1^2 - \frac{1}{2}|D_x^2\psi_1|^2h - \frac{1}{2h^3}\frac{23^2}{36^2}\psi_1^2 - \frac{1}{2}|D_x^2\psi_2|^2h \\
&\quad - \frac{1}{2h^3}\frac{1^2}{8^2}\psi_1^2 - \frac{1}{2}|D_x^2\psi_3|^2h \\
&\ge \frac{2\psi_1^2}{h^3} - \frac{1}{2}h(|D_x^2\psi_1|^2 + |D_x^2\psi_2|^2 + |D_x^2\psi_3|^2)\,.
\end{aligned} \tag{4.2.30}$$

where we use the fact that $\frac{25}{6} - \frac{1}{2}(\frac{115^2}{72^2} + \frac{23^2}{36^2} + \frac{1^2}{8^2}) \ge 2$. Then we can also arrive at $\mathcal{B} \ge -\frac{1}{2}\|D_x^2\psi\|^2$ as in (4.2.20). Lemma 4.2.1, which controls the term $\|D_x^2\psi\|^2$ by

Reproduced with permission of the copyright owner. Further reproduction prohibited without permission.

the diffusion term $\|\varpi\|^2$, is still valid here. Finally, repeating (4.2.25), (4.2.26), we obtain (4.2.27), which shows that the fourth order scheme (4.2.5) with the vorticity boundary condition (4.2.11) is also stable.

4.2.3 Numerical Tests and Accuracy Check

We now present accuracy check for the fourth order scheme with boundary conditions we mentioned above. The exact solution of (4.2.3) with $k = 1$, the viscosity $\nu = 0.01$, and the corresponding $\mu = 2.88335565358979$ which is determined by $k = 1$ will be used for comparison in our numerical experiments. The final time is taken to be $t = 1.0$. Explicit treatment of the diffusion term and the fourth order Runge-Kutta time stepping were used (see E and Liu [ELV1] for detail). Table 4.1 and Table 4.2 list the numerical results of fourth order schemes with two different boundary conditions for the vorticity. As can be seen in the tables, the EC4 method with Briley's boundary condition achieves fourth order accuracy for the stream function, and gets more than fourth order accuracy for the vorticity. The EC4 scheme with our new 4th order boundary condition on the boundary also achieves the fourth order accuracy for the stream function, and gets almost fifth order accuracy for the vorticity. In other words, the orders of accuracy of these two formulas for the stream function are almost the same, yet our new fourth order boundary condition performs better than Briley's formula in the accuracy for vorticity.

4.2.4 Convergence Analysis of the Fourth order scheme

In this section, we will give a convergence analysis of the fourth order method. The stability of it, with both Briley's formula (4.2.7) and our new 4-th order vorticity boundary condition (4.2.11), has been been established in 4.2.2. We only analyze the convergence of the one with Briley's formula here, since the consistency analysis of it will turn out to be more technical than that

Reproduced with permission of the copyright owner. Further reproduction prohibited without permission.

of our new 4-th order formula, by which we hope to explain the methodology of Strang type expansion. As we can see, direct truncation error analysis gives us fourth order accuracy for the momentum equation, but only third order accuracy for the vorticity on the boundary if Briley's formula is used. Below, a more careful truncation error analysis will be carried out by including a higher order term, which is known as Strang type analysis to construct approximate stream function. In addition, the construction of the approximate vorticity needs some technique: first, the approximate intermediate vorticity variable will be constructed via finite difference of the approximate stream function; then, our approximate vorticity field will be constructed by solving a linear system through the approximate intermediate vorticity variable. The eigenvalues corresponding to the linear system are controlled. To maintain higher order consistency for the approximate vorticity, we add an $O(h^4)$ correction term to the exact vorticity on the boundary when we set its boundary condition, which leads to the convenience when its finite differences are computed.

All the analysis in this section can be carried out to our new formula, which is more straightforward, no expansion is needed.

4.2.4.1 Consistency Analysis

Denote ψ_e, ω_e as the exact solutions, extend ψ_e smoothly to $[-1-\delta, 1+\delta]$, and construct the approximate stream function $\Psi = \psi_e + h^4\widehat{\psi}$ with

$$\widehat{\psi}(x,t) = \frac{1}{4}\alpha(t)(x+1)(1-x)^2 - \frac{1}{4}\beta(t)(x+1)^2(1-x)\,. \tag{4.2.31}$$

where $\alpha(t) = -\frac{30}{11}\partial_x^5\psi_e(-1)$, $\beta(t) = -\frac{30}{11}\partial_x^5\psi_e(1)$. The choices of $\alpha(t)$ and $\beta(t)$ will guarantee Ψ to satisfy higher order truncation errors in Briley's formula, which we can see later. It is obvious that (say at the left boundary $x_0 = -1$)

$$\widehat{\psi}(-1) = 0\,, \qquad \partial_x\widehat{\psi}(-1) = -\frac{30}{11}\partial_x^5\psi_e(-1)\,. \tag{4.2.32}$$

Reproduced with permission of the copyright owner. Further reproduction prohibited without permission.

To estimate $\hat{v}$, we can see that $\partial_x^4 \hat{v} = 0$, which implies that

$$\|\hat{v}\|_{C^m} = \|\hat{v}\|_{C^3} \le C\|v_e\|_{C^3}, \qquad \text{if } m \ge 3. \tag{4.2.33}$$

Moreover, our definition of $\alpha(t)$ and $\beta(t)$ implies that $|\partial_t \alpha(t)|, |\partial_t \beta(t)| \le C\|\partial_t \partial_x^5 v_e\|_{C^0}$. To have a good estimate of $\|\partial_t \partial_x^5 v_e\|_{C^0}$, which is exactly $\|\partial_x^5 \partial_t v_e\|_{C^0}$, we see that $\partial_t v_e$ satisfies

$$\begin{cases} (\partial_x^2 - 1)\partial_t v_e = \partial_t \omega_e, & \text{in } [-1, 1], \\ \partial_t v_e = 0 & \text{at } x = -1, 1. \end{cases} \tag{4.2.34}$$

which implies that $\|\partial_t v_e\|_{C^3} \le C\|\partial_t \omega_e\|_{C^1}$. On the other hand, $\|\partial_t \omega_e\|_{C^1}$ can be controlled by the order of $\|\omega_e\|_{C^3}$ from our original vorticity equation that $\partial_t \omega_e = (\partial_x^2 - 1)\omega_e$. The combination of the above arguments indicates that

$$|\partial_t \alpha(t)|, |\partial_t \beta(t)| \le C\|\partial_t \partial_x^5 v_e\|_{C^0} \le C\|\partial_t \omega_e\|_{C^1} \le C\|\omega_e\|_{C^3} \le C\|v_e\|_{C^7}. \tag{4.2.35}$$

and the fact that $\partial_t \hat{v} = \frac{1}{4}(x+1)(1-x)^2 \partial_t \alpha(t) - \frac{1}{4}(x+1)^2(1-x)\partial_t \beta(t)$ gives

$$\|\partial_t \hat{v}\|_{C^m} = \|\partial_t \hat{v}\|_{C^3} \le C\|v_e\|_{C^7}, \qquad \text{if } m \ge 3. \tag{4.2.36}$$

The construction of the approximate vorticity is quite tricky. First we define

$$\overline{\Omega}_i = \Big((1 - \frac{h^2}{12})D_x^2 - 1\Big)\Psi_i, \qquad \text{for } 1 \le i \le N-1, \tag{4.2.37}$$

and then recover Ω by solving the following system

$$\Big(1 + \frac{h^2}{12} D_x^2\Big)\Omega_i = \overline{\Omega}_i. \tag{4.2.38}$$

We should mention that (4.2.38) always has a solution since the eigenvalues of the matrix corresponding to $1 + \frac{h^2}{12} D_x^2$ are all non-zero. On the other hand, the implementation of (4.2.38) requires the boundary value for Ω. To maintain the higher order consistency needed in the truncation error estimate below for the discrete derivatives of the constructed vorticity, we introduce

$$\hat{\omega} = \hat{\omega}_1 + \hat{\omega}_2, \qquad \text{where } \hat{\omega}_1 = -\frac{1}{240}\partial_x^6 v_e, \quad \hat{\omega}_2 = (\partial_x^2 - 1)\hat{v}. \tag{4.2.39}$$

Reproduced with permission of the copyright owner. Further reproduction prohibited without permission.

where $h^4\tilde{\omega}_1$ is the $O(h^4)$ truncation error of $\left((1-\frac{h^2}{12})D_x^2-1\right)\omega_e-(1+\frac{h^2}{12}D_x^2)\omega_e$. $h^4\tilde{\omega}_2$ is the $O(h^4)$ part of $h^4\left((1-\frac{h^2}{12})D_x^2-1\right)\tilde{\psi}$. The boundary condition for Ω (say at $x_0=-1$) is imposed as

$$\Omega_0=\omega_e(x_0)+h^4\tilde{\omega}_0\,. \tag{4.2.40}$$

and Ω_N can be determined similarly. The purpose of this choice can be seen in the following lemma.

Lemma 4.2.2 *We have on the grid points x_i, $0\le i\le N$,*

$$\Omega=\omega_e+h^4\tilde{\omega}+O(h^6)\|\psi_e\|_{C^8}\,. \tag{4.2.41}$$

Proof. First we note that

$$\begin{aligned}\left(1+\frac{h^2}{12}D_x^2\right)\Omega &= \left((1-\frac{h^2}{12})D_x^2-1\right)\Psi\\ &= \left((1-\frac{h^2}{12})D_x^2-1\right)\psi_e+h^4\left((1-\frac{h^2}{12})D_x^2-1\right)\tilde{\psi}\,.\end{aligned} \tag{4.2.42}$$

where the first term can be estimated via local Taylor expansion

$$\begin{aligned}\left((1-\frac{h^2}{12})D_x^2-1\right)\psi_e &= (1+\frac{h^2}{12}D_x^2)\omega_e-\frac{1}{240}h^4\partial_x^6\psi_e+O(h^6)\|\psi_e\|_{C^8}\\ &= (1+\frac{h^2}{12}D_x^2)\omega_e+h^4\tilde{\omega}_1+O(h^6)\|\psi_e\|_{C^8}\,,\end{aligned} \tag{4.2.43}$$

where $\tilde{\omega}_1$ was introduced in (4.2.39). and the second term appearing on the right hand side of (4.2.42) can be treated as

$$\begin{aligned}h^4\left((1-\frac{h^2}{12})D_x^2-1\right)\tilde{\psi} &= h^4(\partial_x^2-1)\tilde{\psi}+O(h^6)\|\tilde{\psi}\|_{C^4}\\ &= h^4\tilde{\omega}_2+O(h^6)\|\psi_e\|_{C^8}\,,\end{aligned} \tag{4.2.44}$$

where we applied (4.2.33) and $\tilde{\omega}_2$ was also introduced in (4.2.39). The combination of (4.2.42). (4.2.43) and (4.2.44) gives us

$$\begin{aligned}\left(1+\frac{h^2}{12}D_x^2\right)\Omega &= (1+\frac{h^2}{12}D_x^2)\omega_e+h^4\tilde{\omega}_1+h^4\tilde{\omega}_2+O(h^6)\|\psi_e\|_{C^8}\\ &= (1+\frac{h^2}{12}D_x^2)\omega_e+h^4\tilde{\omega}+O(h^6)\|\psi_e\|_{C^8}\,.\end{aligned} \tag{4.2.45}$$

Reproduced with permission of the copyright owner. Further reproduction prohibited without permission.

On the other hand, the fact that $\|D_x^2\tilde{\omega}\|_{C^0}$ is bounded by the order of $\|\psi_e\|_{C^6}$ from our construction of $\tilde{\omega}$ gives

$$(4.2.46)\qquad \Big(1+\frac{h^2}{12}D_x^2\Big)(\omega_e+h^4\tilde{\omega}) = (1+\frac{h^2}{12}D_x^2)\omega_e + h^4\tilde{\omega} + O(h^6)\|\psi_e\|_{C^6}\,.$$

The combination of (4.2.45) and (4.2.46) shows that at interior grid points x_i, $1 \le i \le N-1$,

$$(4.2.47)\qquad \Big|\Big(1+\frac{h^2}{12}D_x^2\Big)(\Omega-\omega_e-h^4\tilde{\omega})\Big| \le Ch^6\|\psi_e\|_{C^6}\,.$$

On the boundary (say at $i=0$), (4.2.40) indicates

$$(4.2.48)\qquad \Omega_0 - (\omega_e+h^4\tilde{\omega})_0 = 0\,.$$

Since the matrix $I+\frac{h^2}{12}D_x^2$ is uniformly diagonally dominant, we obtain (4.2.41) from (4.2.47) and (4.2.48). Lemma 4.2.2 is proved.

Next we look at the truncation error of the diffusion term. By Lemma 4.2.2 and the fact that $\tilde{\omega}$ and its divided differences up to second order are bounded by the order of $\|\psi_e\|_{C^6}$, we have

$$(4.2.49)\qquad |D_x^2(\Omega-\omega_e)| \le Ch^4\|\psi_e\|_{C^6}\,,$$

which along with (4.2.41) gives us

$$(4.2.50)\qquad \Big((1-\frac{h^2}{12})D_x^2-1\Big)\Omega = \Big((1-\frac{h^2}{12})D_x^2-1\Big)\omega_e + O(h^4)\|\psi_e\|_{C^6}\,.$$

On the other hand, local Taylor expansion of ω_e shows that

$$(4.2.51)\qquad \Big((1-\frac{h^2}{12})D_x^2-1\Big)\omega_e = (1+\frac{h^2}{12}\partial_x^2)(\partial_x^2-1)\omega_e + O(h^4)\|\omega_e\|_{C^6}\,.$$

The combination of (4.2.50) and (4.2.51) implies that

$$(4.2.52)\qquad \Big((1-\frac{h^2}{12})D_x^2-1\Big)\Omega = (1+\frac{h^2}{12}\partial_x^2)(\partial_x^2-1)\omega_e + O(h^4)\|\psi_e\|_{C^6}\,.$$

Reproduced with permission of the copyright owner. Further reproduction prohibited without permission.

Now we estimate the time marching term. At the interior grid points x_i, $1 \le i \le N-1$.

$$\begin{aligned} \partial_t \widehat{\Omega} &= \partial_t \Big((1 - \frac{h^2}{12}) D_x^2 - 1 \Big) \Psi \\ &= \partial_t \Big((1 - \frac{h^2}{12}) D_x^2 - 1 \Big) \omega_e + h^4 \partial_t \Big((1 - \frac{h^2}{12}) D_x^2 - 1 \Big) \widehat{\psi}. \end{aligned} \tag{4.2.53}$$

where the first term can be treated via local Taylor expansion and the kinematic relation between ψ_e and ω_e

(4.2.54)

$$\partial_t \Big((1 - \frac{h^2}{12}) D_x^2 - 1 \Big) \psi_e = \partial_t (1 + \frac{h^2}{12} \partial_x^2) \omega_e + h^4 \partial_t (\frac{1}{360} \partial_x^6 \psi_e - \frac{1}{144} \partial_x^4 \psi_e) + O(h^6) \| \partial_t \psi_e \|_{C^6} .$$

and the second term can also be controlled by

$$h^4 \partial_t \Big((1 - \frac{h^2}{12}) D_x^2 - 1 \Big) \widehat{\psi} = h^4 \partial_t (\partial_x^2 - 1) \widehat{\psi} + O(h^6) \| \partial_t \widehat{\psi} \|_{C^4} . \tag{4.2.55}$$

Again, by (4.2.34), we have the following estimate

$$\| \partial_t \psi_e \|_{C^6} \le C \| \partial_t \omega_e \|_{C^4} \le C \| \omega_e \|_{C^6} \le C \| \psi_e \|_{C^8} , \tag{4.2.56}$$

where the original PDE that $\partial_t \omega_e = \nu (\partial_x^2 - 1) \omega_e$ was applied in the second step. The term $\| \partial_t \widehat{\psi} \|_{C^4}$ appearing in (4.2.55) can be controlled by (4.2.36). The combination of (4.2.53)-(4.2.56) shows that

$$\partial_t (1 + \frac{h^2}{12} D_x^2) \Omega - \partial_t (1 + \frac{h^2}{12} \partial_x^2) \omega_e = O(h^4) \| \psi_e \|_{C^8} . \tag{4.2.57}$$

Combining (4.2.57) and (4.2.52), the estimate for time marching term and diffusion term respectively, and applying the original vorticity equation which implies that $(1 + \frac{h^2}{12} \partial_x^2) \Big(\partial_t \omega_e - \nu (\partial_x^2 - 1) \omega_e \Big) = 0$, we arrive at

$$\partial_t (1 + \frac{h^2}{12} D_x^2) \Omega - \nu \Big((1 - \frac{h^2}{12}) D_x^2 - 1 \Big) \Omega = O(h^4) \| \psi_e \|_{C^8} . \tag{4.2.58}$$

at grid points x_i, $1 \le i \le N-1$.

Reproduced with permission of the copyright owner. Further reproduction prohibited without permission.

Finally we look at the boundary condition for Ω. We will show that Ω satisfies Briley's formula applied to Ψ up to $O(h^4)$ error. To verify it, first we have a look at the expression appearing in Briley's formula (say near the left boundary $x_0 = -1$)

(4.2.59)
$$6\Psi_1 - \frac{3}{2}\Psi_2 + \frac{2}{9}\Psi_3 = \left(6w_e(x_1) - \frac{3}{2}w_e(x_2) + \frac{2}{9}w_e(x_3)\right) + h^4(6\widehat{w}_1 - \frac{3}{2}\widehat{w}_2 + \frac{2}{9}\widehat{w}_3).$$

The first term can be estimated via Taylor expansion of w_e, keeping in mind that $w_e(x_0) = \partial_x w_e(x_0) = 0$

(4.2.60)
$$6w_e(x_1) - \frac{3}{2}w_e(x_2) + \frac{2}{9}w_e(x_3) = h^2\partial_x^2 w_e(x_0) + \frac{1}{10}h^5\partial_x^5 w_e(x_0) + O(h^6)\|w_e\|_{C^6}.$$

The estimate of the second term appearing in (4.2.59) can also be carried out via Taylor expansion and our construction of $\widehat{w}$

(4.2.61)
$$\begin{aligned} h^4(6\widehat{w}_1 - \frac{3}{2}\widehat{w}_2 + \frac{2}{9}\widehat{w}_3) &= \frac{11}{3}h^5\partial_x\widehat{w}(x_0) + O(h^6)\|\widehat{w}\|_{C^2} \\ &= -\frac{1}{10}h^5\partial_x^5 w_e(x_0) + O(h^6)\|w_e\|_{C^6}. \end{aligned}$$

where we used (4.2.32) and (4.2.33). As we can see, the $O(h^5)$ terms appearing in (4.2.60) and (4.2.61) cancel each other if we put them into a combined term $6\Psi_1 - \frac{3}{2}\Psi_2 + \frac{2}{9}\Psi_3$ because of our special choice of $\alpha(t)$ and $\beta(t)$. The reason of the choice can be seen more clearly here. The combination of (4.2.59), (4.2.60) and (4.2.61), along with the fact that $w_e(x_0) = (\partial_x^2 - 1)w_e(x_0) = \partial_x^2 w_e(x_0)$ since w_e vanishes on the boundary, gives us

(4.2.62)
$$6\Psi_1 - \frac{3}{2}\Psi_2 + \frac{2}{9}\Psi_3 = h^2 w_e(x_0) + O(h^6)\|w_e\|_{C^6}.$$

in other words,

(4.2.63)
$$w_e(x_0) = \frac{1}{h^2}(6\Psi_1 - \frac{3}{2}\Psi_2 + \frac{2}{9}\Psi_3) + O(h^4)\|w_e\|_{C^6}.$$

Reproduced with permission of the copyright owner. Further reproduction prohibited without permission.

On the other hand, our definition of Ω_0 in (4.2.40) and the fact that $|\tilde{\omega}_0| \le C\|\psi_e\|_{C^6}$ implies that the difference between Ω_0 and $\omega_e(x_0)$ is of order $O(h^4)\|\psi_e\|_{C^6}$. Then we obtain the boundary condition for Ω:

$$\Omega_0 = \frac{1}{h^2}(6\Psi_1 - \frac{3}{2}\Psi_2 + \frac{2}{9}\Psi_3) + h^4 e_0 . \qquad \text{where} \quad |e_0| \le C\|\psi_e\|_{C^6} . \tag{4.2.64}$$

4.2.4.2 Error estimates

For $0 \le i \le N$, we define

$$\tilde{\psi}_i = \psi_i - \Psi_i . \qquad \tilde{\omega}_i = \omega_i - \Omega_i . \tag{4.2.65}$$

and the error function for $\overline{\omega}$ is defined at grid points x_i, $1 \le i \le N-1$,

$$\tilde{\overline{\omega}}_i = \overline{\omega}_i - \overline{\Omega}_i = (1 + \frac{h^2}{12}D_x^2)\tilde{\omega}_i . \tag{4.2.66}$$

Our consistency analysis carried out above gives a closed system for error functions

$$\begin{cases} \left(1 + \frac{h^2}{12}D_x^2\right)\partial_t\tilde{\omega} = \nu\left((1 - \frac{h^2}{12})D_x^2 - 1\right)\tilde{\omega} + \boldsymbol{f} . \\ \left((1 - \frac{h^2}{12})D_x^2 - 1\right)\tilde{\psi} = \left(1 + \frac{h^2}{12}D_x^2\right)\tilde{\omega} . \qquad \tilde{\psi}_0 = \tilde{\psi}_N = 0 . \end{cases} \tag{4.2.67}$$

where the local truncation error $\boldsymbol{f}$ satisfies $|\boldsymbol{f}_i| \le Ch^4\|\psi_e\|_{C^6}$. On the boundary, (say at the left boundary point $x_0 = -1$)

$$\tilde{\omega}_0 = \frac{1}{h^2}(6\tilde{\psi}_1 - \frac{3}{2}\tilde{\psi}_2 + \frac{2}{9}\tilde{\psi}_3) + h^4 e_0 , \tag{4.2.68}$$

where $|e_0| \le C\|\psi_e\|_{C^6}$. (4.2.68) comes from Briley's formula (4.2.7) and our estimate for Ω_0 (4.2.64). In other words, the error function of vorticity and the error function of stream function satisfy Briley's formula up to $O(h^4)$ error.

The system of the error functions (4.2.67) along with (4.2.68) is very similar to the fourth order scheme (4.2.5) with Briley's formula (4.2.7), except for local truncation error terms $\boldsymbol{f}$, $\boldsymbol{h^4 e_0}$. The procedure of stability analysis carried out in **4.2.2.1** can be implemented here similarly.

Reproduced with permission of the copyright owner. Further reproduction prohibited without permission.

Multiplying (4.2.67) by $-(1+\frac{h^2}{12}D_x^2)\tilde{\omega}$ gives

(4.2.69)
$$\langle -(1+\frac{h^2}{12}D_x^2)\tilde{\psi},(1+\frac{h^2}{12}D_x^2)\partial_t\tilde{\omega}\rangle + \Big\langle (1+\frac{h^2}{12}D_x^2)\tilde{\omega},\big((1-\frac{h^2}{12})D_x^2-1\big)\tilde{\omega}\Big\rangle = \langle -(1+\tfrac{h^2}{12}D_x^2)\tilde{\omega},\boldsymbol{f}\rangle .$$

The term corresponding to local truncation error can be controlled by Cauchy inequality

(4.2.70)
$$\langle -(1+\frac{h^2}{12}D_x^2)\tilde{\omega},\boldsymbol{f}\rangle \le C\|\tilde{\omega}\|^2 + C\|\boldsymbol{f}\|^2 .$$

and the results corresponding to the time marching term and diffusion term are analogous to (4.2.15) and (4.2.16)

(4.2.71)
$$\begin{aligned} &-\langle (1+\frac{h^2}{12}D_x^2)\tilde{\psi},(1+\frac{h^2}{12}D_x^2)\partial_t\tilde{\omega}\rangle \\ &= \frac{1}{2}\frac{d}{dt}\Big((1-\frac{h^2}{6})\|\nabla_h\tilde{\omega}\|^2 + \|\tilde{\omega}\|^2 - \frac{h^2}{12}(1-\frac{h^2}{12})\|D_x^2\tilde{\omega}\|^2\Big) . \end{aligned}$$

(4.2.72)
$$\Big\langle \big(1+\frac{h^2}{12}D_x^2\big)\tilde{\omega},\big((1-\frac{h^2}{12})D_x^2-1\big)\tilde{\omega}\Big\rangle = \|(1+\frac{h^2}{12}D_x^2)\tilde{\omega}\|^2 + \frac{1}{h}(\tilde{\omega}_1\tilde{\omega}_0 + \tilde{\omega}_{N-1}\tilde{\omega}_N) .$$

The estimate of the boundary term $\mathcal{B}=\mathcal{B}_1+\mathcal{B}_2$, where $\mathcal{B}_1=\frac{1}{h}(\tilde{\psi}_1\tilde{\omega}_0)$ and $\mathcal{B}_2=\frac{1}{h}(\tilde{\omega}_{N-1}\tilde{\omega}_N)$ is similar to that in **4.2.2.1**. The boundary condition for $\tilde{\omega}_0$ in (4.2.68) gives us

(4.2.73)
$$\mathcal{B}_1 = \tilde{\psi}_1\Big(\frac{1}{h^3}(6\tilde{\psi}_1 - \frac{3}{2}\tilde{\psi}_2 + \frac{2}{9}\tilde{\psi}_3) + h^3\boldsymbol{e}_0\Big) .$$

Analogous to (4.2.18), we can rewrite the term $6\tilde{\psi}_1-\frac{3}{2}\tilde{\psi}_2+\frac{2}{9}\tilde{\psi}_3$ as $\frac{11}{3}\tilde{\psi}_1 - \frac{19}{18}h^2D_x^2\tilde{\psi}_1+\frac{2}{9}h^2D_x^2\tilde{\psi}_2$. Then the procedure in (4.2.19) can be repeated to estimate $\mathcal{B}_1$ here, where we will use Cauchy inequality to estimate the error term

(4.2.74)
$$\begin{aligned} \mathcal{B}_1 = &\ \frac{\tilde{\psi}_1}{h^3}(\frac{11}{3}\tilde{\psi}_1 - \frac{19}{18}h^2D_x^2\tilde{\psi}_1 + \frac{2}{9}h^2D_x^2\tilde{\psi}_2) + h^3\tilde{\psi}_1\boldsymbol{e}_0 \\ \ge &\ \frac{11\tilde{\psi}_1^2}{3h^3} - \frac{1}{2h^3}\frac{19^2}{18^2}\tilde{\psi}_1^2 - \frac{1}{2}|D_x^2\tilde{\psi}_1|^2h - \frac{1}{2h^3}\frac{2^2}{9^2}\tilde{\psi}_1^2 - \frac{1}{2}|D_x^2\tilde{\psi}_2|^2h - \frac{1}{4}\frac{\tilde{\psi}_1^2}{h^3} - h^9\boldsymbol{e}_0^2 \\ \ge &\ \frac{\tilde{\psi}_1^2}{h^3} - \frac{1}{2}|D_x^2\tilde{\psi}_1|^2h - \frac{1}{2}|D_x^2\tilde{\psi}_2|^2h - h^9\boldsymbol{e}_0^2 . \end{aligned}$$

Reproduced with permission of the copyright owner. Further reproduction prohibited without permission.

Similar to (4.2.20), we arrive at

$$\mathcal{B} \geq -\frac{1}{2}\sum_{i=1,2N-1,N-2} h|D_x^2\tilde{e}_i|^2 - h^9(\boldsymbol{e}_0^2 + \boldsymbol{e}_N^2) \geq -\frac{1}{2}\|D_x^2\tilde{e}\|^2 - h^8 . \tag{4.2.75}$$

if h is small enough since $|\boldsymbol{e}_0|, |\boldsymbol{e}_N| \leq C\|v_e\|_{C^8}$.

Since $\tilde{e}_0 = \tilde{e}_N = 0$, we can use the same argument as in Lemma 4.2.1 to conclude that

$$\|(1 - \frac{h^2}{12})D_x^2\tilde{\psi}\| \leq \|\Big((1 - \frac{h^2}{12})D_x^2 - 1\Big)\tilde{e}\| = \|(1 + \frac{h^2}{12}D_x^2)\tilde{w}\| . \tag{4.2.76}$$

Substitute (4.2.76) into (4.2.75) and (4.2.72), we obtain

$$\Big\langle (1 + \frac{h^2}{12}D_x^2)\tilde{\psi}, \Big((1 - \frac{h^2}{12})D_x^2 - 1\Big)\tilde{w}\Big\rangle \geq -h^8 \tag{4.2.77}$$

Combining (4.2.77), (4.2.72) and (4.2.71), denoting $\tilde{E}$ as

$$\tilde{E} = (1 - \frac{h^2}{6})\|\nabla_h\tilde{\psi}\|^2 + \|\tilde{e}\|^2 - \frac{h^2}{12}(1 - \frac{h^2}{12})\|D_x^2\tilde{e}\|^2 . \tag{4.2.78}$$

along with the Poincare inequality for $\tilde{w}$ which states that $\|\tilde{w}\| \leq C\|\nabla_h\tilde{e}\|$ since $\tilde{e}$ vanishes on the boundary, we arrive at

$$\frac{1}{2}\frac{d\tilde{E}}{dt} \leq C\|\boldsymbol{f}\|^2 + C\|\tilde{\psi}\|^2 + h^8 \leq C\|\boldsymbol{f}\|^2 + C\|\nabla_h\tilde{e}\|^2 + h^8 . \tag{4.2.79}$$

Integrating in time, we obtain

$$\tilde{E} \leq C\int_0^T \|\boldsymbol{f}\|^2\,dt + C\int_0^T \|\nabla_h\tilde{e}\|^2\,dt + 2Th^8 + O(h^8) . \tag{4.2.80}$$

where $O(h^8)$ is the initial term of $\tilde{E}(\cdot,0)$. By our construction of Ψ, we have $\tilde{e}(\cdot,0) = h^4\tilde{e}(\cdot,0)$. Moreover, we get $O(h^8) \leq Ch^8\|v_e\|_{C^8}^2$. The fact that $\|D_x^2\tilde{e}\|^2 \leq \frac{4}{h^2}\|\nabla_h\tilde{e}\|^2$, which implies that $\|\nabla_h\tilde{\psi}\|^2 \leq \tilde{E}$, along with (4.2.80) leads to

$$\|\nabla_h\tilde{e}\|^2 \leq C\int_0^T \|\boldsymbol{f}\|^2\,dt + C\int_0^T \|\nabla_h\tilde{w}\|^2\,dt + CTh^8 + O(h^8) . \tag{4.2.81}$$

By Gronwall inequality, we have

$$\|\nabla_h\tilde{e}\|^2 \leq C\int_0^T \|\boldsymbol{f}(\cdot,s)\|^2\,ds + CTh^8 + O(h^8) \leq Ch^8(\|v_e\|_{C^8}^2 + T) . \tag{4.2.82}$$

Reproduced with permission of the copyright owner. Further reproduction prohibited without permission.

Thus, we have proved

$$\|\nabla_h(\psi(\cdot,t)-\psi_e(t))\|_{L^2}\le Ch^4(\|\psi_e\|_{C^6}+T)\,. \tag{4.2.83}$$

which gives the convergence of the fourth order scheme along with Briley's formula (4.2.7).

4.3 Analysis of EC4 Scheme for 2-D NSE

4.3.1 Description of the scheme

Essentially Compact Fourth order scheme (EC4) for NSE (4.1.1), (4.1.2) was proposed by E and Liu in [ELV2]. Motivated by the fourth order approximation to $\triangle$ in 2-D

$$\triangle=\frac{\triangle_h+\frac{h^2}{6}D_x^2D_y^2}{1+\frac{h^2}{12}\triangle_h}+O(h^4)\,. \tag{4.3.1}$$

they discretize NSE in 2-D by

$$\begin{cases}\partial_t\overline{\omega}=(\triangle_h+\dfrac{h^2}{6}D_x^2D_y^2)\omega-\mathcal{NL}\,.\\ (\triangle_h+\dfrac{h^2}{6}D_x^2D_y^2)\psi=\overline{\omega}\,.\qquad \psi\,|_\Gamma=0\,.\\ (1+\dfrac{h^2}{12}\triangle_h)\omega=\overline{\omega}\,.\end{cases} \tag{4.3.2}$$

where the intermediate variable $\overline{\omega}$ was introduced as $\overline{\omega}=(1+\frac{h^2}{12}\triangle_h)\omega$, and the approximate nonlinear term $\mathcal{NL}$ is given by

$$\mathcal{NL}=\widetilde{D}_x(1+\frac{h^2}{6}D_y^2)(u\omega)+\widetilde{D}_y(1+\frac{h^2}{6}D_x^2)(v\omega)-\frac{h^2}{12}\triangle_h(u\widetilde{D}_x\omega+v\widetilde{D}_y\omega)\,. \tag{4.3.3}$$

Note that the implementation of the third term of (4.3.3) needs the boundary value of $u\widetilde{D}_x\omega+v\widetilde{D}_y\omega$. Since the velocity $\boldsymbol{u}$ vanishes on the boundary, we can set

$$(u\widetilde{D}_x\omega+v\widetilde{D}_y\omega)\,\big|_\Gamma=0\,. \tag{4.3.4}$$

Reproduced with permission of the copyright owner. Further reproduction prohibited without permission.

The velocity $\boldsymbol{u} = (-\partial_y \psi, \partial_x \psi)$ can be valued by using the standard long-stencil 4-th order formulas:

$$u = -\widetilde{D}_y(1 - \frac{h^2}{6} D_y^2)\psi; \quad v = \widetilde{D}_x(1 - \frac{h^2}{6} D_x^2)\psi . \tag{4.3.5}$$

Note that the implementation of (4.3.5) near the boundary needs "ghost point" values of ψ, which was discussed in Section 4.2 Corresponding to the new 4-th order vorticity boundary condition we will state below, we adopt the following 6-th order one-sided approximations for ψ at "ghost" points, (say, near Γ_x, $j = 0$), which are 2-D versions analogous to (4.2.9) and (4.2.10) as we presented in 1-D case

$$\psi_{i,-1} = 10\psi_{i,1} - 5\psi_{i,2} + \frac{5}{3}\psi_{i,2} - \frac{1}{4}\psi_{i,2} - 5h(\frac{\partial \psi}{\partial y})_{i,0} + O(h^6) , \tag{4.3.6}$$

$$\psi_{i,-2} = 80\psi_{i,1} - 45\psi_{i,2} + 16\psi_{i,3} - \frac{5}{2}\psi_{i,4} - 30h(\frac{\partial \psi}{\partial y})_{i,0} + O(h^6) . \tag{4.3.7}$$

On the boundary, we use the no-slip boundary condition $\boldsymbol{u}\,|_\Gamma = 0$.

The boundary condition for vorticity has been discussed in Section 4.2. For simplicity of our analysis below, which does not need the correction term $h^4\widehat{\psi}$ as we added in **4.2.4.1**, we use our new 4-th order vorticity boundary formula corresponding to (4.2.11) in 1-D case, which can be derived from (4.3.6) and (4.3.7)

$$\omega_{i,0} = \frac{1}{h^2}(8\psi_{i,1} - 3\psi_{i,2} + \frac{8}{9}\psi_{i,3} + \frac{1}{8}\psi_{i,4}) - \frac{25}{6h}(\frac{\partial \psi}{\partial x})_{i,0} . \tag{4.3.8}$$

The last terms in (4.3.6), (4.3.7) and (4.3.8) vanish if no-slip boundary condition for velocity is assumed.

Reproduced with permission of the copyright owner. Further reproduction prohibited without permission.

Theorem 4.3.1 *Let* $\boldsymbol{u}_e \in L^\infty([0,T]; C^{7,\alpha}(\overline{\Omega}))$ *be the solution of the Navier-Stokes equations (4.1.1)-(4.1.2) and* $\boldsymbol{u}_h$ *be the approximate solution of EC4, then we have*

(4.3.9)

$$\|\boldsymbol{u} - \boldsymbol{u}_h\|_{L^\infty([0,T],L^2)} \le Ch^4 \|\boldsymbol{u}_e\|_{L^\infty([0,T],C^{7,\alpha})}(1 + \|\boldsymbol{u}_e\|_{L^\infty([0,T],C^5)})\exp\left\{\frac{CC^*T}{\nu}\right\}.$$

where $C^* = (1 + \|\boldsymbol{u}_e\|_{L^\infty([0,T],C^5)})^2$.

4.3.2. Consistency Analysis

We denote $\psi_e, \boldsymbol{u}_e, \omega_e$ as the exact solutions of NSE, and extend ψ_e smoothly to $[-\delta, 1+\delta]^2$. Let $\Psi_{i,j} = \psi_e(x_i, y_j)$ for $-2 \le i, j \le N+2$, and construct U, V via the finite differences of Ψ

(4.3.10)

$$U_{i,j} = -\widetilde{D}_y(1 - \frac{h^2}{6}D_y^2)\Psi\,, \qquad V_{i,j} = \widetilde{D}_x(1 - \frac{h^2}{6}D_x^2)\Psi\,. \qquad \text{for } 0 \le i, j \le N\,.$$

The construction of the approximate vorticity is similar to that of 1-D case. First we define

$$\overline{\Omega}_{i,j} = (\triangle_h + \frac{h^2}{6}D_x^2 D_y^2)\Psi\,. \qquad \text{for } 1 \le i, j \le N-1\,. \tag{4.3.11}$$

and then recover Ω by solving the following system

$$(1 + \frac{h^2}{12}\triangle_h)\Omega_{i,j} = \overline{\Omega}_{i,j}\,. \tag{4.3.12}$$

once again, (4.3.12) always has a solution with suitable boundary condition for Ω since the eigenvalues of the matrix corresponding to $(1 + \frac{h^2}{12}\triangle_h)$ are all non-zero. The boundary condition for Ω (say on Γ_x, $j = 0$) is set to be

$$\Omega_{i,0} = (\omega_e)_{i,0} + h^4\tilde{\omega}_{i,0}\,. \qquad 0 \le i \le N\,. \tag{4.3.13}$$

where the function $\tilde{\omega}$ is introduced as

$$\tilde{\omega} = (-\frac{1}{240}\partial_x^4 - \frac{1}{240}\partial_y^4 + \frac{1}{90}\partial_x^2\partial_y^2)\omega_e\,. \tag{4.3.14}$$

Reproduced with permission of the copyright owner. Further reproduction prohibited without permission.

We should mention here that $h^4\hat{\omega}$ is just the $O(h^4)$ truncation error of $(\Delta_h + \frac{h^2}{6}D_x^2D_y^2)\psi_e - (1+\frac{h^2}{12}\Delta_h)\omega_e$, which is corresponding to $h^4\hat{\omega}_1$ as in (4.2.39) when we dealt with the 1-D case. Here we don't need the $h^4\hat{\omega}_2$ term appearing in (4.2.39), which corresponded to the correction term $h^4\hat{\psi}$, since we adopted the new 4-th order vorticity formula (4.3.8) instead of Briley's formula. The purpose of the introduction of $h^4\hat{\omega}$ is still to maintain the higher order consistency needed in the truncation error estimate below for the discrete derivatives of the constructed vorticity, as we can see in the following lemma, which is analogous to Lemma 4.2.2.

Lemma 4.3.1 *We have at grid points* $0 \le i, j \le N$,

$$\Omega = \omega_e + h^4\hat{\omega} + O(h^6)\|\psi_e\|_{C^8}. \tag{4.3.15}$$

Proof. Our construction of Ω and Ψ and Taylor expansion of ψ_e and ω_e indicate that at grid points (x_i, y_j), $1 \le i, j \le N-1$,

$$(1+\frac{h^2}{12}\Delta_h)\Omega = (\Delta_h+\frac{h^2}{6}D_x^2D_y^2)\Psi_e = (1+\frac{h^2}{12}\Delta_h)\omega_e+h^4\hat{\omega}+O(h^6)\|\psi_e\|_{C^8}. \tag{4.3.16}$$

where $\hat{\omega}$ was introduced in (4.3.14). (4.3.16) gives

$$(1+\frac{h^2}{12}\Delta_h)(\Omega-\omega_e-h^4\hat{\omega}) = -\frac{h^6}{12}\Delta_h\hat{\omega}+O(h^6)\|\psi_e\|_{C^8} = O(h^6)\|\psi_e\|_{C^8}. \tag{4.3.17}$$

since the second order differences of $\hat{\omega}$ is bounded by $\|\psi_e\|_{C^8}$. (4.3.17) along with (4.3.13), the boundary condition for Ω, and the property that the matrix $I+\frac{h^2}{12}\Delta_h$ is uniformly diagonally dominant, lead to (4.3.15). Lemma 4.3.1 is proved.

One direct consequence of (4.3.15) is that

$$(\Delta_h + \frac{h^2}{6}D_x^2D_y^2)\Omega = (\Delta_h + \frac{h^2}{6}D_x^2D_y^2)\omega_e + O(h^4)\|\psi_e\|_{C^8}. \tag{4.3.18}$$

which along with Taylor expansion of ω_e that

$$(\Delta_h + \frac{h^2}{6}D_x^2D_y^2)\omega_e = (1 + \frac{h^2}{12}\Delta)\Delta\omega_e + O(h^4)\|\psi_e\|_{C^8}. \tag{4.3.19}$$

Reproduced with permission of the copyright owner. Further reproduction prohibited without permission.

indicates the estimate of our truncation error for the diffusion term

$$(\triangle_h + \frac{h^2}{6}D_x^2D_y^2)\Omega = (1 + \frac{h^2}{12}\triangle)\triangle\omega_e + O(h^4)\|\psi_e\|_{C^6}. \tag{4.3.20}$$

Next we look at the convection term, which is the $\mathcal{NL}$ term applied to U, V and Ω introduced in (4.3.3). First we estimate the difference between U, V and u_e. Our definition of U, V and Taylor expansion of ψ_e shows that at the grid points (x_i, y_j), $0 \le i, j \le N$:

(4.3.21)

$$U = u_e + \frac{1}{30}h^4\partial_y^5\psi_e + O(h^5)\|\psi_e\|_{C^6}, \quad V = v_e - \frac{1}{30}h^4\partial_x^5\psi_e + O(h^5)\|\psi_e\|_{C^6}.$$

The combination of (4.3.21) and (4.3.15) gives that

$$\widetilde{D}_x(1 + \frac{h^2}{6}D_y^2)(U\Omega) = \widetilde{D}_x(1 + \frac{h^2}{6}D_y^2)(u_e\omega_e) + O(h^4)\|\psi_e\|_{C^6}\|\psi_e\|_{C^6}. \tag{4.3.22}$$

which along with the Taylor expansion of $u_e\omega_e$ that

$$\begin{aligned}\widetilde{D}_x(1 + \frac{h^2}{6}D_y^2)(u_e\omega_e) &= (1 + \frac{h^2}{6}\triangle)\partial_x(u_e\omega_e) + O(h^4)\|u_e\omega_e\|_{C^5} \\ &= (1 + \frac{h^2}{6}\triangle)\partial_x(u_e\omega_e) + O(h^4)\|\psi_e\|_{C^6}\|\psi_e\|_{C^6}.\end{aligned} \tag{4.3.23}$$

leads to the estimate that

$$\widetilde{D}_x(1 + \frac{h^2}{6}D_y^2)(U\Omega) = (1 + \frac{h^2}{6}\triangle)\partial_x(u_e\omega_e) + O(h^4)\|\psi_e\|_{C^6}\|\psi_e\|_{C^6}. \tag{4.3.24}$$

The other convection terms can be treated similarly

$$\widetilde{D}_y(1 + \frac{h^2}{6}D_x^2)(V\Omega) = (1 + \frac{h^2}{6}\triangle)\partial_y(v_e\omega_e) + O(h^4)\|\psi_e\|_{C^6}\|\psi_e\|_{C^6}. \tag{4.3.25}$$

$$\frac{h^2}{12}\triangle_h(U\widetilde{D}_x\Omega + V\widetilde{D}_y\Omega) = \frac{h^2}{12}\triangle(u_e\partial_x\omega_e + v_e\partial_y\omega_e) + O(h^4)\|\psi_e\|_{C^6}\|\psi_e\|_{C^6}. \tag{4.3.26}$$

The treatment of time marching term is also similar to that of 1-D case. Note that at the grid points (x_i, y_j), $1 \le i, j \le N-1$.

(4.3.27)

$$\begin{aligned}\partial_t(1 + \frac{h^2}{12}\triangle_h)\Omega &= (\triangle_h + \frac{h^2}{6}D_x^2D_y^2)\partial_t\psi_e \\ &= \Big(\triangle + \frac{h^2}{12}(\partial_x^4 + \partial_y^4) + \frac{h^2}{6}\partial_x^2\partial_y^2\Big)\partial_t\psi_e + O(h^4)\|\partial_t\psi_e\|_{C^6}.\end{aligned}$$

Reproduced with permission of the copyright owner. Further reproduction prohibited without permission.

where the first term is exactly $(1+\frac{h^2}{12}\triangle)\partial_t\omega_e$, and the estimate of the second term will resort to the Schauder estimate to the following Poisson equation satisfied by $\partial_t v_e$

$$\text{(4.3.28)} \qquad \begin{cases} \triangle(\partial_t v_e) = \partial_t\omega_e\,, & \text{in } \Omega\,. \\ \partial_t v_e = 0\,, & \text{on } \Gamma\,. \end{cases}$$

which leads to

$$\text{(4.3.29)} \qquad \|\partial_t v_e\|_{C^{3,\alpha}} \le C\|\partial_t\omega_e\|_{C^{1,\alpha}} \le C(\|v_e\|_{C^{3,\alpha}} + \|v_e\|_{C^{2,\alpha}}\|v_e\|_{C^{3,\alpha}})\,.$$

where in the second step we applied our original NSE again, as we did in the 1-D case. Then we arrive at

$$\text{(4.3.30)} \quad \partial_t(1+\frac{h^2}{12}\triangle_h)\Omega = (1+\frac{h^2}{12}\triangle)\partial_t\omega_e + O(h^4)(\|v_e\|_{C^{3,\alpha}} + \|v_e\|_{C^{2,\alpha}}\|v_e\|_{C^{3,\alpha}})\,.$$

Finally, the combination of (4.3.20), (4.3.24)-(4.3.26) and (4.3.30) completes the truncation error analysis for the momentum equation: at grid points (x_i, y_j), $1 \le i, j \le N-1$,

$$\text{(4.3.31)} \quad \begin{aligned} &(1+\frac{h^2}{12}\triangle_h)\partial_t\Omega + \widetilde{D}_x(1+\frac{h^2}{6}D_y^2)(U\Omega) + \widetilde{D}_y(1+\frac{h^2}{6}D_x^2)(V\Omega) - \frac{h^2}{12}\triangle_h(U\widetilde{D}_x\Omega + V\widetilde{D}_y\Omega) \\ &\quad = \nu(\triangle_h + \frac{h^2}{6}D_x^2D_y^2)\Omega + O(h^4)(\|\boldsymbol{u}_e\|_{C^{2,\alpha}} + \|\boldsymbol{u}_e\|_{C^3}\|\boldsymbol{u}_e\|_{C^2})\,. \end{aligned}$$

where we applied the NSE, which implies that $(1+\frac{h^2}{12}\triangle)\big(\partial_t\omega_e + \nabla\cdot(\boldsymbol{u}_e\omega_e) - \nu\triangle\omega_e\big) = 0$.

The estimate of Ω on the boundary is very straightforward here. As we can see, one-sided Taylor expansion of v_e at the boundary shows that

$$\text{(4.3.32)} \qquad (\omega_e)_{i,0} = \frac{1}{h^2}(8\Psi_{i,1} - 3\Psi_{i,2} + \frac{8}{9}\Psi_{i,3} - \frac{1}{8}\Psi_{i,4}) + O(h^4)\|v_e\|_{C^6}\,.$$

whose combination with our definition of $\Omega_{i,0}$ in (4.3.13) and the fact that $|\Omega_{i,0}| \le C\|v_e\|_{C^6}$, indicates the vorticity boundary condition up to $O(h^4)$ error:

$$\text{(4.3.33)} \qquad \Omega_{i,0} = \frac{1}{h^2}(8\Psi_{i,1} - 3\Psi_{i,2} + \frac{8}{9}\Psi_{i,3} - \frac{1}{8}\Psi_{i,4}) + O(h^4)\|v_e\|_{C^6}\,.$$

Reproduced with permission of the copyright owner. Further reproduction prohibited without permission.

4.3.3 Error estimates

For $0 \le i, j \le N$, we define

(4.3.34)

$$\tilde{\psi}_{i,j} = \psi_{i,j} - \Psi_{i,j}\,, \quad \tilde{\omega}_{i,j} = \omega_{i,j} - \Omega_{i,j}\,, \quad \tilde{u}_{i,j} = u_{i,j} - U_{i,j}\,, \quad \tilde{v}_{i,j} = v_{i,j} - V_{i,j}\,.$$

In addition, the error function for ϖ is introduced here at grid points (x_i, y_j), $1 \le i, j \le N-1$

$$\tilde{\varpi}_{i,j} = \varpi_{i,j} - \overline{\Omega}_{i,j} = (1 + \frac{h^2}{12}\triangle_h)\tilde{\omega}_{i,j}\,. \tag{4.3.35}$$

Our consistency analysis in **4.3.1** shows that

$$\begin{cases} \partial_t \tilde{\varpi} + \mathcal{L} = \nu(\triangle_h + \dfrac{h^2}{6}D_x^2 D_y^2)\tilde{\omega} + \boldsymbol{f}\,. \\ (\triangle_h + \dfrac{h^2}{6}D_x^2 D_y^2)\tilde{\psi} = (1 + \dfrac{h^2}{12}\triangle_h)\tilde{\omega}\,, \qquad \tilde{\psi}\,|_\Gamma = 0\,. \\ \tilde{u} = -\widetilde{D}_y(1 - \dfrac{h^2}{6}D_y^2)\tilde{\psi}\,, \quad \tilde{v} = \widetilde{D}_x(1 - \dfrac{h^2}{6}D_x^2)\tilde{\psi}\,. \end{cases} \tag{4.3.36}$$

where the local truncation error $|\boldsymbol{f}| \le Ch^4\|\boldsymbol{u}_e\|_{C^{7,\alpha}}(1+\|\boldsymbol{u}_e\|_{C^5})$, and the linearized convection error $\mathcal{L}$ is represented as

$$\begin{aligned} \mathcal{L} = {} & \widetilde{D}_x\Big(1 + \frac{h^2}{6}D_y^2\Big)(\tilde{u}\Omega + u\tilde{\omega}) + \widetilde{D}_y\Big(1 + \frac{h^2}{6}D_x^2\Big)(\tilde{v}\Omega + v\tilde{\omega}) \\ & - \frac{h^2}{12}\Delta_h(u\widetilde{D}_x\tilde{\omega} + v\widetilde{D}_y\tilde{\omega}) - \frac{h^2}{12}\Delta_h(\tilde{u}\widetilde{D}_x\Omega + \tilde{v}\widetilde{D}_y\Omega)\,. \end{aligned} \tag{4.3.37}$$

On the boundary (say near Γ_x, $j = 0$), we have

$$\begin{aligned} \tilde{\omega}_{i,0} &= \frac{1}{h^2}(8\tilde{\psi}_{i,1} - 3\tilde{\psi}_{i,2} + \frac{8}{9}\tilde{\psi}_{i,3} - \frac{1}{8}\tilde{\psi}_{i,4}) + h^4 e_i\,. \\ \tilde{\psi}_{i,-1} &= 10\tilde{\psi}_{i,1} - 5\tilde{\psi}_{i,2} + \frac{5}{3}\tilde{\psi}_{i,3} - \frac{1}{4}\tilde{\psi}_{i,4} + O(h^5)\|\boldsymbol{u}_e\|_{C^5}\,. \end{aligned} \tag{4.3.38}$$

where $|\boldsymbol{g}| \le C\|\boldsymbol{u}_e\|_{C^5}$. The first equality in (4.3.38) comes from our numerical boundary condition (4.3.8) and our estimate (4.3.33); the second estimate in (4.3.38) comes from our numerical "ghost point" value (4.3.5) and Taylor expansion of ψ_e.

Reproduced with permission of the copyright owner. Further reproduction prohibited without permission.

Our strategy of estimating the error functions is similar to that of 1-D case. Multiplying the vorticity error equation in (4.3.36) by $-(1+\frac{h^2}{12}\triangle_h)\tilde{\omega}$, using the fact that $\tilde{\omega}$ vanishes on the boundary which indicates that (the derivation of the following identity is similar to that of (4.2.14))

$$-\langle(1+\frac{h^2}{12}\triangle_h)\tilde{\omega},\partial_t\tilde{\psi}\rangle=-\langle(1+\frac{h^2}{12}\triangle_h)\tilde{\psi},(\triangle_h+\frac{h^2}{6}D_x^2D_y^2)\partial_t\tilde{\omega}\rangle=\frac{1}{2}\frac{d\tilde{E}}{dt}, \tag{4.3.39}$$

where $\tilde{E}$ is denoted as

(4.3.40)

$$\tilde{E}=\|\nabla_h\tilde{\psi}\|^2-\frac{h^2}{12}\|\triangle_h\tilde{\psi}\|^2-\frac{h^2}{6}\|D_xD_y\tilde{\psi}\|^2+\frac{h^4}{72}(\|D_xD_y^2\tilde{\psi}\|^2+\|D_yD_x^2\tilde{\psi}\|^2),$$

and applying Cauchy inequality for $\langle(1+\frac{h^2}{12})\triangle_h\tilde{\psi},\boldsymbol{f}\rangle$, we arrive at

$$\begin{aligned}&\frac{1}{2}\frac{d\tilde{E}}{dt}+\nu\Big\langle(1+\frac{h^2}{12}\triangle_h)\tilde{\psi},(\triangle_h+\frac{h^2}{6}D_x^2D_y^2)\tilde{\omega}\Big\rangle-\Big\langle(1+\frac{h^2}{12}\triangle_h)\tilde{\psi},\mathcal{L}\Big\rangle\\&\qquad\le C\|\tilde{\psi}\|^2+C\|\boldsymbol{f}\|^2.\end{aligned} \tag{4.3.41}$$

The estimates of the diffusion and convection terms are presented in the following two lemmas. The proofs of them will be given in Section 4.4.

Lemma 4.3.2 *For sufficiently small h, we have*

$$\langle(1+\frac{h^2}{12}\triangle_h)\tilde{\psi},(\triangle_h+\frac{h^2}{6}D_x^2D_y^2)\tilde{\omega}\rangle\ge\frac{3}{16}\|\tilde{\omega}\|^2-h^8. \tag{4.3.42}$$

Lemma 4.3.3 *Assume a-prior that the error function for the velocity field satisfy*

$$\|\tilde{\boldsymbol{u}}\|_{L^\infty}\le h, \tag{4.3.43}$$

then we have

$$\Big|\Big\langle(1+\frac{h^2}{12}\triangle_h)\tilde{\psi},\mathcal{L}\Big\rangle\Big|\le\tilde{C}\|\nabla_h\tilde{\psi}\|^2+\frac{\nu}{8}\|\tilde{\omega}\|^2+h^8, \tag{4.3.44}$$

where $\mathcal{L}$ was defined in (4.3.37) and $\tilde{C}=\frac{32(1+\|\boldsymbol{u}_e\|_{C^0})^2}{\nu}+C(2+\|\boldsymbol{u}_e\|_{C^1})^2+C\|\boldsymbol{u}_e\|_{C^\infty}$.

Then we go back to our convergence analysis. First we assume that (4.3.43) holds. Plugging (4.3.44), (4.3.42) back into (4.3.41), we obtain

$$\frac{1}{2}\frac{d\tilde{E}}{dt}\le(1+\nu)h^8+C\|\boldsymbol{f}\|^2+C\|\tilde{\psi}\|^2+(\tilde{C}+C)\|\nabla_h\tilde{\psi}\|^2-\frac{\nu}{16}\|\tilde{\omega}\|^2. \tag{4.3.45}$$

Reproduced with permission of the copyright owner. Further reproduction prohibited without permission.

As we can see, $\|\tilde{\omega}\|^2$ can be absorbed in the coefficient of $\|\nabla_h\tilde{\omega}\|^2$ since the Poincare inequality for $\tilde{\omega}$: $\|\tilde{\omega}\|^2 \le C\|\nabla_h\tilde{\omega}\|^2$ can be applied here. Integrating in time for (4.3.45) gives us

$$\tilde{E} + \frac{\nu}{8}\int_0^T \|\tilde{\omega}\|^2 dt \le C\int_0^T \|\boldsymbol{f}\|^2\,dt + \tilde{C}\int_0^T \|\nabla_h\tilde{\omega}\|^2\,dt + CTh^8\,. \tag{4.3.46}$$

Since the property of $\tilde{\omega}$ that it vanishes on the boundary indicates

$$\|\nabla_h\tilde{\omega}\|^2 \le 3(\|\nabla_h\tilde{\omega}\|^2 - \frac{h^2}{12}\|\Delta_h\tilde{\omega}\|^2 - \frac{h^2}{6}\|D_xD_y\tilde{\omega}\|^2)\,. \tag{4.3.47}$$

which implies that $\frac{1}{3}\|\nabla_h\tilde{\omega}\|^2 \le \tilde{E}$, we arrive at

$$\|\nabla_h\tilde{\omega}\|^2 + \frac{3\nu}{8}\int_0^T \|\tilde{\omega}\|^2\,dt \le C\int_0^T (\|\boldsymbol{f}\|^2 + h^8)\,dt + \tilde{C}\int_0^T \|\nabla_h\tilde{\omega}\|^2\,dt\,. \tag{4.3.48}$$

By Gronwall inequality, we have

$$\begin{aligned}\|\nabla_h\tilde{\omega}\|^2 &\le C\exp\left\{\tilde{C}T\right\}\int_0^T (\|\boldsymbol{f}(\cdot,s)\|^2 + h^8)\,ds \\ &\le Ch^8\exp\left\{\frac{CC^*T}{\nu}\right\}\|\boldsymbol{u}_e\|^2_{C^{7,\alpha}}(1+\|\boldsymbol{u}_e\|_{C^5})^2\,.\end{aligned} \tag{4.3.49}$$

since $\tilde{C} \le \frac{CC^*T}{\nu}$ where C^* was introduced after (4.3.9). Thus, we have proved

$$\|\boldsymbol{u}(\cdot,t) - \boldsymbol{u}(t)\|_{L^2} \le Ch^4\|\boldsymbol{u}_e\|_{C^{7,\alpha}}(1+\|\boldsymbol{u}_e\|_{C^5})\exp\left\{\frac{CC^*T}{\nu}\right\}\,. \tag{4.3.50}$$

which implies (4.3.9). Using the inverse inequality, we have

$$\|\tilde{\boldsymbol{u}}\|_{L^\infty} \le Ch^3\,. \tag{4.3.51}$$

Now we can resort to a standard trick which asserts that (4.3.43) will never be violated if h is small enough. Theorem 4.3.1 is proved.

Reproduced with permission of the copyright owner. Further reproduction prohibited without permission.

4.4 Proof of the Lemmas in Section 4.3

For the convenience of the analysis below, we define $\|\tilde{\omega}\|_W$ by

$$\|\tilde{\omega}\|_W^2 = \sum_{0\le i,j\le N} \tilde{\omega}_{i,j}^2 h^2 . \tag{4.4.1}$$

Note that the difference between $\|\tilde{\omega}\|_W$ and $\|\tilde{\omega}\|$ is that $\|\tilde{\omega}\|_W$ involves the boundary values of $\tilde{\omega}$.

To prove Lemma 4.3.2, the estimate of the diffusion term, some preliminary results in the following Lemma 4.4.1 are needed.

Lemma 4.4.1 *We have*

$$\|D_x^2\tilde{\psi}\|^2 + \|D_y^2\tilde{\psi}\|^2 \le \frac{9}{8}\|\tilde{\omega}\|^2 . \tag{4.4.2}$$

$$\|(1+\frac{h^2}{6}D_y^2)D_x^2\tilde{\psi}\|^2 + \|(1+\frac{h^2}{6}D_x^2)D_y^2\tilde{\psi}\|^2 \le \|\tilde{\omega}\|^2 . \tag{4.4.3}$$

Proof of Lemma 4.4.1 The proof of Lemma 4.4.1 is similar to Lemma 4.2.1 in 1-D case. Since $\tilde{\psi}_{i,j}|_\Gamma = 0$, we can Sine transform $\{\tilde{\psi}_{i,j}\}$ on both directions, i.e.,

$$\tilde{\psi}_{i,j} = \sum_{k,\ell} \hat{\tilde{\psi}}_{k,\ell} \sin(k\pi x_i)\sin(\ell\pi y_j) . \tag{4.4.4}$$

Again, Parserval equality gives

$$\sum_{i,j}(\tilde{\psi}_{i,j})^2 = \sum_{k,\ell}\left|\hat{\tilde{\psi}}_{k,\ell}\right|^2 . \tag{4.4.5}$$

If we introduce

$$f_k = -\frac{4}{h^2}\sin^2(\frac{k\pi h}{2}), \qquad g_\ell = -\frac{4}{h^2}\sin^2(\frac{\ell\pi h}{2}), \tag{4.4.6}$$

we obtain the Fourier expansions of $D_x^2\tilde{\psi}$ and $D_y^2\tilde{\psi}$

$$D_x^2\tilde{\psi}_{i,j} = \sum_{k,l} f_k\,\hat{\tilde{\psi}}_{k,l}, \qquad D_y^2\tilde{\psi}_{i,j} = \sum_{k,l} g_\ell\,\hat{\tilde{\psi}}_{k,l} . \tag{4.4.7}$$

Reproduced with permission of the copyright owner. Further reproduction prohibited without permission.

which in turn implies that

$$(4.4.8)\quad \sum_{i,j}|\tilde{\bar{\omega}}_{i,j}|^2=\sum_{i,j}|(\triangle_h+\frac{h^2}{6}D_x^2D_y^2)\tilde{\omega}_{i,j}|^2=\sum_{k,\ell}(g_\ell+f_k+\frac{h^2}{6}f_kg_\ell)^2\left|\tilde{\hat{\omega}}_{k,\ell}\right|^2.$$

Similarly, we have

$$(4.4.9)\quad \begin{aligned}\sum_{i,j}|(1+\frac{h^2}{6}D_y^2)D_x^2\tilde{\omega}_{i,j}|^2&=\sum_{k,\ell}|(1+\frac{h^2}{6}g_\ell)f_k|^2\left|\tilde{\hat{\omega}}_{k,\ell}\right|^2,\\ \sum_{i,j}|(1+\frac{h^2}{6}D_x^2)D_y^2\tilde{\omega}_{i,j}|^2&=\sum_{k,\ell}|(1+\frac{h^2}{6}f_k)g_\ell|^2\left|\tilde{\hat{\omega}}_{k,\ell}\right|^2.\end{aligned}$$

On the other hand, the fact that $-\frac{4}{h^2}\le f_k,g_\ell\le 0$ shows that

$$(4.4.10)\qquad |g_\ell+f_k+\frac{h^2}{6}f_kg_\ell|^2\ge|(1+\frac{h^2}{6}g_\ell)f_k|^2+|(1+\frac{h^2}{6}f_k)g_\ell|^2.$$

$$(4.4.11)\qquad |g_\ell+f_k+\frac{h^2}{6}f_kg_\ell|^2\ge(f_k^2+g_\ell^2-\frac{2}{9}f_kg_\ell)\ge\frac{8}{9}(f_k^2+g_\ell^2).$$

by direct calculations. The combination of (4.4.8), (4.4.9) and (4.4.10) gives us (4.4.3). (4.4.2) can be argued in a similar fashion. Lemma 4.4.1 is proved.

Now we go back our proof of Lemma 4.3.2.

Proof of Lemma 4.3.2 Summing by parts and keeping in mind that $\tilde{\omega}|_\Gamma=0$, (which is similar to the process in (4.2.15)), we have

(4.4.12)
$$\left\langle(1+\frac{h^2}{12}\triangle_h)\tilde{\omega},(\triangle_h+\frac{h^2}{6}D_x^2D_y^2)\tilde{\omega}\right\rangle=\left\langle(\triangle_h+\frac{h^2}{6}D_x^2D_y^2)\tilde{\omega},(1+\frac{h^2}{12}\triangle_h)\tilde{\omega}\right\rangle+\mathcal{B},$$

where the first term is exactly $\|\tilde{\bar{\omega}}\|^2$ since $(\triangle_h+\frac{h^2}{6}D_x^2D_y^2)\tilde{\omega}=(1+\frac{h^2}{12}\triangle_h)\tilde{\omega}=\tilde{\bar{\omega}}$, and the boundary term $\mathcal{B}$ can be decomposed as three parts $\mathcal{B}=\mathcal{B}_1+\mathcal{B}_2+\mathcal{B}_3$.

Reproduced with permission of the copyright owner. Further reproduction prohibited without permission.

where

$$\begin{aligned}
\mathcal{B}_1 &= \sum_{i=1}^{N-1}\Big((1+\frac{h^2}{6}D_x^2)\tilde{\omega}_{i,1}\cdot\tilde{\omega}_{i,0}+(1+\frac{h^2}{6}D_x^2)\tilde{\omega}_{i,N-1}\cdot\tilde{\omega}_{i,N}\Big)\\
&+\sum_{j=1}^{N-1}\Big((1+\frac{h^2}{6}D_y^2)(\tilde{\omega}_{1,j}\cdot\tilde{\omega}_{0,j}+(1+\frac{h^2}{6}D_y^2)\tilde{\omega}_{N-1,j}\cdot\tilde{\omega}_{N,j})\Big)\\
\mathcal{B}_2 &= \frac{h^4}{72}\sum_{i=1}^{N-1}(D_x^2\tilde{\omega}_{i,1}D_x^2\tilde{\omega}_{i,0}+D_x^2\tilde{\omega}_{i,N-1}D_x^2\tilde{\omega}_{i,N})\\
&+\frac{h^4}{72}\sum_{j=1}^{N-1}D_y^2\tilde{\omega}_{1,j}D_y^2\tilde{\omega}_{0,j}+D_y^2\tilde{\omega}_{N-1,j}D_y^2\tilde{\omega}_{N,j})\\
\mathcal{B}_3 &= \frac{1}{6}(\tilde{\omega}_{1,1}\tilde{\omega}_{0,0}+\tilde{\omega}_{1,N-1}\tilde{\omega}_{0,N}+\tilde{\omega}_{N-1,1}\tilde{\omega}_{N,0}+\tilde{\omega}_{N-1,N-1}\tilde{\omega}_{N,N}).
\end{aligned}\tag{4.4.13}$$

Next we estimate the three boundary terms separately.

Lemma 4.4.2 *We have the estimate*

$$\mathcal{B}_1 \geq \frac{1}{3h^2}\mathcal{B}_v-\frac{3}{4}\|\tilde{\bar{\omega}}\|^2-Ch^9,\tag{4.4.14}$$

where $\mathcal{B}_v$ is introduced as

$$\mathcal{B}_v=\sum_{i=1}^{N-1}(\tilde{v}_{i,1}^2+\tilde{v}_{i,N-1}^2)+\sum_{j=1}^{N-1}(\tilde{\psi}_{1,j}^2+\tilde{\psi}_{N-1,j}^2).\tag{4.4.15}$$

Proof. The boundary condition for $\tilde{\omega}$ in (4.3.38) implies that $\sum_{i=1}^{N-1}(1+\frac{h^2}{6}D_x^2)\tilde{v}_{i,1}\tilde{\omega}_{i,0}$ includes two parts: I_1 and I_2, where

$$\begin{aligned}
I_1 &= \frac{1}{h^2}\sum_{i=1}^{N-1}(1+\frac{h^2}{6}D_x^2)\tilde{\psi}_{i,1}(8\tilde{\psi}_{i,1}-3\tilde{\psi}_{i,2}+\frac{8}{9}\tilde{\psi}_{i,3}-\frac{1}{8}\tilde{\psi}_{i,4}).\\
I_2 &= h^4\sum_{i=1}^{N-1}(1+\frac{h^2}{6}D_x^2)\tilde{v}_{i,1}\boldsymbol{e}_i.
\end{aligned}\tag{4.4.16}$$

The term I_2 can be controlled by Cauchy inequality directly: first, summing by parts gives $I_2=h^4\sum_{i=1}^{N-1}\tilde{v}_{i,1}(1+\frac{h^2}{6}D_x^2)\boldsymbol{e}_{i,0}$, then we have

$$I_2\geq-\frac{1}{36}\sum_{i=1}^{N-1}\frac{\tilde{v}_{i,1}^2}{h^2}-9\sum_{i=1}^{N-1}h^{10}\Big((1+\frac{h^2}{6}D_x^2)\boldsymbol{e}_i\Big)^2\geq-\frac{1}{36}\sum_{i=1}^{N-1}\frac{\tilde{v}_{i,1}^2}{h^2}-Ch^9.\tag{4.4.17}$$

Reproduced with permission of the copyright owner. Further reproduction prohibited without permission.

since $|e_{i,0}| \le C\|u_e\|_{C^5}$. Our main concern will be I_1. Similar to the argument in (4.3.2.29), the term $8\tilde{\omega}_{i,1} - 3\tilde{\omega}_{i,2} + \frac{8}{9}\tilde{\omega}_{i,3} - \frac{1}{8}\tilde{\omega}_{i,4}$ can be rewritten as

(4.4.18)
$$8\tilde{\omega}_{i,1}-3\tilde{\omega}_{i,2}+\frac{8}{9}\tilde{\omega}_{i,3}-\frac{1}{8}\tilde{\omega}_{i,4} = \frac{25}{6}\tilde{\omega}_{i,1}-\frac{115}{72}h^2(D_y^2\tilde{\psi})_{i,1}+\frac{23}{36}h^2(D_y^2\tilde{\omega})_{i,2}-\frac{1}{8}h^2(D_y^2\tilde{\omega})_{i,3},$$

which in turn implies that I_1 can be expressed as

(4.4.19)
$$\begin{aligned} I_1 = \; & \frac{25}{6h^2}\sum_{i=1}^{N-1}(\tilde{\omega}_{i,1}^2 + \frac{h^2}{6}\tilde{\omega}_{i,1}D_x^2\tilde{\omega}_{i,1}) - \frac{115}{72}\sum_{i=1}^{N-1}\tilde{\psi}_{i,1}(1+\frac{h^2}{6}D_x^2)(D_y^2\tilde{\omega})_{i,1} \\ & +\frac{23}{36}\sum_{i=1}^{N-1}\tilde{\omega}_{i,1}(1+\frac{h^2}{6}D_x^2)(D_y^2\tilde{\psi})_{i,2} - \frac{1}{8}\sum_{i=1}^{N-1}\tilde{\psi}_{i,1}(1+\frac{h^2}{6}D_x^2)(D_y^2\tilde{\omega})_{i,3}, \end{aligned}$$

where we summed by parts again, since $\tilde{\psi}|_\Gamma = 0$. Each term in I_1 can be estimated by Cauchy inequality

(4.4.20)
$$\begin{aligned} & \sum_{i=1}^{N-1}(\tilde{\omega}_{i,1}^2 + \frac{h^2}{6}\tilde{\omega}_{i,1}D_x^2\tilde{\omega}_{i,1}) \ge \frac{1}{3}\sum_{i=1}^{N-1}\tilde{\omega}_{i,1}^2, \\ & -\frac{115}{72}\tilde{\omega}_{i,1}\Big(1+\frac{h^2}{6}D_x^2\Big)(D_y^2\tilde{\omega})_{i,1} \ge -\frac{1}{3h^2}\frac{115^2}{72^2}|\tilde{\omega}_{i,1}|^2 - \frac{3}{4}h^2\Big|\Big(1+\frac{h^2}{6}D_x^2\Big)(D_y^2\tilde{\omega})_{i,1}\Big|^2h^2 \\ & \frac{23}{36}\tilde{\omega}_{i,1}\Big(1+\frac{h^2}{6}D_x^2\Big)(D_y^2\tilde{\omega})_{i,2} \ge -\frac{1}{3h^2}\frac{23^2}{36^2}|\tilde{\omega}_{i,1}|^2 - \frac{3}{4}h^2\Big|\Big(1+\frac{h^2}{6}D_x^2\Big)(D_y^2\tilde{\omega})_{i,2}\Big|^2h^2, \\ & \frac{1}{8}\tilde{\omega}_{i,1}\Big(1+\frac{h^2}{6}D_x^2\Big)(D_y^2\tilde{\omega})_{i,3} \ge -\frac{1}{3h^2}\frac{1^2}{8^2}|\tilde{\omega}_{i,1}|^2 - \frac{3}{4}h^2\Big|\Big(1+\frac{h^2}{6}D_x^2\Big)(D_y^2\tilde{\omega})_{i,3}\Big|^2h^2. \end{aligned}$$

Since $\frac{1}{3}\cdot\frac{25}{6} - \frac{1}{3}(\frac{115^2}{72^2} + \frac{23^2}{36^2} + \frac{1^2}{8^2}) \ge \frac{13}{36}$, we have

$$I_1 \ge \frac{13}{36h^2}\sum_{i=1}^{N-1}|\tilde{\omega}_{i,1}|^2 - \frac{3}{4}h^2\sum_{i=1}^{N-1}\sum_{j=1,2,3}\Big|\Big(1+\frac{h^2}{6}D_x^2\Big)D_y^2\tilde{\omega}_{i,j}\Big|^2. \tag{4.4.21}$$

The combination of I_1 and I_2 gives

$$\begin{aligned} & \sum_{i=1}^{N-1}\Big(1+\frac{h^2}{6}D_x^2\Big)\tilde{\omega}_{i,1}\tilde{\omega}_{i,0} \\ & \ge \frac{1}{3h^2}\sum_{i=1}^{N-1}|\tilde{\omega}_{i,1}|^2 - \frac{3}{4}\sum_{i}\sum_{j=1,2,3}\Big|\Big(1+\frac{h^2}{6}D_x^2\Big)D_y^2\tilde{\omega}_{i,j}\Big|^2h^2 - Ch^9. \end{aligned} \tag{4.4.22}$$

Reproduced with permission of the copyright owner. Further reproduction prohibited without permission.

The treatment of the other three boundary terms is exactly the same. Finally we obtain

$$\begin{aligned}\mathcal{B}_1 \geq \frac{1}{3h^2}\mathcal{B}_v - \frac{3}{4}h^2\sum_{i=1}^{N-1}\sum_{j=1}^{N-1}|(1+\frac{h^2}{6}D_y^2)D_x^2\tilde{v}_{i,j}|^2 \\ -\frac{3}{4}h^2\sum_{i=1}^{N-1}\sum_{j=1}^{N-1}|(1+\frac{h^2}{6}D_x^2)D_y^2\tilde{v}_{i,j}|^2 - Ch^9\,.\end{aligned} \tag{4.4.23}$$

where $\mathcal{B}_v$ was defined in (4.4.15). The combination of (4.4.23) and (4.4.3) in Lemma 4.4.1 implies (4.4.14). This completes the proof of Lemma 4.4.2.

$\mathcal{B}_2$ can be treated in a similar fashion. We still only look at the term $\sum_i D_x^2\tilde{v}_{i,1}D_x^2\tilde{\omega}_{i,0}$ here. Once again, (4.3.38), the boundary condition for $\tilde{\omega}$ indicates that $\sum_i D_x^2\tilde{v}_{i,1}D_x^2\tilde{\omega}_{i,0}$ includes two parts: I_3 and I_4, which are denoted as

$$\begin{aligned}I_3 &= \frac{1}{h^2}\sum_{i=1}^{N-1}D_x^2\tilde{v}_{i,1}\left(8D_x^2\tilde{\psi}_{i,1} - 3D_x^2\tilde{\psi}_{i,2} + \frac{8}{9}D_x^2\tilde{v}_{i,3} - \frac{1}{8}D_x^2\tilde{v}_{i,4}\right), \\ I_4 &= h^4\sum_{i=1}^{N-1}D_x^2\tilde{v}_{i,1}D_x^2\mathbf{e}_i\,.\end{aligned} \tag{4.4.24}$$

The estimate of I_3 and I_4 is similar to that of I_1 and I_2, respectively. Repeating the arguments in the proof of Lemma 4.4.2, we can get (the detail is omitted here)

$$\mathcal{B}_2 \geq -\frac{1}{144}h^4\|D_y^2D_x^2\tilde{\psi}\|^2 - Ch^9\,. \tag{4.4.25}$$

On the other hand, the fact that $\|D_y^2D_x^2\tilde{\psi}\| \leq \frac{4}{h^2}\|D_x^2\tilde{\psi}\|$ and $\|D_y^2D_x^2\tilde{v}\| \leq \frac{1}{h^2}\|D_y^2\tilde{v}\|$ implies

(4.4.26)

$$\|D_y^2D_x^2\tilde{v}\|^2 = \frac{1}{2}(\|D_y^2D_x^2\tilde{v}\|^2 + \|D_y^2D_x^2\tilde{v}\|^2) \leq \frac{8}{h^4}\|D_x^2\tilde{\psi}\|^2 + \frac{8}{h^4}\|D_y^2\tilde{\psi}\|^2 \leq \frac{9}{h^4}\|\tilde{\varpi}\|^2\,.$$

where in the last step we applied (4.4.2) in Lemma 4.4.1. Substituting (4.4.26) into (4.4.25), we arrive at

$$\mathcal{B}_2 \geq -\frac{1}{16}\|\tilde{\varpi}\|^2 - Ch^9\,. \tag{4.4.27}$$

Reproduced with permission of the copyright owner. Further reproduction prohibited without permission.

Finally, $\mathcal{B}_3$ can be controlled by standard Cauchy inequality (still, we only look at the term $\frac{1}{6}\tilde{v}_{1,1}\tilde{\omega}_{0,0}$)

$$\frac{1}{6}\tilde{v}_{1,1}\tilde{\omega}_{0,0} \geq -\frac{1}{12}\frac{\tilde{v}_{1,1}^2}{h^2} - \frac{1}{12}h^2\tilde{\omega}_{0,0}^2 \geq -\frac{1}{12}\frac{\tilde{v}_{1,1}^2}{h^2} - Ch^{10}\|v_e\|_{C^8}^2, \tag{4.4.28}$$

where in the last step we used the fact that $|\tilde{\omega}_{0,0}| \leq Ch^4\|v_e\|_{C^8}$ by our numerical ω and our construction of Ω in §3.3.1. As we can see, the first term appearing on the right hand side of (4.4.28) can be absorbed in the $\mathcal{B}_v$ term.

$$\mathcal{B}_3 \geq -\frac{1}{12h^2}\mathcal{B}_v - Ch^9, \tag{4.4.29}$$

Finally, the combination of (4.4.14), (4.4.27) and (4.4.29) shows that $\mathcal{B} \geq -\frac{13}{16}\|\tilde{\bar{\omega}}\|^2 - h^8$, whose substitution in (4.4.12) is exactly (4.3.42). Thus we finish the proof of Lemma 4.3.2.

Before we proceed to the proof of Lemma 4.3.3, we need to have a good estimate of $\|\tilde{\omega}\|_{1,h}^2$, introduced in (4.4.1), which includes the boundary values of $\tilde{\omega}$.

Lemma 4.4.3 *We have*

$$\|\tilde{\omega}\|_{1,h}^2 \leq C\|\tilde{\bar{\omega}}\|^2 + \frac{C}{h^2}\|\nabla_h\tilde{\psi}\|^2 + Ch^9. \tag{4.4.30}$$

Proof. Step 1. Establish a bound for $\|\tilde{\omega}\|^2$

We follow the pattern of analysis in the proof of Lemma 4.4.1 We need to decompose $\tilde{\omega}$ since it does not vanish on the boundary: let $\tilde{\omega}^0$ and $\tilde{\omega}^b$ be the interior part and boundary part of $\tilde{\omega}$, respectively, i.e. $\tilde{\omega} = \tilde{\omega}^0 + \tilde{\omega}^b$, such that

$$\begin{aligned} &\tilde{\omega}_{i,j}^0 = \tilde{\omega}_{i,j}, \qquad \tilde{\omega}_{i,j}^b = 0, \qquad \text{for } 1 \leq i,j \leq N-1, \\ &\tilde{\omega}_{i,j}^0 = 0, \qquad \tilde{\omega}_{i,j}^b = \tilde{\omega}_{i,j}, \qquad \text{on } \Gamma, \end{aligned} \tag{4.4.31}$$

and define $\tilde{\bar{\omega}}^0 = (1 + \frac{1}{12}\Delta_h)\tilde{\omega}^0$. Since $\tilde{\omega}^0$ vanishes on the boundary, we can Sine transform $\left\{\tilde{\omega}_{i,j}^0\right\}$ both in the i-direction and j-direction, i.e.

$$\tilde{\omega}_{i,j}^0 = \sum_{k,\ell}\hat{\tilde{\omega}}_{k,\ell}^0 \sin(k\pi x_i)\sin(\ell\pi y_j). \tag{4.4.32}$$

Reproduced with permission of the copyright owner. Further reproduction prohibited without permission.

Then, Parserval equality applied to $\bar{\omega}^0$ gives

$$\sum_{i,j}(\bar{\omega}^0_{i,j})^2 = \sum_{k,\ell}\left|\hat{\bar{\omega}}^0_{k,\ell}\right|^2 . \tag{4.4.33}$$

Similarly, we have $D_x^2\bar{\omega}^0_{i,j} = \sum_{k,l} f_k\,\hat{\bar{\omega}}^0_{k,l}$, and $D_y^2\bar{\omega}^0_{i,j} = \sum_{k,l} g_\ell\,\hat{\bar{\omega}}^0_{k,l}$, as in (4.4.6) and (4.4.7), which in turn indicates that

$$\sum_{i,j}|\bar{\bar{\omega}}^0_{i,j}|^2 = \sum_{i,j}|(1+\frac{h^2}{12}\Delta_h)\bar{\omega}^0_{i,j}|^2 = \sum_{k,\ell}|1+\frac{h^2}{12}(f_k+g_\ell)|^2\left|\hat{\bar{\omega}}^0_{k,\ell}\right|^2 . \tag{4.4.34}$$

The combination of (4.4.33), (4.4.34), along with the fact that $\frac{1}{3} \le 1+\frac{h^2}{12}(f_k+g_\ell) \le 1$, shows that

$$\|\bar{\bar{\omega}}^0\|^2 \ge \frac{1}{9}\|\bar{\omega}\|^2 . \tag{4.4.35}$$

On the other hand, we note that $\bar{\bar{\omega}}^0_{i,j} = \bar{\bar{\omega}}_{i,j}$ for $2 \le i,j \le N-2$, and near the boundary (say at $j=1$),

$$|\bar{\bar{\omega}}^0_{i,1}|^2 = (\bar{\bar{\omega}}_{i,1} - \frac{1}{12}\bar{\omega}_{i,0})^2 \le \frac{13}{12}\bar{\bar{\omega}}^2_{i,1} + \frac{13}{144}\bar{\omega}^2_{i,0} . \tag{4.4.36}$$

and near the corner (say at $i=1$, $j=1$)

$$|\bar{\bar{\omega}}^0_{1,1}|^2 = (\bar{\bar{\omega}}_{1,1} - \frac{1}{12}\bar{\omega}_{1,0} - \frac{1}{12}\bar{\omega}_{0,1})^2 \le \frac{7}{6}\bar{\bar{\omega}}^2_{1,1} + \frac{7}{72}(\bar{\omega}^2_{1,0}+\bar{\omega}^2_{0,1}) . \tag{4.4.37}$$

which indicates that

$$\|\bar{\bar{\omega}}^0\|^2 \le \frac{7}{6}\|\bar{\bar{\omega}}\|^2 + \frac{7}{72}\Big(\sum_{i=1}^{N-1} h^2(|\bar{\omega}_{i,0}|^2+|\bar{\omega}_{i,N}|^2) + \sum_{j=1}^{N-1} h^2(|\bar{\omega}_{0,j}|^2+|\bar{\omega}_{N,j}|^2)\Big) . \tag{4.4.38}$$

The combination of (4.4.38) and (4.4.35) gives us

$$\|\bar{\omega}\|^2 \le \frac{21}{2}\|\bar{\bar{\omega}}\|^2 + \frac{7}{8}h^2\mathcal{B}_\omega , \tag{4.4.39}$$

where $\mathcal{B}_\omega$ is the total sum of boundary terms for $\bar{\omega}$:

$$\mathcal{B}_\omega = \sum_{i=1}^{N-1}(|\bar{\omega}_{i,0}|^2+|\bar{\omega}_{i,N}|^2) + \sum_{j=1}^{N-1}(|\bar{\omega}_{0,j}|^2+|\bar{\omega}_{N,j}|^2) . \tag{4.4.40}$$

Reproduced with permission of the copyright owner. Further reproduction prohibited without permission.

Step 2. (4.4.30) is a direct consequence of (4.4.39) and our boundary condition for vorticity error function as in (4.3.38):

By our definition of $\|\tilde{\omega}\|_W$ in (4.4.1), we have $\|\tilde{\omega}\|_W^2 = \|\tilde{\omega}\|^2 + h^2\mathcal{B}_\omega$, where $\mathcal{B}_\omega$ was defined in (4.4.40), whose substitution into (4.4.30) leads to $\|\tilde{\omega}\|^2 \le \frac{21}{2}\|\tilde{\psi}\|^2 + 2h^2\mathcal{B}_\omega$. Then the remaining task is to control $\mathcal{B}_\omega$. For simplicity we just look at the first term $\sum_{i=1}^{N-1}\tilde{\omega}_{i,0}^2$. Similar to the proof of the diffusion term in Lemma 4.3.2, we can apply (4.3.38), the boundary condition for $\tilde{\omega}$, to recover $\mathcal{B}_\omega$. The term appearing in the parenthesis in (4.3.38) can be rewritten as (4.4.18), whose substitution into (4.3.38) shows that

(4.4.41)
$$\tilde{\omega}_{i,0}^2 \le \frac{4}{h^4}\Big(\frac{25^2}{6^2}\tilde{\psi}_{i,1}^2 + \frac{115^2}{72^2}h^4(D_y^2\tilde{\psi})_{i,1}^2 + \frac{23^2}{36^2}h^4(D_y^2\tilde{\psi})_{i,2}^2 + \frac{1^2}{8^2}h^4(D_y^2\tilde{\psi})_{i,3}^2\Big) + 2h^8\boldsymbol{e}_{i,0}^2 .$$

Similar results are available for $\tilde{\omega}_{i,N}^2$, $\tilde{\omega}_{0,j}^2$, and $\tilde{\omega}_{N,j}^2$. Then we arrive at

$$\begin{aligned}\mathcal{B}_\omega &\le \frac{C}{h^4}\mathcal{B}_\psi + C\sum_{i=1}^{N-1}\sum_{j=1}^{N-1}(D_x^2\tilde{\psi}_{i,j})^2 + C\sum_{i=1}^{N-1}\sum_{j=1}^{N-1}(D_y^2\tilde{\psi}_{i,j})^2 + 2h^8\mathcal{E} \\ &\le \frac{C}{h^4}\|\nabla_h\tilde{\psi}\|^2 + \frac{C}{h^2}(\|D_x^2\tilde{\psi}\|^2 + \|D_y^2\tilde{\psi}\|^2) + 2h^8\mathcal{E} ,\end{aligned} \tag{4.4.42}$$

where $\mathcal{B}_\psi$ was defined in (4.4.15) and $\mathcal{E}$ is introduced as

$$\mathcal{E} = \sum_{i=1}^{N-1}(\boldsymbol{e}_{i,0}^2 + \boldsymbol{e}_{i,N}^2) + \sum_{j=1}^{N-1}(\boldsymbol{e}_{0,j}^2 + \boldsymbol{e}_{N,j}^2) . \tag{4.4.43}$$

In the second step of (4.4.42), we absorbed all the terms of $\mathcal{B}_\psi$ appearing in (4.4.15) into $\|\nabla_h\tilde{\psi}\|^2$, since $h^2(\frac{\tilde{\psi}_{i,1}-\tilde{\psi}_{i,0}}{h})^2 = \tilde{\psi}_{i,1}^2$ (by the fact that $\tilde{\psi}_{i,0} = 0$) is included in $\|\nabla_h\tilde{\psi}\|^2$. Moreover, the second term appearing on the right hand side of (4.4.42) can be controlled by the order of $\|\tilde{\omega}\|^2$ via (4.4.2) in Lemma 4.4.1. In addition, we can see that $2h^8\mathcal{E} \le Ch^9\|\boldsymbol{u}_e\|_{C^5}^2$ since $|\boldsymbol{e}_{i,0}| \le C\|\boldsymbol{u}_e\|_{C^5}$. Plugging these estimates back into (4.4.42), along with our previous argument that $\|\tilde{\omega}\|^2 \le \frac{21}{2}\|\tilde{\psi}\|^2 + 2h^2\mathcal{B}_\omega$, we obtain (4.4.30).

Now we can continue our proof of Lemma 4.3.3.

Reproduced with permission of the copyright owner. Further reproduction prohibited without permission.

Proof of Lemma 4.3.3 We decompose $\mathcal{L}$ into four parts: $\mathcal{L} = \mathcal{L}_1 + \mathcal{L}_2 + \mathcal{L}_3 + \mathcal{L}_4$, where

(4.4.44)

$$\mathcal{L}_1 = \widetilde{D}_x\Big(1 + \frac{h^2}{6}D_y^2\Big)(\tilde{u}\Omega + u\tilde{\omega})\,. \qquad \mathcal{L}_2 = \widetilde{D}_y\Big(1 + \frac{h^2}{6}D_x^2\Big)(\tilde{v}\Omega + v\tilde{\omega})\,.$$
$$\mathcal{L}_3 = -\frac{h^2}{12}\triangle_h\Big(u\widetilde{D}_x\tilde{\omega} + v\widetilde{D}_x\tilde{\omega}\Big)\,. \qquad \mathcal{L}_4 = -\frac{h^2}{12}\triangle_h\Big(\tilde{u}\widetilde{D}_x\Omega + \tilde{v}\widetilde{D}_x\Omega\Big)\,.$$

We will show that the inner product of $(1 + \frac{h^2}{12}\triangle_h)\tilde{\omega}$ with each term in (4.4.44) is bounded by the following result

$$\Big|\langle(1 + \frac{h^2}{12}\triangle_h)\tilde{\omega}\,,\ \mathcal{L}_i\rangle\Big| \le \frac{1}{4}\tilde{C}\|\nabla_h\tilde{\omega}\|^2 + \frac{\nu}{32}\|\tilde{\omega}\|^2 + h^9\,. \tag{4.4.45}$$

for $i = 1, 2, 3, 4$, where $\tilde{C} = \dfrac{32(1 + \|\boldsymbol{u}_e\|_{C^0})^2}{\nu} + C(2 + \|\boldsymbol{u}_e\|_{C^1})^2 + C\|\boldsymbol{u}_e\|_{C^5}$.

We only give the estimate of $\langle(1 + \frac{h^2}{12}\triangle_h)\tilde{\omega}, \mathcal{L}_1\rangle$. The other three terms can be treated in a similar fashion. Summing by parts, we have

$$\begin{aligned}&\Big\langle(1 + \frac{h^2}{12}\triangle_h)\tilde{\omega}, \widetilde{D}_x(1 + \frac{h^2}{6}D_y^2)(\tilde{u}\Omega + u\tilde{\omega})\Big\rangle \\ &= -\Big\langle\widetilde{D}_x(1 + \frac{h^2}{6}D_y^2)\tilde{\omega}, (1 + \frac{h^2}{12}\triangle_h)(\tilde{u}\Omega + u\tilde{\omega})\Big\rangle + \mathcal{BL}_1\,.\end{aligned} \tag{4.4.46}$$

where $\mathcal{BL}_1$ includes boundary terms

(4.4.47)

$$\begin{aligned}\mathcal{BL}_1 \ &= \frac{1}{6}h^2\sum_i(1 + \frac{h^2}{12}\triangle_h)\tilde{\omega}_{i,1}\cdot\widetilde{D}_x(\tilde{u}\Omega)_{i,0} + \frac{1}{6}h^2\sum_i(1 + \frac{h^2}{12}\triangle_h)\tilde{\omega}_{i,N-1}\cdot\widetilde{D}_x(\tilde{u}\Omega)_{i,N} \\ &+ \frac{1}{12}h^2\sum_i\widetilde{D}_x(1 + \frac{h^2}{6}D_y^2)\tilde{\omega}_{i,1}\cdot(\tilde{u}\Omega)_{i,0} + \frac{1}{12}h^2\sum_i\widetilde{D}_x(1 + \frac{h^2}{6}D_y^2)\tilde{\omega}_{i,N-1}\cdot(\tilde{u}\Omega)_{i,N}\,.\end{aligned}$$

We look at the right hand side of (4.4.46) term by term. By our construction of Ω as in (4.3.11)-(4.3.14) indicates that

$$\|\Omega\|_{L^\infty} \le C(\|\overline{\Omega}\|_{L^\infty} + \|\Omega\,|_\Gamma\,\|_{L^\infty}) \le C(\|v_e\|_{C^2} + \|\psi_e\|_{C^5}) \le C\|\boldsymbol{u}_e\|_{C^5}\,. \tag{4.4.48}$$

which in turn gives that

$$\|(1 + \frac{h^2}{12}\triangle_h)(\tilde{u}\Omega)\| \le \|\Omega\|_{L^\infty}\|(1 + \frac{h^2}{12}\triangle_h)\tilde{u}\| \le C\|\boldsymbol{u}_e\|_{C^5}\|\nabla_h\tilde{\omega}\|\,. \tag{4.4.49}$$

Reproduced with permission of the copyright owner. Further reproduction prohibited without permission.

where in the last step we applied the result that $\|\tilde{u}\| \le 2\|\nabla_h \tilde{\psi}\|$ by the relation between $\tilde{u}$ and $\tilde{\psi}$. (4.4.49) along with the fact that

$$\|\widetilde{D}_x(1+\frac{h^2}{6}D_y^2)\tilde{\psi}\| \le \|\widetilde{D}_x\tilde{\psi}\| \le \|\nabla_h\tilde{\psi}\|, \tag{4.4.50}$$

since $\tilde{\psi}$ vanishes on the boundary, and Cauchy inequality gives

$$\left|\left\langle \widetilde{D}_x(1+\frac{h^2}{6}D_y^2)\tilde{\psi}, (1+\frac{h^2}{12}\triangle_h)(\tilde{u}\Omega)\right\rangle\right| \le C\|\boldsymbol{u}_e\|_{C^3}\|\nabla_h\tilde{\psi}\|^2. \tag{4.4.51}$$

Now we look at the inner product of $-\widetilde{D}_x(1+\frac{h^2}{6}D_y^2)\tilde{\psi}$ with $(1+\frac{h^2}{12}\triangle_h)(u\tilde{\omega})$. First, we can rewrite the latter as

$$(1+\frac{h^2}{12}\triangle_h)(u\tilde{\omega})_{i,j} = u_{i,j}(1+\frac{h^2}{12}\triangle_h)\tilde{\omega}_{i,j} + \mathcal{DL} = u_{i,j}\tilde{\bar{\omega}}_{i,j} + \mathcal{DL}, \tag{4.4.52}$$

where $\mathcal{DL}$ includes four parts: $\frac{1}{12}(u_{i-1,j}-u_{i,j})\tilde{\omega}_{i-1,j}$, $\frac{1}{12}(u_{i+1,j}-u_{i,j})\tilde{\omega}_{i+1,j}$, $\frac{1}{12}(u_{i,j-1}-u_{i,j})\tilde{\omega}_{i,j-1}$, $\frac{1}{12}(u_{i,j+1}-u_{i,j})\tilde{\omega}_{i,j+1}$. Our construction of U in (4.3.10) and the a-prior assumption (4.3.43) gives

$$\|u\|_{L^\infty} \le \|U\|_{L^\infty} + \|\tilde{u}\|_{L^\infty} \le \|\psi_e\|_{C^1} + h \le \|\boldsymbol{u}_e\|_{C^0} + 1 \equiv C_1, \tag{4.4.53}$$

which leads to

$$\left|\left\langle \widetilde{D}_x(1+\frac{h^2}{6}D_y^2)\tilde{\psi}, u\tilde{\bar{\omega}}\right\rangle\right| \le \frac{32C_1^2}{\nu}\|\nabla_h\tilde{\psi}\|^2 + \frac{\nu}{32}\|\tilde{\bar{\omega}}\|^2. \tag{4.4.54}$$

Furthermore, we have

$$\|u_{i,j}-u_{i-1,j}\|_{L^\infty} \le \|U_{i,j}-U_{i-1,j}\|_{L^\infty} + \|\tilde{u}_{i,j}-\tilde{u}_{i-1,j}\|_{L^\infty} \le h\|\psi_e\|_{C^2} + 2h, \tag{4.4.55}$$

and similar result holds for the other three neighboring points, which shows that $\|\mathcal{DL}\| \le C(\|\boldsymbol{u}_e\|_{C^1}+2)h\|\tilde{\omega}\|_W$. Note that $\|\tilde{\omega}\|_W$ involves the boundary values of $\tilde{\omega}$. Then we arrive at

$$\left|\left\langle \widetilde{D}_x(1+\frac{h^2}{6}D_y^2)\tilde{\psi}, \mathcal{DL}\right\rangle\right| \le C(\|\boldsymbol{u}_e\|_{C^1}+2)^2\|\nabla_h\tilde{\psi}\|^2 + h^2\|\tilde{\omega}\|_W^2. \tag{4.4.56}$$

Reproduced with permission of the copyright owner. Further reproduction prohibited without permission.

and applying Lemma 4.4.3, we obtain

$$(4.4.57)\quad \left|\left\langle \widetilde{D}_x(1+\frac{h^2}{6}D_y^2)\tilde{\omega}, \mathcal{DL}\right\rangle\right| \le C(\|\boldsymbol{u}_e\|_{C^1}+2)^2\|\nabla_h\tilde{\omega}\|^2 + Ch^2\|\tilde{\omega}\|^2 + Ch^{11}.$$

The combination of (4.4.52), (4.4.55) and (4.4.57) shows that

$$(4.4.58)\quad \left|\left\langle \widetilde{D}_x(1+\frac{h^2}{6}D_y^2)\tilde{\omega}, (1+\frac{h^2}{12}\Delta_h)(u\tilde{\omega})\right\rangle\right| \le C_2\|\nabla_h\tilde{\omega}\|^2 + \frac{\nu}{32}\|\tilde{\omega}\|^2 + \frac{1}{2}h^9.$$

where $C_2 = \frac{32C_1^2}{\nu} + C(\|\boldsymbol{u}_e\|_{C^1}+2)^2$.

Applying the similar argument to $\mathcal{BL}_1$ we can get

$$(4.4.59)\qquad \mathcal{BL}_1 \le C\|\nabla_h\tilde{\omega}\|^2 + \frac{1}{2}h^9.$$

We omit the detail here. Finally, combining (4.4.51), (4.4.58), (4.4.59), we arrive at (4.4.45) for $i=1$. The other three terms can be estimated in a similar fashion. Then we proved Lemma 4.3.3.

Reproduced with permission of the copyright owner. Further reproduction prohibited without permission.

Table 4.1: Errors and order of accuracy for stream function and vorticity at $t = 1$ when the fourth order schemes with **Briley's formula** at the boundary are used. CFL=$\frac{1}{2}$, where CFL= $\frac{2\nu\Delta t}{\Delta x^2}$. we took $\Delta t = \frac{1}{2}\Delta x$ when N=32.

	N	L^1 error	L^1 order	L^2 error	L^2 order	L^∞ error	L^∞ order
ψ	32	4.01e-06		3.22e-06		3.75e-06	
	64	2.60e-07	3.95	2.17e-07	3.90	2.67e-07	3.81
	128	1.67e-08	3.96	1.43e-08	3.92	1.77e-08	3.91
	256	1.06e-09	3.98	9.18e-10	3.96	1.14e-09	3.96
ω	32	6.15e-05		8.75e-05		1.81e-04	
	64	3.41e-06	4.17	4.71e-06	4.21	9.60e-06	4.23
	128	1.96e-07	4.12	2.66e-07	4.14	5.30e-07	4.18
	256	1.16e-08	4.07	1.56e-08	4.09	3.06e-08	4.11

Table 4.2: Errors and order of accuracy for stream function and vorticity at $t = 1$ when the fourth order scheme with **new vorticity boundary condition** are used. CFL=$\frac{1}{2}$, where CFL= $\frac{2\nu\Delta t}{\Delta x^2}$. we took $\Delta t = \frac{1}{2}\Delta x$ when N=32.

	N	L^1 error	L^1 order	L^2 error	L^2 order	L^∞ error	L^∞ order
ψ	32	7.52e-06		6.20e-06		6.87e-06	
	64	4.38e-07	4.10	3.68e-07	4.07	4.14e-07	4.05
	128	2.63e-08	4.06	2.23e-08	4.04	2.53e-08	4.03
	256	1.61e-09	4.03	1.37e-09	4.02	1.57e-09	4.01
ω	32	1.24e-05		1.58e-05		3.29e-05	
	64	4.74e-07	4.71	5.38e-07	4.87	1.10e-06	4.90
	128	1.76e-08	4.75	1.69e-08	5.00	3.04e-08	5.17
	256	7.37e-10	4.58	6.29e-10	4.74	7.56e-10	5.32

Reproduced with permission of the copyright owner. Further reproduction prohibited without permission.

CHAPTER 5
FLOW ON MULTI-CONNECTED DOMAIN

5.1 Preliminary

The homogeneous, incompressible Navier-Stokes equations (NSE) in velocity-pressure formulation with no-slip boundary condition can be written as

$$\begin{cases} \boldsymbol{u}_t + (\boldsymbol{u}\cdot\nabla)\boldsymbol{u} + \nabla p = \dfrac{1}{Re}\triangle\boldsymbol{u}, & \text{in } \Omega, \\ \nabla\cdot\boldsymbol{u} = 0, & \text{in } \Omega, \\ \boldsymbol{u} = 0, & \text{on } \partial\Omega, \end{cases} \tag{5.1.1}$$

where $\boldsymbol{u} = (u, v)$ is the velocity, p is the pressure and Re is the Reynolds number. For simplicity, we denote $\nu = \frac{1}{Re}$. For the multi-connected domain, $\partial\Omega$ is assumed to be composed of closed, non-intersecting segments Γ_i, $i = 1, ..., k$, enclosed by the closed curve Γ_0, i.e. $\partial\Omega = \Gamma_0 \cup \Gamma_1 \cup \Gamma_2 ... \cup \Gamma_k$. The k regions with the boundaries Γ_1, Γ_2, ... Γ_k are called the k holes of the domain Ω. See Fig. 5.1 below.

The no penetration, no-slip boundary condition for the velocity is given by $\boldsymbol{u}\,|_{\Gamma_0} = 0$, $\boldsymbol{u}\,|_{\Gamma_1} = 0$, ... $\boldsymbol{u}\,|_{\Gamma_k} = 0$.

There are three main difficulties in the numerical simulation of incompressible flow in the primitive formulation:

1. The implementation of the incompressibility constraint $\nabla\cdot\boldsymbol{u} = 0$.

2. There is no dynamic equation and no boundary condition for the pressure p. Indeed, p is mainly a Lagrange multiplier to assure the incompressibility.

Reproduced with permission of the copyright owner. Further reproduction prohibited without permission.

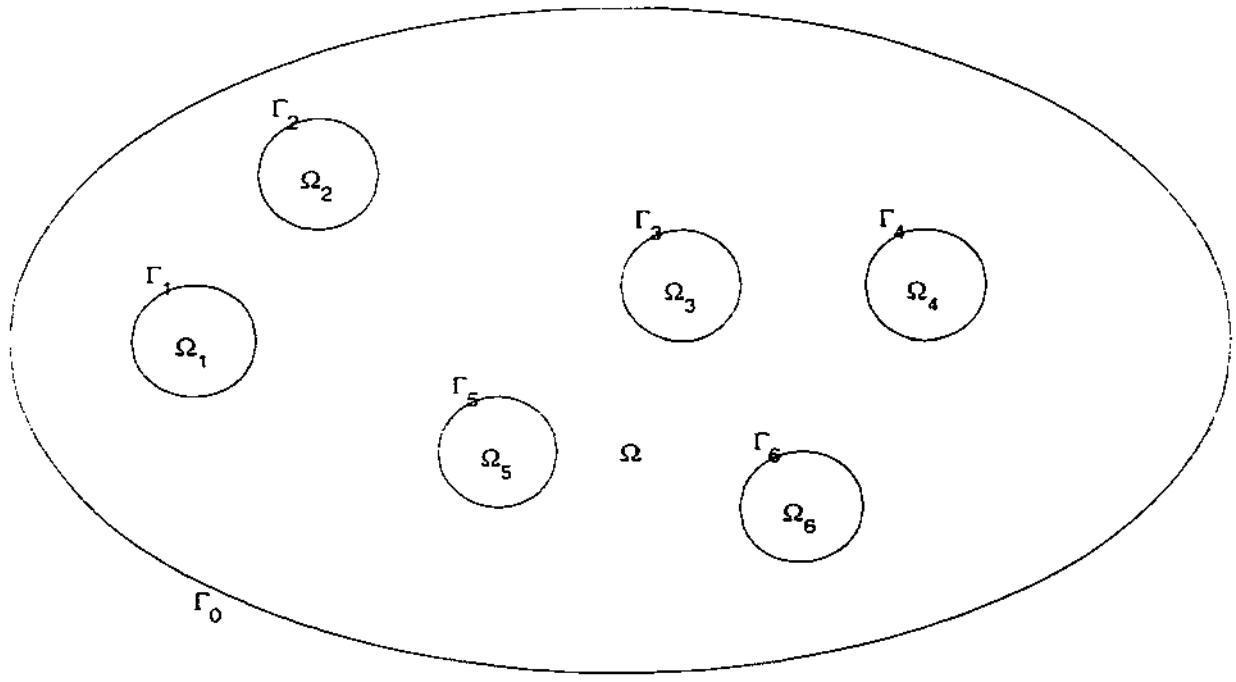

Figure 5.1: A multi-connected Domain

3. The implementation of the no penetration and no-slip boundary condition.

In 2D case, the first and second difficulties can be eliminated in the vorticity-stream function formulation

$$\begin{cases} \partial_t \omega + (\boldsymbol{u}\cdot\nabla)\omega = \nu\triangle\omega\,. \\ \triangle\psi = \omega\,. \\ u = -\partial_y\psi\,. \qquad v = \partial_x\psi\,. \end{cases} \tag{5.1.2}$$

where the vorticity is introduced as $\omega = \nabla \times \boldsymbol{u} = -\partial_y u + \partial_x v$.

The no penetration boundary condition for $\boldsymbol{u}$ indicates that

$$\psi|_{\Gamma_i} = C_i\,, \qquad \text{for } 0 \le i \le k\,. \tag{5.1.3}$$

where C_i are constants; while the no-slip boundary condition for $\boldsymbol{u}$ shows that

$$\frac{\partial\psi}{\partial\boldsymbol{n}} = 0\,, \qquad \text{at each } \Gamma_i\,. \tag{5.1.4}$$

Reproduced with permission of the copyright owner. Further reproduction prohibited without permission.

The remaining difficulty involved in the formulation (5.1.2) is the boundary condition:

1. There are two boundary conditions (5.1.3), (5.1.4) for the stream function, while there is no boundary condition for the vorticity.

2. How to determine the constants of the stream function, C_1, C_2, ... ,C_k, at the k "holes", respectively?

The methodology to overcome the first difficulty has been described in detail in [ELV1], [ELV2] by E and Liu: the Dirichlet boundary condition (5.1.3) can be applied to solve the stream function by the Poisson equation in (5.1.2), which states the kinematic relationship between ψ and ω; the no-slip boundary condition (5.1.4) can be converted into the local formula for the vorticity boundary condition, which can be implemented very effectively by the explicit treatment.

This approach works perfectly in the case of the simply-connected domain. However, if the domain is multi-connected, the second difficulty, which is a well-known difficulty, arises. This topic will be the main focus of this chapter.

The starting point of our method is the following equivalent formulation of the incompressible NSE for the multi-connected domain in terms of vorticity-stream function formulation

$$\partial_t \omega + (\boldsymbol{u}\cdot\nabla)\omega = \nu\triangle\omega\,. \tag{5.1.5a}$$

$$\triangle\psi = \omega\,. \tag{5.1.5b}$$

$$\psi|_{\Gamma_i} = C_i\,, \qquad \frac{\partial\psi}{\partial\boldsymbol{n}} = 0\,, \qquad \text{at each } \Gamma_i\,. \tag{5.1.5c}$$

$$\int_{\Gamma_i}\frac{\partial\omega}{\partial\boldsymbol{n}} = 0\,, \qquad \text{for } 0\le i\le k\,. \tag{5.1.5d}$$

$$u = -\partial_y\psi\,, \qquad v = \partial_x\psi\,. \tag{5.1.5e}$$

Reproduced with permission of the copyright owner. Further reproduction prohibited without permission.

Since the stream function is uniquely determined up to a constant, the constant at the outer boundary Γ_0 can be automatically set as 0, i.e. $C_0 = 0$.

The derivation of the boundary condition $\int_{\Gamma_i} \frac{\partial \omega}{\partial \boldsymbol{n}} = 0$ in (5.1.5d) is given below: on each boundary Γ_i, multiplying the momentum equation in (5.1.1) with τ, where τ is the unit tangential vector along the boundary, and using the fact that the velocity $\boldsymbol{u}$ vanishes on the boundary lead to

$$\frac{\partial p}{\partial \tau} = -\nu \frac{\partial \omega}{\partial \boldsymbol{n}}, \qquad \text{on } \Gamma_i. \tag{5.1.6}$$

Integrating (5.1.6) along the boundary Γ_i, keeping in mind that p is a single-valued function, we arrive at the boundary condition in (5.1.5d). Such derivation can also been found in [GPM], [GMD], [MA], [TTE].

5.2 The Second Order Scheme

For simplicity of presentation, the domain in Fig. 5.2 is used to describe the scheme.

In Fig. 5.2, $\partial\Omega$ is composed of the outer closed boundary Γ_0: $A_1B_1C_1D_1$ and only one segment Γ_1: $ABCD$, where $A_1B_1C_1D_1$, $ABCD$ are $[0,3]^2$ and $[1,2]^2$ boxes, respectively. The other geometries of multi-connected domain can be dealt with in a similar way. In more detail, A, B, C, D have grid indices (n,n), (n,m), (m,m), and (m,n), and A_1, B_1, C_1, D_1 have grid indices $(0,0)$, $(0,N)$, (N,N), $(N,0)$, respectively. n and m are given by $n = \frac{1}{3}N$, $m = \frac{2}{3}N$, and the grid size is chosen as $\Delta x = \Delta y = h$. N_i is denoted as the number of interior grid points. $\widetilde{D}_x$, D_x^2 are denoted as the standard centered difference operators corresponding to ∂_x, ∂_x^2, respectively.

The key part in the numerical simulation of the system (5.1.5) is the computation of Poisson equation (5.1.5b) and enforcement of boundary conditions

Reproduced with permission of the copyright owner. Further reproduction prohibited without permission.

(5.1.5c), (5.1.5d). We first describe the basic computational strategy to deal with this part. The Laplacian operator in (5.1.5b) can be approximated by second order finite difference operator $\triangle_h = D_x^2 + D_y^2$, and the use of Dirichlet boundary condition in (5.1.5c) leads to the following discrete system

$$\begin{cases} \triangle_h \psi = \omega, & \text{in } \Omega, \\ \psi|_{\Gamma_0} = 0, \quad \psi|_{\Gamma_1} = C_1. \end{cases} \tag{5.2.1}$$

Yet, the constant C_1 is not known yet. The remaining task is to obtain such constant by the boundary condition in (5.1.5d).

The no-slip boundary condition $\frac{\partial \psi}{\partial \boldsymbol{n}} = 0$ can be converted into the boundary condition for the vorticity by local formulas, such as **Thom's formula**, as argued in [ELV1]. For example, on the boundary section A_1D_1, $j = 0$, Thom's formula gives

$$\omega_{i,0} = \frac{2\psi_{i,1} - 2\psi_{i,0}}{h^2}. \tag{5.2.2}$$

and on AD, one boundary section of Γ_1, Thom's formula indicates

$$\omega_{i,n} = \frac{2\psi_{i,n-1} - 2\psi_{i,n}}{h^2}. \tag{5.2.3}$$

Similar formulas can be applied to other boundary sections.

The boundary condition $\int_{\Gamma_1} \frac{\partial \omega}{\partial \boldsymbol{n}} = 0$ can be implemented by finite difference approximation. For the convenience of the presentation below, some notations are introduced.

Notation. For any discrete field f on the grid points (i, j), we define

$$\int_{\Gamma_1}^{(\mathbf{k})} f = \int_{AB} f_{n-k,j} + \int_{BC} f_{i,m-k} + \int_{CD} f_{m-k,j} + \int_{DA} f_{i,n-k}, \tag{5.2.4}$$

where the trapezoid rule is applied to the integration at each boundary sections. For example, on the section AB,

$$\int_{AB} f_{n-k,j} = h\left(\frac{1}{2} f_{n-k,n} + \sum_{j=n-1}^{m-1} f_{n-k,j} + \frac{1}{2} f_{n-k,m}\right). \tag{5.2.5}$$

Reproduced with permission of the copyright owner. Further reproduction prohibited without permission.

Using the one-sided difference operator $\frac{4\omega_{n-1,j}-\omega_{n-2,j}-3\omega_{n,j}}{2h}$ as the second order approximation to $\frac{\partial\omega}{\partial n}$ (at the boundary section AB), and plugging into the boundary condition (5.1.5d) results in

$$\int_{\Gamma_1}^{(0)}\omega=\frac{4}{3}\int_{\Gamma_1}^{(1)}\omega-\frac{1}{3}\int_{\Gamma_1}^{(2)}\omega. \tag{5.2.6}$$

The substitution of Thom's formula (5.2.3) into the left hand side of (5.2.6), along with the fact that ψ is a constant C_1 on the boundary Γ_1, gives

$$C_1=\frac{1}{|\Gamma_1|}\Big(\int_{\Gamma_1}^{(1)}\psi-\frac{4}{3}h^2\int_{\Gamma_1}^{(1)}\omega+\frac{1}{3}h^2\int_{\Gamma_1}^{(2)}\omega\Big), \tag{5.2.7}$$

where $|\Gamma_1|$ is the length of the boundary Γ_1. In the case of Fig. 5.2, $|\Gamma_1|=4$.

The formula (5.2.7) plays the role of a bridge between the constant C_1 and the boundary condition $\int_{\Gamma_1}\frac{\partial\omega}{\partial n}=0$: Different C_1 leads to different $\psi_{i,j}$, which, in turn, results in different vorticity ω on the boundary, by Thom's formula (5.2.2) and (5.2.3), then different $\int_{\Gamma_1}\frac{\partial\omega}{\partial n}$. On the other hand, this integration has to be 0 according to (5.1.5d), the equivalent formulation of incompressible NSE in vorticity-stream function formulation.

The coupled system (5.2.1), (5.2.7) will be used to compute ψ and the constant C_1 by iteration, as will be explained in detail later. Let's first count the number of equations and unknowns of it: there are N_i+1 unknowns (where N_i is the number of interior grid points), including N_i number of $\psi_{i,j}$ at interior grid points and the boundary value C_1; the number of equations is also N_i+1: N_i equations in (5.2.1) and one additional equation (5.2.7).

As argued above, the right hand side of (5.2.7) depends on C_1. An operator o can be introduced by (5.2.7): for any constant C, denote ψ as the solution of the system

$$\begin{cases}\Delta_h\psi=\omega, & \text{in } \Omega,\\ \psi|_{\Gamma_0}=0, \quad \psi|_{\Gamma_1}=C.\end{cases} \tag{5.2.8}$$

Reproduced with permission of the copyright owner. Further reproduction prohibited without permission.

and define

$$o(C) = \frac{1}{|\Gamma_1|}\Big(\int_{\Gamma_1}^{(1)} v - \frac{4}{3}h^2 \int_{\Gamma_1}^{(1)} \omega + \frac{1}{3}h^2 \int_{\Gamma_1}^{(2)} \omega\Big)\,. \tag{5.2.9}$$

It should be noted that the term related to v at the right side of (5.2.9) depends on C, according to (5.2.8). Obviously, the fixed point of o, i.e. the constant C such that $o(C) = C$, along with v determined by (5.2.8), is exactly the solution of the coupled system (5.2.1), (5.2.7). The existence and uniqueness of the fixed point can be guaranteed by the following Proposition, which states that o is in fact a contraction mapping.

Proposition 5.2.1 *For any C_1, $C_2 \in R$, we have*

$$|o(C_1) - o(C_2)| \le C^*|C_1 - C_2|\,, \qquad \text{where } C^* = 1 - h\,. \tag{5.2.10}$$

Proof. Denote v^1, v^2 be the solutions of the system (5.2.8) with the boundary condition $v^1\,|_{\Gamma_1} = C_1$, $v^2\,|_{\Gamma_1} = C_2$, respectively. Define $\tilde{v} = v^1 - v^2$. It can be seen that

$$\begin{cases} \triangle_h \tilde{v} = 0\,, & \text{in } \Omega\,, \\ \tilde{v}\,|_{\Gamma_0} = 0\,, & \tilde{v}\,|_{\Gamma_1} = C_1 - C_2\,. \end{cases} \tag{5.2.11}$$

The definition of $o(C_1)$ and $o(C_2)$, which was indicated by (5.2.9), gives

$$o(C_1) - o(C_2) = \frac{1}{|\Gamma_1|}\int_{\Gamma_1}^{(1)} \tilde{v}\,. \tag{5.2.12}$$

The estimate of the right side of (5.2.12) is obtained by the following Lemma.

Lemma 5.2.2 *Let u be the solution of the system*

$$\begin{cases} \triangle_h u = 0\,, & \text{in } \Omega\,, \\ u\,|_{\Gamma_0} = 0\,, & u\,|_{\Gamma_1} = 1\,. \end{cases} \tag{5.2.13}$$

then we have

$$0 \le u_{n-1,j} \le C^*\,, \qquad \text{for } n \le j \le m\,, \qquad \text{where} \quad C^* = 1 - h\,. \tag{5.2.14}$$

Reproduced with permission of the copyright owner. Further reproduction prohibited without permission.

Proof. The left half of (5.2.14) comes directly from the maximum principle of the discrete Laplacian operator $\triangle_h$. For the right half, the region Ω can be partitioned into four sub-regions: A_1ABB_1, A_1ADD_1, D_1DCC_1, C_1CBB_1, denoted by Ω_1, Ω_2, Ω_3, Ω_4, respectively, as shown in Fig. 5.3.

It can be seen that the function

$$v = \begin{cases} x\,, \text{in } \Omega_1\,, \\ y\,, \text{in } \Omega_2\,, \\ 3-x\,, \text{in } \Omega_3\,, \\ 3-y\,, \text{in } \Omega_4\,, \end{cases} \tag{5.2.15}$$

satisfies

$$\begin{cases} \triangle_h v = \begin{cases} -\frac{2}{h}\,, & \text{on } AA_1\,, BB_1\,, CC_1\,, DD_1\,, \\ 0\,, & \text{otherwise}\,. \end{cases} \\ v\,|_{\Gamma_0} = 0\,. \qquad v\,|_{\Gamma_1} = 1\,. \end{cases} \tag{5.2.16}$$

Denote $f = -\triangle_h v$. Obviously, $f \geq 0$. Then u can be decomposed into two parts: $u = v + w$, where w is the solution of the following system

$$\begin{cases} \triangle_h w = f\,. \qquad \text{in } \Omega\,. \\ w\,|_{\Gamma_0} = 0\,. \qquad w\,|_{\Gamma_1} = 0\,. \end{cases} \tag{5.2.17}$$

Since $\triangle_h w = f \geq 0$, and w vanishes on the boundary, the maximum principle of $\triangle_h$ shows that $w \leq 0$ at all grid points. Then we have

$$u \leq v\,, \qquad \text{at all grid points}\,. \tag{5.2.18}$$

and especially, $u_{n-1,j} \leq v_{n-1,j} = 1 - h = C^*$. Lemma 2.2 is proven.

Obviously, $\tilde{w} = (C_1 - C_2)u$ where u is given in Lemma 5.2.2. This results in

$$|\tilde{w}_{n-1,j}| \leq C^*|C_1 - C_2|\,. \qquad \text{for } n \leq j \leq m\,. \tag{5.2.19}$$

Reproduced with permission of the copyright owner. Further reproduction prohibited without permission.

Similar arguments can be used to $\tilde{v}_{i,m+1}$, $\tilde{v}_{m+1,j}$, $\tilde{v}_{i,n-1}$. Proposition 4.2.1 is a direct consequence of (5.2.19), along with (5.2.12).

By Proposition 5.2.1, there is an unique fixed point under the operator o, i.e., $o(C) = C$. That's exactly the solution of the system (5.2.1), (5.2.7). Thus the existence and uniqueness of the system is proven.

Remark 5.2.1 The above procedure can be applied to a set of very general cases: general domain (either symmetric or non-symmetric ones), the domain with more "holes", different boundary conditions for the vorticity. We can even extend it to 4-th order scheme, as will be explained in Section 5.3.

Remark 5.2.2 The other choices for the vorticity boundary condition includes **Wilkes' formula**

$$\omega_{i,0} = \frac{4\psi_{i,1} - \frac{1}{2}\psi_{i,2} - \frac{7}{2}\psi_{i,0}}{h^2}, \qquad \omega_{i,n} = \frac{4\psi_{i,n-1} - \frac{1}{2}\psi_{i,n-2} - \frac{7}{2}\psi_{i,n}}{h^2}, \tag{5.2.20}$$

which are analogous to (5.2.2), (5.2.3). The combination of (5.2.6) and (5.2.20) gives the corresponding formula for C_1

$$C_1 = \frac{1}{|\Gamma_1|}\Big(\frac{8}{7}\int_{\Gamma_1}^{(1)} \psi - \frac{1}{7}\int_{\Gamma_1}^{(1)} v - \frac{4}{3}h^2\int_{\Gamma_1}^{(1)} \omega + \frac{1}{3}h^2\int_{\Gamma_1}^{(2)} \omega\Big). \tag{5.2.21}$$

Again, the coupled system (5.2.1), (5.2.21) has to be solved to obtain ψ and the constant C_1 by iteration. The existence of the solution can be guaranteed by introducing a similar contraction mapping o: for any constant C, denote v as the solution of (5.2.8), and define

$$\phi(C) = \frac{1}{|\Gamma_1|}\Big(\frac{8}{7}\int_{\Gamma_1}^{(1)} \psi - \frac{1}{7}\int_{\Gamma_1}^{(1)} v - \frac{4}{3}h^2\int_{\Gamma_1}^{(1)} \omega + \frac{1}{3}h^2\int_{\Gamma_1}^{(2)} \omega\Big). \tag{5.2.22}$$

Proposition 2.1 is still valid here, the only difference is that $C^* = 1 - \frac{6}{7}h + O(h^2)$. It should be mentioned that C^* is the convergence rate corresponding to different vorticity boundary conditions. For example, $1 - h$ is the convergence rate for Thom's formula, and $1 - \frac{6}{7}h$ is the convergence rate for Wilkes' formula.

Reproduced with permission of the copyright owner. Further reproduction prohibited without permission.

The detailed derivation of convergence rates comes from a simple 1-D model. This convergence rate is consistent with the numerical experiments which will be presented in Section 5.4.

5.2.1 Iteration Procedure: Fixed Point Iteration

Proposition 5.2.2 also provides a means for solving the system (5.2.1), (5.2.7) by iteration procedure: once the k-th iteration for the constant $C_1^{(k)}$ is obtained, solve the stream function $\psi^{(k)}$ using the boundary condition $C_1^{(k)}$, then update the constant $C_1^{(k+1)}$by $(k+1)$-th iteration: $C_1^{(k+1)} = \phi(C_1^{(k)})$. Proposition 5.2.1 indicates that this iteration procedure converges to the real solution of (5.2.1), (5.2.7).

It should be pointed out that with the constant $C_1^{(k)}$ obtained at each iteration stage, a linear system solver for (5.2.1) is required. The Schwarz iteration is extremely efficient to solve this (discrete) Poisson equation in the overlapping region. At each sub-domain, which is a rectangle with uniform grids, some fast Poisson solvers, e.g. FFT, can be applied. The computational evidence indicates that the combination of the Schwarz iteration and FFT solver gives an excellent convergence speed in the overlapping region.

Our numerical experiment also shows that Schwarz iteration and the iteration formula (5.2.9) can be combined into a single iteration to facilitate the computation.

The momentum equation in (5.1.5a) can be discretized by the second order finite difference method

$$\partial_t \omega + u\widetilde{D}_x\omega + v\widetilde{D}_y\omega = \nu\triangle_h\omega\,. \tag{5.2.23}$$

The velocity field $\boldsymbol{u} = (u, v) = (-\partial_y\psi, \partial_x\psi)$ can be updated via the finite difference of ψ

$$u = -\widetilde{D}_y\psi\,, \qquad v = \widetilde{D}_x\psi\,. \tag{5.2.24}$$

Reproduced with permission of the copyright owner. Further reproduction prohibited without permission.

5.2.2 Explicit Time Stepping Procedure

The above scheme can be implemented very effectively through the explicit treatment of (5.2.23), as discussed in detail in [ELV1]. The convection and diffusion term can be updated explicitly, which does not result in any problem caused by the cell-Reynolds number constraint if the Runge-Kutta method is applied. Such explicit treatment is especially effective in Poisson solver (5.2.1), (5.2.7) when we apply the iteration formula (5.2.2), (5.2.3). For simplicity we only present the forward Euler time-discretization. The extension to multi-step or Runge-Kutta methods is straightforward.

Time-stepping: Given the vorticity ω^n at time t^n, we compute all the profiles at the time step t^{n+1} via the following steps.

Step 1. Update $\left\{\omega_{i,j}^{n+1}\right\}$, at interior points (x_i, y_j), using

$$\frac{\omega^{n+1}-\omega^n}{\Delta t} + u^n \widetilde{D}_x \omega^n + v^n \widetilde{D}_y \omega^n = \nu \triangle_h \omega^n . \tag{5.2.25}$$

Step 2. Solve for $\left\{v_{i,j}^{n+1}\right\}$, at interior points (x_i, y_j), by the following coupled system

$$\begin{cases} \triangle_h v^{n+1} = \omega^{n+1} , & \text{in} \quad \Omega , \\ v^{n+1}\,|_{\Gamma_0} = 0 , & v^{n+1}\,|_{\Gamma_1} = C_1^{n+1} , \end{cases} \tag{5.2.26}$$

and

$$C_1^{n+1} = \frac{1}{|\Gamma|}\Big(\int_{\Gamma_1}^{(1)} v^{n+1} + \frac{4}{3}h^2 \int_{\Gamma_1}^{(1)} \omega^{n+1} - \frac{1}{3}h^2 \int_{\Gamma_1}^{(2)} \omega^{n+1}\Big) . \tag{5.2.27}$$

The iteration procedure described above is used to solve (5.2.26), (5.2.27).

Step 3. Obtain the boundary value for ω^{n+1} by Thom's formula (5.2.2), (5.2.3).

Step 4. Update the velocity $u_{i,j}^{n+1}, v_{i,j}^{n+1}$ using the second order difference scheme at the interior points, and set $\boldsymbol{u}^{n+1}\,|_\Gamma = 0$

$$u^{n+1} = -\widetilde{D}_y v^{n+1} , \qquad v^{n+1} = \widetilde{D}_x v^{n+1} . \tag{5.2.28}$$

Reproduced with permission of the copyright owner. Further reproduction prohibited without permission.

5.3 The Fourth Order Method

A fourth order method, Essentially Compact Fourth Order Scheme (EC4), which was proposed by E and Liu in [ELV2], can be used here. The starting point of the scheme is the fact that Laplacian operator $\triangle$ can be approximated with the fourth order by

$$\triangle = \frac{\triangle_h + \frac{h^2}{6} D_x^2 D_y^2}{1 + \frac{h^2}{12}\triangle_h} + O(h^4)\,. \tag{5.3.1}$$

Multiplying the denominator difference operator $1 + \frac{h^2}{12}\triangle_h$ by the momentum equation gives

$$(1 + \frac{h^2}{12}\triangle_h)\partial_t\omega + (1 + \frac{h^2}{12}\triangle_h)(\boldsymbol{u}\cdot\nabla)\omega = \nu\Big(\triangle_h + \frac{h^2}{6} D_x^2 D_y^2\Big)\omega\,. \tag{5.3.2}$$

Multiplying the same operator by the kinematic equation results in

$$\Big(\triangle_h + \frac{h^2}{6} D_x^2 D_y^2\Big)v = (1 + \frac{h^2}{12}\triangle_h)\omega\,, \tag{5.3.3}$$

with the boundary condition

$$v\,|_{\Gamma_0} = 0\,. \qquad v\,|_{\Gamma_1} = C_1\,. \tag{5.3.4}$$

Similar to the system (5.2.1) in the second order case, the constant C_1 is not known yet, which has to be obtained by the boundary condition in (5.1.5d).

The implementation of the boundary condition $\int_{\Gamma_1} \frac{\partial\omega}{\partial\boldsymbol{n}} = 0$ is a little different from the second order case. As can be seen later, the vorticity in the interior points has to be determined by a Poisson-like equation and the boundary condition for ω, which, in turn, depends on the stream function and C_1, by Briley's formula, which will be presented later. To avoid the coupling between the two systems, we express $\frac{\partial\omega}{\partial\boldsymbol{n}}$ in terms of a third order derivative of ψ, so that only (5.3.3), (5.3.4) needs to be concentrated, which can facilitate a lot of computations as shown in our numerical experiments. As can be seen, on the boundary

Reproduced with permission of the copyright owner. Further reproduction prohibited without permission.

section AD of Γ_1, $\omega = \triangle v = \partial_y^2 v$, which is implied by the fact that $v = C_1$ on the boundary AD. Accordingly, $\frac{\partial \omega}{\partial \boldsymbol{n}} = -\partial_y^3 v$ on AD. On the other hand, ∂_y^3 can be approximated by

$$\partial_y^3 v_{i,n} \sim \frac{1}{h^3}\left(15v_{i,n-1} - 6v_{i,n-2} + v_{i,n-3} - 10v_{i,n}\right). \tag{5.3.5}$$

The third order derivative of v at other boundary sections of Γ_1 can be obtained similarly. Plugging into the boundary condition $\int_{\Gamma_1} \frac{\partial \omega}{\partial \boldsymbol{n}} = 0$, we arrive at an equality similar to (5.2.6)

$$\int_{\Gamma_1}^{(0)} v = \frac{3}{2}\int_{\Gamma_1}^{(1)} v - \frac{3}{5}\int_{\Gamma_1}^{(2)} v + \frac{1}{10}\int_{\Gamma_1}^{(3)} v. \tag{5.3.6}$$

Since v is a constant C_1 on Γ_1, we have

$$C_1 = \frac{3}{2|\Gamma_1|}\int_{\Gamma_1}^{(1)} v - \frac{3}{5|\Gamma_1|}\int_{\Gamma_1}^{(2)} v + \frac{1}{10|\Gamma_1|}\int_{\Gamma_1}^{(3)} v. \tag{5.3.7}$$

Again, the formula (5.3.7) plays the role of a bridge between the constant C_1 and the boundary condition $\int_{\Gamma_1} \frac{\partial \omega}{\partial \boldsymbol{n}} = 0$: Different C_1 leads to different $\psi_{i,j}$, which, in turn, results in different $\int_{\Gamma_1} \frac{\partial \omega}{\partial \boldsymbol{n}}$, while (5.1.5d) indicates that this integration has to be 0.

The coupled system (5.3.3), (5.3.4), (5.3.7) is used to obtain ψ and the constant C_1 by iteration. The similar argument can be applied here that the number of both equations and unknowns is $N_1 + 1$.

Of course, the right hand side of (5.3.7) depends on C_1. A similar procedure of iteration can be applied. First, we define the operator o: for any constant C, let v be the solution satisfying

$$\begin{cases} \left(\triangle_h + \frac{h^2}{6}D_x^2 D_y^2\right) v = (1 + \frac{h^2}{12}\triangle_h)\omega, \\ v\,|_{\Gamma_0} = 0, \qquad v\,|_{\Gamma_1} = C. \end{cases} \tag{5.3.8}$$

and $o(C)$ is defined by

$$o(C) = \frac{3}{2|\Gamma_1|}\int_{\Gamma_1}^{(1)} v - \frac{3}{5|\Gamma_1|}\int_{\Gamma_1}^{(2)} v + \frac{1}{10|\Gamma_1|}\int_{\Gamma_1}^{(3)} v. \tag{5.3.9}$$

Reproduced with permission of the copyright owner. Further reproduction prohibited without permission.

The following proposition shows that ϕ is a contraction mapping. Its argument is similar to that of proposition 5.2.1 in the second order case and the proof of it will be provided in Section 5.5.

Proposition 5.3.1 *For any two constants C_1, C_2, we have*

$$|\phi(C_1) - \phi(C_2)| \le C^*|C_1 - C_2|\,, \qquad \text{where } C^* = 1 - O(h)\,. \tag{5.3.10}$$

By Proposition 5.3.1, there is a fixed point for the operator ϕ, i.e., $\phi(C) = C$, which is exactly the solution of the system (5.3.3), (5.3.4), (5.3.7). Thus the existence and uniqueness of the system is proven.

5.3.1 Iteration Procedure: Fixed Point Iteration

A similar method for solving the system (5.3.3), (5.3.4), (5.3.7) can be obtained by the iteration procedure: once the k-th iteration for the constant $C_1^{(k)}$ is obtained, solve the stream function $\psi^{(k)}$ using the boundary condition $C_1^{(k)}$ in (5.3.8), then update the constant $C_1^{(k+1)}$ by $(k+1)$-th iteration: $C_1^{(k+1)} = \phi(C_1^{(k)})$. This iteration procedure converges to the real solution of (5.3.3), (5.3.4), (5.3.7), as was guaranteed by Proposition 5.3.1.

Again, it should be pointed out that with the constant $C_1^{(k)}$ obtained at each iteration stage, the Schwarz iteration combined with FFT is needed to solve the discrete Poisson-like equation in the overlapping region. In addition, Schwarz iteration and the iteration formula can be combined into a single iteration to facilitate the computation.

Let's go back to the momentum equation. As in [ELV2], the corresponding nonlinear convection term in the vorticity dynamic equation can be estimated as

$$\begin{aligned}(1 + \frac{h^2}{12}\triangle_h)(\boldsymbol{u}\cdot\nabla\omega) = \;& \widetilde{D}_x\Big(1 + \frac{h^2}{6}D_y^2\Big)(u\omega) + \widetilde{D}_y\Big(1 + \frac{h^2}{6}D_x^2\Big)(v\omega) \\ & - \frac{h^2}{12}\triangle_h\Big(u\widetilde{D}_x\omega + v\widetilde{D}_y\omega\Big) + O(h^4)\,.\end{aligned} \tag{5.3.11}$$

Reproduced with permission of the copyright owner. Further reproduction prohibited without permission.

The first and the second terms in (5.3.11) are compact. The third term is not compact, yet it does not cause any problem in practical computations since $u^n\widetilde{D}_x\omega^n + v^n\widetilde{D}_y\omega^n$ can be taken as 0 on the boundary. The case of boundary condition with slip can be treated similarly, as discussed in [ELV2]. Finally, by the introduction of an intermediate variable ϖ

$$\varpi = (1 + \frac{h^2}{12}\triangle_h)\omega\,. \tag{5.3.12}$$

and combining the discussions in (5.3.2), (5.3.11), (5.3.12), the whole momentum equation can be approximated by

$$\begin{aligned}&\partial_t\varpi + \widetilde{D}_x\Big(1 + \frac{h^2}{6}D_y^2\Big)(u\omega) + \widetilde{D}_y\Big(1 + \frac{h^2}{6}D_x^2\Big)(v\omega)\\ &\qquad -\frac{h^2}{12}\triangle_h(u\widetilde{D}_x\omega + v\widetilde{D}_y\omega) = \nu\Big(\triangle_h + \frac{h^2}{6}D_x^2D_y^2\Big)\omega\,.\end{aligned} \tag{5.3.13}$$

The velocity field $\boldsymbol{u} = \nabla^\perp\psi = (-\partial_y\psi, \partial_x\psi)$ can be obtained by the long-stencil approximation to ∂_x, ∂_y

$$u = -\widetilde{D}_y(1 - \frac{h^2}{6}D_y^2)\psi\,, \quad v = \widetilde{D}_x(1 - \frac{h^2}{6}D_x^2)\psi\,. \tag{5.3.14}$$

The vorticity is determined by ϖ via (5.3.12). The implementation of (5.3.12) needs the boundary condition for ω. As already discussed in [ELV2], the main point of the vorticity boundary condition is to use the no-slip boundary condition $\frac{\partial\psi}{\partial\boldsymbol{n}} = 0$, and convert it into $\omega\,|_{\partial\Omega}$ by the kinematic relation $\triangle\psi = \omega$. We can use Briley's formula

$$\omega_{i,0} = \frac{1}{18h^2}(108\psi_{i,1} - 27\psi_{i,2} + 4\psi_{i,3} - 85\psi_{i,0})\,. \tag{5.3.15}$$

along with the one-sided Taylor expansions of the stream function

$$\psi_{i,-1} = 6\psi_{i,1} - 2\psi_{i,2} + \frac{1}{3}\psi_{i,3} - \frac{10}{3}\psi_{i,0} - 4h\left(\frac{\partial\psi}{\partial y}\right)_{i,0}\,. \tag{5.3.16}$$

$$\psi_{i,-2} = 40\psi_{i,1} - 15\psi_{i,2} + \frac{8}{3}\psi_{i,3} - \frac{80}{3}\psi_{i,0} - 12h\left(\frac{\partial\psi}{\partial y}\right)_{i,0}\,. \tag{5.3.17}$$

Reproduced with permission of the copyright owner. Further reproduction prohibited without permission.

On the boundary section AD, Briley's formula gives

$$\omega_{i,n} = \frac{1}{18h^2}(108v_{i,n-1} - 27v_{i,n-2} + 4v_{i,n-3} - 85v_{i,n}) . \tag{5.3.18}$$

It should be mentioned that the system (5.3.12) and the boundary condition (5.3.15), (5.3.18) can be solved very efficiently by the combination of the Schwarz iteration and FFT solver.

5.3.2 Time Stepping Procedure

Similar to the second order case, all terms in the momentum equation can be updated explicitly. Again, we only present the forward Euler time-discretization. The extension to multi-step or Runge-Kutta methods is straightforward.

Initialization: Given $\{\omega_{ij}^0\}$, compute

$$\Big(1 + \frac{h^2}{12}\Delta_h\Big)\omega^0 = \varpi^0 . \tag{5.3.19}$$

Time-stepping:

Step 1. Update $\left\{\varpi_{ij}^{n+1}\right\}$ at interior points (x_i, y_j) using

$$\begin{aligned} &\frac{\varpi^{n+1} - \varpi^n}{\Delta t} + \widetilde{D}_x\Big(1 + \frac{h^2}{6}D_y^2\Big)(u^n\omega^n) + \widetilde{D}_y\Big(1 + \frac{h^2}{6}D_x^2\Big)(v^n\omega^n) \\ &\quad - \frac{h^2}{12}\Delta_h(u^n\widetilde{D}_x\omega^n + v^n\widetilde{D}_y\omega^n) = \nu\Big(\Delta_h + \frac{h^2}{6}D_x^2D_y^2\Big)\omega^n . \end{aligned} \tag{5.3.20}$$

Step 2. Solve for $\left\{v_{ij}^{n+1}\right\}$ at interior points (x_i, y_j) using

$$\begin{cases} \Big(\Delta_h + \dfrac{h^2}{6}D_x^2D_y^2\Big)v^{n+1} = \varpi^{n+1} . \\ v^{n+1}|_{\Gamma_0} = 0 . \qquad v^{n+1}|_{\Gamma_1} = C_1^{n+1} . \end{cases} \tag{5.3.21}$$

and

$$C_1^{n+1} = \frac{3}{2|\Gamma_1|}\int_{\Gamma_1}^{(1)} v^{n+1} - \frac{3}{5|\Gamma_1|}\int_{\Gamma_1}^{(2)} v^{n+1} + \frac{1}{10|\Gamma_1|}\int_{\Gamma_1}^{(3)} v^{n+1} . \tag{5.3.22}$$

Reproduced with permission of the copyright owner. Further reproduction prohibited without permission.

The iteration procedure described above is used to solve the system (5.3.21). (5.3.22).

Compute v^{n+1} at the "ghost points" using (5.3.16). (5.3.17).

Step 3. Obtain the boundary value for ω^{n+1} by Briley's formula (5.3.15). (5.3.18).

Step 4. With the boundary values for ω^{n+1} updated in Step 3 at hand, we solve for $\left\{\omega_{i,j}^{n+1}\right\}$ at interior points using

$$\left(1+\frac{h^2}{12}\triangle_h\right)\omega^{n+1}=\varpi^{n+1}. \tag{5.3.23}$$

The combination of Schwarz iteration and FFT is applied. Only Sine transformations are needed.

Step 5. Update the velocity $u_{i,j}^{n+1}$, $v_{i,j}^{n+1}$ using the 4-th order difference scheme

$$u^{n+1}=-\widetilde{D}_y(1-\frac{h^2}{6}D_y^2)v^{n+1}. \qquad v^{n+1}=\widetilde{D}_x(1-\frac{h^2}{6}D_x^2)\psi^{n+1}. \tag{5.3.24}$$

5.4 Numerical Experiment

Two numerical examples will be presented to show the validity of the methods proposed above. The first example is a flow with a force term. The accuracy of both the second order and fourth order method is documented. The second example is a flow passing through an engine, e.g. a cooling system. Detailed structures of vorticity at different time steps will be given.

5.4.1 Accuracy Check

A Taylor vortex type flow in a multi-connected domain is computed by the methods proposed earlier. The exact stream function is chosen as

$$\psi_e(\boldsymbol{x},t)=\left(\cos x+\cos y+\cos x\cos y\right)\cos t. \tag{5.4.1}$$

Reproduced with permission of the copyright owner. Further reproduction prohibited without permission.

Accordingly, the exact velocity and vorticity are determined by

$$
\begin{aligned}
u_e(\boldsymbol{x}, t) &= -\partial_y \psi_e = (\sin y + \cos x \sin y)\cos t\,. \\
v_e(\boldsymbol{x}, t) &= \partial_x \psi_e = (-\sin x - \sin x \cos y)\cos t\,. \\
\omega_e(\boldsymbol{x}, t) &= \triangle \psi_e = (-\cos x - \cos y - 2\cos x \cos y)\cos t\,.
\end{aligned} \tag{5.4.2}
$$

The kinematic viscosity is taken as $\nu = 0.001$. Substitution of (5.4.2) into the momentum equation gives

$$\partial_t \omega_e + (\boldsymbol{u}_e \cdot \nabla)\omega_e = \nu \triangle \omega_e + \boldsymbol{f}\,. \tag{5.4.3}$$

where $\boldsymbol{f}$ is the force term. The domain has the same shape as in Fig. 0.3. Yet the dimensions of the boxes $A_1B_1C_1D_1$ and $ABCD$ are $[-3\pi, 3\pi]^2$ and $[-\pi, \pi]^2$, respectively. Using the same notations as before, denote the outer boundary $A_1B_1C_1D_1$ as Γ_0, and the inner boundary $ABCD$ as Γ_1. It is obvious that the boundary condition for the stream function at the outer boundary is

$$\psi(\boldsymbol{x}, t)\mid_{\Gamma_0} = -\cos t\,. \tag{5.4.4}$$

which is a constant varying with time t. The stream function is also a constant on Γ_1 (at each fixed time), denoted by C_1. Yet, C_1 is not given explicitly. We need to obtain such constant by the procedure described in Section 4.2 and Section 4.3 to determine it.

5.4.1.1 Second Order Scheme

(5.4.3) can be solved via our second order method coupled with the 4-th order Runge-Kutta time discretization, as discussed in (5.2.25)-(5.2.28). Thom's formula (5.2.2), (5.2.3) are chosen as our boundary condition for vorticity. The results using Wilkes' formula are similar. The force term $\boldsymbol{f}$ is added when (5.4.3) is updated. The final time is taken to be $t = 6.0$. The CFL number, which is defined as $\frac{\triangle t}{\triangle x}$, is taken to be 0.5. The absolute errors of stream function and vorticity are listed in Table 5.1. As can be seen, the stream function achieves

Reproduced with permission of the copyright owner. Further reproduction prohibited without permission.

almost exactly second order accuracy, while the vorticity achieves second order accuracy in L^1, L^2 norms, and obviously loses accuracy in L^∞ norm. The reason for it is still under investigation. All the errors are measured in L^1, L^2 and L^∞ norms, where the L^p norm is defined as

$$\|f\|_{L^p} = \Big(\frac{1}{|\Omega|}\int_\Omega f^p d\boldsymbol{x}\Big)^{\frac{1}{p}}. \qquad \text{for} \quad 0 < p < \infty, \tag{5.4.5}$$

where $|\Omega|$ is taken to be $32\pi^2$ in this case.

5.4.1.2 Fourth Order Scheme

The fourth order method coupled with the 4-th order Runge-Kutta time discretization, as discussed in (5.3.19)-(5.3.24), can also be used to compute the flow. The force term which will be added to the vorticity equation (5.4.3) becomes $(1+\frac{h^2}{12}\triangle_h)\boldsymbol{f}$, since we applied the operator $1+\frac{h^2}{12}\triangle_h$ to the momentum equation. The final time is still taken to be $t = 6.0$ and the CFL number is taken to be 0.5. The absolute errors of stream function, vorticity are listed in Table 5.2. It is indicated in the table that the stream function achieves more than fourth order accuracy in L^1, L^2 and L^∞ norms. The vorticity achieves fourth order accuracy in L^1, L^2 norms and more than third order accuracy in L^∞ norm.

5.4.2 A Flow Past a Cooling System

An impulsively-started incompressible flow in the following region (see Fig. 5.4) was computed using the fourth order method we proposed.

The flow region is similar to a cooling engine. The detailed dimensions of it are given by: $OO_1 = OT = 1$, $OR = O_1R_1 = \frac{1}{8}$. The inlet points B and M have coordinates (w.r.t. the origin O) $(0, \frac{1}{4})$, $(0, \frac{3}{8})$, respectively. The coordinates of other corner points are

$$A(0, \frac{1}{8}), \quad C(\frac{3}{16}, \frac{1}{4}), \quad D(\frac{3}{16}, \frac{3}{4}), \quad E(\frac{9}{32}, \frac{3}{4}), \quad F(\frac{9}{32}, \frac{1}{8}). \tag{5.4.6}$$

Reproduced with permission of the copyright owner. Further reproduction prohibited without permission.

The positions of the outlet points are also determined by their coordinates

$$P(\frac{3}{16}, 0)\,, \quad Q(\frac{3}{16}, -\frac{1}{8})\,, \quad R(0, -\frac{1}{8})\,. \tag{5.4.7}$$

In addition, there are three boxes in the middle, which are denoted by $S_1S_2U_2U_1$, $S_3S_4U_4U_3$, and $S_5S_6U_6U_5$. The $x-$coordinates of S_1, S_2, S_3, S_4, S_5, S_6 are given by $\frac{11}{32}$, $\frac{13}{32}$, $\frac{15}{32}$, $\frac{17}{32}$, $\frac{19}{32}$, $\frac{21}{32}$, and the $y-$coordinates of U_1 and S_1 are given by $\frac{3}{8}$, $\frac{3}{4}$, respectively. The coordinates of A_1-T_1 can be obtained by symmetry.

The no-penetration, no-slip boundary condition $\boldsymbol{u}\,|_\Gamma = 0$ is imposed at the boundaries of the region, except for the inlet BM, B_1M_1, and outlet QR, Q_1R_1. At the inlet BM, the velocity field is given by the standard parabola profile

$$u = 384(\frac{3}{8} - y)(y - \frac{1}{4})\,, \quad v = 0\,, \tag{5.4.8}$$

and consequently, the velocity profile at the inlet B_1M_1 is

$$u = -384(\frac{3}{8} - y)(y - \frac{1}{4})\,, \quad v = 0\,. \tag{5.4.9}$$

By the relationship between velocity and stream function that $\boldsymbol{u} = \nabla^\perp \psi$, we can integrate our velocity field at the inlet and set our boundary condition for ψ as:

$$\text{On } BM\,, \quad \psi_b = -1.5(y - \frac{1}{4}) + 128(y - \frac{5}{16})^3 + \frac{3}{32}\,. \tag{5.4.10}$$

and

$$\text{On } B_1M_1\,, \quad \psi_b = 1.5(y - \frac{1}{4}) - 128(y - \frac{5}{16})^3 - \frac{3}{32}\,. \tag{5.4.11}$$

Then the other boundary values for ψ is given by

$$\begin{aligned}
&\text{On } RA\,.\,AF\,.\,FE\,.\,ED\,.\,DC\,.\,CB\,.\,BA\,. \quad \psi_b = \tfrac{1}{8}\,.\\
&\text{On } R_1A_1\,.\,A_1F_1\,.\,F_1E_1\,.\,E_1D_1\,.\,D_1C_1\,.\,C_1B_1\,.\,B_1A_1\,. \quad \psi_b = -\tfrac{1}{8}\,.\\
&\text{On } MT\,.\,TT_1\,.\,T_1M_1\,. \quad \psi_b = 0\,.\\
&\text{On } QP\,.\,PP_1\,.\,P_1Q_1\,. \quad \psi_b = 0\,.
\end{aligned} \tag{5.4.12}$$

Reproduced with permission of the copyright owner. Further reproduction prohibited without permission.

At the outlet RQ and R_1Q_1, we adopt the natural normal boundary condition

$$\text{On } RQ, R_1Q_1, \quad \frac{\partial \psi}{\partial \boldsymbol{n}} = 0, \quad \frac{\partial \boldsymbol{u}}{\partial \boldsymbol{n}} = 0, \quad \frac{\partial \omega}{\partial \boldsymbol{n}} = 0. \tag{5.4.13}$$

The boundary value for ψ on the middle box $\Gamma_2 = S_3S_4U_4U_3$ can be obtained by symmetry

$$\psi_b = 0. \qquad \text{On} \quad \Gamma_2. \tag{5.4.14}$$

Yet, the boundary condition for ψ at the other two cooling boxes: $\Gamma_1 = S_1S_2U_2U_1$, $\Gamma_3 = S_5S_6U_6U_5$ can not be obtained directly. The fixed point iteration process described earlier has to be carried out to get such constants.

The fourth order method proposed in Section 5.3 was used to compute the flow, with Reynolds number $Re = 2000$. The calculations were carried out by two grid sizes: $\triangle x = \triangle y = \frac{1}{512}$ and $\triangle x = \triangle y = \frac{1}{768}$, (which corresponds to two resolutions: 512×576, 768×864, respectively). The vorticity profiles computed by the grid $\triangle x = \triangle y = \frac{1}{512}$ at a sequence of times, i.e. $t_1 = 0.5$, $t_2 = 1$, $t_3 = 1.5$, $t_4 = 2$ are shown in Fig. 5.5-5.8, respectively. Fig. 5.9 shows the vorticity profile at $t = 6$, which is close to a steady state.

Reproduced with permission of the copyright owner. Further reproduction prohibited without permission.

5.5 Proof of Proposition 5.3.1

Proof. Using the similar notations as in Section 5.2: denote $\tilde{\omega} = \omega^1 - \omega^2$, where ω^1, ω^2 are the solutions of the (5.3.8) with the boundary condition $\omega^1 |_{\Gamma_1} = C_1$, $\omega^2 |_{\Gamma_1} = C^2$, respectively. It can be seen that

$$\text{(5.5.2)} \qquad \begin{cases} \left(\triangle_h + \frac{h^2}{6} D_x^2 D_y^2\right)\tilde{\omega} = 0\,. \\ \tilde{\omega} |_{\Gamma_0} = 0\,. \qquad \tilde{\omega} |_{\Gamma_1} = C_1 - C_2\,. \end{cases}$$

The definition of ϕ in (5.3.9) indicates that

$$\text{(5.5.3)} \qquad \phi(C_1) - \phi(C_2) = \frac{1}{|\Gamma_1|}\Big(\frac{3}{2}\int_{\Gamma_1}^{(1)} \tilde{\omega} - \frac{3}{5}\int_{\Gamma_1}^{(2)} \tilde{\omega} + \frac{1}{10}\int_{\Gamma_1}^{(3)} \tilde{\omega}\Big)\,.$$

As can be seen, the right side of (5.5.3) is different from (5.2.12) in the second order case: three integrals, $\int_{\Gamma_1}^{(1)} \tilde{\omega}$, $\int_{\Gamma_1}^{(2)} \tilde{\omega}$, $\int_{\Gamma_1}^{(3)} \tilde{\omega}$ are involved in (5.5.3), where only $\int_{\Gamma_1}^{(1)} \tilde{\omega}$ was involved in (5.2.12). The better control of (5.5.3) is obtained by rewriting it. Motivated by the idea of the stability analysis of vorticity boundary conditions, which were shown in [ELV2], we can rewrite $\frac{3}{2}\tilde{\omega}_{n-1,j} - \frac{3}{5}\tilde{\omega}_{n-2,j} + \frac{1}{10}\tilde{\omega}_{n-3,j}$ as

$$\text{(5.5.4)} \qquad \begin{aligned} &\frac{3}{2}\tilde{\psi}_{n-1,j} - \frac{3}{5}\tilde{\psi}_{n-2,j} + \frac{1}{10}\tilde{\psi}_{n-3,j} \\ &= \frac{2}{5}\tilde{\psi}_{n,j} + \frac{3}{5}\tilde{\psi}_{n-1,j} - \frac{2}{5}h^2 D_x^2\tilde{\omega}_{n-1,j} + \frac{1}{10}h^2 D_x^2\tilde{\omega}_{n-2,j}\,. \end{aligned}$$

The substitution of (5.5.4) into (5.5.3), along with the fact that $\tilde{\psi}$ is a constant $C_1 - C_2$ on Γ_1, gives

(5.5.5)

$$\phi(C_1) - \phi(C_2) = \frac{1}{|\Gamma_1|}\Big(\frac{2}{5}(C_1 - C_2)|\Gamma_1| + \frac{3}{5}\int_{\Gamma_1}^{(1)} \tilde{\omega} - \frac{2}{5}h^2\int_{\Gamma_1}^{(2)} D_{\boldsymbol{n}}^2\tilde{\omega} + \frac{1}{10}h^2\int_{\Gamma_1}^{(3)} D_{\boldsymbol{n}}^2\tilde{\psi}\Big)\,,$$

where $D_{\boldsymbol{n}}^2\tilde{\omega}$ is $D_x^2\tilde{\omega}$ on the boundary sections AB, CD, and $D_y^2\tilde{\omega}$ on the boundary sections BC, DA.

The following Lemma, which is analogous to Lemma 5.2.2 in the second order case, gives the estimate of $\tilde{\omega}$ near the boundary Γ_1. The strategy of the

Reproduced with permission of the copyright owner. Further reproduction prohibited without permission.

proof is also similar to that of Lemma 5.2.2: applying the maximum principle to the operators $\left(\triangle_h + \frac{h^2}{6} D_x^2 D_y^2\right)$.

Lemma 5.5.1 Let u be the solution of the system

$$\begin{cases} \left(\triangle_h + \dfrac{h^2}{6} D_x^2 D_y^2\right) u = 0 . \\ u\,|_{\Gamma_0} = 0 . \qquad u\,|_{\Gamma_1} = 1 . \end{cases} \tag{5.5.6}$$

then we have

$$0 \le u_{n-k,j} \le 1 - kh . \qquad \text{for } n \le j \le m . \tag{5.5.7}$$

Proof. Using the same notations as in the proof of Lemma 5.2.2, the region Ω can be partitioned into four regions: A_1ABB_1, A_1ADD_1, D_1DCC_1, C_1CBB_1, denoted by Ω_1, Ω_2, Ω_3, Ω_4, respectively, as shown in Fig. 5.3. The same function v as in (5.2.15) is considered. Detailed calculations indicate that the constructed function v in (5.2.15) is concave, which satisfies

$$\begin{cases} \left(\triangle_h + \dfrac{h^2}{6} D_x^2 D_y^2\right) v \le 0 . \\ v\,|_{\Gamma_0} = 0 . \qquad v\,|_{\Gamma_1} = 1 . \end{cases} \tag{5.5.8}$$

Then of course, $f = -\left(\triangle_h + \frac{h^2}{6} D_x^2 D_y^2\right) v \ge 0$. Then u can be decomposed into two parts: $u = v + w$, where w is the solution of the following system

$$\begin{cases} \left(\triangle_h + \frac{h^2}{6} D_x^2 D_y^2\right) w = f \ge 0 . \\ w\,|_{\Gamma_0} = 0 . \qquad w\,|_{\Gamma_1} = 0 . \end{cases} \tag{5.5.9}$$

It can be argued similarly as in Section 5.2 that the maximum principle holds for the operator $\left(\triangle_h + \frac{h^2}{6} D_x^2 D_y^2\right)$. In the uniform grid, the operator has the form

$$\begin{aligned} \left(\triangle_h + \frac{h^2}{6} D_x^2 D_y^2\right) u_{i,j} = \; & \frac{1}{6h^4} \big((u_{i-1,j-1} + 4u_{i,j-1} + u_{i+1,j-1}) \\ & + (4u_{i-1,j} - 20u_{i,j} + 4u_{i+1,j}) \\ & + (u_{i-1,j+1} + 4u_{i,j+1} + u_{i+1,j+1}) \big) . \end{aligned} \tag{5.5.10}$$

Reproduced with permission of the copyright owner. Further reproduction prohibited without permission.

which indicates the maximum principle. This principle together with (5.5.9) shows that $w \le 0$ at all grid points. Then we have

(5.5.11) $$u \le v. \qquad \text{at all grid points.}$$

and especially, $u_{n-k,j} \le v_{n-k,j} = 1 - kh$. The left half of (5.5.7) comes directly from the maximum principle of the operator $\left(\triangle_h + \frac{h^2}{6} D_x^2 D_y^2\right)$. Lemma 5.5.1 is proven.

Obviously, $\tilde{\psi} = (C_1 - C_2)u$, where $\tilde{\psi}$ was given in (5.5.1) and u is the solution of (5.5.6), which results in the control of the second term in (5.5.5):

(5.5.12) $$\frac{3}{5}\left|\int_{\Gamma_1}^{(1)} \tilde{\psi}\right| \le \frac{3}{5}(1-h)|C_1 - C_2||\Gamma_1|.$$

The estimates of the last two terms in (5.5.5) are obtained by the following Lemma.

Lemma 5.5.2 Let u be the solution of (5.5.6), then we have

(5.5.13) $$h^2\left|\int_{\Gamma_1}^{(1)} D_{\boldsymbol{n}}^2 u\right|, \quad h^2\left|\int_{\Gamma_1}^{(2)} D_{\boldsymbol{n}}^2 u\right| \le 4h.$$

Proof. For simplicity of the presentation, only the integral on the boundary section AB is discussed here. The boundary sections BC, CD, DA can be dealt with in the same way. The equation in (5.5.6) gives $D_x^2 u = -\left(D_y^2 + \frac{h^2}{6} D_x^2 D_y^2\right)u$, whose application to the grid point $(n-1, j)$ results in

(5.5.14)
$$D_x^2 u_{n-1,j} = -\left(D_y^2 + \frac{h^2}{6} D_x^2 D_y^2\right)u_{n-1,j} = -\frac{1}{6} D_y^2 u_{n-2,j} - \frac{2}{3} D_y^2 u_{n-1,j} - \frac{1}{6} D_y^2 u_{n,j}.$$

Integration of (5.5.14) along the boundary AB (by trapezoid rule) gives

(5.5.15)
$$\begin{aligned} h^2 \int_{AB} D_x^2 u_{n-1,j} = \; & -\frac{1}{6}h^2\left(\frac{1}{2}\frac{u_{n-2,m+1} - u_{n-2,m-1}}{h} - \frac{1}{2}\frac{u_{n-2,n+1} - u_{n-2,n-1}}{h}\right) \\ & -\frac{2}{3}h^2\left(\frac{1}{2}\frac{u_{n-1,m+1} - u_{n-1,m-1}}{h} - \frac{1}{2}\frac{u_{n-1,n+1} - u_{n-1,n-1}}{h}\right) \\ & -\frac{1}{6}h^2\left(\frac{1}{2}\frac{u_{n,m+1} - u_{n,m-1}}{h} - \frac{1}{2}\frac{u_{n,n+1} - u_{n,n-1}}{h}\right). \end{aligned}$$

Reproduced with permission of the copyright owner. Further reproduction prohibited without permission.

As argued earlier, the application of the maximum principle in (5.5.6) shows that

$$0 \le u_{i,j} \le 1 , \qquad \text{for} \qquad (x_i, y_j) \in \Omega . \tag{5.5.16}$$

The combination of (5.5.15) and (5.5.16) gives

$$h^2 \left| \int_{AB} D_x^2 u_{n-1,j} \right| \le h . \tag{5.5.17}$$

Similar estimates can be applied to boundary sections BC, CD, DA. Lemma A.2.2 is proven.

As said earlier, $\tilde{\psi} = (C_1 - C_2)u$. The combination of (5.5.5), Lemma A.1, Lemma A.2, gives

$$|\phi(C_1) - \phi(C_2)| \le (1 - \frac{3}{5}h + \frac{2}{|\Gamma_1|}h)|C_1 - C_2| = (1 - \frac{1}{10}h)|C_1 - C_2| , \tag{5.5.18}$$

since $|\Gamma_1| = 4$. Proposition 5.3.1 is proven.

Reproduced with permission of the copyright owner. Further reproduction prohibited without permission.

Table 5.1: Errors and orders of accuracy at $t = 6$ when the second order method, which was described in Section 5.2, is used. CFL=$\frac{1}{2}$, where CFL= $\frac{\Delta t}{\Delta x}$.

	N	L^∞ error	L^∞ order	L^1 error	L^1 order	L^2 error	L^2 order
c	48	5.17e-02		1.57e-02		2.08e-02	
	72	2.20e-02	2.10	6.35e-03	2.23	8.68e-03	2.16
	96	1.26e-02	1.94	3.58e-03	1.99	4.95e-03	1.95
	144	5.49e-03	2.05	1.54e-03	2.08	2.14e-03	2.06
	192	3.11e-03	1.98	8.64e-04	2.01	1.20e-03	2.01
ω	48	1.02e-01		1.98e-02		2.83e-02	
	72	6.72e-02	1.03	8.50e-03	2.08	1.27e-02	1.98
	96	5.03e-02	1.01	4.88e-03	1.93	7.53e-03	1.82
	144	2.98e-02	1.29	2.14e-03	2.03	3.38e-03	1.98
	192	1.98e-02	1.42	1.23e-03	1.93	1.96e-03	1.90

Table 5.2: Errors and orders of accuracy at $t = 6$ when the fourth order method, which was described in Section 5.3, is used. CFL=$\frac{1}{2}$, where CFL= $\frac{\Delta t}{\Delta x}$.

	N	L^∞ error	L^∞ order	L^1 error	L^1 order	L^2 error	L^2 order
c	48	4.08e-03		1.31e-03		1.68e-03	
	72	6.24e-04	4.63	1.90e-04	4.76	2.40e-04	4.79
	96	1.72e-04	4.48	5.08e-05	4.58	6.41e-05	4.59
	144	2.70e-05	4.57	7.76e-06	4.63	9.74e-06	4.65
	192	7.59e-06	4.41	2.18e-06	4.41	2.74e-06	4.41
ω	48	2.23e-02		2.81e-03		3.93e-03	
	72	5.70e-03	3.36	5.01e-04	4.25	7.52e-04	4.08
	96	2.22e-03	3.28	1.57e-04	4.03	2.49e-04	3.85
	144	5.12e-04	3.62	2.92e-05	4.15	4.82e-05	4.05
	192	2.02e-04	3.23	9.24e-06	4.00	1.59e-05	3.86

Reproduced with permission of the copyright owner. Further reproduction prohibited without permission.

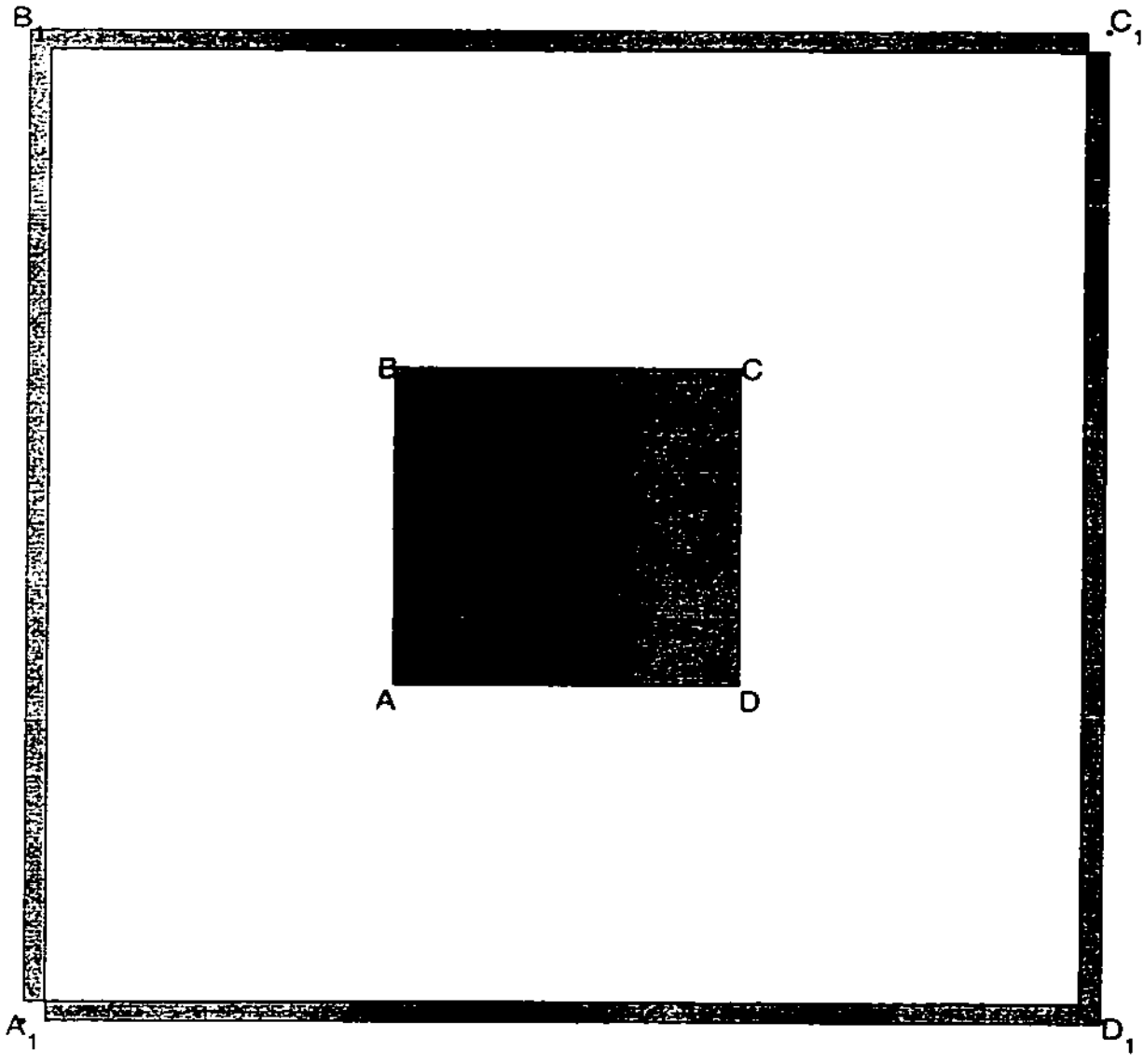

Figure 5.2: An example of multi-connected Domain

Reproduced with permission of the copyright owner. Further reproduction prohibited without permission.

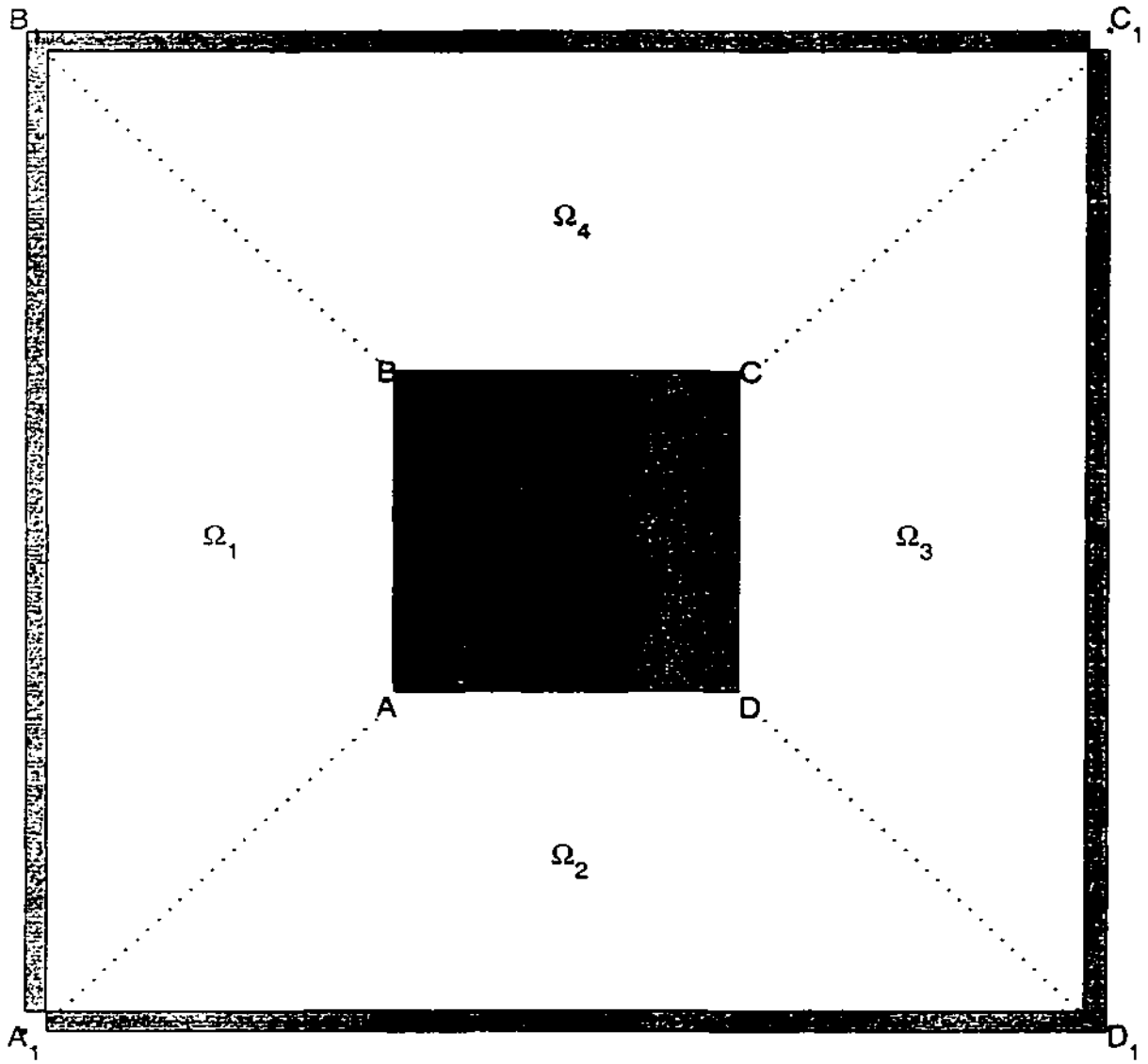

Figure 5.3: A decomposition of the domain

Reproduced with permission of the copyright owner. Further reproduction prohibited without permission.

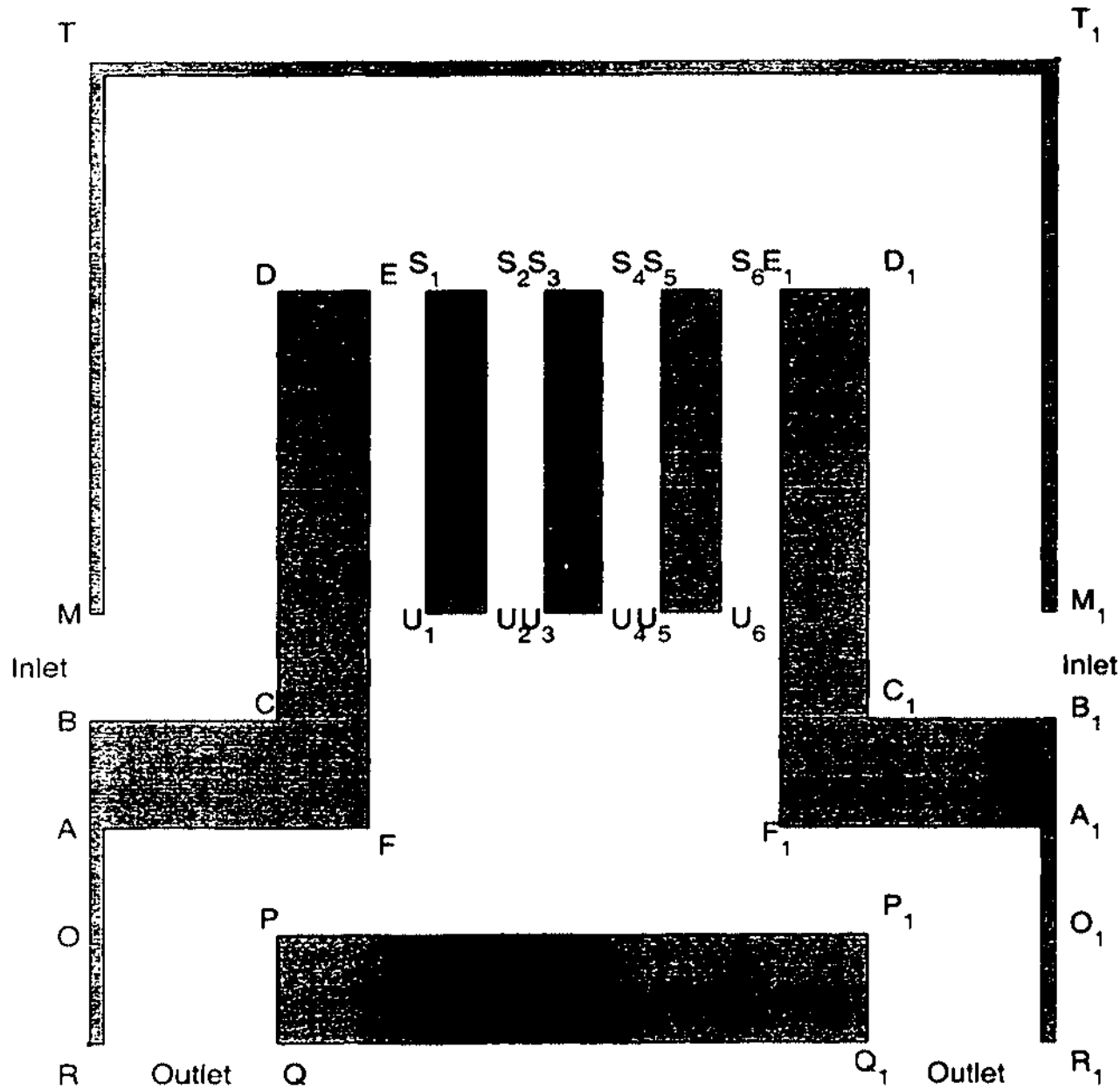

Figure 5.4: A cooling system

Reproduced with permission of the copyright owner. Further reproduction prohibited without permission.

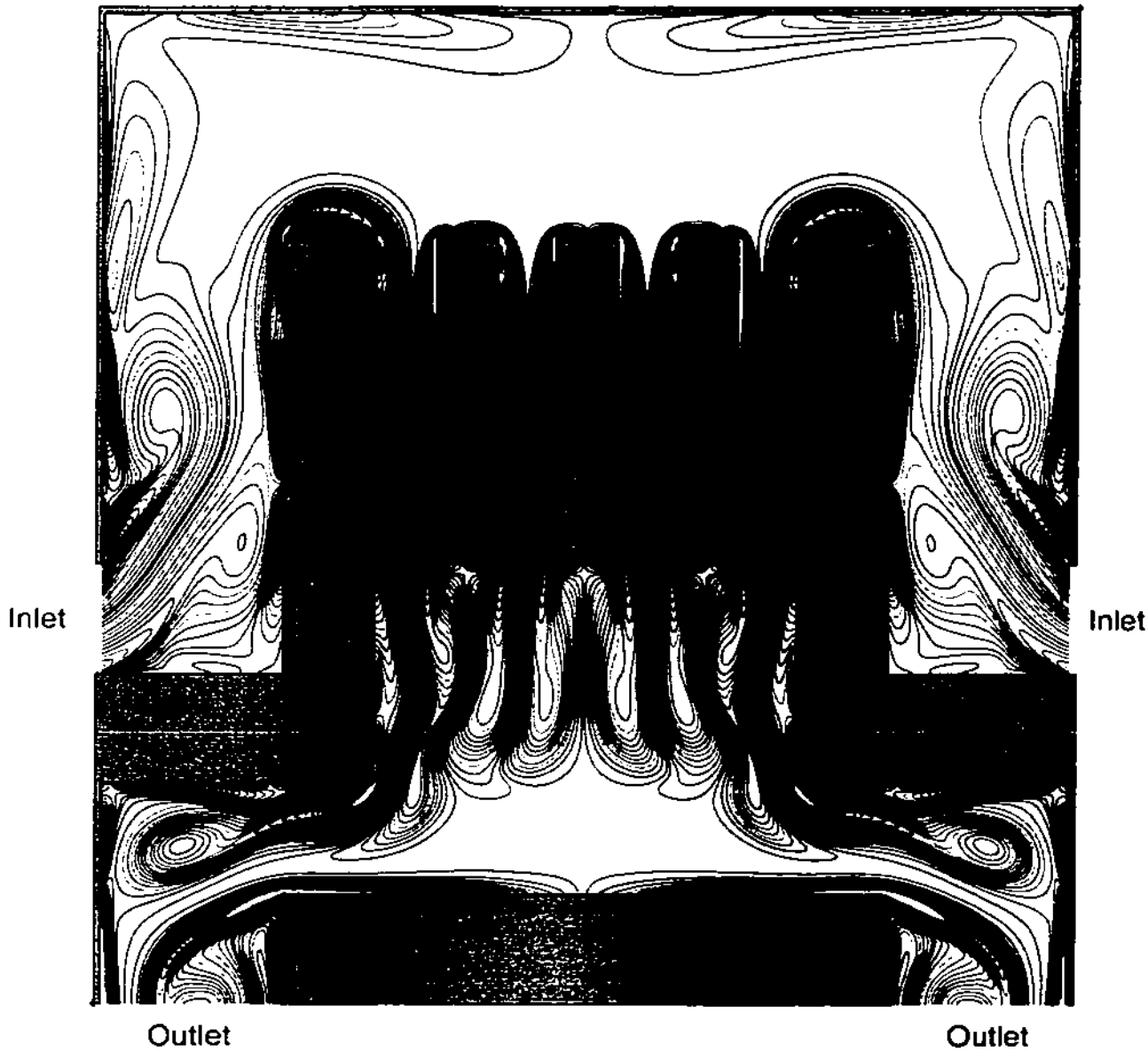

Figure 5.5: Vorticity plot with 30 equally spaced contours from 1 to 100 and from -100 to -1, at time $t_1 = 0.5$, of the flow past the cooling system. $Re = 2000$. The computation is based on EC4 method with the resolution $\triangle x = \triangle y = \frac{1}{512}$.

Reproduced with permission of the copyright owner. Further reproduction prohibited without permission.

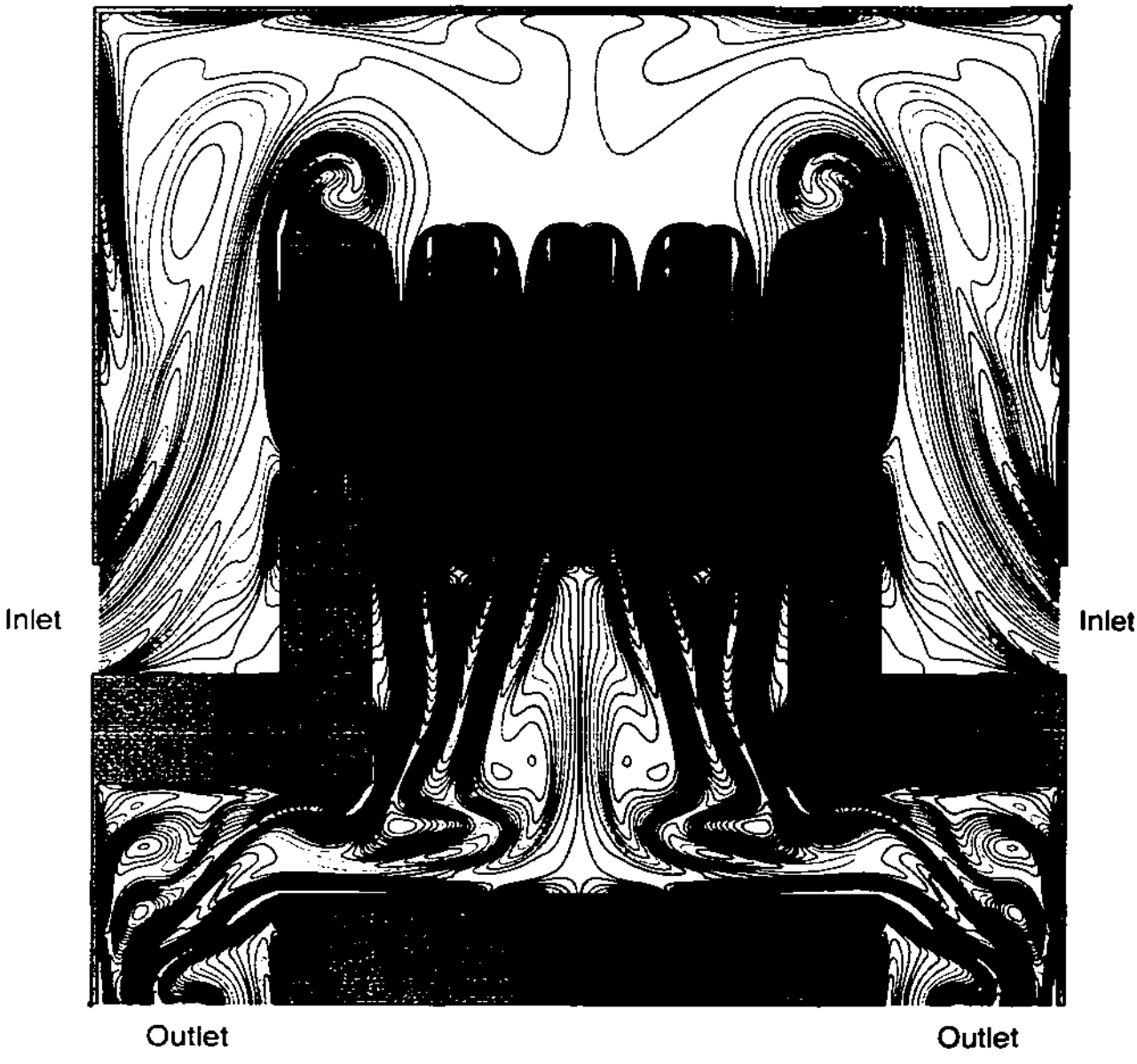

Figure 5.6: Vorticity plot with 30 equally spaced contours from 1 to 100 and from -100 to -1. at time $t_2 = 1$. of the flow past the cooling system. $Re = 2000$. The computation is based on EC4 method with the resolution $\triangle x = \triangle y = \frac{1}{512}$.

Reproduced with permission of the copyright owner. Further reproduction prohibited without permission.

Figure 5.7: Vorticity plot with 30 equally spaced contours from 1 to 100 and from -100 to -1, at time $t_3 = 1.5$, of the flow past the cooling system. $Re = 2000$. The computation is based on EC4 method with the resolution $\triangle x = \triangle y = \frac{1}{512}$.

Reproduced with permission of the copyright owner. Further reproduction prohibited without permission.

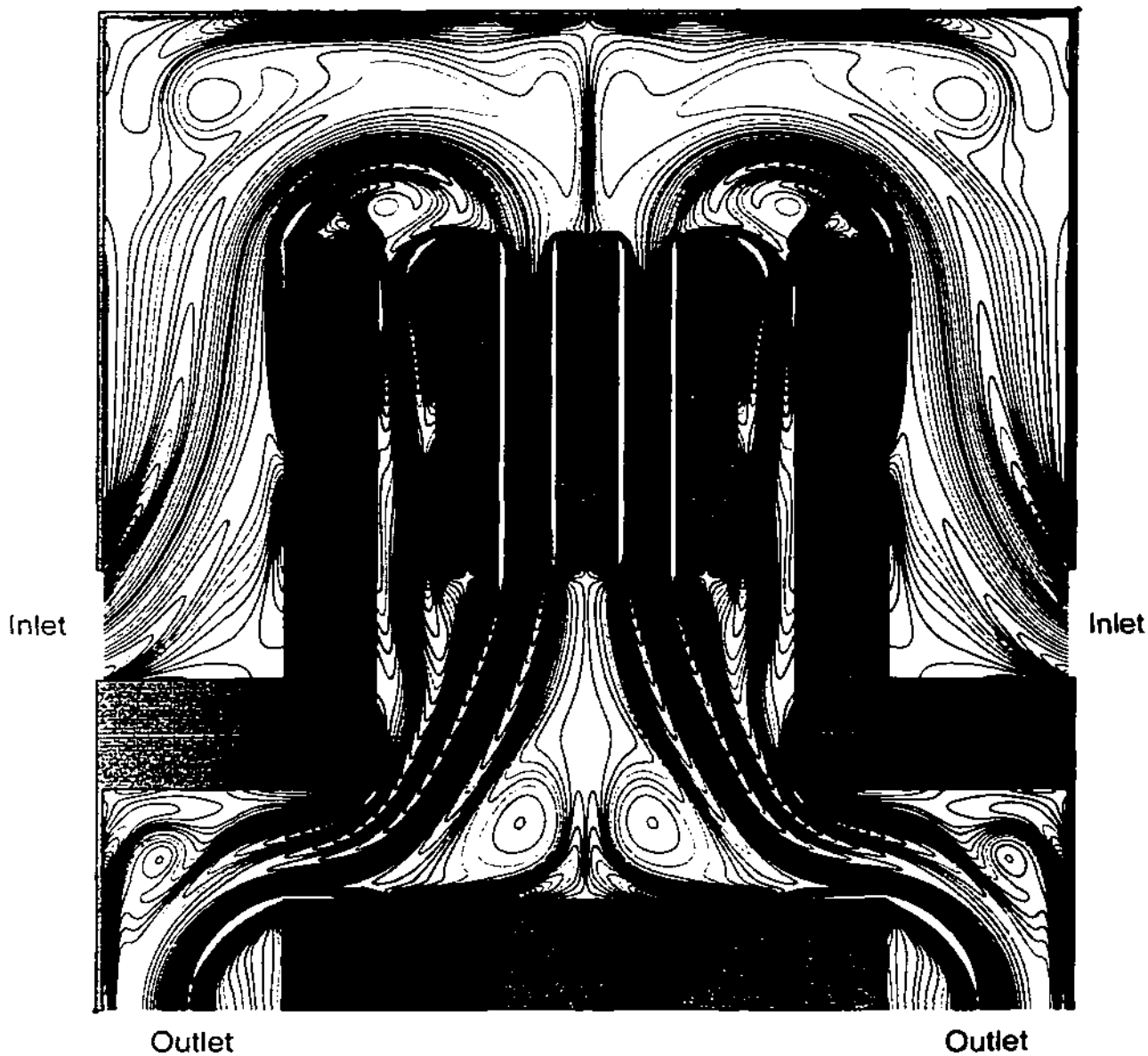

Figure 5.8: Vorticity plot with 30 equally spaced contours from 1 to 100 and from -100 to -1, at time $t_4 = 2$, of the flow past the cooling system. $Re = 2000$. The computation is based on EC4 method with the resolution $\triangle x = \triangle y = \frac{1}{512}$.

Reproduced with permission of the copyright owner. Further reproduction prohibited without permission.

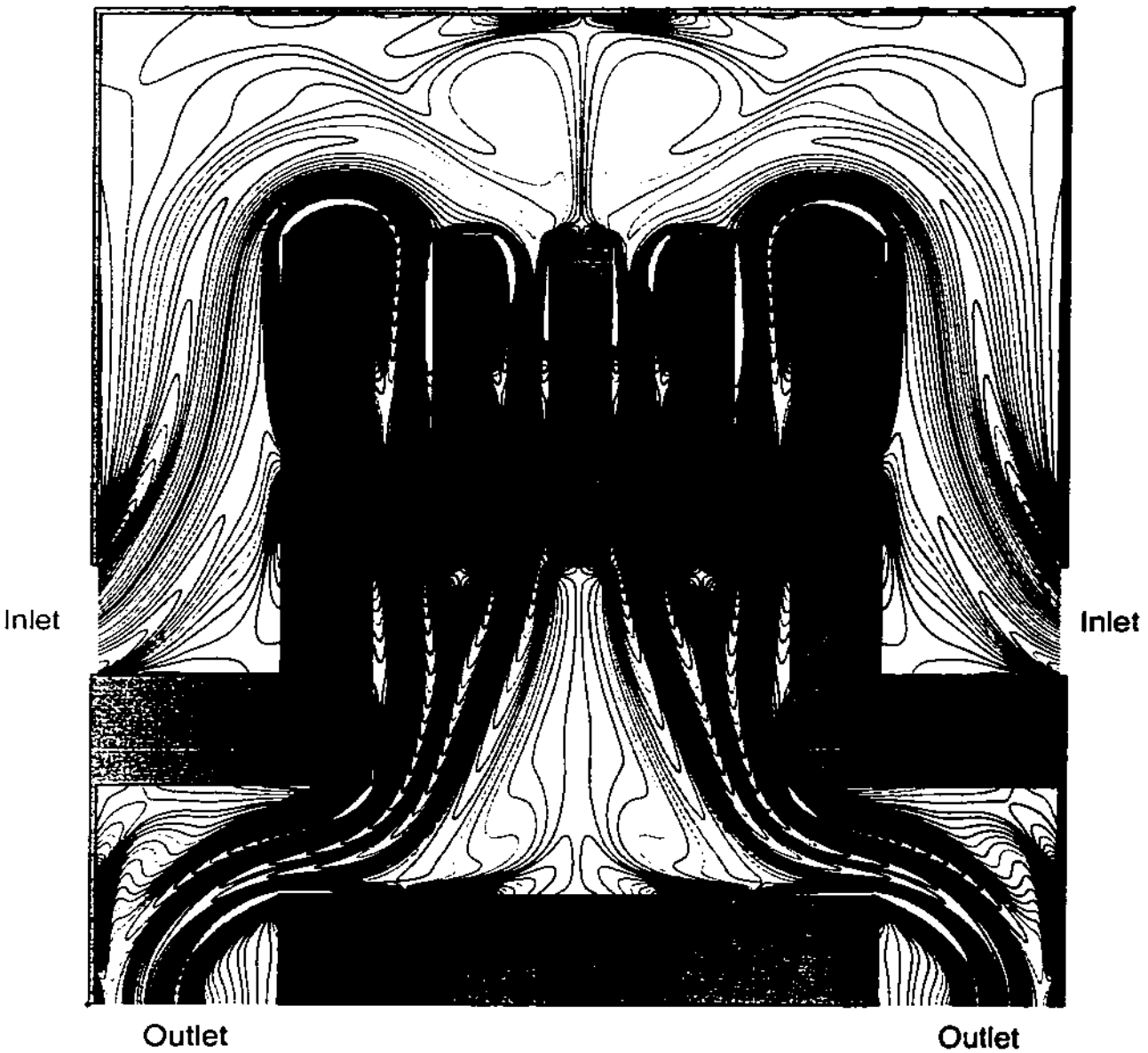

Figure 5.9: Vorticity plot with 30 equally spaced contours from 1 to 100 and from -100 to -1. at time $t = 6$, which is close to the steady state, of the flow past the cooling system. $Re = 2000$. The computation is based on EC4 method with the resolution $\triangle x = \triangle y = \frac{1}{512}$.

Reproduced with permission of the copyright owner. Further reproduction prohibited without permission.

CHAPTER 6
APPLICATION TO BOUSSINESQ EQUATIONS

6.1 Preliminary

The 2-D dimensionless incompressible Navier-Stokes equations in the Boussinesq approximation are given by

$$\begin{cases} \partial_t\theta + (\boldsymbol{u}\cdot\nabla)\theta = \dfrac{1}{Re\cdot Pr}\triangle\theta\,, \\ \partial_t\boldsymbol{u} + (\boldsymbol{u}\cdot\nabla)\boldsymbol{u} + \nabla p = Ri\cdot\theta\cdot\begin{pmatrix} 0 \\ 1 \end{pmatrix} + \dfrac{1}{Re}\triangle\boldsymbol{u}\,, \\ \nabla\cdot\boldsymbol{u} = 0\,. \end{cases} \tag{6.1.1}$$

where $\boldsymbol{u}$ is the velocity, p is the pressure, θ is the temperature, Re is the Reynolds number of the flow, Pr represents the Prandtl number, which is the ratio of the kinematic viscosity to the heat conductivity, Ri, the Richardson number, corresponds to the gravity force effect and the thermal expansion of the fluid. Sometimes there are different dimensionless quantities in the above equations based on the scales relating to the purposes of different setups in physics. Some other parameters can be introduced in different problems in physics, such as the Rayleigh number $Ra = Ri\cdot Re^2\cdot Pr$ appearing in the Rayleigh-B'enard problem, and Gr, the Grashof number, which is defined as $Gr = \frac{Ra}{Pr} = Ri\cdot Re^2$. For brevity of our presentation below, we denote $\nu = \frac{1}{Re}$, and $\kappa = \frac{1}{RePr}$. The system (6.1.1) is usually identified as Oberbeck-Boussinesq equations, (or, simply, Boussinesq

Reproduced with permission of the copyright owner. Further reproduction prohibited without permission.

equations).

(6.1.1) can also be written in the vorticity-stream function formulation

$$\text{(6.1.2)} \qquad \begin{cases} \partial_t \theta + (\boldsymbol{u}\cdot\nabla)\theta = \kappa\triangle\theta\,. \\ \partial_t \omega + (\boldsymbol{u}\cdot\nabla)\omega = Ri\partial_x\theta + \nu\triangle\omega\,. \\ \triangle\psi = \omega\,. \\ u = -\partial_y\psi\,, \qquad v = \partial_x\psi \end{cases}$$

where $\omega = \nabla \times \boldsymbol{u}$ is the vorticity, ψ is the stream function.

The natural no-slip boundary condition $\boldsymbol{u}\,|_\Gamma = 0$ is imposed in (6.1.1), which in turn can be written in terms of the stream function ψ if the computational domain is a simply-connected domain

$$\text{(6.1.3)} \qquad \psi = 0, \quad \frac{\partial\psi}{\partial\mathbf{n}} = 0\,.$$

For the temperature θ, we can either impose the Dirichlet boundary condition

$$\text{(6.1.4)} \qquad \theta\,|_\Gamma = \theta_b\,.$$

where θ_b is a given distribution for the temperature on the boundary; or, we can impose the Neumann boundary condition

$$\text{(6.1.5)} \qquad \frac{\partial\theta}{\partial\boldsymbol{n}} = \theta_f\,, \quad \text{on } \Gamma\,.$$

where θ_f is a given heat flux on the boundary. If the adiabatic boundary condition is assumed, θ_f can be taken to be 0.

The strategy of developing the fourth order numerical method of the Boussinesq equations in vorticity formulation is similar to that of the Navier-Stokes equations. See [ELV1], [ELV2]. A 4-th order essentially compact approach will be used to treat the momentum equation. The purpose of this approach is to reduce the number of numerical boundary conditions for ψ. This is important

Reproduced with permission of the copyright owner. Further reproduction prohibited without permission.

for the momentum equation since v is coupled with ω by a Poisson equation. The main issue of determining the vorticity on the boundary is that there are two boundary conditions for stream function as in (6.1.3). The no-penetration boundary condition $\psi\,|_\Gamma = 0$ can be directly applied in the Poisson solver. The no-slip boundary condition $\frac{\partial v}{\partial n}\,|_\Gamma = 0$, along with the kinematic relationship between v and ω, will be converted into a vorticity boundary condition, such as Briley's formula or a new 4-th order vorticity boundary formula proposed in Chapter 4. Moreover, the main difference between the momentum equation in Boussinesq equations and the usual fluid equations is the addition of the gravity term, i.e. the temperature is coupled in the momentum equation with the gravity term. This coupling will be treated explicitly. Consequently, no numerical difficulty will be anticipated.

The evolution of temperature in the temperature equation can be treated as a standard convection-diffusion equation, mainly a passive scalar. This equation can be updated very efficiently by the 4-th order long stencil difference operators. The numerical values at the "ghost" computation points near the boundary can be estimated by one-sided extrapolation. To reduce the number of interior points for both computational convenience and better stability, we can also apply some information obtained by the temperature equation on the boundary. Similar idea can be found in [HKR]. The resulting boundary condition can be proven to be stable, both numerically and theoretically.

The 4-th order Runge-Kutta method will be used in our time discretization to avoid cell-Reynolds constraint, as discussed by E and Liu in [ELV1], [ELV2]. The numerical scheme, including the implementation of the time-stepping procedure, is described in Section 6.2.

In Section 6.3, a well-recognized model dealing with Rayleigh-Bénard convection is used to check the accuracy of our numerical scheme. The stream

Reproduced with permission of the copyright owner. Further reproduction prohibited without permission.

function and the temperature in the two-dimensional flow can be represented by three parameters with the help of single and double mode analyses. By making appropriate transformations, the evolution of the three parameters can be described as a nonlinear system of ODEs, which is known as the Lorenz system. An accuracy check is carried out for our computational method applied to the Boussinesq equations (with a single source term) based on the Lorenz system. Full fourth order accuracy was shown for this flow.

In Section 6.4, we demonstrate the robustness of our numerical method by simulating an example of strong shear flow induced by a temperature jump, of the ratio 1.5:1, in an insulated box. The complicated structure of rolling up, resulting from the vortex sheet and the consequent Kelvin-Helmholtz instability, is completely resolved. The accuracy of our computation is checked by the perfect match of the two resolutions: 2048×256 and 4096×512.

6.2 Description of the Scheme

For simplicity of presentation, we take the same computation domain as in Chapter 3: $\Omega = [0,1] \times [0,1]$ with grid size $\triangle x = \triangle y = h$. The boundary is composed of Γ_x: $\{y = 0, 1\}$ and Γ_y: $\{x = 0, 1\}$. The associated numerical grids will be denoted by $\{x_i = i/N, y_j = j/N,\ i, j = 0, 1, \cdots, N\}$.

6.2.1 Temperature Transport Equation

For the temperature transport equation $\partial_t \theta + \boldsymbol{u} \cdot \nabla \theta = \kappa \triangle \theta$, one can approximate ∂_x, ∂_y by the standard fourth order long-stencil operator

$$\partial_x = \widetilde{D}_x(1 - \frac{h^2}{6} D_x^2) + O(h^4), \qquad \partial_y = \widetilde{D}_y(1 - \frac{h^2}{6} D_y^2) + O(h^4), \tag{6.2.1}$$

where $\widetilde{D}_x$, D_x^2 are standard centered difference operators corresponding to ∂_x, ∂_x^2.

Reproduced with permission of the copyright owner. Further reproduction prohibited without permission.

respectively. To approximate $\triangle$ in the diffusion term, one can see that

$$\triangle = \triangle_h - \frac{h^2}{12}(D_x^4 + D_y^4) + O(h^4)\,. \tag{6.2.2}$$

Thus we have the approximation for the temperature equation

$$\partial_t\theta + u\widetilde{D}_x(1 - \frac{h^2}{6}D_x^2)\theta + v\widetilde{D}_y(1 - \frac{h^2}{6}D_y^2)\theta = \kappa\Big(\triangle_h - \frac{h^2}{12}(D_x^4 + D_y^4)\Big)\theta\,. \tag{6.2.3}$$

6.2.2 Temperature at Ghost Point(s)

As can be seen, the implementation of (6.2.3) requires the determination of θ at the "ghost points", which are grid points outside the computational domain. Its derivation needs the one-sided approximation near the boundary. Shorter one-sided stencils usually result in better stability and computational convenience. For brevity of the presentation, we concentrate on the boundary Γ_x, $j = 0$.

6.2.2.1 Dirichlet boundary condition for Temperature

If the Dirichlet boundary condition for the temperature (6.1.4) is imposed, $\theta_{i,0}$ can be given accurately on the boundary to be $\theta_b(x_i, 0)$. Accordingly, under this boundary condition for the temperature, (6.2.3) shall be updated at interior points (x_i, y_j), $1 \le i, j \le N-1$. This indicates that only one "ghost point" value $\theta_{i,-1}$ needs to be obtained. Local Taylor expansion near the boundary gives us

$$\theta_{i,-1} = \frac{20}{11}\theta_{i,0} - \frac{6}{11}\theta_{i,1} - \frac{4}{11}\theta_{i,2} + \frac{1}{11}\theta_{i,3} + \frac{12}{11}h^2\partial_y^2\theta_{i,0} + O(h^5)\,. \tag{6.2.4}$$

Sometimes we can even use information from the PDE, or derivatives of PDE, near the boundary to reduce the number of required points in the stencil. As can be seen, the term $\partial_y^2\theta$ on $j = 0$ in (6.2.4) can be evaluated with the help of the following evaluation on the boundary

$$\partial_t\theta\,|_{\Gamma_x} = \kappa\triangle\theta\,|_{\Gamma_x} = \kappa(\partial_x^2 + \partial_y^2)\theta\,|_{\Gamma_x} = \kappa(\partial_x^2\theta_b + \partial_y^2\theta\,|_{\Gamma_x})\,. \tag{6.2.5}$$

Reproduced with permission of the copyright owner. Further reproduction prohibited without permission.

where in the first step we used the no-slip boundary condition for u and v, which implies that the convection term disappears on the boundary for the equation in (6.1.2). (6.2.5) leads to

$$\partial_y^2\theta\,|_{\Gamma_x} = \frac{1}{\kappa}\partial_t\theta_b - \partial_x^2\theta_b\,. \tag{6.2.6}$$

where the right hand side is a known function since θ is given on the boundary. Substituting (6.2.6) into (6.2.4), we have

$$\theta_{i,-1} = \frac{20}{11}\theta_{i,0} - \frac{6}{11}\theta_{i,1} - \frac{4}{11}\theta_{i,2} + \frac{1}{11}\theta_{i,3} + \frac{12}{11}h^2(\frac{1}{\kappa}\partial_t\theta_b - \partial_x^2\theta_b) + O(h^5)\,. \tag{6.2.7}$$

The same applies to the other three boundaries. It can be shown that this formula gives full 4-th order accuracy. See the results in Table 6.1.

Remark 6.2.1 In (6.2.4), we used 5-th order one-sided approximation for the temperature near the boundary. In fact, the 4-th order Taylor expansion near the boundary can also be used, which results in only one interior point in the formula

$$\theta_{i,-1} = 2\theta_{i,0} - \theta_{i,1} + h^2\partial_y^2\theta_{i,0} + O(h^4)\,. \tag{6.2.8}$$

The derivation of $\partial_y^2\theta_{i,0}$ on Γ_x, (6.2.5) and (6.2.6), is still valid here. The combination of (6.2.8) and (6.2.6) results in

$$\theta_{i,-1} = 2\theta_{i,0} - \theta_{i,1} + h^2(\frac{1}{\kappa}\partial_t\theta_b - \partial_x^2\theta_b) + O(h^4)\,. \tag{6.2.9}$$

which is a $O(h^4)$ formula analogous to (6.2.7). Our computation shows that both (6.2.7) and (6.2.9) provides stability and full accuracy, as explained in Section 6.3. Since (6.2.9) only requires one interior point, we suggest using (6.2.9) in practical computation for convenience.

Reproduced with permission of the copyright owner. Further reproduction prohibited without permission.

6.2.2.2 Neumann Boundary Condition for the Temperature

Under Neumann boundary condition, the temperature distribution on the boundary is not known explicitly. In this case, (6.2.3) is updated at every computational point (x_i, y_j), $0 \leq i, j \leq N$. This in turn requires that we determine two "ghost point" values $\theta_{i,-1}$ and $\theta_{i,-2}$ to carry out (6.2.3). The same strategy of one-sided approximations is applied. It can be seen that the local Taylor expansion near the boundary gives

$$\theta_{i,-1} = \theta_{i,1} - 2h\partial_y\theta_{i,0} - \frac{h^3}{3}\partial_y^3\theta_{i,0} + O(h^5)\,. \tag{6.2.10}$$

and

$$\theta_{i,-2} = \theta_{i,2} - 4h\partial_y\theta_{i,0} - \frac{8h^3}{3}\partial_y^3\theta_{i,0} + O(h^5)\,. \tag{6.2.11}$$

The term $\partial_y\theta_{i,0}$ appearing in (6.2.10), (6.2.11) has already been given by θ_f. In the no-flux case, this term disappears. Then the remaining task is to determine $\partial_y^3\theta_{i,0}$. As discussed above, the information from the PDE, or derivatives of PDE, near the boundary can be used for the derivation of "ghost point" values of the temperature. If the normal derivative on the boundary, which is ∂_y on Γ_x, is taken for the original temperature transport equation, we arrive at

$$\theta_{yt} + u_y\theta_x + u\theta_{xy} + v_y\theta_y + v\theta_{yy} = \kappa(\theta_{yxx} + \partial_y^3\theta)\,, \qquad \text{on } \Gamma_x\,. \tag{6.2.12}$$

All the terms in (6.2.12) are evaluated on the boundary Γ_x. The first term on the left side of (6.2.12) is a known function θ_{ft}, which in the no-flux case disappears; the third and fifth terms on the left side of (6.2.12) disappear because of no-slip boundary condition; the fourth term on the left side also disappears because of the no-slip boundary condition and the incompressibility which implies that $v_y = -u_x = 0$ on Γ_x; the first term on the right side of (6.2.12) is also a known function θ_{fxx}, which disappears in the case that no heat flux is on the

Reproduced with permission of the copyright owner. Further reproduction prohibited without permission.

boundary. Then the remaining task is to determine the second term on the left side of (6.2.12), $u_y\theta_x$. As can be seen, u_y is in fact $-\omega$ on the boundary Γ_x because $\omega = -u_y + v_x$ and v_x vanishes on the boundary. Moreover, since (6.2.3) is updated at all grid points, including the boundary points, θ_x on Γ_x can be calculated by the standard fourth order long-stencil operator (6.2.1). Combining all the arguments above and substituting back into (6.2.12), we obtain $\partial_y^3\theta$ on Γ_x

$$\partial_y^3\theta_{i,0} = \frac{1}{\kappa}\Big(\theta_{ft} - \omega_{i,0}\widetilde{D}_x(1 - \frac{h^2}{6}D_x^2)\theta_{i,0}\Big) - \theta_{fxx}\,. \tag{6.2.13}$$

Plugging (6.2.13) back into (6.2.10), (6.2.11), we get the two "ghost point" values for θ near the boundary Γ_x

$$\theta_{i,-1} = \theta_{i,1} - 2h\theta_f - \frac{h^3}{3}\Big(\frac{1}{\kappa}\theta_{ft} - \frac{1}{\kappa}\omega_{i,0}\widetilde{D}_x(1 - \frac{h^2}{6}D_x^2)\theta_{i,0} - \theta_{fxx}\Big)\,. \tag{6.2.14}$$

$$\theta_{i,-2} = \theta_{i,2} - 4h\theta_f - \frac{8h^3}{3}\Big(\frac{1}{\kappa}\theta_{ft} - \frac{1}{\kappa}\omega_{i,0}\widetilde{D}_x(1 - \frac{h^2}{6}D_x^2)\theta_{i,0} - \theta_{fxx}\Big)\,. \tag{6.2.15}$$

In the no-flux case (in other words, θ_f disappears), the above formulas can be simplified to

$$\theta_{i,-1} = \theta_{i,1} + \frac{h^3}{3}\frac{\omega_{i,0}}{\kappa}\widetilde{D}_x(1 - \frac{h^2}{6}D_x^2)\theta_{i,0}\,. \tag{6.2.16}$$

$$\theta_{i,-2} = \theta_{i,2} + \frac{8h^3}{3}\frac{\omega_{i,0}}{\kappa}\widetilde{D}_x(1 - \frac{h^2}{6}D_x^2)\theta_{i,0}\,. \tag{6.2.17}$$

Still, the other three boundaries can be treated in a similar manner.

6.2.3 Momentum Equation

To solve the fluid part equations, we can use the Essentially Compact Fourth Order Scheme (EC4), which was proposed by E and Liu. The starting point of the scheme is the fact that Laplacian operator $\triangle$ can be approximated with the fourth order by

$$\triangle = \frac{\triangle_h + \frac{h^2}{6}D_x^2D_y^2}{1 + \frac{h^2}{12}\triangle_h} + O(h^4)\,. \tag{6.2.18}$$

Reproduced with permission of the copyright owner. Further reproduction prohibited without permission.

Multiplying the denominator difference operator $1 + \frac{h^2}{12}\triangle_h$ to the momentum equation gives

(6.2.19)
$$(1 + \frac{h^2}{12}\triangle_h)\partial_t\omega + (1 + \frac{h^2}{12}\triangle_h)\nabla\cdot(\boldsymbol{u}\omega) - Ri(1 + \frac{h^2}{12}\triangle_h)\partial_x\theta = \nu\Big(\triangle_h + \frac{h^2}{6}D_x^2D_y^2\Big)\omega\,.$$

and multiplying the same operator to the kinematic equation leads to

$$\Big(\triangle_h + \frac{h^2}{6}D_x^2D_y^2\Big)\psi = (1 + \frac{h^2}{12}\triangle_h)\omega\,. \tag{6.2.20}$$

As in [ELV2], the corresponding nonlinear convection term in the vorticity dynamic equation can be estimated as

$$\begin{aligned}(1 + \frac{h^2}{12}\triangle_h)(\boldsymbol{u}\cdot\nabla\omega) = \;& \widetilde{D}_x\Big(1 + \frac{h^2}{6}D_y^2\Big)(u\omega) + \widetilde{D}_y\Big(1 + \frac{h^2}{6}D_x^2\Big)(v\omega)\\ -\;& \frac{h^2}{12}\triangle_h\Big(u\widetilde{D}_x\omega + v\widetilde{D}_y\omega\Big) + O(h^4)\,.\end{aligned} \tag{6.2.21}$$

The first and the second terms in (6.2.21) are compact. The third term is not compact, yet it does not cause any trouble in practical computations since $u^n\widetilde{D}_x\omega^n + v^n\widetilde{D}_y\omega^n$ can be taken as 0 on the boundary. The case of boundary condition with slip can be treated similarly, as discussed in [ELV2]. The gravity term $(1 + \frac{h^2}{12}\triangle_h)\partial_x\theta$ can be dealt with in a similar fashion. The formal Taylor expansion gives

$$\begin{aligned}(1 + \frac{h^2}{12}\triangle)\partial_x = \;& \widetilde{D}_x(1 + \frac{h^2}{12}D_y^2 - \frac{h^2}{12}D_x^2) + O(h^4)\\ =\;& \widetilde{D}_x + \frac{h^2}{12}\widetilde{D}_xD_y^2 - \frac{h^2}{12}\widetilde{D}_xD_x^2 + O(h^4)\,.\end{aligned} \tag{6.2.22}$$

where the first and the second terms can be updated easily, yet the third term has to be implemented by "ghost points" value of θ, which was discussed in the last subsection. Finally, by the introduction of an intermediate variable ϖ

$$\varpi = (1 + \frac{h^2}{12}\triangle_h)\omega\,, \tag{6.2.23}$$

Reproduced with permission of the copyright owner. Further reproduction prohibited without permission.

and combining the discussions in (6.2.19)-(6.2.22), the whole momentum equation can be approximated by

(6.2.24)

$$\partial_t\overline{\omega} + \widetilde{D}_x\Big(1 + \frac{h^2}{6}D_y^2\Big)(u\omega) + \widetilde{D}_y\Big(1 + \frac{h^2}{6}D_x^2\Big)(v\omega)$$
$$-\frac{h^2}{12}\triangle_h(u\widetilde{D}_x\omega + v\widetilde{D}_y\omega) - Ri\widetilde{D}_x\Big(1 + \frac{h^2}{12}(D_y^2 - D_x^2)\Big)\theta = \nu\Big(\triangle_h + \frac{h^2}{6}D_x^2D_y^2\Big)\omega .$$

The stream function can be solved by (6.2.20) with the boundary condition $\psi\,|_\Gamma = 0$. The velocity $\boldsymbol{u} = \nabla^\perp\psi = (-\partial_y\psi, \partial_x\psi)$ can be obtained by (6.2.1), the long-stencil approximation to ∂_x, ∂_y

$$u = -\widetilde{D}_y(1 - \frac{h^2}{6}D_y^2)\psi , \quad v = \widetilde{D}_x(1 - \frac{h^2}{6}D_x^2)\psi . \tag{6.2.25}$$

The vorticity is determined by $\overline{\omega}$ via (6.2.23). The implementation of (6.2.23) needs the boundary condition for ω, which is discussed in the next subsection.

6.2.4 Fourth Order Boundary Condition for the Vorticity

We only see the boundary Γ_x where $j = 0$ here. As already discussed in Chapter 3, the main point of the boundary vorticity is to use the boundary condition $\psi\,|_\Gamma = 0$, $\frac{\partial\psi}{\partial\boldsymbol{n}} = 0$, and convert it into $\omega\,|_\Gamma$ by the kinematic relation $\triangle\psi = \omega$. We can either use Briley's formula

$$\omega_{i,0} = \frac{1}{18h^2}(108\psi_{i,1} - 27\psi_{i,2} + 4\psi_{i,3}) . \tag{6.2.26}$$

along with the one-sided Taylor expansions of the stream function

$$\psi_{i,-1} = 6\psi_{i,1} - 2\psi_{i,2} + \frac{1}{3}\psi_{i,3} - 4h\left(\frac{\partial\psi}{\partial y}\right)_{i,0} . \tag{6.2.27}$$

$$\psi_{i,-2} = 40\psi_{i,1} - 15\psi_{i,2} + \frac{8}{3}\psi_{i,3} - 12h\left(\frac{\partial\psi}{\partial y}\right)_{i,0} . \tag{6.2.28}$$

Or, we can use a new 4-th order formula for the vorticity, which was proposed in Chapter 3

$$\omega_{i,0} = \frac{1}{h^2}(8\psi_{i,1} - 3\psi_{i,2} + \frac{8}{9}\psi_{i,3} - \frac{1}{8}\psi_{i,4}) . \tag{6.2.29}$$

Reproduced with permission of the copyright owner. Further reproduction prohibited without permission.

along with the estimate of the stream function at "ghost points"

$$\psi_{i,-1} = 10\psi_{i,1} - 5\psi_{i,2} + \frac{5}{3}\psi_{i,3} - \frac{1}{4}\psi_{i,4} - 5h\left(\frac{\partial \psi}{\partial y}\right)_{i,0} + O(h^6)\,. \tag{6.2.30}$$

and

$$\psi_{i,-2} = 80\psi_{i,1} - 45\psi_{i,2} + 16\psi_{i,3} - \frac{5}{2}\psi_{i,4} - 30h\left(\frac{\partial \psi}{\partial y}\right)_{i,0} + O\left(h^6\right)\,. \tag{6.2.31}$$

As pointed out in Chapter 4, both formulae give us fourth order accuracy for the 2-D Navier-Stokes equations. For computational convenience, we suggest using Briley's formula along with (6.2.27), (6.2.28) in the calculation.

Remark 6.2.3 This one-sided vorticity boundary condition was proven to be stable and be consistent with the centered difference applied at interior points. The whole scheme, including the one-sided approximations of the temperature near the boundary and the vorticity boundary condition, has been shown to have full 4-th order accuracy.

6.2.5 Time Discretization

As discussed in [ELV1], [ELV2], the convection, diffusion terms and the gravity term appearing in the Boussinesq equations, together with the 4-th order spatial discretizations discussed above, can be updated explicitly. Such explicit treatment does not result in any problem caused by the cell-Reynolds number constraint if the Runge-Kutta method is applied. For simplicity we only present the forward Euler time-discretization. The extension to multi-step or Runge-Kutta methods is straightforward.

Initialization: Given $\{\omega_{ij}^0\}$, compute

$$\left(1 + \frac{h^2}{12}\triangle_h\right)\omega^0 = \overline{\omega}^0\,. \tag{6.2.32}$$

Time-stepping: Given the vorticity ω^n and the temperature θ^n at time t^n, we compute all the profiles at the time step t^{n+1} via the following steps.

Reproduced with permission of the copyright owner. Further reproduction prohibited without permission.

Step 1. Update $\left\{\varpi_{i,j}^{n+1}\right\}$, at interior points (x_i, y_j), for $1 \le i, j \le N-1$ using

(6.2.33)
$$\frac{\varpi^{n+1}-\varpi^n}{\triangle t} + \widetilde{D}_x\Big(1+\frac{h^2}{6}D_y^2\Big)(u^n\omega^n) + \widetilde{D}_y\Big(1+\frac{h^2}{6}D_x^2\Big)(v^n\omega^n)$$
$$-\frac{h^2}{12}\triangle_h(u^n\widetilde{D}_x\omega^n + v^n\widetilde{D}_y\omega^n) - Ri\widetilde{D}_x\Big(1+\frac{h^2}{12}(D_y^2-D_x^2)\Big)\theta^n = \nu\Big(\triangle_h + \frac{h^2}{6}D_x^2D_y^2\Big)\omega^n .$$

Step 2. Obtain $\theta_{i,j}^{n+1}$ using

(6.2.34)
$$\frac{\theta^{n+1}-\theta^n}{\triangle t} + u^n\widetilde{D}_x(1-\frac{h^2}{6}D_x^2)\theta^n + v^n\widetilde{D}_y(1-\frac{h^2}{6}D_y^2)\theta^n = \kappa\Big(\triangle_h - \frac{h^2}{12}(D_x^4+D_y^4)\Big)\theta^n .$$

If the Dirichlet boundary condition is imposed for the temperature, (6.2.34) is updated at interior points (x_i, y_j), $1 \le i, j \le N-1$, and the boundary value of θ^{n+1} is given by (6.1.4); if the Neumann boundary condition is imposed for the temperature, (6.2.34) is updated at all computational points (x_i, y_j), $0 \le i, j \le N$.

Step 3. Solve for $\left\{\psi_{i,j}^{n+1}\right\}_{1\le i,j\le N-1}$ using

(6.2.35)
$$\begin{cases} \Big(\triangle_h + \dfrac{h^2}{6}D_x^2D_y^2\Big)\psi^{n+1} = \varpi^{n+1} , \\ \psi^{n+1}\,|_\Gamma = 0 , \end{cases}$$

where only Sine transformations are needed. Compute ψ^{n+1} at the "ghost points" using (6.2.27), (6.2.28) (together with Briley's vorticity boundary condition (6.2.26)), or using (6.2.30), (6.2.31) (together with the new vorticity boundary condition (6.2.29)). We note that solving (6.2.35) only requires ϖ^{n+1} at interior points (x_i, y_j), $1 \le i, j \le N-1$, which has been updated in Step 1.

Step 4. If the Dirichlet boundary condition is imposed for the temperature, calculate "ghost point" value $\theta_{i,-1}$ by the formula (6.2.7) or (6.2.9); if the Neumann boundary condition is imposed for the temperature, use (6.2.14), (6.2.15) to calculate θ at "ghost points".

Step 5. Since ψ^{n+1} (including the "ghost point" value) has been computed

Reproduced with permission of the copyright owner. Further reproduction prohibited without permission.

in Step 3. now we are able to obtain the boundary value for ω^{n+1} by Briley's formula (6.2.26) or the new fourth order formula (6.2.29).

Step 6. Now we use the boundary values for ω^{n+1} updated in Step 5. to solve for $\left\{\omega_{i,j}^{n+1}\right\}_{i\geq 1, j\geq 1}$ using

$$\left(1+\frac{h^2}{12}\Delta_h\right)\omega^{n+1}=\varpi^{n+1}. \tag{6.2.35}$$

Step 7. Update the velocity $u_{i,j}^{n+1}$, $v_{i,j}^{n+1}$ using the 4-th order difference scheme

$$u^{n+1}=-\widetilde{D}_y(1-\frac{h^2}{6}D_y^2)\psi^{n+1}, \qquad v^{n+1}=\widetilde{D}_x(1-\frac{h^2}{6}D_x^2)\psi^{n+1}, \tag{6.2.36}$$

for $i, j \geq 1$, and $u^{n+1}\mid_\Gamma = 0$, $v^{n+1}\mid_\Gamma = 0$.

Remark 6.2.4 In the above time-stepping procedure, the most computations involved are the solvers for the two Poisson-like equations appearing in Step 3 and Step 5, respectively. Our numerical experiment shows that over 90 percent of the CPU is spent in the two Poisson solvers. That makes the method extremely efficient.

6.3 Accuracy Check Using the Lorenz System

We consider a well-known model dealing with Rayleigh-Bénard convection, which was proposed by Lorenz(1963). He expanded the equations describing two-dimensional nonlinear convection on a uniformly heated plane with free-free boundaries in double Fourier series. The resulting system of equations was then truncated radically, so that only three ODEs remained. These are the so-called

Reproduced with permission of the copyright owner. Further reproduction prohibited without permission.

Lorenz system

$$\begin{cases} \dfrac{dX}{dT} = -\sigma X + \sigma Y \,, \\ \dfrac{dY}{dT} = rX - Y - ZX \,, \\ \dfrac{dZ}{dT} = -bZ + XY \,. \end{cases} \tag{6.3.1}$$

in which X is proportional to the amplitude of the convection motions, Y is proportional to the temperature difference between the ascending and descending motions, i.e. the horizontal temperature difference across a roll, and Z is proportional to the deviation of the vertical temperature profile from the linear profile; σ stands for Prandtl number, $r = \dfrac{Ra}{R_c}$, the ratio of the Rayleigh number to the critical Rayleigh number, b is a parameter related to the wavenumber as can be shown later.

Now we fit the Lorenz system to the Boussinesq equations. A single-mode stream function can be chosen as

$$\psi_e(\boldsymbol{x}, t) = P(t)\sin(kx)\sin(y) \,. \tag{6.3.2}$$

and the temperature can be chosen as

$$\theta_e(\boldsymbol{x}, t) = A(t)\cos(kx)\sin(y) + B(t)\sin(2y) + (\pi - y) \,. \tag{6.3.3}$$

where k is the wavenumber. It shall be noted that two different modes were used in the temperature profile. The interaction between these two modes reveal a rich nonlinear dynamics phenomenon. The term $\pi - y$ in the temperature stands for the linear profile. Accordingly, the corresponding velocity $\boldsymbol{u}_e = (-\partial_y \psi_e, \partial_x \psi_e)$ and the vorticity $\omega_e = \triangle \psi_e$ are computed to be

$$\begin{aligned} &u_e(\boldsymbol{x}, t) = -P(t)\sin(kx)\cos(y) \,, \quad v_e(\boldsymbol{x}, t) = k\,P(t)\cos(kx)\sin(y) \,. \\ &\omega_e(\boldsymbol{x}, t) = \lambda_k P(t)\sin(kx)\sin(y) \,. \end{aligned} \tag{6.3.4}$$

Reproduced with permission of the copyright owner. Further reproduction prohibited without permission.

where $\lambda_k = -(k^2+1)$. Plugging (6.3.2)-(6.3.4) into the momentum equation,

$$\partial_t \omega_e + (\boldsymbol{u}_e \cdot \nabla)\omega_e - Ri\partial_x \theta_e = \nu \triangle \omega_e . \tag{6.3.5}$$

we obtain the following nonlinear ODE

$$\frac{dP}{dt} = \nu\lambda_k P - Ri\frac{k}{\lambda_k}A . \tag{6.3.6}$$

However, these profiles do not satisfy the temperature transport equation exactly. In the original derivation of the Lorenz equation, the high order production term was truncated, which leads to the Lorenz system (6.3.1). This can be reformulated by adding a force term, which represents the truncated term, to the heat transport equation, so that the profiles satisfy

$$\partial_t \theta_e + \boldsymbol{u}_e \cdot \nabla \theta_e = \kappa \triangle \theta_e + \boldsymbol{f} . \tag{6.3.7}$$

where

$$\boldsymbol{f} = 2PB\cos(kx)\sin(y)\big(\cos(2y) - 1\big) . \tag{6.3.8}$$

(6.3.7) and (6.3.8) result in the following ODEs

$$\begin{cases} \dfrac{dA}{dt} = kP + \kappa\lambda_k A - 2kBP . \\ \dfrac{dB}{dt} = -4\kappa B - \dfrac{k}{2}PA . \end{cases} \tag{6.3.9}$$

We can see that (6.3.6), (6.3.9) form a closed system of ODEs for the parameters $P(t)$, $A(t)$, $B(t)$. The equivalence between them and the parameters X, Y, Z appearing in the Lorenz system (6.3.1) can be derived by the following scaling transformations: denoting $X = \alpha P$, $Y = \beta A$, $Z = \gamma B$, $t = -\frac{\tau}{\kappa\lambda_k}$ and substituting into (6.3.1), we get

$$\sigma = \frac{\nu}{\kappa} , \quad r = -\frac{Ri \cdot k^2}{\nu\kappa\lambda_k^3} , \quad b = -\frac{4}{\lambda_k} . \tag{6.3.10}$$

Reproduced with permission of the copyright owner. Further reproduction prohibited without permission.

and

$$\alpha = \frac{k}{\kappa\lambda_k}, \quad \beta = \frac{Ri\cdot k^2}{\nu\kappa\lambda_k^3}, \quad \gamma = -\frac{2Rik^2}{\nu\kappa\lambda_k^3}. \tag{6.3.11}$$

from which it can be seen that σ is the Prandtl number. b is one parameter related to the wavenumber. r is the ratio of the Rayleigh number to the critical Rayleigh number.

6.3.1 Accuracy Check

We use our fourth order method proposed in §2 to solve the Boussinesq flow with force term (6.3.5), (6.3.7), (6.3.8). The initial data is taken as the profiles (6.3.2)-(6.3.4) when $t = 0$, and $A(0)$, $B(0)$, $C(0)$ are chosen to be 1. The vorticity boundary condition is taken to be the new 4-th order formula (6.2.29). The application of Briley's formula (6.2.26) leads to a similar accuracy result. Both the Dirichlet and Neumann boundary condition for the temperature can be imposed in this example. In the case of the Dirichlet boundary condition, the 5-th order formula (6.2.7) is used as our extrapolation for the temperature near the boundary, while the 4-th order formula (6.2.9) leads to almost the same result in our computation. In the case of the Neumann boundary condition, (6.2.14), (6.2.15) is used as our extrapolation for the temperature near the boundary, while the force term has to be added and the slip velocity on the boundary, which can be seen from (6.3.4), will be taken into consideration when we derive $\partial_y^3\theta$ on Γ_x.

We choose the wave number $k = 1$. The final time is taken to be $t = 2.0$. The other physical parameters are chosen as: $Ri = 1$, $\nu = \kappa = 0.001$. Accordingly, $r = 1.25 \times 10^5$, $\sigma = 1$ and $b = 2$. The computational domain is chosen as $[0, \pi]^2$ with uniform spatial grids $\Delta x = \Delta y = h$, and the time step $\Delta t = \frac{1}{2}\Delta x$.

The exact solutions of stream function and temperature are given by (6.3.2), (6.3.3), where the coefficients $P(t)$, $A(t)$ and $B(t)$ are computed by the 4-th order Runge-Kutta method applied to the system (6.3.6), (6.3.9).

Reproduced with permission of the copyright owner. Further reproduction prohibited without permission.

32^2, 64^2, 128^2, 256^2. The absolute errors of stream function, vorticity and temperature are listed in Table 6.1 and Table 6.2, with Dirichlet and Neumann boundary conditions for the temperature imposed, respectively. We can see in the tables that the temperature and the stream function achieve exactly fourth order accuracy. The vorticity achieves almost fourth order accuracy in L^1, L^2 norms and a little less than fourth order accuracy in L^∞ norms.

Reproduced with permission of the copyright owner. Further reproduction prohibited without permission.

6.4 Computation of Marsigli Flow

To illustrate the performance of the fourth order method, we compute an example of Marsigli flow which has been known since the 17th century. This example can be found in the work of Marsigli (1681). The detailed story is described in Gill's book "Atmosphere-Ocean Dynamics" [GILL] as follow.

> It seems that when Marsigli went to Constantinople in 1679 he was told about a well-known undercurrent in the Bosphorous: "... for the fisherman of the towns on the Bosphorous say that the whole stream does not flow in the direction of Byzantium, but while the upper current which we can see plainly does flow in this direction, the deep water of the abyss, as it is called, moves in a direction exactly opposite to that of the upper current and so flows continuously against the current which is seen". That is, the undercurrent water flows toward the Black Sea from the Mediterranean. Marsigli reasoned that the effect was due to density differences: water from the Black Sea is lighter than water from the Mediterranean. The lower density of the Black Sea can be attributed to lower salinity resulting from river runoff. He then performed a laboratory experiment: A container is initially divided in two by a partition. The left side contained water taken from the undercurrent in the Bosphorous, while the right side contained dyed water having the density of surface water in the Black Sea. The experiment was to put two holes in the partition to observe the resulting flow. The flow through the lower hole was in the direction of the undercurrent in the Bosphorous, while the flow through the upper hole was in the direction of the surface flow.

Reproduced with permission of the copyright owner. Further reproduction prohibited without permission.

We simulated the above physical process in a simple setup: Boussinesq flow with two initially piecewise constant temperatures in an insulated box $\Omega = [0, 8] \times [0, 1]$. The partition was located at $x = 4$. The temperature was chosen to be 1.5 at the left half, which indicated the lower density, 1 at the right half, which indicated the higher density. (By Boussinesq assumption, the density difference can be converted into temperature difference with the reverse ratio). The whole flow was at rest at $t = 0$. A no-slip boundary condition was imposed for the velocity and adiabatic boundary condition was imposed for the temperature. The computational method was based on the fourth order scheme discussed above coupled with 4-th order Runge-Kutta time stepping, as described in **2.5**. Briley's formula (6.2.26) was used as the boundary condition for the vorticity. The adiabatic boundary condition imposed for the temperature indicated the use of (6.2.16), (6.2.17) to evaluate the temperature at "ghost point". In our computation, the Reynolds number was chosen to be $Re = 5000$, the Prandtl number was chosen to be 1, and the Richardson number Ri, which corresponds to the gravity effect, was chosen to be 4. We repeated the computations using two resolutions: 2048×256, 4096×512.

The computation results on the resolution of 2048×256 of temperature and vorticity at a sequence of times: $t_1 = 2$, $t_2 = 4$, $t_3 = 6$, $t_4 = 8$ are shown in Fig. 6.1, Fig. 6.2, respectively. To save the space, we only plot the vorticity on the left-half domain $[0, 4] \times [0, 1]$. The vorticity on the right-half domain $[4, 8] \times [0, 1]$ is axis-symmetric to that of the left-half domain. Like Riemann shock-tube problem, once the partition was removed, the flow was driven by the gravity force. The results indicated clearly the appearance of an upper current flow, which moved from the left side to the right side, and an undercurrent flow, which moved in the opposite direction. It coincided with the phenomenon observed by Marsigli. Consequently, a sharp interface was formed between the

Reproduced with permission of the copyright owner. Further reproduction prohibited without permission.

two currents. In other words, two currents with different moving directions were separated by an interface. Strong shear flow and vortex sheet came into being along the interface. This vortex sheet exhibited the Kelvin-Helmholtz instability. As a result, at $t_1 = 2$, two symmetric vortices and the rolling up structures were formed. As the time goes on, more and more rolling-up structures were generated and swelled. To see the details, we plot the temperature and vorticity in a zooming region of $[2.5, 3.5] \times [0, 1]$ at $t_3 = 6$, on the resolution of 4096×512, in Fig. 6.3 and Fig. 6.4, respectively.

The numerical simulation for this type of Kelvin-Helmholtz instability is quite challenging. To verify the accuracy of our method, we compare the temperature and the vorticity at time $t = 6$ on a $y = \frac{1}{2}$ cut between two resolutions: 2048×256, 4096×512 in Fig. 6.5 and Fig. 6.6, respectively. It is evident that even though there are so many rolling up structures and sharp transitional areas for temperature and vorticity profiles, the results using two resolutions match perfectly well.

Reproduced with permission of the copyright owner. Further reproduction prohibited without permission.

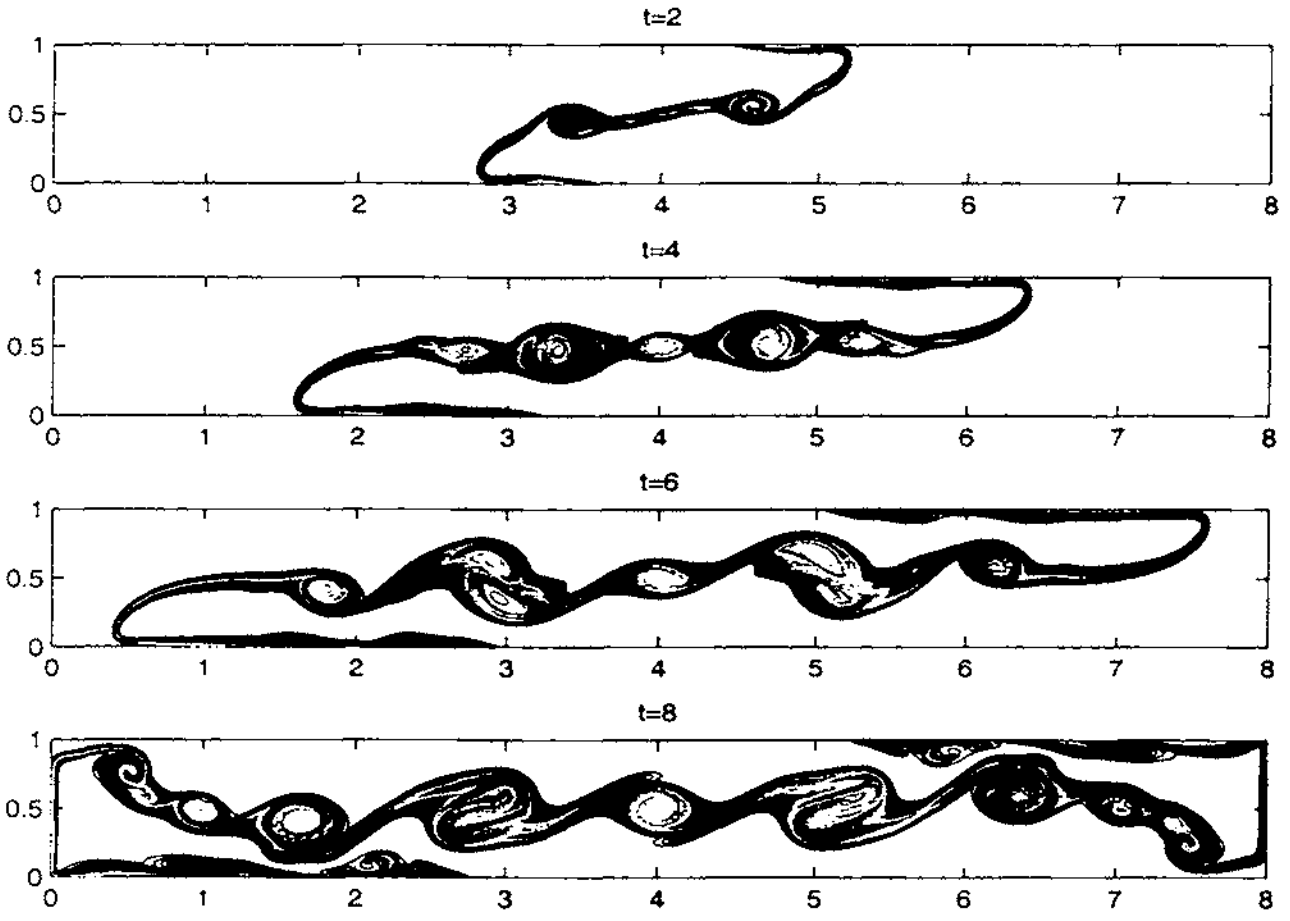

Figure 6.1: Temperature plots at a sequence of times at $t_1 = 2$, $t_2 = 4$, $t_3 = 6$, $t_4 = 8$, of the interaction between two flow with different densities $\frac{3}{2} : 1$ in an insulated box $\Omega = [0, 8] \times [0, 1]$. Initially, the two flows are partitioned at $x = 4$. Other physical parameters: $Re = 5000$, $Pr = 1$, $Ri = 4$. The computation is based on the fourth order method with 2048×256 resolution.

Reproduced with permission of the copyright owner. Further reproduction prohibited without permission.

Table 6.1: Errors and orders of accuracy for Boussinesq equation at $t = 2$ when the fourth order method is used and the Dirichlet boundary condition for the temperature is imposed. CFL=$\frac{1}{2}$, where CFL= $\frac{\triangle t}{\triangle x}$.

	N	L^∞ error	L^∞ order	L^1 error	L^1 order	L^2 error	L^2 order
θ	32	1.25e-04		4.82e-04		2.00e-04	
	64	7.85e-06	3.99	3.11e-05	3.96	1.27e-05	3.98
	128	4.89e-07	4.00	1.96e-06	3.99	7.95e-07	4.00
	256	3.07e-08	4.00	1.23e-07	4.00	4.99e-08	4.00
v	32	4.97e-05		1.46e-04		6.50e-05	
	64	3.21e-06	3.95	9.45e-06	3.95	4.21e-06	3.95
	128	2.01e-07	4.00	5.94e-07	3.99	2.64e-07	4.00
	256	1.27e-08	3.99	3.74e-08	3.99	1.66e-08	3.99
ω	32	6.38e-04		8.50e-04		3.93e-04	
	64	4.46e-05	3.84	4.88e-05	4.12	2.33e-05	4.07
	128	4.31e-06	3.37	3.07e-06	3.99	1.57e-06	3.90
	256	4.69e-07	3.20	2.07e-07	3.89	1.15e-07	3.77

Table 6.2: Errors and orders of accuracy for Boussinesq equation at $t = 2$ when the fourth order method is used and the Neumann boundary condition for the temperature is imposed. CFL=$\frac{1}{2}$, where CFL= $\frac{\triangle t}{\triangle x}$.

	N	L^∞ error	L^∞ order	L^1 error	L^1 order	L^2 error	L^2 order
θ	32	1.23e-04		4.92e-04		2.01e-04	
	64	7.78e-06	3.98	3.16e-05	3.96	1.28e-05	3.97
	128	4.86e-07	4.00	1.99e-06	3.99	8.01e-07	4.00
	256	3.05e-08	4.00	1.25e-07	3.99	5.03e-08	3.99
v	32	5.04e-05		1.49e-04		6.63e-05	
	64	3.23e-06	3.96	9.57e-06	3.96	4.26e-06	3.96
	128	2.02e-07	4.00	6.00e-07	4.00	2.67e-07	4.00
	256	1.27e-08	3.99	3.78e-08	3.99	1.68e-08	3.99
ω	32	4.01e-04		6.69e-04		2.79e-04	
	64	3.44e-05	3.54	4.07e-05	4.04	1.72e-05	4.02
	128	3.55e-06	3.28	2.69e-06	3.92	1.27e-06	3.76
	256	2.85e-07	3.64	1.83e-07	3.88	9.33e-08	3.77

Reproduced with permission of the copyright owner. Further reproduction prohibited without permission.

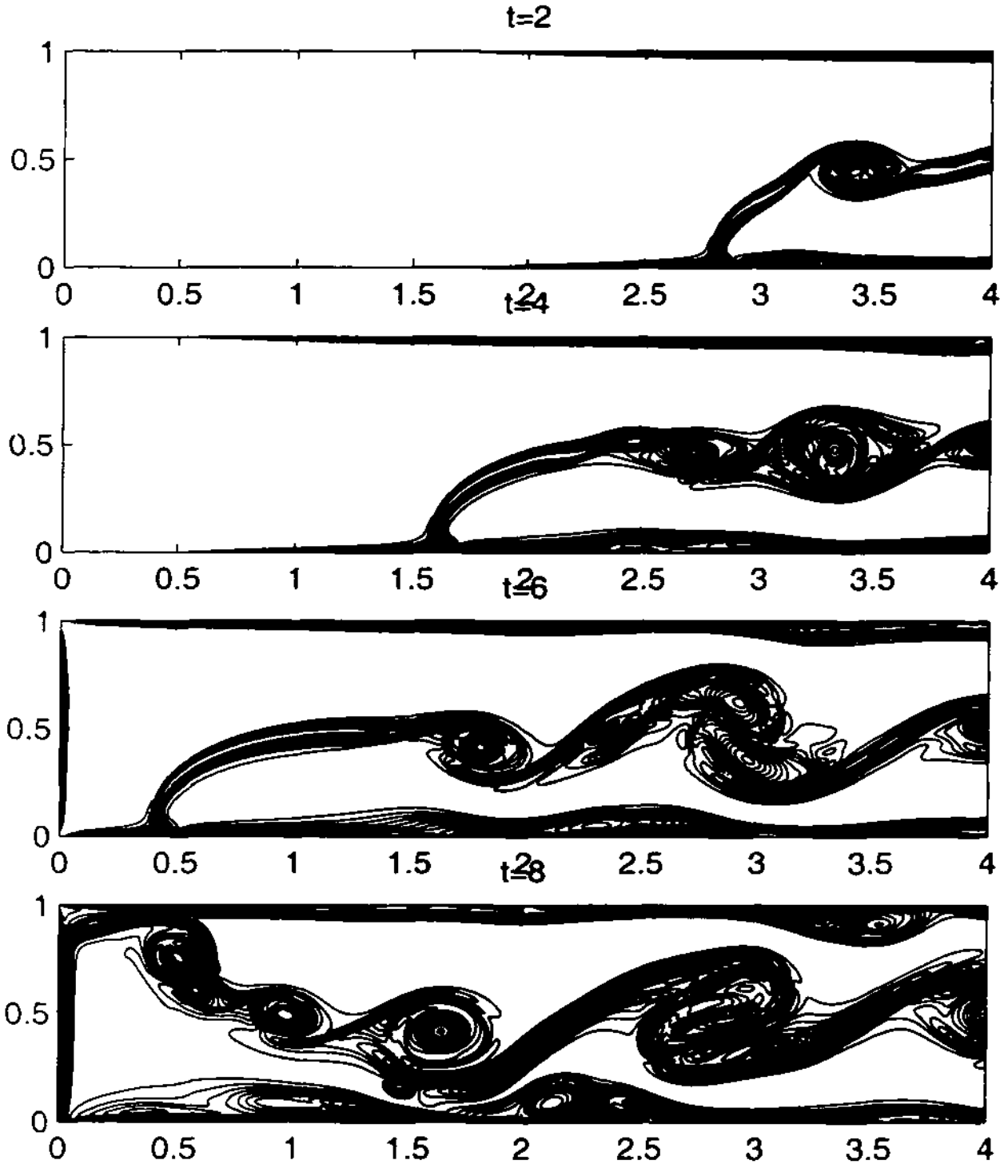

Figure 6.2: Vorticity plots on the left half domain $[0,4] \times [0,1]$, at the same sequence of times with the same physical parameters in Fig. 5.1 and the same resolution. 40 equally spaced contours from -21 to 31. We omit the vorticity plots on the right half domain $[4,8] \times [0,1]$, which is axis-symmetric to the left half domain.

Reproduced with permission of the copyright owner. Further reproduction prohibited without permission.

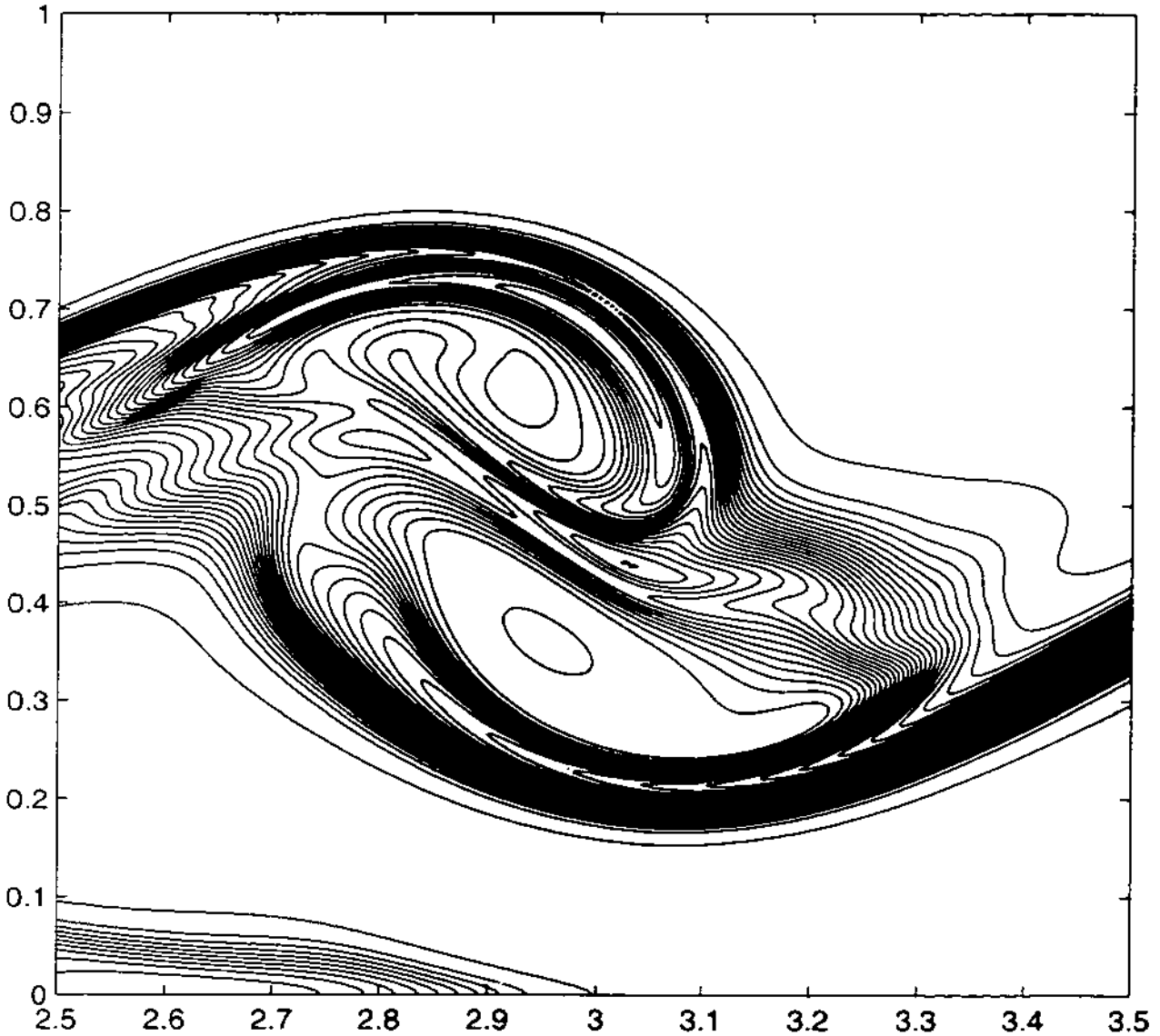

Figure 6.3: Zooming plot of temperature at $t = 6$ in $[2.5, 3.5] \times [0, 1]$. 40 equally spaced contours from 1.001 to 1.499.

Reproduced with permission of the copyright owner. Further reproduction prohibited without permission.

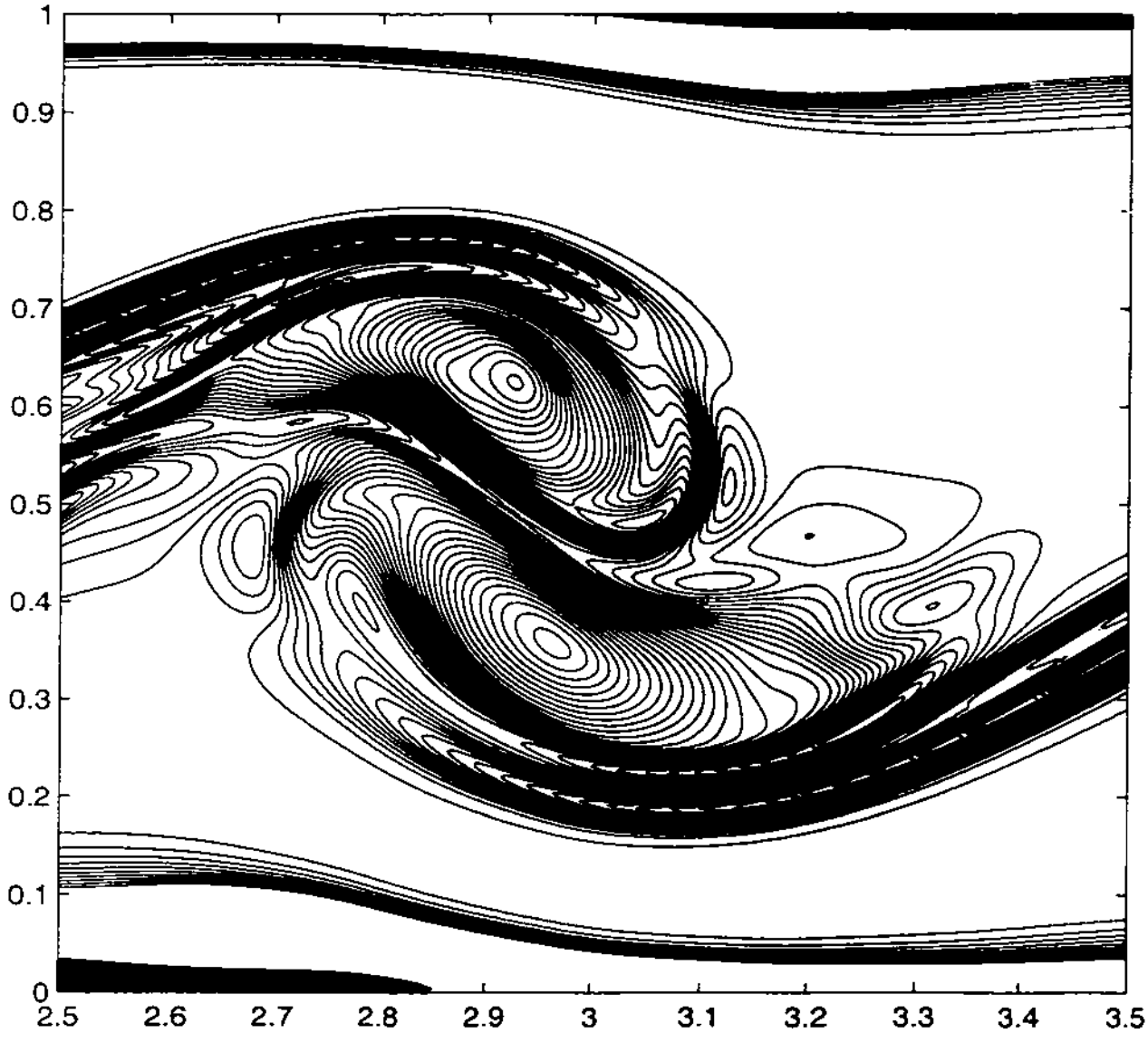

Figure 6.4: Zooming plot of vorticity at $t = 6$ in $[2.5, 3.5] \times [0, 1]$. 40 equally spaced contours from -16.6 to 5.4.

Reproduced with permission of the copyright owner. Further reproduction prohibited without permission.

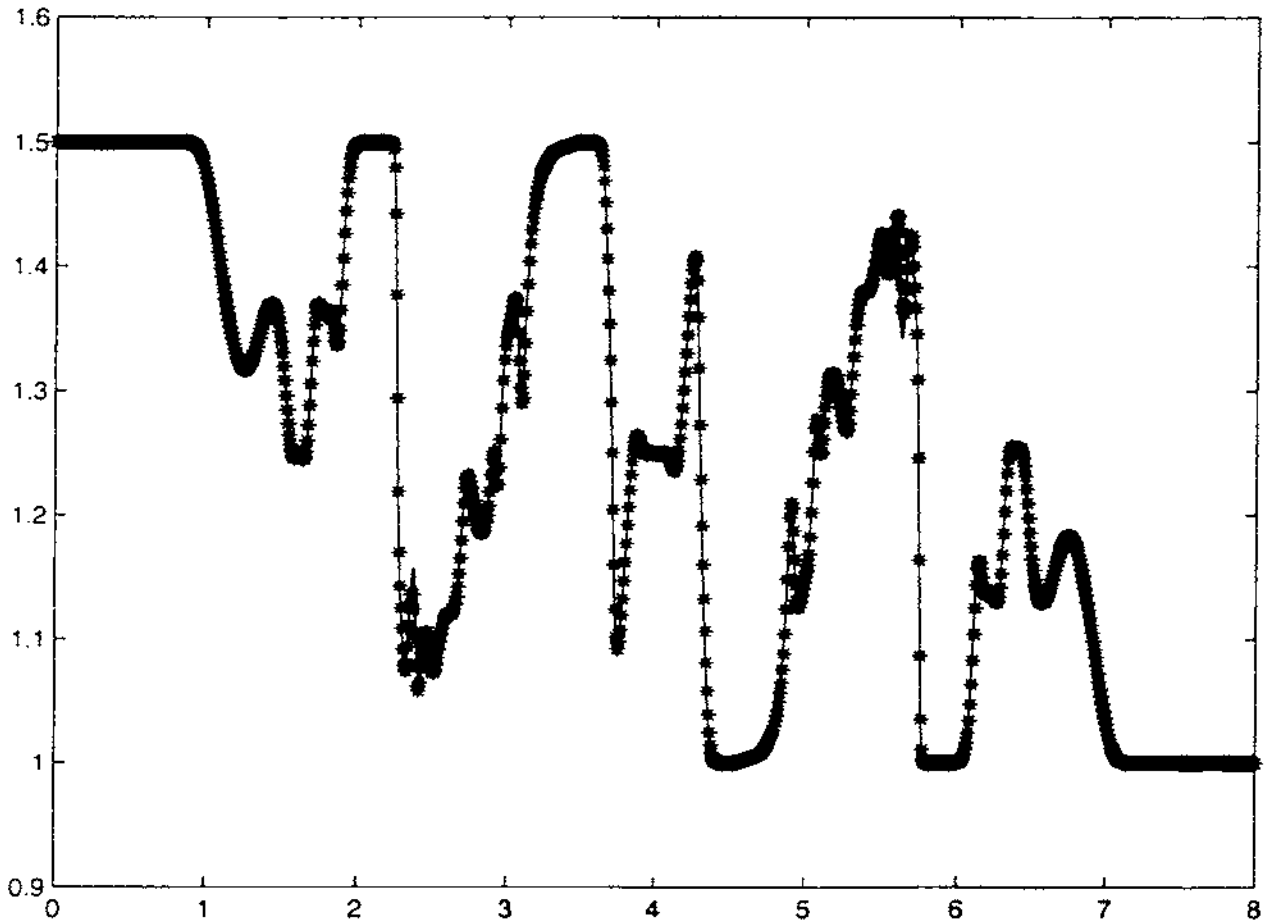

Figure 6.5: Comparison of temperature profile at $y = \frac{1}{2}$ cut, $t = 6$ between two resolutions: the solid line represents the result computed by the resolution 4096×512, while the star line represents that of 2048×256. To make the plot clearly, we only plot the even points in the start line. In other words, the graph of the star line only shows 1025 points.

Reproduced with permission of the copyright owner. Further reproduction prohibited without permission.

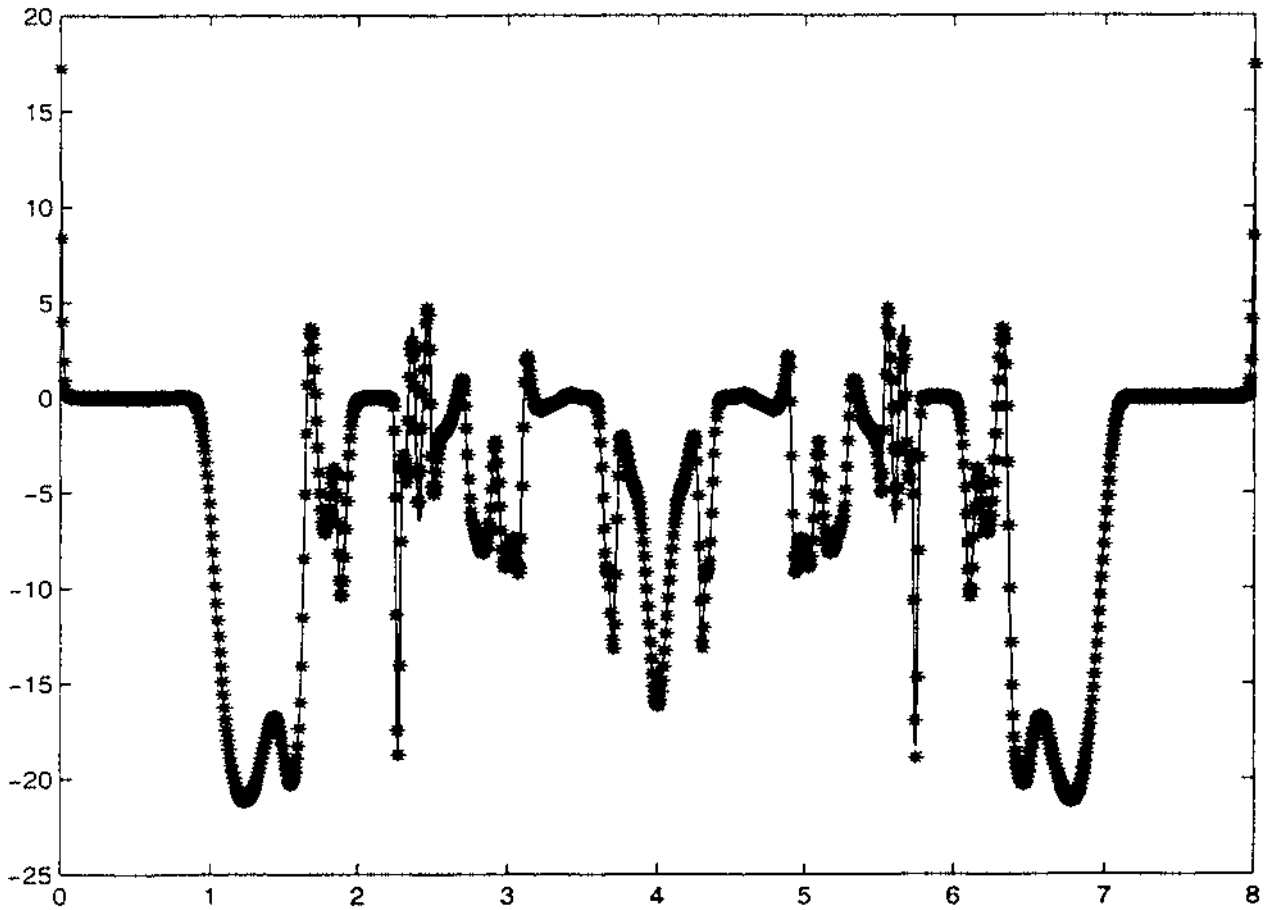

Figure 6.6: The comparison between the two resolutions for the vorticity with the same horizontal line and time.

Reproduced with permission of the copyright owner. Further reproduction prohibited without permission.

REFERENCES CITED

[ABS] Almgren, A.S., Bell, J.B., Szymczak, W.G., 1996, *A Numerical Method for the Incompressible Navier-Stokes Equations Based on an Approximate projection*, SIAM J. Sci. Comput. **17**, 358–369.

[AR] Anderson, C.R., M.B. Reider, M.B., 1996, *A High Order Explicit Method for the Computation of Flow about a Circular Cylinder*, J. Comput. Phys. **125**, 207-224.

[BC] Buttke, T., Chorin, A.J., 1993, *Turbulence calculation using magnetization variables* , J. Appl. Numer. Math. **12**, 47–54.

[BCG] Bell, J.B., Colella, P., and Glaz, H.M., 1989, *A Second Order Projection Method for the Incompressible Navier-Stokes Iquations*, J. Comput. Phys. **85**, 257–283.

[BM] Bell, J.B., Marcus, D.L., 1992, *A Second-Order Projection Method for Variable-Density Flows* , J. Comput. Phy., **101**, 334-348.

[BRL] Briley, W.R., 1971, *A Numerical Study of Laminar Separation Bubbles uUing the Navier-Stokes Equations*, J. Fluid Mech. **47**, 713–736.

[BT] Buttke, T., 1993, *Velocity Methods: Lagrangian Numerical Methods Which Preserve the Hamiltonian Structure of Incompressible Fluid flow* , Vortex Flows and Related Numerical Methods, J. T. Beale, G. H. Cottet and S. Huberson ed.

[C] Chorin, A.J., 1968, *Numerical Solution of Navier-Stokes Equations*, Math. Comp. **22**, 745–762.

[DH] Dennis, S.C.R., Hudson, J.D., 1989, *Compact h^4 Finite-Difference Approximations to Operators of Navier-Stokes Type*, J. Comput. Phys., **85**, 390–416.

[ELG1] E, Weinan, Liu, J.-G., 1996, *Gauge Method for Viscous Incompressible Flows*, submitted to J. Comp. Phys.

[ELG2] E, Weinan, Liu, J.-G., 1997, *Gauge Finite Element Method For Incompressible Flows*, submitted to Int. J. Num. Meth. Fluids.

Reproduced with permission of the copyright owner. Further reproduction prohibited without permission.

[ELG3] E. Weinan, Liu. J.-G.. 1997. *Finite Difference Schemes for Incompressible Flows in the Impulse-Velocity Formulation* . J. Comput. Phys. **130**. 67–76.

[ELP1] E. Weinan, Liu, J.-G.. 1995. *Projection Method I: Convergence and Numerical Boundary Layers*. SIAM J. Numer. Anal. **32**. 1017–1057.

[ELP3] E. Weinan, Liu, J.-G.. 1995. *Projection Method III: Spatial Discretizations On the Staggered Grid*. to appear Math. Comp.

[ELV1] E. Weinan, Liu, J.-G., 1996. *Vorticity Boundary Condition for Finite Difference Schemes*. J. Comput. Phys.. **124**. 368–382.

[ELV2] E. Weinan, Liu, J.-G., 1996. *Essentially Compact Schemes for Unsteady Viscous Incompressible Flows*. J. Comput. Phys.. **126**. 122-138.

[ELV3] E. Weinan, Liu, J.-G., 1997. *Finite Difference Methods for 3D Viscous Incompressible Flows in the Vorticity-Vector Potential Formulation on non-staggered grids*. J. Comput. Phys. **138**. 57-82.

[ES] E. Weinan. Shu, Chi-Wang. 1994. *Small-Scale Structures in Boussinesq Convection* , Phys. Fluids **6** (1). 49-54.

[GILL] Gill. Adrian E., *Atmosphere-Ocean Dynamics*. Academic Press.

[GMD] Gunzburger, M.D.. 1989. *Finite Element Methods for Viscous Incompressible Flows: A Guide to Theory. Practice. and Algorithms*, Boston: Academic Press. Inc.

[GPM] Gresho. P.M., 1991, *Incompressible Fluid Dynamics: Some Fundamental Formulation Issues*. Annu. Rev. Fluid Mech. **23**. 413–453.

[GS] Gresho. P.M., Sani R.L.. 1987, *On Pressure Boundary Conditions for the Incompressible Navier-Stokes Equations*. Int. J. Numer. Methods Fluids **7**. 1111–1145.

[HKR] Henshaw, W.D., Kreiss, H.O., Reyna. L.G.M.. 1994. *A Fourth-Order Accurate Difference Approximation for the Incompressible Navier-Stokes Equations*, Comput. and Fluids **23**. 575-593.

[HW] Hou. Y.T., Wetton, B.R.. 1992. *Convergence of a Finite Difference Scheme for the Navier-Stokes Equations Using Vorticity Boundary Conditions*. SIAM J. Numer. Anal. **29** . 615-639.

[KHO] Kreiss. H.O., 1972, *Comparison of Accurate Methods for the Integration of Hyperbolic Equations*. Tellus. XXIV. **3**. 199 215.

Reproduced with permission of the copyright owner. Further reproduction prohibited without permission.

[KM] Kim, J., Moin, P., 1985. *Application of a Fractional-Step Method to Incompressible Navier-Stokes Equations*. J. Comp. Phys. **59**. 308-323.

[MA] Mizukami, A., 1983. *A Stream Function-Vorticity Finite Element Formulation for Navier-Stokes Equations in Multi-Connected Domain*. Int. J. Numer. Methods Eng. **19**. 1403-1409.

[MKZ] Meth, K.Z., 1988, *A Vortex and Finite Difference Hybrid Method to Compute the Flow of an Incompressible, Inviscid Fluid Past a Semi-Infinite Plate*., Ph.D. thesis, NYU, (unpublished).

[MP] Maddocks, J.H., Pego, R.L., 1995. *An Unconstrained Hamiltonian Formulation for Incompressible Fluid* , Comm. Math. Phys. **170**. 207-217.

[OI1] Orszag, S.A., Israeli, M., 1974. *Numerical Simulation of Viscous Incompressible Flows*, Ann. Rev. Fluid Mech., **6**. 281-318.

[OI2] Orszag, S.A., Israeli, M., Deville, M.O., 1986. *Boundary Conditions for Incompressible Flows*, J. Scientific Computing **1**. 75-111.

[OV] Oseledets, V.I., 1989, *On a New Way of Writing the Navier-Stokes Equation: The Hamiltonian Formulation* , J. Russ. Math. Surveys **44**. 210-211.

[PT] Peyret, R., Taylor, T., 1983, *Computational Methods for Fluid Flow*. (Springer-Verlag, New York/Berlin).

[QL] Quartapelle, L., 1983, *Numerical Solution of the Incompressible Navier-Stokes Equations*, (Birkhauser, Berlin).

[RS] Russo, G., Smereka, P., *Impulse Formulation of the Euler Equations: General Properties and Numerical Methods* , appear in J. Fluid Mech.

[TM] Temam, R., 1969, *Sur l'Approximation de la Solution Des Dquation de Navier-Stokes Par la Méthode Des Fractionnarires II*, Arch. Rational Mech. Anal. **33**, 377-385.

[S1] Shen, J., 1992. *On Error Estimates of Projection Methods for Navier-Stokes Equation: First Order Schemes*. SIAM J. Numer. Anal. **29**. 57-77.

[S2] Shen, J., 1992. *On Error Estimates of Some Higher Order Projection and Penalty-Projection Methods for Navier-Stokes Equations*. Numer. Math. **62**. 49-73.

[STR] Strang, G., 1964. *Accurate Partial Differential Methods II. Non-Linear Problems*. Numerische Mathematik **6** (1964). 37-46.

Reproduced with permission of the copyright owner. Further reproduction prohibited without permission.

[THOM] Thom, A., 1933, *Proc. Roy. Soc. London Sect. A* , **141**, 651.

[TS1] Thorpe, S.A., 1968, *On Standing Internal Gravity Waves of Finite Amplitude*, J. Fluid Mech., **32**, 489-528.

[TS2] Thorpe, S.A., 1969, *Experiments on the Instability of Stratified Shear Flows: immiscible fluids*, J. Fluid Mech., **39**, 25-48.

[TS3] Thorpe, S.A., 1971, *Experiments on the Instability of Stratified Shear Flows: mMscible Fluids*, J. Fluid Mech., **46**, 299-320.

[TTE] Tezduyar, T.E., 1989, *Finite Element Formulation for the Vorticity-Stream Function Form of the Incompressible Euler Equations on Multi-Connected Domains*, Comput. Meth. Appl. Mech. Eng. **73(3)**, 331-340.

[VKJ] Van Kan, J., 1986, *A Second Order Accurate Pressure Correction Scheme for Viscous Incompressible Flow* , SIAM J. Sci. Comput. **7**, 870-891.

[WB] Wetton, Brian R., 1997, *Error Analysis for Chorin's Original Fully Discrete Projection Method and Regularizations in Space and Time*, SIAM J. Numer. Anal. **34**, 1683-1697.

Reproduced with permission of the copyright owner. Further reproduction prohibited without permission.